NASA Contractor Report 3714

Analysis and Correlation of Test Data From an Advanced Technology Rotor System

D. Jepson, R. Moffitt, K. Hilzinger,
and J. Bissell

CONTRACT NAS2-10211
AUGUST 1983

25th Anniversary
1958-1983

NASA

NASA Contractor Report 3714

Analysis and Correlation of Test Data From an Advanced Technology Rotor System

D. Jepson, R. Moffitt, K. Hilzinger,
and J. Bissell
United Technologies Corporation
Stratford, Connecticut

Prepared for
Ames Research Center
under Contract NAS2-10211

NASA
National Aeronautics
and Space Administration

Scientific and Technical
Information Branch

1983

TABLE OF CONTENTS

TABLE OF CONTENTS (continued)

ANALYSIS AND CORRELATION OF TEST DATA FROM AN ADVANCED TECHNOLOGY ROTOR SYSTEM

By D. Jepson, R. Moffitt, K. Hilzinger and J. Bissell
Sikorsky Aircraft Division
United Technologies Corporation
Stratford, Connecticut

SUMMARY

Comparisons have been made of the performance and blade vibratory loads characteristics for an advanced rotor system as predicted by analysis and as measured in a 1/5 scale model wind tunnel test, a full scale model wind tunnel test and flight test.

The principal objective of the study was to determine the accuracy with which the various tools available at the various stages in the design/development process (analysis, model test etc.) could predict final characteristics as measured on the aircraft. A secondary objective was to evaluate the accuracy of the analyses in predicting the effects of systematic tip planform variations investigated in the full scale wind tunnel test. The principal analysis employed was the Sikorsky Y201 aeroelastic analysis which considered the effects of rotor induced and fuselage-induced flow fields. A steady two-dimensional aerodynamic representation was used.

The test data from the full scale model were shown to predict forward flight performance within $\pm 5\%$. Hover performance measurements taken in the wind tunnel predicted corrected hover performance data measured at the contractor's rotor whirlstand facility. Blade vibratory loads were found to be underpredicted by the full scale model and this was indicated by analysis to be mostly the result of rotor inflow distortions imparted by the flow over the fuselage.

Blade tip sweep and to a lesser extent tip planform taper were shown to be effective in reducing rotor forward flight power requirements and blade vibratory loads. When these configuration features are combined together, the resulting swept tapered tip was found to be even more effective for improving these rotor system attributes.

The 1/5 scale model rotor predicted conservative full scale rotor performance as expected due to Reynolds number effects. Although blade vibratory moment trends with advance ratio were predicted by the 1/5 scale model, differences in mass and edgewise stiffness distributions (due to the model fabrication early in the design stage of the full scale ATRS and, due to provisions in the model- to allow interchangeable tips) caused the absolute values of the blade vibratory moments to be underpredicted. Analytical corrections correctly accounted for most of the differences between model and full scale results.

The Contractor's Coupled Normal Modes (Y201) elastic rotor blade analysis incorporating variable inflow was able to predict most of the trends of the test data at the higher advance ratios. In addition, using rotor inflow distortions due to fuselage flow as computed by Sikorsky Aircraft's Wing and Body Aerodynamic Technique (WABAT), the Y201 program predicted increases in blade vibratory moments reasonably consistent in magnitude and phase relation with the test data. However, the analysis was unable to predict the absolute magnitude of the blade ½ peak to peak moments at all cruise speed and rotor lift conditions. The ½ peak to peak moments were best predicted when constant inflow was assumed. Y201 gave good performance predictions below rotor stall but optimistic rotor power predictions at high lift.

To eliminate these discrepancies, it is believed that a better representation of the aerodynamics of the blade is required. Emphasis should be placed on improving skewed, unsteady airfoil characteristics, and three-dimensional tip effects.

INTRODUCTION

It is well known that helicopter rotors operate in a complex aerodynamic environment. This presents a challenging problem of accurately predicting the characteristics of new designs that differ significantly from past practice. To minimize the risk entailed in developing a new rotor, it would be highly desirable to surface potential problems through early analysis and/or early wind tunnel tests. Reynolds number effects, of course, exist at model scale and it is not always possible to duplicate in a model all dynamic characteristics of the full scale hardware. Such differences can exist due to scale problems and/or the fact that the model may not reflect fully the developed full scale rotor. On the other hand, wind tunnel tests of large (or even full) scale rotors usually cannot be conducted until the design/development process is well along. Nevertheless, such a test can be valuable for several reasons. It can be used to confirm the design, to reduce the risk of the flight program, to provide a solid data base on the "isolated" rotor for the purpose of validating analyses and to interpret aircraft system performance.

During the development of the advanced main rotor for a recent modern helicopter, Sikorsky conducted analyses and model and full scale wind tunnel tests of the main rotor (hereafter referred to as Advance Technology Rotor System, ATRS). See Figure 1. Not only are rotor wind tunnel data available at both full and 1/5 scale (from an aerodynamically and dynamically similar model), but rotor flight test data and airfoil data appropriate to the Reynolds number both of the full and 1/5th scale model are also available. Accordingly, there became available a sufficient data base on one rotor configuration to evaluate the usefulness of models and analysis for predicting full scale rotor attributes. In addition, during the course of the full scale wind tunnel program, systematic tests of tip shapes were conducted.

The prime objective of this program was to determine the ability to use analytical, model and full scale wind tunnel test results to predict rotor flight performance and blade dynamic loading characteristics. More specifically, the objectives were to:

1. To assess the degree to which full scale wind tunnel data for an "isolated" rotor agree with flight test results.

2. To evaluate the applicability of model rotor results through comparisons with full scale wind tunnel and flight test results.

3. To assess the possibility of extending the applicability of model results through the application of analyses employing airfoil data appropriate to model scale airfoils.

4. To evaluate the accuracy of analytic predictions of rotor performance and vibratory loads, identifying important areas where improvements in the analytical methods should be developed.

5. To evaluate the accuracy of analyses in predicting the effects of systematic tip planform variations.

This study has brought these data into a comparable format and employed this data base to address the objectives cited above. It should be noted that wind tunnel data on the full scale rotor has presented an opportunity to correlate analyses with less uncertainties due to the effects of fuselage forces and rotor-fuselage aerodynamic interactive effects present in flight data.

The flight test data for the baseline ATRS comes from demonstration testing of the Sikorsky "SPIRIT™" helicopter. See Figure 2. The general arrangement of the helicopter is shown in Figure 3. The ATRS incorporates an advanced tip configuration that combines the features of sweep and planform taper which the study will show proved to provide significant rotor system benefits. These same full scale rotor blades were also tested in the NASA Ames 40 ft. (12.2 m) by 80 ft (24.4 m) Large Subsonic Wind Tunnel. The test configuration is shown in Figure 4. Here the ATRS is mounted above the NASA's Rotor Test Apparatus (RTA) which was powered with two 1500 hp electric motors. During this series of tests, the three 5% span alternate tip configurations were demonstrated. These tips provide the opportunity to study systematically the effects of tip planform taper and tip sweep and the combination thereof with the results from a conventional rectangular planform tip at full scale Reynolds numbers. Blade spanwise twist and airfoil section were held constant. The four tips are shown in Figure 5 and are described more fully below. These tips are interchangeable with the baseline, swept tapered tip so that only one set of inboard blades were used for the test. Therefore, these tips are compared avoiding potential inboard blade differences that could occur if four sets of blades had been used. Some of the results of these tests are reported in References 1 and 3. The 1/5 scale model data were obtained in United Technology Research Center's (UTRC) 18 foot (5.49 m) large subsonic Wind Tunnel. The model included a powered rotor, and a replica of the flight vehicles fuselage. The blade was an aerodynamic and dynamically scaled replica of the then defined ATRS blade; it was capable of operating at full scale Mach numbers. Figure 5 shows the model installation. The performance results of this test series are reported in Reference 2.

From these three tests, level rotor performance and blade vibratory moment data were compared where data were available. The rotor system attributes that were selected for comparison were those that are considered to be some of the more important rotor design parameters and, were available from the three tests over the cruise envelope. They are rotor power, blade root torsion (push rod load) and flatwise bending moment at the 70% span (NB-7). Other blade flatwise and edgewise bending moment data are also presented for selected flight conditions.

LIST OF FIGURES

LIST OF FIGURES - CONTINUED

LIST OF FIGURES - CONTINUED

LIST OF FIGURES - CONTINUED

LIST OF FIGURES - CONCLUDED

LIST OF TABLES

LIST OF SYMBOLS

a — speed of sound

b — number of blades in the rotor system

C — blade chord

C_D — rotor drag coefficient = $\frac{D}{\pi\rho\ \Omega^2\ R^4}$

C_{EB-X} — blade edgewise bending moment coefficient at the 10 x X% span station = $\frac{EB-X}{\pi\rho\ \Omega^2\ R^5}$

C_L — airfoil lift coefficient = $\frac{L_R}{\frac{1}{2}\ \rho\ V^2 S}$, or

total rotor lift coefficient = $\frac{L_R}{\pi\rho\ \Omega^2\ R^4}$

$C_{L_{AF}}$ — lift coefficient of the airframe = $\frac{L_{AF}}{\pi\rho\ \Omega^2\ R^4}$

C_{LSS} — lateral stationary servo control force coefficient = $\frac{L_{SS}}{\pi\rho\ \Omega^2\ R^4}$

C_{NB-X} — blade flatwise bending moment coefficient at 10 x X% span station = $\frac{NB-X}{\pi\rho\ \Omega^2\ R^5}$

C_P — main rotor power coefficient = $\frac{P}{\pi\rho\ \Omega^3\ R^5}$

C_{PRL} — blade root torsional moment coefficients = $\frac{PRL}{\pi\rho\ \Omega^2\ R^4 \ln}$

C_Q — main rotor torque coefficient = $\frac{Q}{\pi\rho\ \Omega^2\ R^5}$

D — rotor drag, positive rearward

D_{AF} — total airframe drag, positive rearward

EB-X — blade edgewise moment at the 10 x X% span station, positive forward

f — total airframe parasite drag area

kg	kilogram, mass
kgf	kilogram, force
L	airfoil section or blade segment lift, positive upward
L_{AF}	airframe lift, positive upward
l_h	blade push rod horn length
L_R	main rotor lift, positive upward
L_{SS}	lateral stationary servo control force, positive upward
M_T	rotor rotation or hover tip Mach number, $\frac{\Omega R}{a}$
NB-X	blade flatwise bending moment at 10 x X% span station, positive upward
P	main rotor power
p-p	maximum peak minus minimum peak blade moment
PRL	blade push rod load, positive nose up
q	airstream dynamic pressure
Q	main rotor torque
R	blade radius
S	airfoil section or blade segment area
t/c	airfoil maximum thickness to chord ratio
Up	Vertical component of air velocity at the rotor blade, positive upward
U_R	radial component of our velocity of the rotor blade, positive outward
U_T	tangential component of our velocity at the other blade, positive approaching the blade
V	true airspeed
W	aircraft gross weight
w	main rotor downwash velocity; positive downward

α_E	fuselage effective angle of attack relative to the local flow, degrees, positive nose up
α_S	main rotor shaft angle of attack relative to the airstream, degrees, positive inclined rearward
θ	fuselage pitch attitude, degrees, positive nose up
θ_1	blade theoretical center of rotation to tip twist, degrees
μ	rotor advance ratio, $\frac{V}{\pi R}$
ρ	mass density of air
σ	rotor solidity = $\frac{bc}{\pi R}$
ϕ	fuselage roll, degrees, positive right wing down
ψ	rotor blade azimuth, zero over the tail cone, or fuselage yaw, degrees, positive nose right

Subscripts

i	induced power
o	profile power
p	parasite drag power

TEST ROTOR DESCRIPTIONS

Flight Vehicle

The Advanced Technology Rotor System (ATRS), as configured for the flight test vehicle, has 4 blades with coincident flap and lag articulation provided at the blade root by elastomeric bearings. Blade pitch motion is also permitted by elastomeric bearings. The blade employs titanium spar construction with a fiberglass skin and utilizes graphite composite trailing edge strips for the control of edgewise natural frequency. The blade radius is 22 feet (6.706m) with a hinge offset of 10 inches (25.4cm) and the nominal value for chord is 15.5 inches (39.37cm). The blade has an equivalent linear twist of -10° and a 5% span swept tapered tip, whose quarter chord is swept aft 30 degrees.

Figure 1 shows a sketch of the blade with a breakdown of its airfoil characteristics. The advanced combined airfoil sections used on the blade range from SC1013R8 at the 50 inch (1.27m) radius, tapering to SC1095R8 at the 120 inch (3.05m) radius, the SC1095R8 continuing out to 210 inches radius. An SC1095 airfoil is used from 220 inches to the tip with a transition region between 210 (5.33m) and 220 inches (5.59m).

The SC1095R8 has leading edge camber to increase maximum lift at low and mid Mach number, and the blade has a -3° reflexed trailing edge tab to reduce blade pitching moment. The SC1095, SC1095R8 and SC1013R8 airfoils have a (t/c) max = 9.5%, 9%, and 13% respectively. The position of (t/c) max is at the 27% chord for all three airfoils. The amount of camber is .84% on the SC1095 and 2.1% on the SC1095R8 and the SC1013R8 airfoils. The SC1095 airfoil's maximum camber is located at 30% chord; for the other two airfoils it is located at 21% chord. The airfoil surface coordinates are presented in Appendix M.

Structural and mass properties of the ATRS flight test rotor blade are identified in Appendix A. Single value items are listed as well as spanwise variations of blade parameters.

For Flight 30, the blade had a 2.27 lb, 8 to 10 inch long, tungsten counterweight starting at station 249.88 and extending inboard. This weight was not included in the aeroelastic analysis, since natural frequency calculations showed it had a small effect.

Full Scale Model

The baseline full scale model blade is identical to the flight test rotor blade. Therefore, all items in Appendix A are applicable to both rotors. Variations were made in tip configuration to evaluate effects on performance and blade response. Figure 5 shows sketches of the various tip configurations.

The swept-tapered or production tip has a quarter chord sweep of 30° and a taper ratio of 60%. The trapezoidal tip has zero aerodynamic sweep and a taper ratio of 60%. The rectangular tip has no sweep or taper ratio and the swept tip has 20^{0} of aerodynamic sweep with no taper. For the production and swept tips, the summation of tip area times the distance of the centroid of tip area from the blade feathering axis was kept essentially constant. The breakdown of the various tip section properties are tabulated in Appendix B.

The natural frequencies of the blade were calculated by the Y201 program. These natural frequencies were verified where possible during whirl testing. This was done by observing resonances during cyclic pitch shaker frequency sweeps, and also resonances due to natural harmonic forcing during rotor speed sweeps. The results of the calculations and testing are shown in Figure 7. The correlation in general is quite good, with agreement seen over a range of rotor speed. The calculated torsion mode frequency is about 200 cpm below the test data. This difference in frequency is attributed to a low estimated value for root control system stiffness.

Miscellaneous ATRS rotor head and aircraft physical properties are presented in Appendix D. Lag damper and control system geometry, as well as tail rotor and fuselage descriptions, are included.

1/5 Scale Model Description

Early in the design phase of the full scale ATRS, a 8.8 foot (2.68m) diameter (1/5th scale) model rotor was constructed for the purpose of predicting rotor performance and rotor downwash over the fuselage and empennage during powered wind tunnel tests in United Technology Research Center's 18 foot (5.49m) large subsonic wind tunnel.

The main two design requirements for this blade were to match the full scale outside contour (aerodynamic configuration) and to be able to operate at full scale tip Mach numbers. A third requirement was also established to provide an 8% span, interchangeable tip capability in order to study the effects of tip design, economically. A fourth, but lower priority requirement, was to match the then defined mass and stiffness properties as close as possible, while meeting the higher priority requirements.

The model blade was fabricated with a chord of 3.1 inches (7.87 cm) and the same spanwise twist and airfoil section distribution as the full scale blade. It was made using similar composite material construction as the full scale rotor blade.

Two physical properties of the 1/5 scale blade are different from the full scale blades. First, after the 1/5 scale model was fabricated and tested, the full scale blade design was modified to increasing the edgewise stiffness by approximately 50%. Secondly, the model's scaled mass is about 18% higher than the full scale blade. This higher weight comes from two sources, structural provisions for the interchangeable tip and from inboard mass weight growth during construction of the first model blades. Because early wind tunnel testing was desired, and because the primary purposes of the test were directed toward performance and handling qualities objectives, the mass differences were judged acceptable.

The mass and structural properties of the 1/5 scale model blades as fabricated are presented in Appendix C.

ROTOR FORCE TRIM ANALYSIS

To satisfy the objectives of this contract, it is necessary to define the trim state of the flight rotor. This can be accomplished in one of two ways. In the first approach, the rotor trim state can be taken as that defined by the blade pitch control angles and the rotor shaft angle measured in flight. These angles can then be used in an analysis to predict rotor forces and moments. These angles could also be used to interrogate wind tunnel data maps to determine rotor forces and moments. The principal disadvantage to this approach is of course that such angle data are not available until the aircraft flies.

The second approach, and the one employed herein, involves use of model scale fuselage characteristics measured on a sub scale model, together with an aircraft trim analysis, to define the required main rotor lift and propulsive force. Using this approach, aircraft predictions can be updated following wind tunnel tests of models. Such model tests can, of course, be conducted much earlier in the life of the aircraft program. Once rotor lift and propulsive force requirements are known, the analysis or rotor wind tunnel (or flight) data can be interrogated at these values to determine dependent quantities of interest such as power, blade stresses etc. As a final note, rotor pitch and roll moments are not considered since experience has shown that such moments are intentionally kept small by design and that on articulated rotors performance and blade loads are generally insensitive to realistic variations in these parameters. The details of the process by which trim conditions were thus computed are given below.

The main rotor lift coefficient is expressed:

$$C_L = C_W - C_{L_{AF}}$$

where:

C_W = weight coefficient

$$= \frac{w}{\rho \pi R^2 (\Omega R)^2}$$

w = aircraft weight

ρ = ambient air density

$C_{L_{AF}}$ = lift coefficient of the airframe

The value of $C_{L_{AF}}$ is not available from flight test measurements and must be determined either through analysis or from wind tunnel tests. For this study the value was obtained from 1/5 scale configuration model tests. Appendix F presents a method to determine the variation of fuselage lift, divided by the free stream dynamic pressure, with fuselage angle of attack based on the model tests. The main rotor lift coefficient is then expressed:

$$C_L = C_W - \frac{(L_{AF}/q)\ q}{\rho \pi R^2 (\Omega R)^2}$$

where:

L_{AF}/q = fuselage lift/dynamic pressure ratio

q = dynamic pressure = $\frac{1}{2} \rho V^2$

Substituting for the dynamic pressure gives:

$$C_L = C_W - \frac{L_{AF}/q}{\rho \pi R^2 (\Omega R)^2} \left(\tfrac{1}{2} \rho V^2\right)$$

$$= C_W - \frac{L_{AF}/q}{2 \pi R^2} \mu^2$$

or, dividing by the solidity ratio (σ):

$$C_L/\sigma = C_W/\sigma - \frac{L_{AF}/q}{2bcR} \mu^2$$

The 1/5 scale model data of Reference 2 was also the basis for evaluating the flight test vehicle parasite drag. Appendix F presents drag related data from Reference 2, along with appropriate corrections that yield the total airframe drag variation with angle of attack presented in Figure 8. These corrections consisted of additional drags due to miscellaneous protuberances, holes, instrumentation items and momentum losses that were not simulated in the wind tunnel tests. The drag coefficient after substituting for the dynamic pressure and dividing by the solidity ratio, is

$$C_D/\sigma = \frac{D_{AF}/q}{2bcR} \mu^2$$

where D_{AF} is the total airframe drag as evaluated in Appendix F.

The main rotor torque used to compare with analytic and wind tunnel results is measured directly in flight and the torque coefficient is defined:

$$C_Q = \frac{Q}{\rho \pi R^3 (\Omega R)^2}$$

where:

Q = main rotor torque

Profile torque must be estimated and is derived from the measured main rotor torque by subtracting the calculated torques due to parasite drag and an idealized induced drag. This is best accomplished by expressing the contributions of parasite and induced drags as power coefficients, since these are numerically equal to the respective torque coefficients. The parasite drag power may be written (assuming ideal propulsive efficiency):

$$P_p = (D_{AF}/q) \times q \times V = D_{AF} V$$

or, in coefficient form:

$$C_{P_p} = C_{Q_p} = \frac{-D_{AF}\ V}{\rho \pi R^2 (\Omega R)^3} = -C_D \times \mu$$

which is the parasite drag torque coefficient.

Induced drag power may, for small tip path plane angles, be expressed as

$$P_i = L_R \left(\frac{w}{V}\right) V = L_R w$$

where

L_R = main rotor lift

w = main rotor downwash velocity

$$= \frac{C_L}{2\mu} \Omega R$$

Substituting for w, previously defined, and nondimensionalizing gives

$$C_{P_i} = \frac{L_R}{\rho \pi R^2 (\Omega R)^3} \left(\frac{C_L}{2\mu}\right) \Omega R = \frac{C_L^{\,2}}{2\mu}$$

therefore,

$$C_{\tilde{P}_i} = C_{Q_i} \approx \frac{C_L^{\,2}}{2\mu}$$

the idealized induced drag torque coefficient.

The profile torque coefficient is defined:

$$C_{Q_o} = \frac{Q_o}{\rho \pi R^3 (\Omega R)^2}$$

where:

Q_o = profile torque

and in terms of the total main rotor torque, lift, and drag coefficients is expressed:

$$C_{Q_o} = C_Q - \frac{C_L^{\,2}}{2\mu} + C_D \times \mu$$

Tables I and II summarize the main rotor level flight force coefficients used to compare the test and analytical data as a function of advance ratio, rotational tip Mach number and helicopter gross weight. The fuselage body attitudes measured in flight are also given for reference. Most of the advance ratio and tip Mach number conditions were selected to correspond to specific conditions tested during the full scale rotor wind tunnel tests. This rotor was tested over a range of lift and propulsive force values. Flight test data were available at two values of gross weights and also over the advance ratio range shown in the tables, but not necessarily at the specific values. The gross weight values in the tables were chosen to correspond to those values selected for the flight testing. One specific advance ratio was selected based on the flight test results. At a rotational tip Mach number (M_T) equal to .6 and a gross weight of 8200 lb (3719.5 kg), vibratory moments were measured at the most blade spanwise stations up to an advance ratio (μ) equal to .338. Other flights extended the test data to higher speeds, but fewer blade loads were recorded. Therefore, μ = .338 was selected as one condition to compare test data results because it was the highest speed where the most complete blade moment data were available from flight tests.

In all cases, some portion of the test data had to be interpolated to the specific conditions shown in the tables. The flight data were interpolated to a specific advance ratio holding gross weight and M_T fixed. The full scale rotor data were usually interpolated to the specific rotor lift and propulsive forces noted in the tables holding μ and M_T constant. The 1/5 scale model data were interpolated for both rotor forces and advance ratio as required.

Late in this study, as this report was being written, an error was discovered in the evaluation of airframe lift. This error amounts to a 5% overestimation of rotor lift for trimmed level flight due to a discrepancy in calculated fuselage local angle of attack, α_E. Accordingly, the full scale model test data are compared to the flight data at a 5% greater value than should be. Airframe drag was not effected because drag is essentially constant between $\alpha_E = -5^0$ to $+ 5^0$, the range where trim for the conditions studied occurs. The effect of this increase on the full scale model power and the blade vibratory load was estimated and found to be equal to, or less than a 1% increase per 1% increase in rotor lift. Also, a check on the calculated fuselage interference flow on blade vibratory moments revealed only small differences in the computed values. Therefore, the effect of the high estimated rotor lift does not effect the conclusions of this report. The data results of this report have not been connected for this discrepancy and the rotor lift values for the trim conditions presented in Tables I and II are numbers that are 5% high.

Wall effect corrections were applied to all rotor data obtained in a wind tunnel. For the full scale model, this correction was based on a classical Prandtl wall correction previously derived for the 40 x 80 ft wind tunnel. ($\Delta\alpha$ = k x L/q where k = .00197 deg/ft^2). This correction becomes more accurate as test velocities are increased and is adequate at speeds 100 kts and above.

Because wall corrections are approximate, they are another source of error. Even a small error in the calculated angle of attack correction can result in a significant error in the corrected rotor power required. For the ATRS rotor operating at C_L/σ = .095, M_T = .6 and a f/bCR = .107, the approximate percentage change in power required per degree of angle correction varies as a function of advance ratio as follows:

μ	$(\Delta Cq/Cq/\Delta\alpha)$ x 100
.15	7%
.30	9%
.40	10.4%

Accordingly, if the correction to the free air conditions of the rotor performance data taken in the wind tunnel were off by 1 degree, then the rotor performance would be in error by the percentage shown in the above table. But as was noted above, as advance ratio is increased, the estimated wall corrections become more accurate and the angle of attack error becomes much less than one degree.

TABLE I

Main Rotor Force Trim Coefficients, M_T = .6

GW LB (kg)	C.G. Loc. (Fus. Sta.)	V Kts, TAS	ΩR fps (m/sec)	θ_B Deg	ϕ_B Deg	ψ_B Deg	ρ $\frac{slug}{ft^3}$ $(\frac{kg}{m^3})$	μ	M_T	C_W/σ	C_L/σ	$-C_D/\sigma$
8200 (3719.5)	210 210	100	673 (205)	2.87	-1.	-2.	.002229 (1.1488)	.25	.6	.07140	.0747	.00336
8200	210	120	673	2.02	-1.	-2.	.002229	.3	.6	.07140	.0755	.00484
8200	210	135	673	1.40	-.5	-2.	.002229	.338	.6	.07140	.0765	.00615
8200	210	150	673	.8	-1.	-2.	.002229	.375	.6	.07140	.0781	.00757
8200	210	160	673	.36	-1.3	-2.	.002229	.4	.6	.07140	.0797	.00861
10300 (4672)	197 197	100	677 (206)	1.5	-1.4	-2.	.002275 (1.1725)	.25	.6	.08684	.0898	.00336
10300	197	120	677	0.4	-1.	-3.	.002275	.30	.6	.08684	.0911	.00484
10300	197	140	677	-1.3	-.9	-1.	.002275	.35	.6	.08684	.0931	.00659
10300	197	150	677	-1.2	-.7	-1.	.002275	.375	.6	.08684	.0948	.00757

TABLE II

Main Rotor Force Trim Coefficients, M_T = .633 to 6.5

GW LB (kg)	C.G. Loc. (Fus. Sta.)	V Kts, TAS	ΩR fps (m/sec)	θ_B Deg	ϕ_B Deg	ψ_B Deg	ρ $\frac{slug}{ft^3}$ $\left(\frac{kg}{m^3}\right)$	μ	M_T*	C_W/σ	C_L/σ	$-C_D/\sigma$
8200 (3719.5)	210 210	100	719 (219)	3.6	-2.6	-3.	.002229 (1.1488)	.25	.64 .65	.06251	.0657	.00336
8200	210	128	719	2.3	-.4	-2.	.002229	.30	.64 .65	.06251	.0670	.00484
8200	210	149	719	.86	+.4	-2.	.002229	.35	.64 .65	.06251	.0689	.00659
8200	210	160	719	0.	-1.	-1.	.002229	.375	.64 .65	.06251	.0700	.00757
8200	210	170	719	-1.35	-1.4	0.	.002229	.400	.64 .65	.06251	.0718	.00861
10300 (4672)	210 210	106	719	4.7	-	-2.	.00222 (1.144)	.25	.633 .65	.07904	.0822	.00336
10300	210	128	719	3.6	-	-2.	.00222	.30	.633 .65	.07904	.840	.00484
10300	210	149	719	2.25	-	-1.	.00222	.35	.633 .65	.07904	.0870	.00659
10300	210	160	719	1.35	-	-1.	.00272	.375	.65	.07904	.0892	.00751

*First value corresponds to flight test, second to NASA/Ames test.

DISCUSSION OF TEST RESULTS

Baseline Rotor - Flight, Full Scale and 1/5 Scale Model Data Comparisons

Performance Data

Figures 9 through 12 present the variation of trimmed level flight main rotor torque coefficient with advance ratio for two tip Mach numbers, 0.6 and 0.65, and for two representative aircraft weights of 8200 lb (3719.5 kg) and 10,300 lb (4622 kg). The data presented was obtained through flight test and wind tunnel tests conducted on both full scale and 1/5 scale models of the ATRS rotor as discussed in the introduction. (Note: In order to provide all flight test data on a consistent basis, the test flights for Figures 9 through 12 were initially selected as those from which the blade dynamic loads data were obtained.)

The correlation of full scale model and flight data is generally good. However, some random differences are noted in Figures 9 and 12. In Figure 9 the full scale model torques are higher than measured in flight whereas in Figure 12 they are lower. It is believed that these differences are due to small errors in the derived flight drag values. Additional flight conditions were examined to provide a greater number of data points and the results are summarized in Figure 13 where flight and full scale wind tunnel torque values are presented. The correlation is quite good as the data scatter is randomly about the 0% error line with the bulk of the data falling within $\pm 5\%$. In the course of making this comparison, it was noted that those data points giving the smallest errors, were those acquired during dedicated performance (as opposed to structural) testing. The range of rotor performance parameters covered by the data in Figure 13 is:

Parameter	Value Range Minimum	Value Range Maximum
μ	.25	.375
M_T	.6	.635
C_L/σ	.762	.10
C_D/σ	-.0034	-.0076
C_q/σ	.00325	.0087

As expected, the 1/5 scale model torques are consistently higher than both the full scale model and flight test vehicle. (Figures 9 through 11) This is due to Reynolds number effects that result in higher drags at comparable lifts below stall and also to earlier stall. 1/5th scale model torques are typically 20% higher than full scale model results.

Figures 14 through 17 present the variation of level flight main rotor profile torques for the same operating conditions as for the total torques presented in Figures 9 through 12. The profile torque is estimated from the measured total torque by subtracting the torques due to idealized parasite drag and induced drag. Correlation of full scale model profile torques with flight test values is, as for the total torques, good to excellent. However, differences here may, in fact, be exaggerated because small differences in total torque will, dependent on the operating condition, result in a much larger percentage change in the profile torques derived from it since all of the difference will by definition be contained in the profile torque.

Hover Performance Measurements

When the full scale model was installed in the NASA Ames Wind Tunnel, hover performance measurements were made with the tunnel walls open and the rotor shaft axis tilted 10 degrees forward. The shaft tilt was used to reduce rotor recirculation effects. These measurements are compared in Figure 18 with corrected data obtained on Sikorsky Aircraft's 10,000 hp main rotor whirlstand. The whirlstand data has been reduced by three percent in order to correct for test stand interference and ground effects. The figure demonstrates good agreement between the two sets of test data and indicates that for rotors of the size of the ATRS or smaller, good quality hover data can be obtained in the subject wind tunnel.

½ Peak to Peak Blade Moment Data

The vibratory moment data presented in the following sections are blade vibratory loads. They are presented in two forms, either as one half of the maximum load value minus the minimum value experienced by the blade as it moves around the aximuth, i.e. half peak to peak values (½ p-p), or the instantaneous load value as a function of blade azimuth. All moments are presented non-dimensionalized and ratioed to rotor solidity as follows:

$$\frac{C_{PRL}}{\sigma} = \frac{\text{Push Rod Load}}{bc\rho\ \Omega^2\ R^3}$$

$$\frac{C_{NB-X}}{\sigma} = \frac{\text{Flatwise Bending Moment at 10xX\% Span Station}}{bc\rho\ \Omega^2\ R^4}$$

$$\frac{C_{EB-X}}{\sigma} = \frac{\text{Edgewise Bending Moment at 10xX\% Span Station}}{bc\rho\ \Omega^2\ R^4}$$

Figure 19 presents the spanwise distribution ½ p-p flatwise bending moments. These are presented at a gross weight of 8200 lb (3719.51 kg) a normal blade rotational tip Mach number, M_T = .6, and an advance ratio, μ = .338 or 135 knots. Flight test data (from flight 30), and full scale and 1/5 scale model interpolated test data are compared along with analytic results, which will be discussed in a separate section.

The maximum measured flight test values are shown to occur at the root and at the 70% span station. They reduce to zero at the blade tip and to about half the peak values at the 30% span (NB-3) station. Data from the full scale model rotor, interpolated to the equivalent cruise speed and rotor trim lift and propulsive force conditions of the figure, accurately predict the flight test 70% span maximum and the 30% span trough values. In between the values are lower.

The corresponding vibratory edgewise loading distribution is shown in Figure 20. The maximum measured moment in flight occurs near the blade root. The interpolated full scale model test data presented over the mid span stations agrees quite closely with the flight data.

Figure 19 and 20 also present a comparison of the measured 1/5 scale model spanwise ½ p-p moments with the flight test and the full scale model interpolated data. The 1/5 scale data are also interpolated to the estimated trim conditions of the flight vehicle. The two inboard flatwise gages of the 1/5 scale model are in good agreement with the full scale test data while the load measured by the NB-6.5 gage is about 50% low. The 1/5 scale model edgewise load is also low.

Potential reasons for the low 1/5 scale model results were considered. The model data were reviewed to see if calibrations were in error; none were found. The differences in blade characteristics between model and full scale were also reviewed. As discussed in the Test Vehicle Description section, the blade flatwise and torsional spanwise stiffness distributions are very close. However, the model edgewise stiffnesses are two-thirds of the full scale blade because the model was built during the early part of the full scale blade design phase. The full scale blade final design edgewise stiffness was increased after the model blades were completed. In addition, the model blade mass distribution inboard of the 60% span station and also between the 91% to 97% span station is higher resulting in a 18% increase in total equivalent blade weight. This resulted from the practical considerations of building and testing model blades to aid in the development of a new rotor system. For example, these model blades were designed with an interchangeable tip capability to study tip changes economically. Accordingly, the model outboard weight increase results from additional structure for the joint. The inboard mass results from the desire to begin the model testing as early as possible in the full scale blade design phase, and therefore, not providing sufficient time to reduce the model blade's weight. These differences, therefore, result from very real practical considerations faced by a designer confronted with lead time constraints.

In order to estimate the effect of these two differences, the Coupled Normal Modes Elastic Rotor Analysis computer program (Y201) was run with the two sets of blade characteristics and assuming constant rotor inflow and using the same airfoil characteristics. These results are shown in Figures 21 through 24 for two advance ratios, .338 and .375 and at 8200 lb. gross weight and 100% rotor speed. The calculations strongly suggest that these differences in blade characteristics are a significant contributor to the lower model NB-6.5 and EB-3.5 vibratory loads. Although each difference was not calculated separately, the increased mass is believed to be the dominant factor affecting the flatwise stresses, which are significantly changed only between the 50% and 75% spanwise stations. For the edgewise loads, Y201 predicts a reduction in vibratory moments inboard of 55% span station due to the combined effects of increased mass and lower edgewise stiffness. These predicted trends are very similar to the differences observed between the full and 1/5 scale model test data This is illustrated in Figures 19 and 20. The arrows connected to the 1/5 scale model test points indicate the magnitude and the direction that the analytical calculations would correct the test data on a percentage basis. Some differences between 1/5 scale and full scale results remain even with these corrections. These are believed to be due to Reynolds number effects on the airfoil characteristics and due to errors introduced by the need to interpolate the various loads data bases to obtain the loads at particular trim conditions.

The correlation of the three test rotors over the level flight envelope is presented in Figures 25 through 30. The blade vibratory torsional moments, in terms of the blade pushrod load, are given in Figures 25 through 27 at 8200 lb (3719.5 kg) and 10,300 lb (4672 kg) and at two rotational tip Mach numbers, M_T = .6 and .65. Figures 28 through 30 present the blade vibratory bending moments at the 70% span station for the same flight conditions as noted for the vibratory torsional moments. This is a station near the maximum outboard flatwise vibratory moment where data are available for all three test vehicles. As was previously noted, blade spanwise vibratory loads (Figures 19 and 20) were obtained from flight 30 up to μ = .338 at M_T = .6 and gross weight = 8200 lb (3719.5 kg). Because flight 30 did not continue to higher speeds, blade vibratory loads at higher speeds (Figure 28) were obtained from flight 2 for the noted gross weight and rotational tip Mach number. The data from the two flights overlap and can be seen to be in agreement when Figures 19 and 28 are compared.

The full scale model either predicts or slightly overpredicts the ½ p-p torsional and outboard flatwise moments at low advance ratio (μ) up to .25. As μ is increased these unsteady moments are underpredicted, but not by a large amount. For example, at μ = .375, the full scale model underpredicts the flight data by about 20% on the average. As shown in Figure 30, the full scale wind tunnel model interpolated data had some scatter at this condition. The mean of the scatter band falls below the flight data in about the same relative position as other similar data shown in Figures 28 and 29. As will be seen in the later discussion on the analytic results, the analysis suggests that flow distortions due to the aircraft flow over the fuselage is the probable cause of much of this underprediction.

The 1/5 scale model data is also shown on these figures for the conditions where M_T = .6. Figures 25 and 26 show that the model underpredicts the flight blade's root torsional moments at minimum power speeds. However, at the higher advance ratios, the more critical flight test moments are well predicted. This generally good agreement is expected despite the blade design differences noted earlier, because they did not significantly influence blade torsional frequencies.

The 1/5 scale model ½ p-p flatwise bending moments (as measured) at the 65% span station are compared to the 70% span moments from flight test in Figures 28 and 29. Their magnitude is about half of the flight test value over the cruise envelope for both the high and the low gross weight values presented. The reasons for the low 1/5 scale model values have been previously discussed; however, it is encouraging to note that the full scale trends with advance ratio and gross weight are well predicted by the model. This suggests that despite potential unavoidable blade differences, early sub scale model data can be used directly to examine trends.

These data and the data in Figures 19 and 20 are the extent of the available 1/5 scale dynamic data. However, this is sufficient data to conclude that if model blade characteristics are scaled properly, then measured model blade dynamic characteristics will reasonably correlate with the full scale characteristics. A practical constraint faced by the model designer will be the early state of the actual blade design. Corrections for reasonable differences in model and final full scale blade designs can be developed using analytic procedures.

Although the flight and full scale model rotor are expected to be alike in many respects, one potential area of difference is that of the stationary control systems. As a result it is of interest to determine the degree to which the full scale model results could be used to predict the flight aircraft stationary control loads.

An example of the loads comparison between the full scale flight and model rotor is presented in Figures 31 and 32 for the non-rotating portions of the rotor control system. The vibratory lateral stationary servo control loads, nondimensionalized, are compared over the level flight envelope for two rotor speeds and helicopter gross weight values. At the lower gross weight, the flight data and the interpolated wind tunnel data agree very closely and there is no effect of blade tip Mach number on the stationary servo load. At the higher gross weight, the full scale model underpredicts the flight data by about 20%, which is similar to what was observed for the other blade vibratory loads. As will be discussed in the analysis section, the difference is probably due in part to fuselage flow interference.

Blade Moment Time Histories

The time histories of the blade push rod load, NB-7 and EB-6 moments were harmonically analyzed for several flight conditions of interest. These data are derived from the test results of both full scale rotors. The following table summarizes the conditions, loads and the figure numbers where resultant load amplitudes and the corresponding time histories are presented.

TABLE III

TEST CONDITIONS FOR HARMONIC ANALYSIS AND TIME HISTORY PRESENTATIONS OF BASELINE ROTOR LOADS

Test Condition				Blade Loads			Figure No.	
μ	M_T	GW (lb)	GW (kg)	PRL	NB-7	EB-6	Resultant Amplitude	Time History
.338	.60	8200.	(3719.5)	√			33	42
					√		34	46
						√	35	47
.4	.60	8200.		√			36	43
					√		37	48
.375	.60	10300.	(4672)	√			38	44
					√		39	49
.375	.65	10300.		√			40	45
					√		41	50

The harmonic analysis study indicates that the first 7 harmonics of the push rod load are the most significant for both rotors. The resultant harmonics from the flight rotor are generally about the same or higher than from the full scale rotor. For the flatwise bending moment data, the first three harmonics are the most significant for both rotors. The flight test rotor generally has the higher resultant amplitudes. This is consistent with the ½ p-p moment data. However, the full scale model rotor has a 10 to 60% higher first harmonic resultant moment than the flight rotor. At this time, there is no satisfactory explanation of this latter result.

The blade load time histories presented in Figures 42 through 50 were reconstructed using the first eight harmonic amplitudes of the reduced test data. A review of these figures leads to the conclusion that the resulting time histories from the wind tunnel model do tend to predict the overall amplitude and general nature of flight rotor time histories, but the higher harmonic content and associated phase are only occasionally predicted.

Effect of Alternate Tip Configurations

Performance Data

The main rotor power requirement as affected by the alternate tip configurations shown in Figure 5 was investigated for four flight conditions in level flight. Advance ratio and rotational tip Mach number combinations are included which cover the present day cruise envelope (120 to 170 kts). Data are presented for gross weight values of 8200 lb (3719.5 kg) and 10,300 lb (4672 kg) where possible.

Figures 51 to 54 compare the ATRS with the three alternate tips to the baseline rotor in terms of rotor torque coefficient to solidity ratio. Two bars are given for each tip configuration; the left bar presents the test data at two gross weight values, the right bar presents the calculated results. (Analytic results also shown will be discussed in a later section.) In all cases, the swept tapered tip provides the lowest main rotor power. Except at $\mu = .3$ and $M_T = .6$, the constant chord swept tip provides the next best improvement and then the trapezoidal tip. The conventional rectangular tip requires the most power at and above 150 kts ($\mu = .375$), as expected. Table IV summarizes these savings relative to the rectangular tip in terms of rotor horsepower.

TABLE IV

MAIN ROTOR BLADE TIP COMPARISON; CHANGE IN HORSEPOWER RELATIVE TO RECTANGULAR TIP

M_T	μ	G.W. (lb) (kg)	ΔHP(KW) Relative to Rectangular Tip			
			Swept Tapered	Swept	Trapezoidal	Rectangular
.6	.30	8,200 (3719.5)	-19.2 (-14.1)	10.3 (7.6)	3. (2.2)	0. 0.
.6	.30	10,300 (4672.)	-17.7 (-13.0)	0.	4.4 (3.2)	0.
.6	.375	8,200	-59.1 (-43.4)	-32.5 (-23.9)	-26.6 (-19.5)	0.
.6	.375	10,300	-	-	-	0.
.65	.375	8,200	-69.5 (-51.1)	-60.1 (-44.2)	-41.3 (-30.4)	0.
.65	.375	10,300	-75.1 (-55.2)	-18.8 (-13.8)	0.	0.
.68	.375	8,200	-30.* (-22.1)	10* (7.4)	0.*	No data

*Savings relative to the trapezoidal tip.

Half Peak to Peak Blade Moment Data

The effect of blade tip configuration on blade vibratory loads was examined as a function of rotor propulsive force for four flight conditions and at two levels of rotor lift equivalent to level flight at a gross weight of 7900 lb (3583 kg) and 10,300 lb (4672 kg). The flight conditions that were examined are: $\mu = .3$, $M_T = .6$; $\mu = .375$, $M_T = .6$, .65 and .68. Blade push rod load and flatwise and edgewise bending moments at the 60 and 70% span stations were compared when the required data were available for each tip configuration and at each flight condition.

These differences are summarized in Figures 55 through 65 along with analytical predictions which are discussed separately. Each figure compares the four tip configurations on the basis of one blade vibratory load parameter measured in trimmed level flight at one advance ratio and tip Mach number. Two bars are given for each tip configuration; the left bar presents the test data at two gross weight values; the right bar presents the calculated results. The trim propulsive force is used in these figures without loss of generality because the relative magnitude of the blade vibratory loads did not change significantly as rotor propulsive force was varied, i.e. $0 \leq -C_D/\sigma \leq .01$. In fact, for this range, blade loads remained essentially constant or were reduced slightly as propulsive force was increased.

At an advance ratio of 0.3 (120 kts), these tip configurations produced only minor differences in ½ p-p blade moments. See Figures 55, 59 and 63. Increasing rotor lift within the gross weight range investigated also did not induce significant differences. At the higher advance ratio (μ = 0.375), however, some load differences were observed at .6 and .65 blade tip rotational Mach number. These are discussed below.

Blade ½ p-p root torsional moments are shown in Figures 56 and 57 to be the highest for the blade with the rectangular tip configuration at both gross weight and blade tip Mach number values. At M_T = .6, the three advanced tip configurations provide the same or small reductions in vibratory pushrod load. For the higher blade tip speed condition, blade tip sweep is shown to be very benefical. The baseline blade, which has the swept tapered tip, produced the lowest push rod loads. These were 25% lower than experienced by the rectangular tip blade.

The ½ p-p flatwise bending moments at the 70% span station are compared in Figures 60 and 61. Again, the blade with the rectangular tip experienced the highest vibratory loads. For both tip Mach numbers, as taper and sweep are incorporated to reduce tip loading, the NB-7 vibratory moments are reduced with the baseline rotor having the lowest moments. At M_T = .6, its moments are reduced about 15% below the rectangular tipped blade and at least 20% at the higher tip Mach number.

For some conditions at μ = 0.375, there was either suspect or insufficient NB-7 data to enable the swept tip blade to be interpolated to the flight trim condition and included in these figures. (Recall that NB-7 was choosen as a basis for comparison because it was one of three parameters measured on all three test vehicles.) However, insight into the relative blade bending moments among the four blade configurations can be obtained from the moments at the 60% span. A review of the NB-6 data showed that the swept tip blade moments are found to be close to the trapezoidal tip blade. Therefore, the NB-7 bending moments for the swept tip blade were assumed to be equal to those for the trapezoidal tip blade. (Figure 19 shows NB-6 and NB-7 to be quite close in magnitude so that this approach is reasonable.)

The 70% span ½ p-p edgewise bending moments are compared in Figures 64 and 65. The test data show that the advanced tip configurations do not affect EB-7 moments by more than 10% as compared to the rectangular tip blade. At normal tip Mach number, .6, the baseline blade has slightly higher moments than the blade with the rectangular tip, while the blade with the trapezoidal tip has slightly lower moments. At M_T = .65, the baseline blade has slightly lower moments than the rectangular tip blade, which has the highest moments.

Limited test data are also available at blade rotational Mach number equal to .68 and an advance ratio of .375 (170 kts) to allow the three advance tip configurations to be compared. Blade ½ p-p push rod loads are presented in Figure 58 and NB-6 moments in Figure 62. The push rod load for the swept tip blade is not available. These data also demonstrate that the swept tapered tip produces the lowest blade loads.

Blade Moment Time Histories

A comparison of the blade root torsion and 60% span flatwise bending moments as they vary around the rotor azimuth and as affected by the four tip configurations is presented in Figure 66 through 69. These data were originally published in Reference 3. The rotor is being flown in near trimmed level flight at a gross weight of 10,500 lb. Test data are presented at two blade rotational tip Mach numbers, .6 and .65.

As was observed in the discussion on the ½ p-p loads, the blade with the rectangular tip is shown generally to have the largest excursions as it traveled around the rotor azimuth for both root torsion and NB-6 moments. Modifying the tip to incorporate taper or sweep provides a modest reduction in peak loads at M_T = .6 for this moderately twisted blade, and only minor changes in blade wave form. As M_T is increased to .65 the reduction in peak loads and changes in wave form increase. The swept and the tapered tip configuration exhibit very similar moment signatures.

The swept tapered tip induced a substantially different blade moment time history than the other tip configurations, especially for the blade push rod load time history. The blade pitch down moment at the 100^o to 180^o azimuth region was significantly reduced at both tip Mach number flight conditions (Figures 66 and 67). The swept and trapezoidal tips also showed this trend, especially at M_T = .65. As the figures show, the elimination of this peak removes one of the major peaks of the blade torsion response. Correspondingly, the 60% span, peak downward flatwise bending moment is reduced in this azimuth region and the peak upward bending moment is also reduced at the 240^o azimuth location.

Why the combination of sweep and taper produces this benefit is not precisely understood but some insights are suggested by considering some first order effects that appear to be supported by the test data. First recall that for the high tip Mach number condition, the advancing blade tip Mach number is 0.9. Reducing blade tip thickness through taper is beneficial because tip drag is reduced. Reducing tip drag on the advancing blade, when the tip region is bent downward due to negative tip lift, would cause an incremental nose up twisting moment causing the tip to be unloaded. This is supported by the advancing blade negative flatwise bending moments shown in Figures 68 and 69, and the reduced blade torsion peak at $\psi = 140^o$ for the trapezoidal tip blade shown in Figures 66 and 67. Secondly, when aft tip sweep is added to a blade, the aerodynamic center of the swept portion of the blade is moved rearward relative to the main blade's elastic axis. Accordingly, tip lift produces a stabilizing moment which also unloads the tip and redistributes this load change inboard. Correspondingly, when tip lift is downward, as on the advancing side of the rotor disc for a twisted blade, the down lift produces a nose up moment, thus again unloading the tip. Moreover, tip sweep provides local Mach number relief for an advancing blade, thus reducing tip drag. Because the blade is bent downward due to negative lift, drag reduction produces an incremental nose up moment. These latter two tip loading effects combine to reduce a nose down blade torsional moment on the advancing blade as, in fact, the test data shows in Figures 66 and 67 for the swept tip blade. Now, when taper was combined with sweep in the baseline tip, the product of tip area and the offset of the centroid of that area from the blade quarter chord was maintained essentially the same for both this tip and the swept tip. That is, the stabilizing twisting effect of tip lift was designed to be similar for these two tips. Therefore, if sweep and taper are combined in a tip, as was done for the baseline tip, then it is certainly reasonable to expect that the above noted benefits could complement each other, producing a still larger nose down moment reduction than was realized from each component reduction.

The test data does support this hypothesis by showing that the lowest nose down torsional moment at $\psi = 140^{\circ}$ does occur for the baseline blade, and that this benefit is Mach number dependent for all three advanced tip configurations. It is noted that rotor horsepower reductions given in Table IV vary in a similar manner as the nose down moment is reduced at $\psi = 140^{\circ}$. The swept taper tip produced the greatest horsepower reductions at the high advance ratio relative to the rectangular tip while the swept and trapezoidal tips produced similar magnitude lower reductions. There is, however, one area where the test data show an inconsistent trend: the lower tip Mach number condition shows the greatest reduction in blade nose down moment for the swept tapered tip which should occur at the higher tip Mach number condition. Rotor trim moment differences or data interpolation inaccuracies might account for this inconsistency.

DISCUSSION OF ANALYTICAL PREDICTIONS

Assessment of Theoretical Performance Correlation

Theoretical rotor power predictions using variable inflow are compared with test values Figures 70 through 73. Each figure presents rotor C_Q/σ for a range of advance ratios and a constant sea level standard gross weight and rotational tip Mach number. The four presented flight conditions represent 8200 lb (3719.5 kg) gross weight at .60 hover tip Mach number, 10,300 lb (4672 kg) gross weight at .60 hover tip Mach number, 8200 lb at .65 hover tip Mach number, and 10,300 lb at .65 hover tip Mach number. At each gross weight and rotational tip mach number, experimental data is presented from three sources. These are full scale model, flight, and 1/5 scale model tests.

Superimposed on the same plots are predicted performance with full scale and model scale airfoil data. Because the two gross weight conditions present markedly different correlation trends, the correlation will be discussed separately at 8200 lb (3719.5 Kg) and 10,300 lb (4672 Kg) gross weight. Also, the full scale correlation will be discussed separately from the model scale results due to different confidence levels in the applied airfoil coefficient data. Full scale analytical results will be examined relative to the full scale model results rather than the flight data. This reflects the belief that the full scale model data represents a higher degree of test condition control. At 8200 lb (3719.5 Kg) gross weight, full scale predicted performance is considered good to excellent at both .60 and .65 rotational tip Mach numbers. This is illustrated by the fact that the predicted results are a better indicator of full scale flight performance than the full scale model test at the .60 rotational tip Mach number condition. At the higher rotational tip Mach number, the analytic prediction is equally accurate relative to the full scale model, but the full scale model is a better predictor of flight results.

At the higher gross weight of 10,300 lb, the analysis predicts optimistic performance irrespective of the hover tip Mach number. The only exception is the good prediction accuracy obtained at an advance ratio of .25. In all other speed regimes, the full scale test power requirements are under predicted, with the most optimism occurring at the highest advance ratio of 0.4. It is also noted that the under estimation of required power becomes less accurate for the lower rotational tip Mach number condition.

Deterioration of the prediction accuracy at the high load condition is not unexpected and is due to approximations applied to the static airfoil data to account for skewed flow in the existing theoretical model. When the airfoil lift requirements are moderate and the static airfoil lift coefficients adequately represent the rotor load distribution, the current Y201 aerodynamic model is sufficient for power prediction. At high retreating side lift conditions, however, the approximate skewed flow lift model and the lack of unsteady aerodynamics compromise performance predictions. As retreating side angles of attack in Y201 progressively enter the stall regime, the approximate skewed flow lift stall model initially causes optimistic power prediction. At deeper stall conditions, the lack of unsteady lift enhancement predominates and rotor power is largely over predicted. Figure 74 illustrates the skewed flow model stall mechanism that causes optimistic power predictions. The skewed C_L-α curve is constructed by connecting a linear extrapolation of the zero skew lift line to a new curve formed by dividing the zero skew curve by the cosine of the sweep angle. As indicated in the figure, this procedure eliminates the nonlinear region prior to $C_{L_{MAX}}$ and substantially elevates airfoil L/D in the shaded region. When the calculated blade side angle of attack enter the shaded region, the rise in airfoil L/D causes the optimistic performance predictions noted at 10,200 lb (4672 kg) gross weight. This behavior was confirmed by recalculating the 10,200 lb, M_T .60 performance at two advance ratios with the Generalized Rotor Performance Program (GRP), a non-elastic blade rotor analysis. This program has aerodynamics which are similar to those of Y201, except that a more conservative skewed flow stall model is used. In this case, the optimism in the rotor power prediction was reduced to approximately 3%. The GRP calculated performance points are noted in Figure 71. It is anticipated that, had the more conservative model been used in Y201, the good correlation demonstrated at 8200 lb (3719.5 kg) gross weight would have also extended to the higher gross weight.

Although not strongly indicated by the presented correlation, increasing the calculated retreating blade angles of attack beyond the shaded region in Figure 74, will result in premature rotor stall and a sharp rise in predicted power. Both the stall onset and the accompanying power increase occur prematurely in the analysis due to the lack of unsteady aerodynamic lift extension. The beginning of this behavior can be noted in the predicted power curve slope between an advance ratio of 0.38 and 0.40 for the 10,000 lb (4672 kg), .60 rotational tip Mach number case. (See Figure 71.)

The skewed flow stall model used in the Y201 elastic blade analysis was an early attempt to approximate the effects of skew flow on steady 2-D airfoil data. At the time it was initiated, no better modeling was available. The more accurate conservative analysis was later developed for the rigid blade, performance programs to meet the requirement of predicting rotor performance. Because both an oblique and unsteady flow representation of the airfoil data is believed to be required to more accurately predict elastic blade dynamic loads, Sikorsky Aircraft and UTRC are presently developing such a representation. The updating of the Y201 program awaits the results of that analysis development.

Torque prediction for the 1/5th scale model at the 8200 lb (3719.5 kg) condition is as good or better than that achieved for the full scale rotor at both rotational tip Mach numbers. However, since the full scale rotor analysis consistently underpredicts the full scale model tests results for the same conditions, the predicted effect of Reynolds number on the rotor torque is generally too large. The most likely cause of this discrepancy is the accuracy of the model scale airfoil data at high lift. Due to the lack of a suitable balance apparatus, the model scale airfoil drag data was measured in the NASA Langley Research Center 6 x 28 inch (15.3 x 68.5 cm) transonic wind tunnel with a wake rake. At high lift coefficients, which induce flow separation, and tunnel speeds above the critical Mach number, which gives rise to wave drag, the wake rake is not an accurate indicator of airfoil drag. Also, the measured maximum lift coefficient in the test were affected by severe wall interference. This tunnel operational problem was noted by NASA prior to the test. It is noted that the predicted Reynolds number effect is substantially more accurate at the lower advance ratios where the airfoil flow patterns are less severe.

At the higher 10,300 lb (4672 kg) gross weight conditions, the 1/5th scale model torque prediction is also more accurate than the full scale prediction. The error in the model torque prediction, however, is pessimistic as opposed to the optimistic trend noted for the full scale rotor cases. This behavior probably results from either the previously discussed accuracy limits on the model airfoil drag data, the lowered maximum lift coefficients of the model airfoil data, or a combination of the two. As indicated in the prior discussion of the Y201 lift representation in the stall regime, the lack of unsteady aerodynamics causes a pessimistic torque trend when the skewed static maximum lift coefficient is approached. For the 1/5th scale model rotor, this lift limit will be reached at lower load and advance ratio conditions.

In summary, the Y201 elastic blade analysis generally predicts optimistic full scale performance in the rotor C_L/σ range above 0.08. The GRP rigid blade rotor performance analysis predicts well full scale performance. The difference is principally due to the skewed flow models used in each program. The Y201 analysis using 1/5 scale model airfoil data predicts pessimistic performance. This indicates that if full scale performance is derived from 1/5 scale model results using corrections based on the differences in available airfoil at the appropriate Reynolds number, the resulting performance will be optimistic. This means that Reynolds number corrections derived from the available airfoil data are too large.

Alternate Tips

Figures 51 through 54 present comparisons, of predicted performance and full scale model measured performance for 20 alternate tip test conditions. Each of the four figures presents test and analytical results for fixed gross weights, advance ratio, rotational tip Mach number, and propulsive force. Baseline rotor test and calculated performance is also included as a reference. For each figure, test and calculated torques are presented at the propulsive force required to sustain level flight on the flight vehicle. It should be noted that test results are not available for the three alternate tips at the highest gross weight presented at the .375 advance ratio and .6 rotational tip Mach number condition examined in Figure 52. Analytical results, however, are presented for this high C_L/σ condition to highlight analytical trends.

In general, absolute performance prediction accuracy for the three alternate tips is similar to the previously discussed trends for the swept tapered tips. For most low gross weight conditions, prediction accuracy is fair to good. At the high gross weight the performance correlation also holds up quite well except for the .375 advance ratio condition at .60 rotational Mach number.

For this case, the baseline rotor torque is under predicted. Although equivalent experimenal data is not available on the alternate tips, it is anticipated that a similar underprediction of rotor torque would occur.

The ability to predict the differential torque requirement between various tip designs is as important, or more important, than accurate prediction of absolute torque. If differential torque trends can be accurately predicted, then the analysis can be used in the future to choose a specific design configuration over another with a degree of confidence. At the low advance ratio condition, no consistent trend with test data emerges in the accuracy of the predicted torque differential. The differentials are smaller for this conditions. However, for the other advance ratio and rotational tip Mach number conditions, the predicted torque differential trends among the tips compare favorably with the test data. The only exception at the high speed conditions is for $\mu = .375$ and $M_T = .68$. Here, the swept tip is predicted to be superior to the trapezoidal tip, while the test data indicates the opposite.

Assessment of Theoretical Blade Vibratory Moment Correlation

Baseline Rotor

Rotor vibratory moments were computed with the Y201 analysis using both constant inflow and variable inflow assumptions. The results are presented in Figures 19 and 20 as a function of blade span (at a $\mu = .338$) and in Figures 25 through 30 as a function of advance ratio (at selected spanwise stations). Contrary to expectations, it was found that the vibratory moments were predicted most accurately when the constant inflow assumption was employed.

In Figures 19 and 20, the important outboard peak flatwise bending moment from flight test was predicted using constant inflow to within 5% although it is predicted to occur more inboard at 58% span. Between this peak and the 30% span station, the constant inflow analysis overpredicts the test data while further inboard and outboard of the 60% span the test data is underpredicted. The predicted maximum ½ p-p edgewise moment occurs about 20% span more outboard than the test data maximum, which is near the 10% span station. The peak test value is also underpredicted by 12.5%. Further outboard on the blade, the difference between the test and predicted moments increases.

The analysis was also run in the coupled Y201/variable inflow (F389 SR) mode, assuming a skewed helical wake. See Appendix G for a more detailed discussion of this analysis. The calculated ½ p-p moments versus with blade span are very similar to those calculated assuming constant inflow. However, using this variable inflow analysis, the blade ½ p-p moments are significantly underpredicted for the ATRS with its swept tip configuration. This underprediction was typical for the entire cruise envelope.

Figures 25 through 30 show the trends with advance ratio. Blade vibratory root moments expressed in terms of blade pushrod load and flatwise bending at the 70% span (NB-7) are presented for the two values of gross weight and blade rotational Mach number being analyzed. Typically, the analysis using constant inflow underpredicts the test data by 20-30%, but generally predicts the rate of increase in pushrod load and NB-7 moment as speed increases above the speed for minimum power.

Predictions of the blade vibratory loading using variable inflow and the classical wake are shown to be more optimistic in Figures 25 through 30 than when using constant inflow. The analysis is only predicting about 50% of the flight test blade ½ p-p moments. Furthermore, the analysis gives a lower moment sensitivity to increasing speed than the test data unlike that which was predicted using constant inflow. Also included in this correlation study were four high speed dive conditions. The flight and rotor force trim conditions are given in the table below:

TABLE V

ROTOR FORCE TRIM FOR HIGH SPEED DIVE CONDITIONS

Condition No.	μ	M_T	Dive Angle	Load Factor	% Normal Rotor RPM	C_L/σ	$-C_D/\sigma$
1	.488	.593	-6.9	1.07	99.6	.0817	.00335
2	.468	.647	-10.4	.98	107.6	.0658	.00056
3	.463	.603	-5.79	.99	100.2	.0973	.00202
4	.449	.638	-7.75	1.04	106.1	.0872	-.00061

The first two conditions were flown at a gross weight of 8200 lb (3719.5 kg) with true airspeed of about 194 and 210 knots, respectively. The second two conditions were flown at 10,300 lb (4672 kg) and 185 and 190 knots, respectively.

A comparison of the predicted main rotor torque and blade ½ p-p loads using the variable inflow analysis is given in Table VI.

TABLE VI

HIGH SPEED DIVE CORRELATION RESULTS

	Flight Test Data			Predicted Data		
Condition No.	C_{PRL}/σ	C_{NB-7}/σ	C_Q/σ	C_{PRL}/σ	C_{NB-7}/σ	C_Q/σ
1	4.37	2.23	9.09	3.2	1.34	7.61
2	4.64	2.27	6.24	4.7	1.82	6.78
3	6.75	2.72	9.04	5.0	1.68	8.84
4	4.77	2.22	7.66	4.4	1.52	4.98
	$(X10^{-3})$	$(X10^{-4})$	$(X10^{-3})$	$(X10^{-3})$	$(X10^{-4})$	$(X10^{-3})$

At these high forward speeds the variable inflow analyses generally underpredicts the rotor performance and blade vibratory moments test data, but the degree of underprediction is less than for the lower flight speed conditions.

Part of this underprediction of the blade loads can be attributed to assuming isolated, rotor operation (i.e. no fuselage flow perturbations) which would normally be done in the design process. It will be shown below that the flight test data does include at least a 20% increase in the blade vibratory loads due to fuselage flow. However, this is only part of the reason for the difference between test and analysis.

A comparison of the calculated and the full scale model blade bending moment variations around the azimuth provides some insight to one probable reason for the low peak loading predictions. These comparisons are shown in Figures 46 through 50 and they are for flight conditions which cover the higher speed portion of today's cruise speed flight envelope. A review of these figures shows that the wave forms, especially for the lower harmonics, are reasonably in phase with the full scale model rotor data, which have a lesser influence of fuselage flow distortions. This phase agreement is also true for the edgewise moment time history shown in Figure 47. What appears to be missing from the variable inflow analysis is sufficient moment amplitude for the first three or four harmonics.

With the assumption of constant inflow, (Figures 42 and 46) the analyses causes a degradation in phase relation, but provides a larger amplitude excitation. Referring to Figure 56, the constant inflow curve shows greater amplitude at azimuth positions of 120^o and 240^o, resulting in the greater predicted ½ p-p moment than was predicted by the variable inflow analysis. The phase correlation with test data, however, is not as good as with variable inflow, expecially around 270^o azimuth. The variable inflow results do not exhibit any increase in higher harmonic content but rather a reduction in the one and two per rev components. Figure 42 shows the same comparison for push rod load. The constant inflow curve displays a more negative amplitude around 140^o azimuth, resulting in the higher ½ p-p value. The variable inflow does produce a 4/rev component that is present in the test data, but not reflected in the constant inflow results. Accordingly, this comparison suggests that while constant inflow improves correlation of ½ p-p moment values, the improvement is probably fortuitous in light of the poorer phase relationship that results.

Alternate Tips

The predicted (using variable inflow) effects of tip configuration on push rod load and flatwise bending moment are presented in Figures 55 through 65. The analysis predicts a strong beneficial effect due to the addition of sweep and taper on push rod load. The test results show a similar, though less strong, benefit at the higher Mach number - advance ratio conditions. At the lower Mach number - advance ratio condition, the test data do not show similar consistent benefits. The analysis correctly predicts (qualitatively) the beneficial effect of reduced gross weight.

For the 70% span flatwise vibratory bending moments, Figures 59 through 61 (NB-6 in Figure 62), the analysis again predicts benefits in these moments due to planform taper and sweep for both blade tip Mach number and gross weight values. Tip sweep was predicted to be more beneficial than tip taper, while the test data at the high advance ratio generally confirms that tip taper and sweep reduce NB-7 moments relative to a conventional blade. For the swept tapered tip, the NB-7 moments were predicted to be the lowest and this is confirmed by the test results for all conditions presented. The analysis predicts the benefits of tip sweep and taper are additive at M_T = .65 while at M_T - .6 they are not. At the highest value of M_T = .68 (Figure 62), the analysis not only predicts the test data trends with tip configuration and gross weight, it also predicts the absolute value of NB-6. This is also true for the blade vibratory push rod loads (Figure 58) and rotor torque (Figure 54). This agreement is unique and occurs at the highest rotational tip Mach number studied. The reason for this agreement is not understood at this time.

The measured vibratory edgewise moments for all the conditions presented (Figures 63 through 65) show little effect of the various tip configurations. In contrast, the analysis predicts beneficial effects for adding sweep and taper for M_T = .6 conditions, the analysis is overpredicting the effect of increasing gross weight. These are the conditions of the highest rotor lift coefficients. As predicted by the analysis, tip sweep exhibits a strong influence for reducing vibratory edgewise moments of high rotor lift conditions.

Although the Y201 analysis tends to generally predict the trends in the test data, blade bending moments are generally underpredicted as was discussed previously for the baseline blade. However, it is interesting to note that blade pushrod loads are predicted for the tip configurations without sweep. Furthermore, there is a larger increase in the predicted blade moments with gross weight than is demonstrated by the test data for the .6 tip Mach number condition. For the high gross weight, the rotor is operating at C_L/σ = .094, which is considered high. Also note that this predicted jump is diminished as tip sweep is introduced. When the blade tip is not swept, the analysis allows the tip to carry more load at local angles of attack in the neighborhood of stall. With tip sweep the analysis unloads the tip and redistributes the blade lift more inboard thus reducing the blade response. While these predicted tip effects trend correctly, the trend magnitude is not correct. The analysis assumes two-dimensional steady flow in a region that has three-dimensional, unsteady flow, and for skewed flow corrections, mentioned earlier. These assumptions governing the loading in the tip region are clearly subjects for review.

Effect of Fuselage Flow on the Baseline Blade Moments

Sikorsky Aircraft's Wing and Body Aerodynamic Technique (WABAT) computer analysis (Y179) was used to compute the local flow over the flight test vehicle's fuselage and the resulting normal interference velocities at the rotor. See Appendix H for a more detailed description of the analysis. Using these interference velocities as input (listed in Appendix L), the coupled normal modes (Y201)/variable inflow (F389) Elastic Rotor Analysis was employed to calculate the effects of fuselage flow distortions on rotor blade vibratory loads. The conditions analyzed are as follows:

TABLE VII

FLIGHT CONDITIONS FOR CORRELATION STUDY OF FUSELAGE FLOW EFFECTS ON ROTOR BLADE VIBRATORY LOADS

μ	M_T	GW
.388	.60	8200 lb (3719.5 kg)
.4	.60	8200 lb
.375	.60	10,300 lb (4672 kg)
.375	.65	10,300 lb

The effect of the fuselage is summarized in Figures 75 through 82 where the calculated and the full scale test time histories of the blade root torsion and 70% span flatwise bending moments are compared. The top two time histories in each figure are the flight and full scale test data results with the steady values of the time history adjusted (to be nearly equal) so that the harmonic portion of the load variations can be compared more directly. The flight test time history includes the effect of the fuselage flow, while the full scale time history includes the lesser flow distortions from the NASA/Ames RTA. (See Figure 4) The bottom two time histories are calculated, one for the rotor alone and one including inflow distortions due to the fuselage.

In order to obtain an indication of difference in inflow velocities due to the two near bodies, the rotor inflow velocities induced by the RTA were estimated using the WABAT analysis as were the velocities induced by the flight vehicle's fuselage. These calculations are compared in Figure 83 in terms of local angle-of-attack change at the rotor blade, induced by the fuselage flow. The two near bodies are located at their respective test heights below and incidence attitudes to the rotor. As the figure shows, the RTA induces a lesser angle-of-attack distortion than the flight vehicle over entire rotor in the longitudinal plane of symmetry. Because the flight vehicle has a wider body than the RTA, the RTA's flow influence also diminishes more rapidly than the flight vehicle's at all other positions in the plane of the rotor. Therefore, the difference between the two test time histories should be an indication of the influence of the flight vehicle's fuselage flow distortion at the rotor.

For each of the four conditions investigated, the significant differences between the rotor alone and the rotor plus fuselage curves, as indicated by the arrows, for both the test and calculated results, generally occur at about the same azimuth positions. This is particularly true for flatwise bending moments, high or low gross weight. For the calculated root torsion results, most significant differences occur as the blade has just passed over the nose of the aircraft where the upflow is expected to be the strongest. These excitations continue on over the retreating portion of the disc and are small on the advancing side of the disc. The test data tends to demonstrate similar differences but also indicates higher excitations over the tail cone.

The calculated and test differences for flatwise bending are very similar on the retreating side of the rotor disc. However, on the advancing side of the disc the test data shows more excitation and the higher 3 per rev resultant bending moment amplitude between flight test and the full scale model that was previously discussed.

The similarity of the azimuth location and direction of moment of the differences between the test and calculated time histories, especially on the retreating side of the rotor disc, suggests that the fuselage flow is a significant contributor. According to the test data, the effect of the fuselage flow is to increase ½ p-p pushrod loads and blade flatwise bending moments by about 20%. However, if the ATRS could have been tested completely free of nearbody flow effects and the results compared to flight test data, blade vibratory loads increases may have been found to be greater than 20%. The predicted increases in ½ p-p loads range from 14 to 44%.

Some Considerations for Analysis Improvement

The above correlation studies have revealed areas of agreement and disagreement between the test data and the Y201 variable inflow analysis, using a skewed helical wake. Improving loads correlation should be particularly emphasized. In this context, four aerodynamic areas where the mathematical modeling of the Y201 rotor blade response analysis and of industry's analysis in general require improvements have been cited above. Note that they are all items that more accurately characterize the blade and the actual environment in which it must operate. The areas are:

- Skewed flow aerodynamics
- Unsteady stall aerodynamics
- Three dimensional, swept tip aerodynamics
- Rotor inflow velocities and wake structure

A possible fifth mathematical moeling area that may require refinement and that pertains principally to Y201 is that of blade structural modeling. Y201 utilized a modal approach, with a limited number of modes and retains only first order twist coupling terms. In the past this modeling has been acceptable, but it is possible that with the recent trend to higher twist rotor blades, that improvements in this area are required.

Unfortunately, the influence that each of the above items has on blade response is highly interrelated with each of the other items so that it is difficult to identify the exact cause of each correlation difficiency. It is believed, however, that the aerodynamic aspect of the problem is more critical. Further, it is also believed that the inflow and tip aerodynamics modeling are the most critical of the aerodynamic areas for improving the loads correlation at flight conditions studied in this report.

The reasons for these beliefs are:

a) Inadequacies in the structural math modeling tend to affect the torsional response most and for the most part the torsional response is well predicted with the current program.

b) The lack of correlation exists at conditions for which significant blade stall is not present. Thus, unsteady and skewed flow effects should be relatively small. Of course, such effects would become important when stall occurs and work in this area is required from that standpoint.

c) The outboard blade loading is a powerful driver of loads - e.g. the differences between constant and variable inflow loadings tend to be concentrated near the tip.

Further discussion of these critical areas, together with some thoughts on how to approach each, follows.

Three-Dimensional Swept Tip Aerodynamics

Owing to the high dynamic pressures at a rotor tip, the tip region is a powerful contributor to blade response. The present tip aerodynamic model in Y201 is based on a simple two-dimensional sweep theory. The geometric tip sweep is assumed to define the aerodynamic sweep of the tip. The Y201 program thus employs this assumption together with the calculation of the local flow velocity vectors normal to and along the local swept axis of the blade. This approach is based on the classical approach to rotary wing aerodynamics. The validity of simple sweep assumption applied to the tip region of the rotor blade is an area that clearly needs further study. Simple sweep theory is most valid on high aspect ratio yawed wing. Where a wing is truncated (e.g., at the tip) three dimensional departures obviously come into play. A large body of fixed wing lifting surface calculations has confirmed these phenomena. See Reference 5 for example. Consequently, because the tip region is critical to the simulation of accurate blade responses, a dedicated study of the adequacy of two-dimensional sweep theory is justified. This should include experimental work as well as application of the three-dimensional lifting surface analyses applicable to rotating wings and fixed wings. This study might include a comparison of pressures on elastic fixed wings calculated from lifting surface and simple sweep theory. Motivation for including elasticity is that equations for the relative flow velocity vector indicate that elastic displacements can have a significant effect on the velocity component normal to the tip surface. A change in inflow angle ϕ of 1 to 2 degrees can be induced by flatwise deflections between unswept and swept blade regions. Simple sweep theory will magnify the inflow angle ϕ and pressure changes beyond the correct three dimensional values. Thus the appropriateness of the aerodynamic model becomes even more important for elastic blades than for rigid blades.

To complement the analytic work on tip aerodynamics, pressure and/or laser velocometer measurements (of circulation) to measure tip loading details should be made.

Rotor Inflow Velocities and Wake Structure

Rotor blade loading is intimately related to the flow field induced by the rotor. The calculations made herein have employed the rotary wing equivalent to the classical fixed-wing, finite-span, lifting-line theory. Wake distortions are neglected as are lifting surface effects which are expected to be significant near the tip (as discussed in the preceeding section) and in blade-vortex encounters. While these assumptions would appear reasonable (except in the tip area) for computing lower harmonics of loading at the advance ratios considered in this report, a complete experiment to validate the inflow-airloading analysis has not been conducted.

Laser velocimeter technology is now becoming generally available. It is capable of making the desired measurements. UTRC, for example, has measured wake structure and induced velocities under a rotor using laser velocimetry techniques for the U.S. Army Research Office. This work is reported in Reference 4. It is believed that the measurements should be made using moderate scale (2.84 m. diameter) model rotor systems, like the one used in this study (See Figure 6). This model rotor system is sufficiently large to prevent large Reynold number effects. Moreover a model of this size permits an area over which the velocity measures would be required to be of reasonable size. The model can also be made with nonflexible blades or can be scaled to represent full scale structural properties (and, thus the elastic deflections mentioned above) and operate at full scale Mach numbers. Also, it can be internally instrumented to allow detailed blade elastic deformations to be determined. The blades used in this study or the blades built specifically to study elastic deformations for the U.S. Army Research and Technology Laboratories (Reference 6) are specific blade examples.

CONCLUSIONS

Full Scale Baseline Rotor Test Results

1. Rotor hover performance can be measured to within +0 to -4% in the NASA/Ames 40 ft. (12.2 m) by 80 ft. (24.4 m) wind tunnel using rotors of the size of ATRS or smaller.

2. Helicopter rotor forward flight performance can be predicted for substantially unstalled conditions to within +5% of the flight test measurements up to an advance ratio of .4 using aerodynamically similar, full scale wind tunnel models.

3. The maximum outboard rotor blade ½ p-p dynamic loads are generally predicted to about 80% of the flight test values using data from a dynamically similar, full scale wind tunnel model rotor. Closer agreement would result if the aircraft fuselage were included in the wind tunnel test.

1/5 Scale Baseline Rotor Test Results

1. Due to Reynolds number effects, a 1/5 scale model rotor predicts poorer full scale helicopter forward flight performance throughout the flight envelope. At μ = .375 and a rotational Mach number, M_T = .6, the over-prediction of power amounts to nominally 20%.

2. If model blade dynamic characteristics are scaled faithfully, then model blade ½ p-p dynamic loads will reasonably predict full scale dynamic loads.

3. If model blade dynamic characteristics differ, the analysis can be used to provide corrected results that agree well with flight data.

Alternate Tip Effects From Full Scale Test Results

1. Combining tip aft sweep and tip planform taper is effective in reducing main rotor power over the cruise envelope. Applying each individually also provides for reductions in rotor power, but to a lesser extent.

2. The effect on blade ½ p-p vibratory blade loads of three alternate tips is small at μ = .3. However, as advancing blade tip Mach number ($M_{1, 90}$) approaches .9, blade control loads and flatwise ½ p-p loads are significantly reduced for swept, tapered tip configurations covering spans as small as 5% of the rotor radius.

3. The time history signatures of the blade control and bending loads for the various tips at μ = .375 (150 kts) show that when tip sweep and planform taper are utilized alone, modest reductions in peak loads are achieved as compared to the conventional rectangular tip loads. However, when tip sweep and taper are combined, substantial reductions in the higher harmonic loads are achieved.

Analytic Results

Performance

1. The Y201 elastic blade analysis predicts main rotor level flight performance to within ±5% at 150 kts for blade loadings below .08. At the higher blades loadings investigated by this study (.095) the analysis becomes optimistic. This would be improved by using a more accurate skewed flow model in the analysis.

2. Performance-oriented, rigid blade analyses, on the other hand, predict performance well for all conditions except those involving significant retreating blade stall.

3. The effect of reducing Reynolds number to 1/5 scale model values is over-predicted. This is attributed to the 1/5 scale model airfoil data used, which is compromised by wall effects at high lift, shock effects at high Mach number on wake rake drag measurements. (Note, unsteady effects were not used to make this comparison in either the full scale or the 1/5 scale model analysis.)

4. At and above 150 kts, the Y201 analysis predicts improvement trends in rotor performance due to tip sweep, taper and the combination thereof, which are consistent with full scale test results.

Blade Vibratory Loads

1. A comparison of predicted blade vibratory loads with test data using Sikorsky Aircraft's rotor blade dynamic program, normal modes (Y201) shows that the analysis generally is very optimistic when using variable inflow. The use of constant inflow provides the best correlation, still underpredicting, but exhibiting very similar trends (relative to full scale flight data) in ½ p-p vibratory loading.

2. The analysis predicts that, as compared to a conventional rectangular tip design, blade tip sweep or planform taper tends to reduce blade ½ p-p vibratory loads in cruise flight. The test data generally confirm these trends. The magnitude of the predicted reductions tended to be larger than measured.

3. The calculated effect of the fuselage flow field is to increase the blade vibratory flatwise bending and torsional moments relative to those predicted for an isolated rotor. The predicted changes in loads due to fuselage flow were qualitatively similar to, but larger than those observed when full scale flight and wind tunnel model test data are compared. This was consistent with the presence of some flow distortion effects due to the wind tunnel test module.

RECOMMENDATIONS

1. Conduct further analytic studies to understand, in more detail, the sensitivity of the results presented to the assumptions made in the analysis.

2. Conduct analytic studies to develop a better approximation for modeling the three-dimensional flow effects on blades having swept tips.

3. Conduct unsteady airfoil tests to provide aerodynamic load characteristics in the region of stall as a function of skew angle and Mach number.

4. Conduct a sub-scale and full scale model test to measure the details of the flow, air loading and blade response on a rotor blade having swept tips.

LITERATURE CITED

1. Balch, D.T., S-76 Full Scale Test In NASA/Ames 40 Ft. By 80 Ft. Wind Tunnel - Performance Results, SER-760193, June 1980.

2. Blauch, R.S., Performance Results Of The One Fifth Scale S-76 Wind Tunnel Test - Phase III With Powered Main Rotor, SER-760178, December 16, 1977.

3. Niebanck, C. and Rabbott, Jr., J.P., Experimental Effects of Tip Shape On Rotor Control Loads, Preprint No. 78-61, 34th National Forum of the American Helicopter Society, May 1978.

4. Landgrebe, A.J., Taylor, R.B., Investigation Of The Airflow At Rocket Trajectory And Wind Sensor Locations Of A Model Helicopter Simulating Low Speed Flight, UTRC Report No. R79-912985-5, September 1979 Prepared for U.S. Army Research Office, Contract No. DAAG29-77-C-0013.

5. Albano, E., and Rodden, W.P., Doublet-Lattice Method For Calculating Lift Distributions On Oscillating Surfaces In Subsonic Flows, AIAA Journal, Vol. 7, No. 2, February 1969, pp 279-285.

6. Blackwell, R.H., Mirich, P.H., Murrill, R.J., and Yeager, Jr., W.T., Wind Tunnel Evaluation Of Aeroelastically Conformable Rotors. Preprint No. 80-23, 36th National Forum of the American Helicopter Society, May 1980, Prepared with U.S. Army Research and Technology Laboratories, Contract No., DAAJ02-77-C-0047.

7. Arcidiacono, P.J., Prediction of Rotor Instability at High Forward Speeds, Vol. I, Steady Flight Differential Equations of Motion for A Flexible Helicopter Blade with Chordwise Mass Unbalance, USAAVLABS TR 68-18A, February 1969.

8. Bergquist, R.R., Helicopter Gust Response Including Unsteady Aerodynamic Stall Effects, USAAVLABS TR 72-68, May 1973.

9. Landgrebe, A.J., and Egolf, T.A., Rotorcraft Wake Analysis for the Prediction of Induced Velocities, USAAMRDL TR 75-45, January 1976.

10. Landgrebe, A.J. and Egolf, T.A., Prediction of Helicopter Induced Flow Velocities Using the Rotorcraft Wake Analysis, Proceedings of the 32nd Forum of the American Helicopter Society, May 1976.

11. Landgrebe, A.J., Moffitt, R.C., and Clark, D.R., Aerodynamic Technology for Advanced Rotorcraft, Journal of American Helicopter Society, April and July 1977.

12. Hess, J.L., and Smith, A.M.O., Calculation of Potential Flow About Arbitrary Bodies, Progress in Aoernautical Science, Vol. 8, The Pergamon Press, 1967.

13. Rubbert, P.E., Saaris, G.R., et al, A General Method for Determining the Aerodynamic Characteristics of Fan-in-Wing Configurations, USAAMRDL TR 67-61A, Eustis Directorate, Vol. I, USAAMRDL, Ft. Eustis, Va., December, 1967.

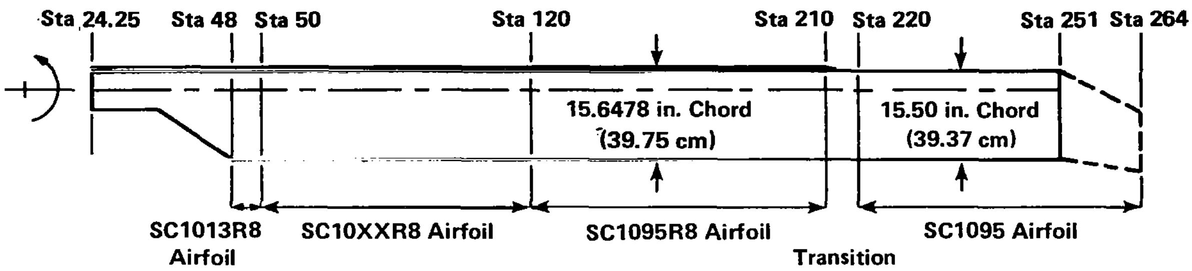

Main rotor blade

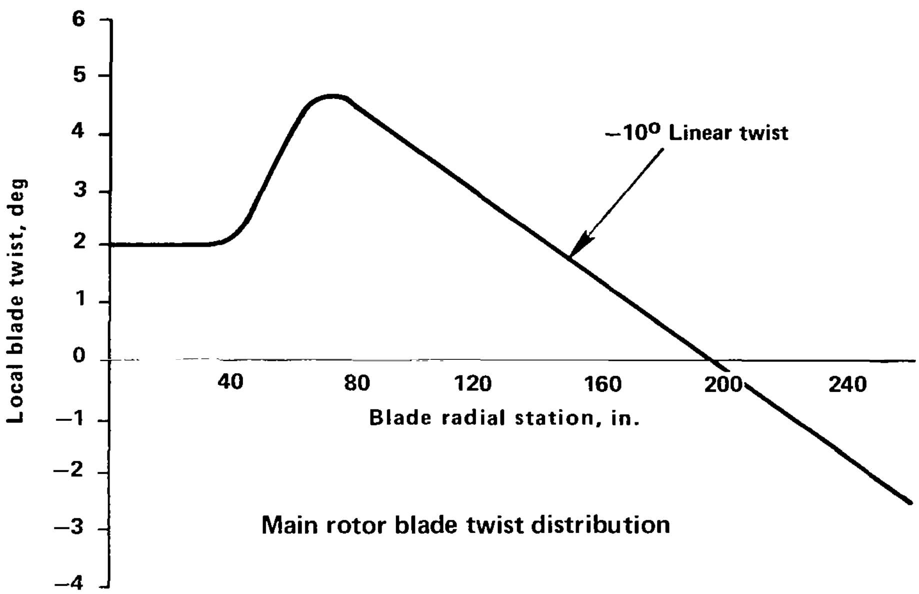

Main rotor blade twist distribution

Main rotor parameters			
Radius	22 ft (6.706 m)	Flapping hinge offset	3.79% radius
Nominal chord	15.5 in. (39.37 cm)	Lock no.	11.6
Solidity ratio	.0748	100% rpm	293
Number of blades	4	100% ΩR	675 fps (205.74 mps)
Airfoils	SC1095 and SC1095R8		

Figure 1 — Geometry details of the advanced technology rotor system main rotor blade.

Figure 2 — Flight test vehicle

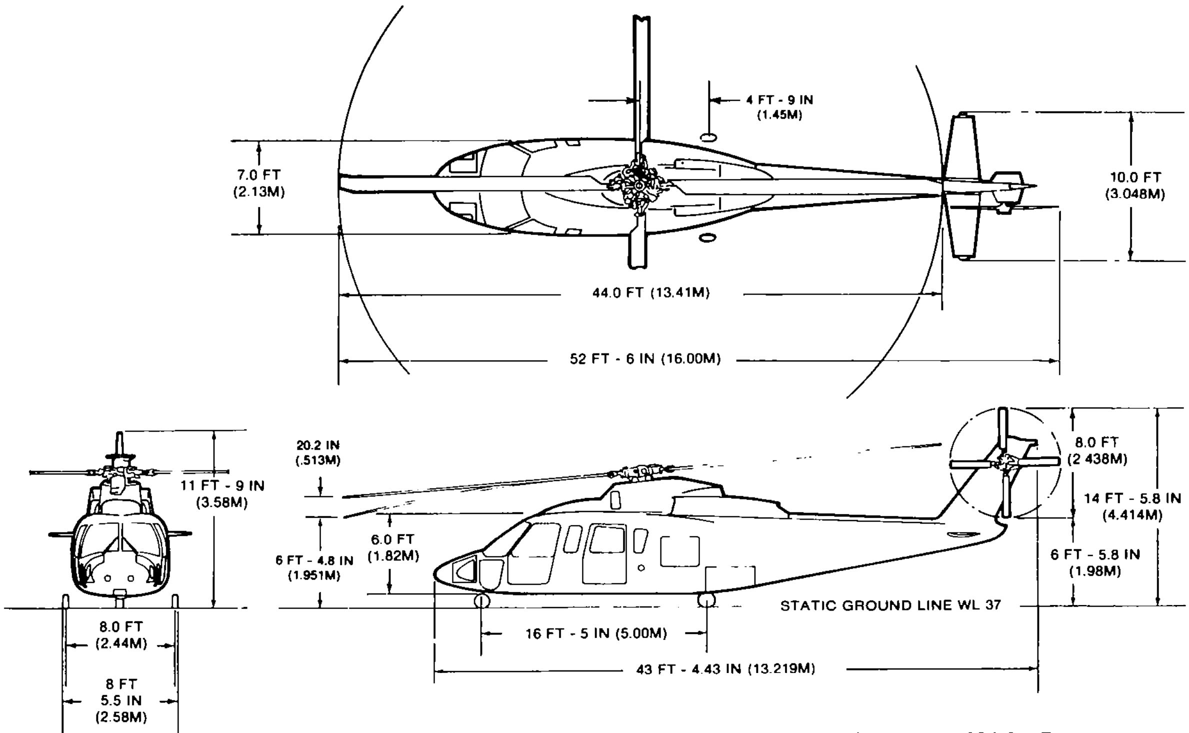

Passenger Cabin Volume	204 Cu. Ft.
Passenger Area	45 Sq. Ft.

Figure 3 — Flight test vehicle for advanced technology rotor system.

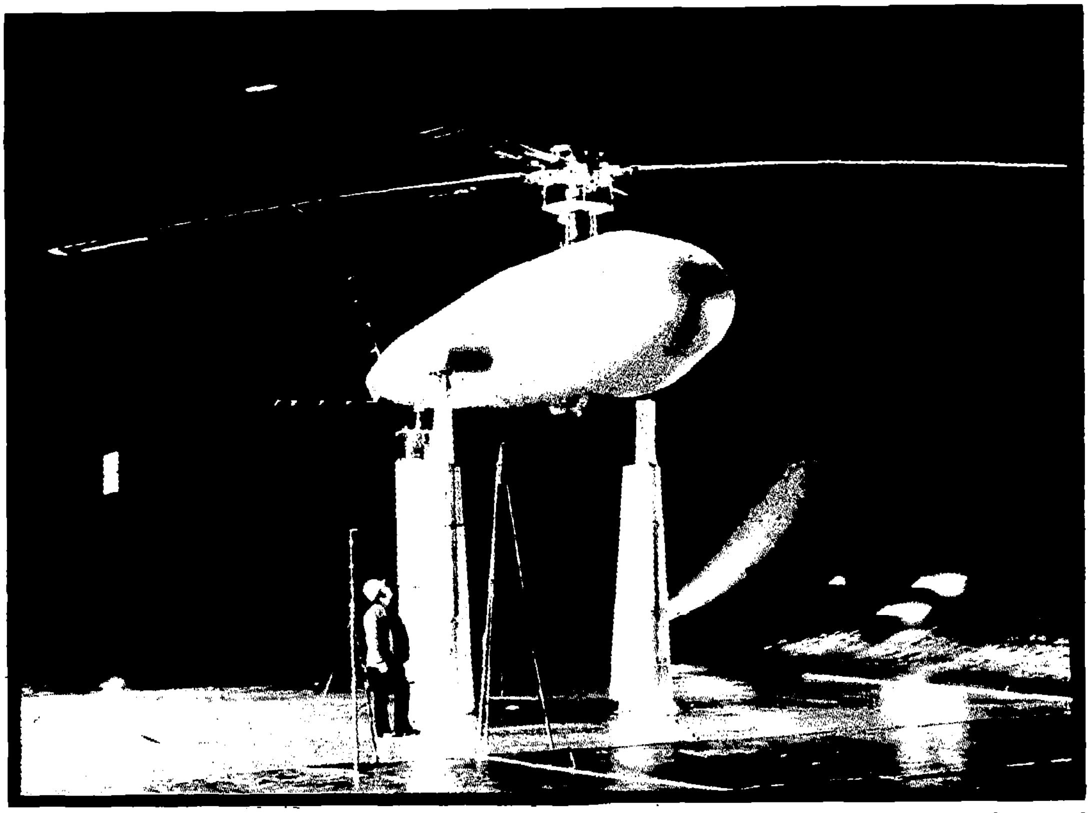

Figure 4 – ATRS full scale model installed in NASA Ames 40 ft x 80 ft wind tunnel.

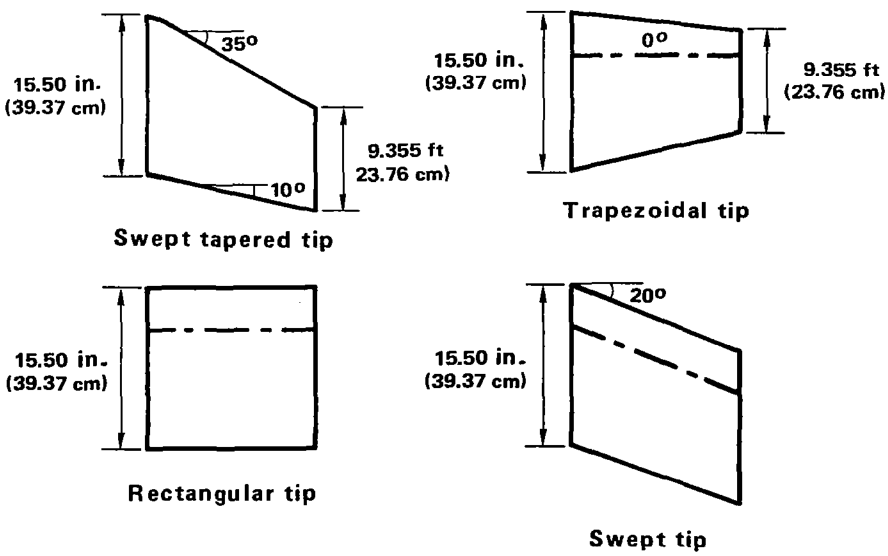

Figure 5 – Advanced technology rotor system swept tapered and alternate tips

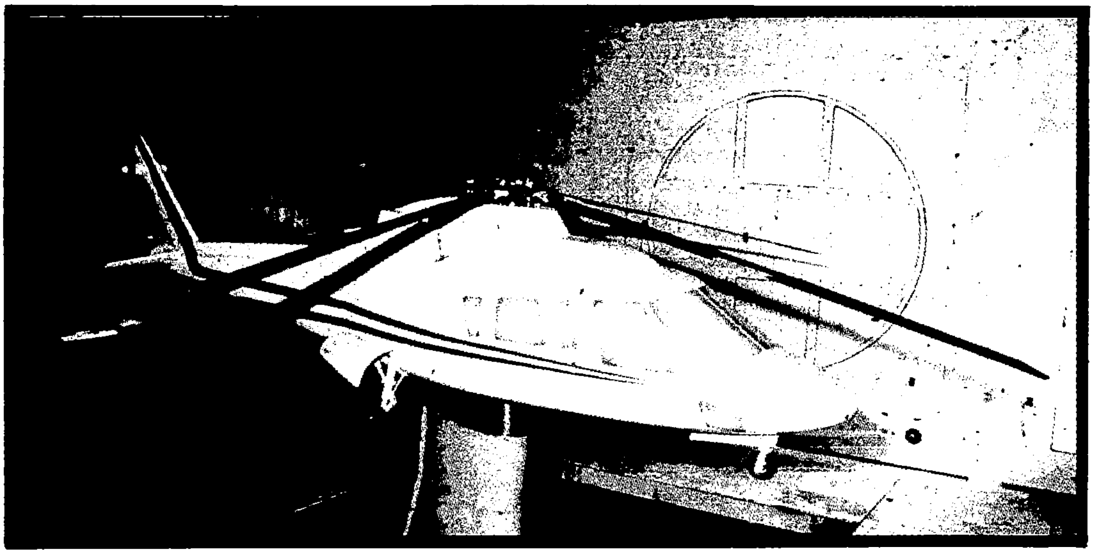

Figure 6 — 1/5 Scale ATRS model installed in the 18 ft section of the UTRC wind tunnel.

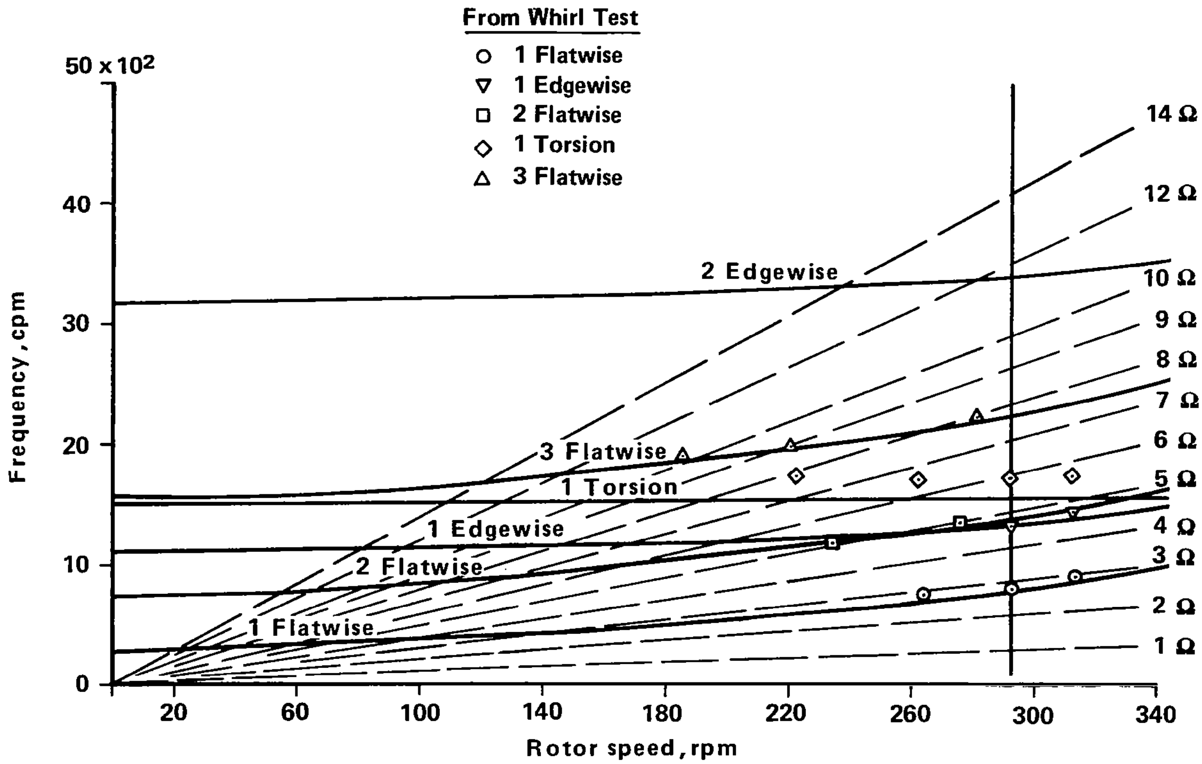

Figure 7 — Sikorsky advanced geometry 44 foot rotor blade bending and torsion frequencies.

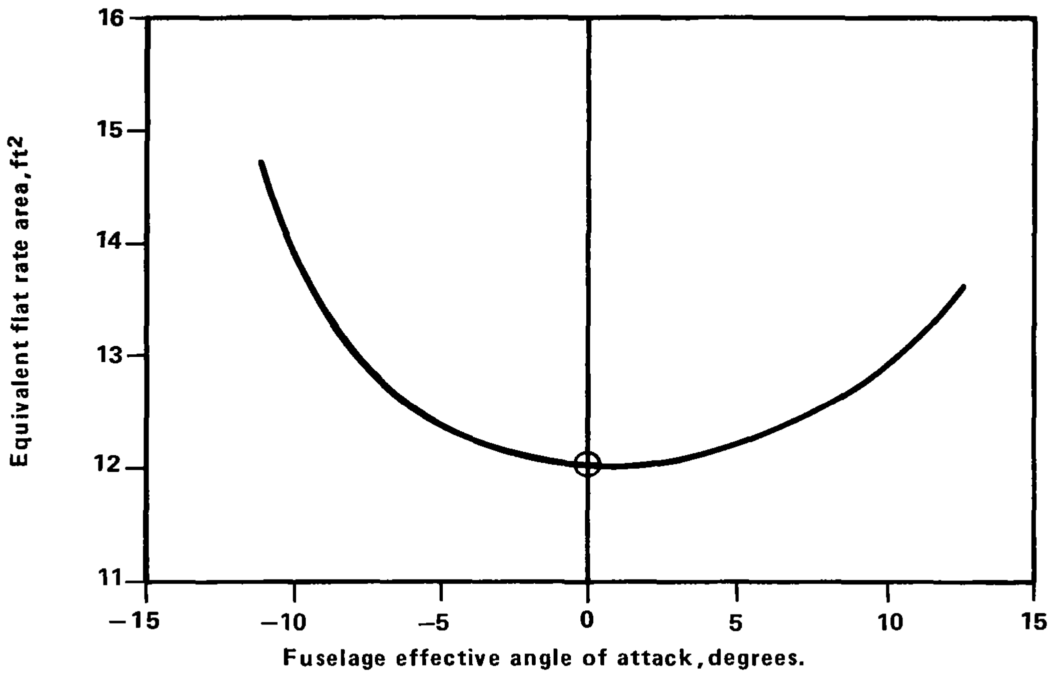

Figure 8 —Flight test vehicle. Total corrected configuration drag.

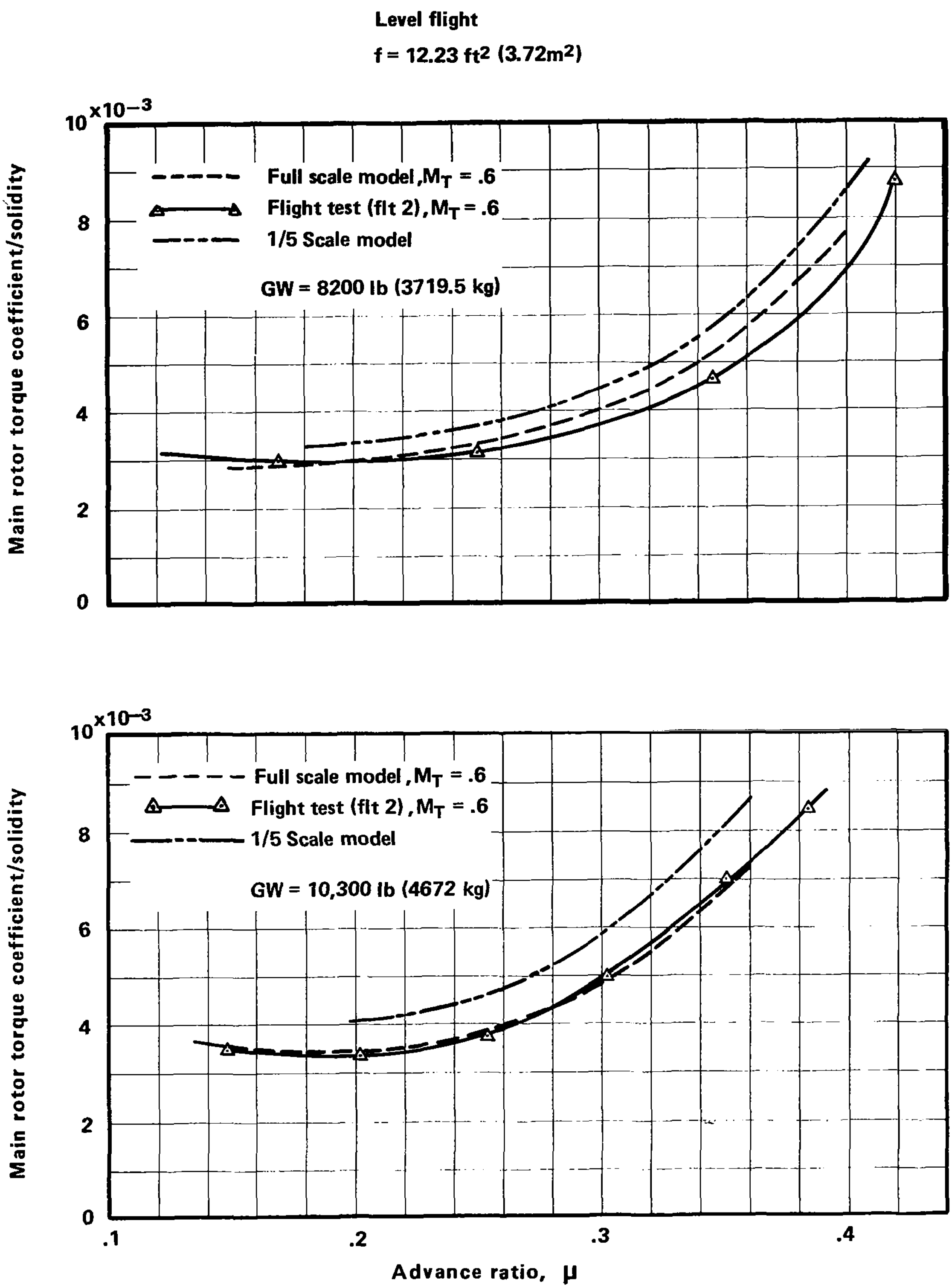

Figure 9, 10 — Main rotor torque coefficient/solidity versus advance ratio. Flight tests compared with model tests.

Level flight
f = 12.23 ft2 (3.72 m2)

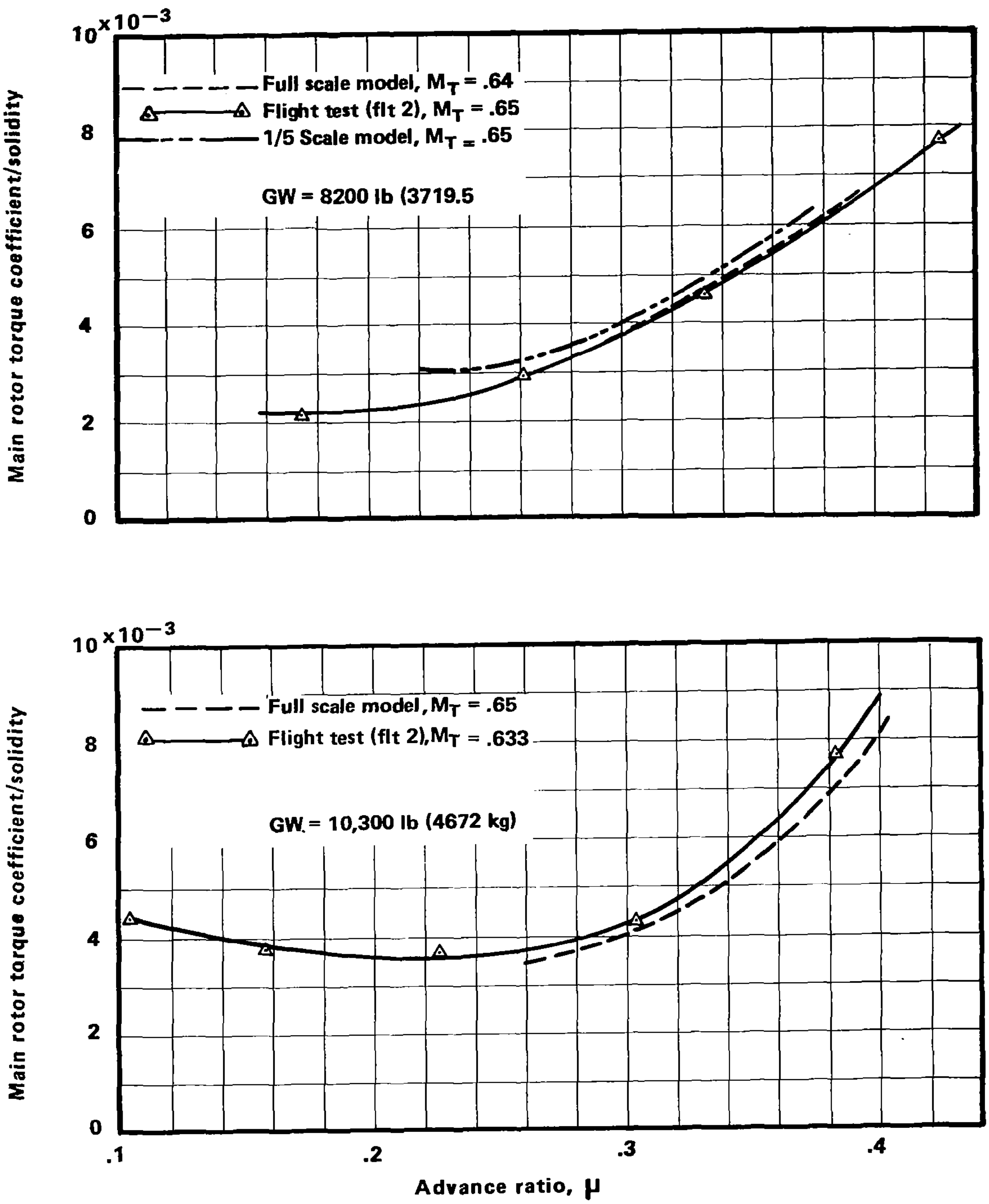

Figures 11, 12 – Main rotor torque coefficient/solidity versus advance ratio. Flight test compared with model tests.

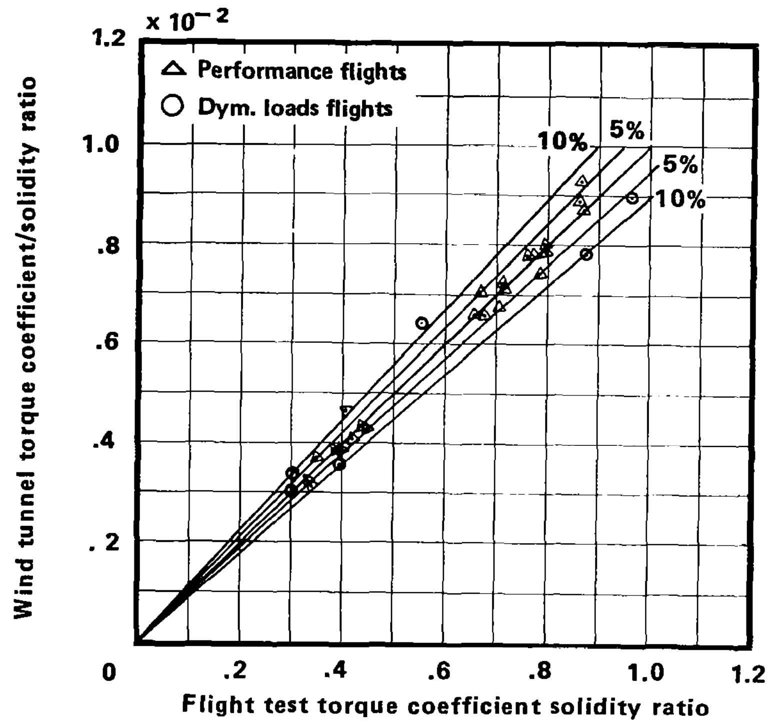

Figure 13 – Comparsion of measured flight and full scale model measured rotor torque coefficient/solidity vlaues.

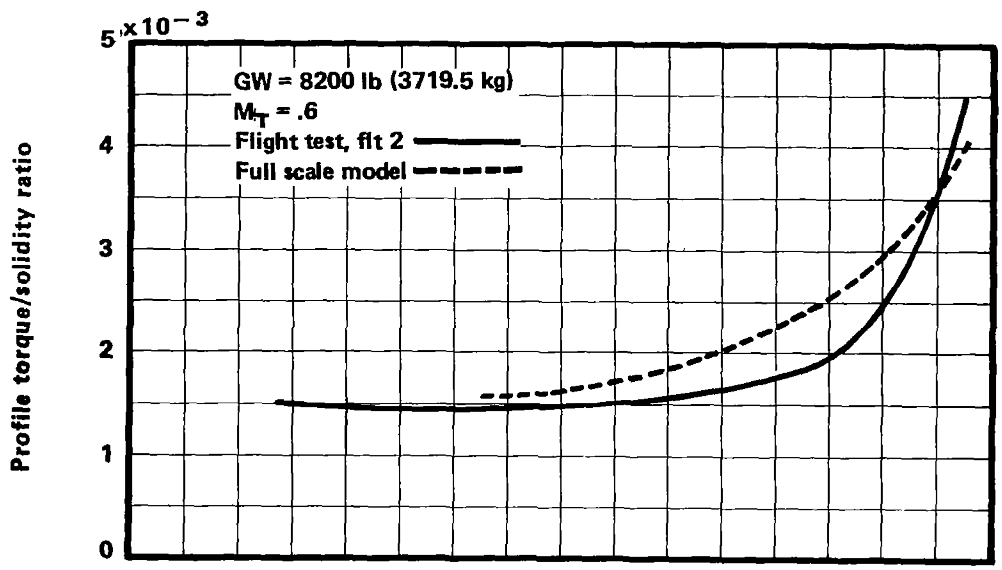

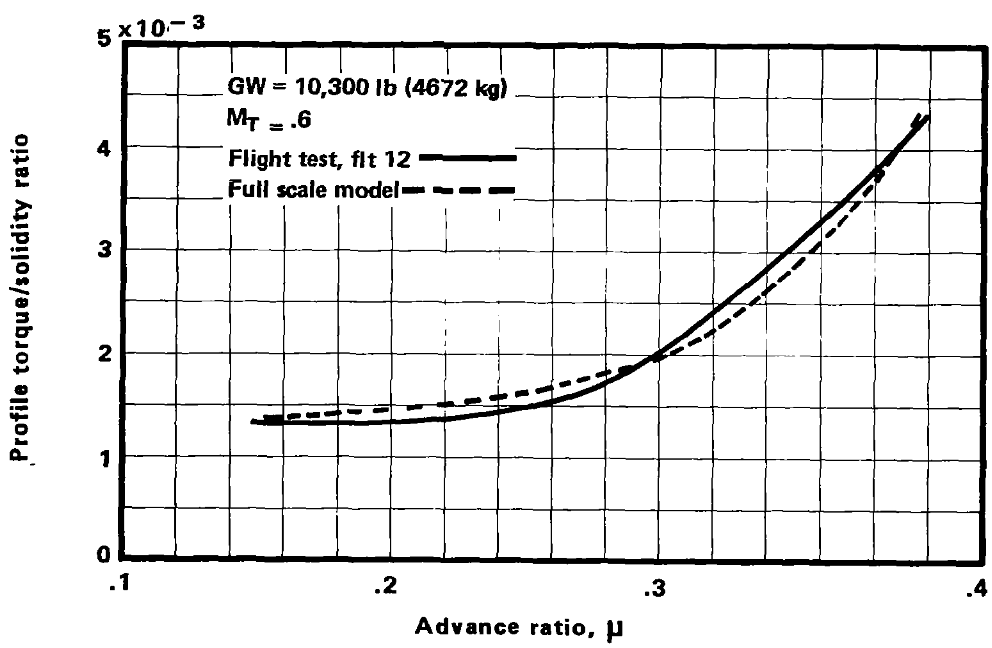

Figures 14, 15 –Main rotor profile torques compared.

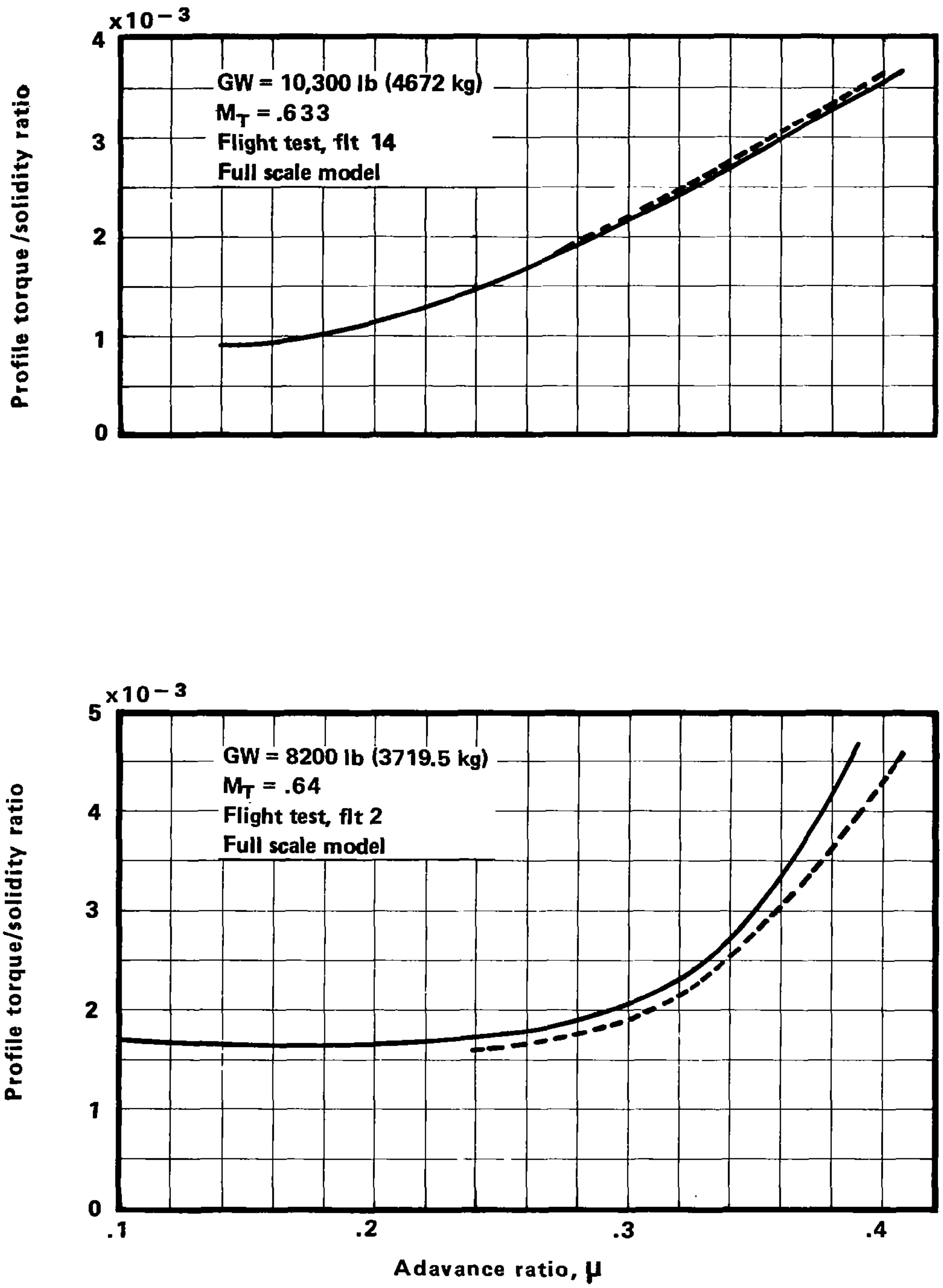

Figure 16,17 —Main rotor profile torques compared.

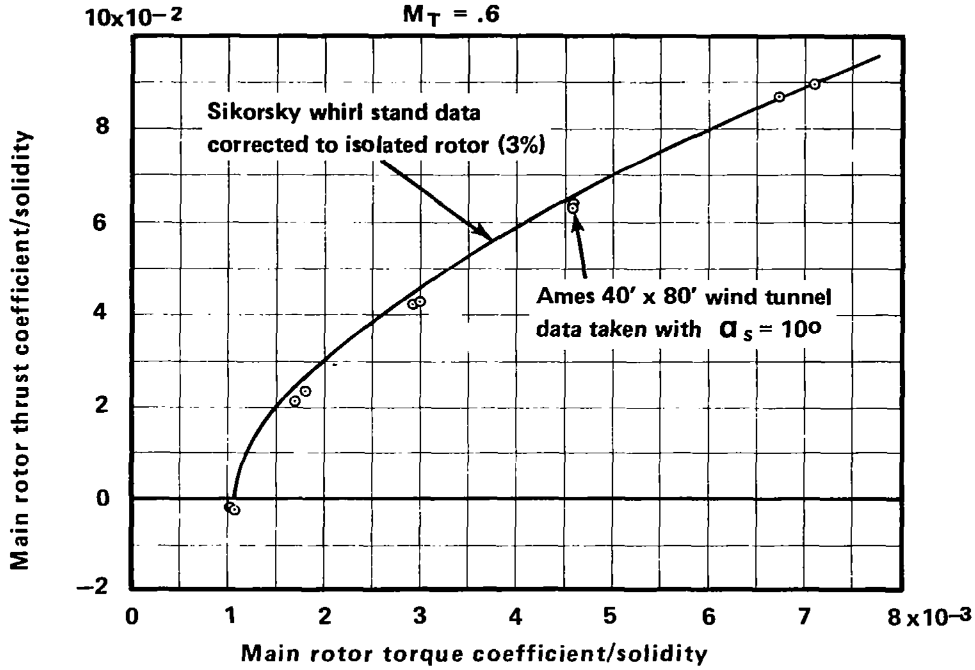

Figure 18 – Advanced technology rotor system hover performance.

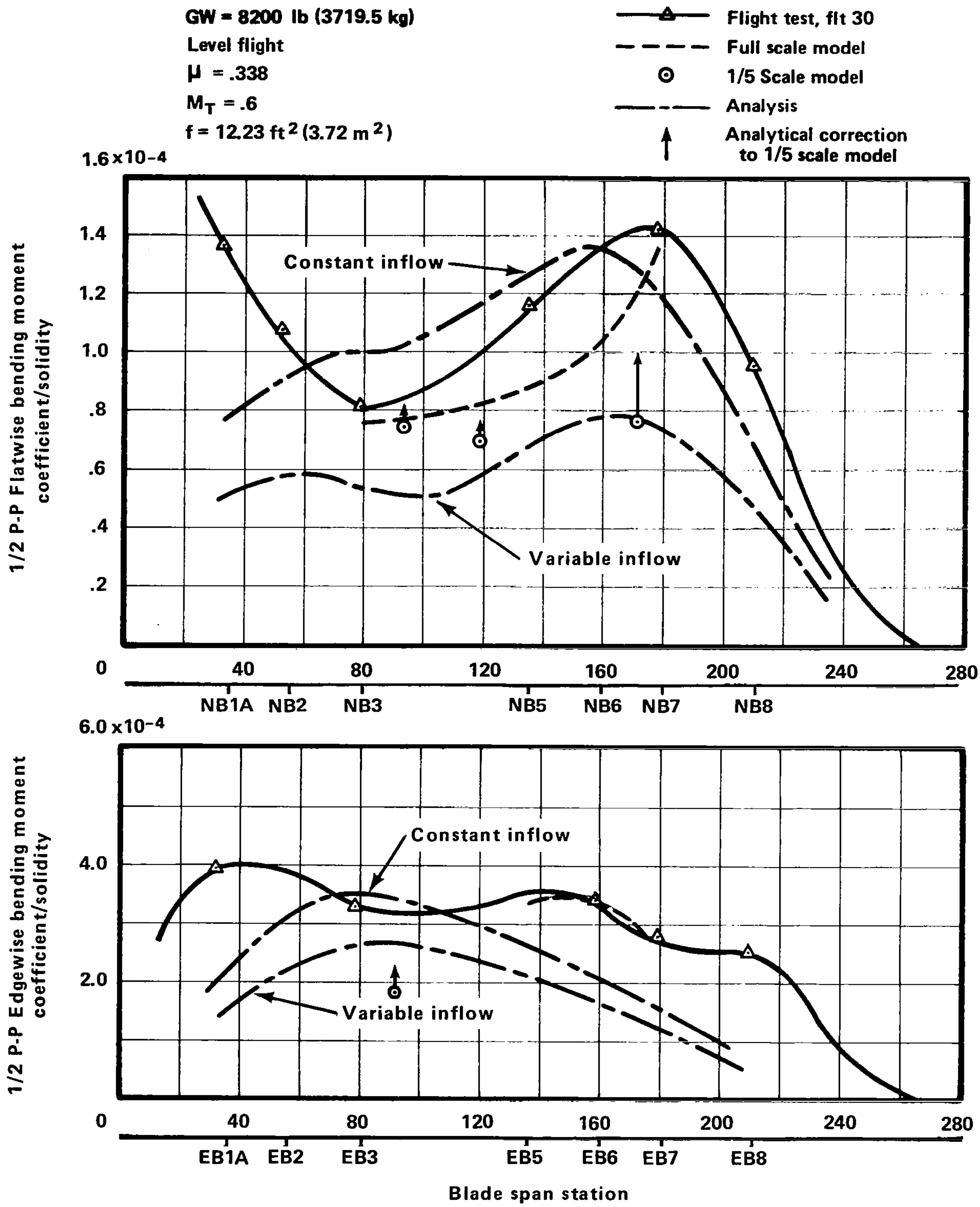

Figures 19, 20 – Main rotor blade vibratory bending moment coefficient/solidity versus blade span. Flight test compared with model tests and analysis.

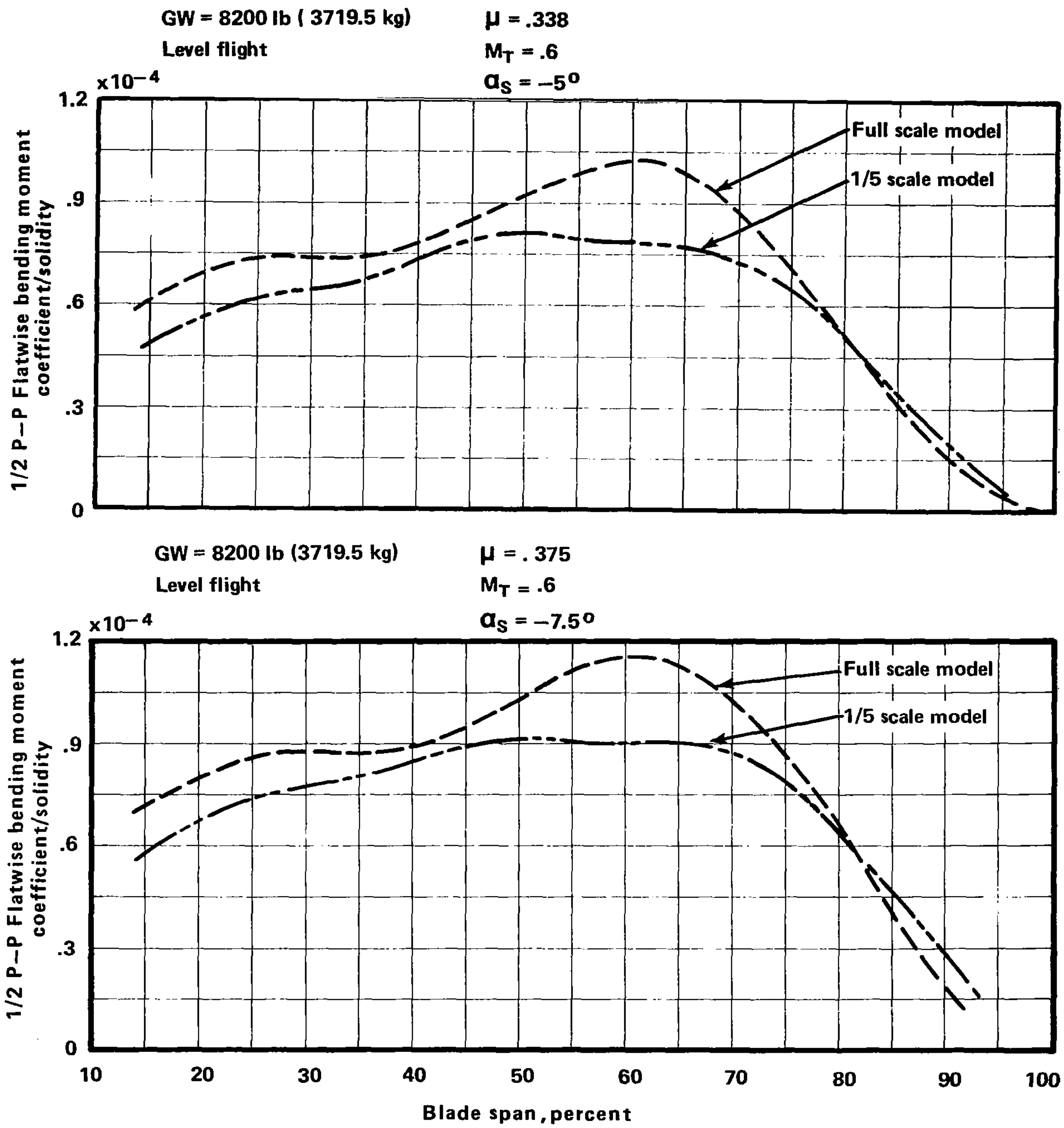

Figures 21, 22 — Calculated 1/2 P—P flatwise bending moment versus blade span. Effect of mass and edgewise stiffness distribution differences between full scale and 1/5 scale model blades.

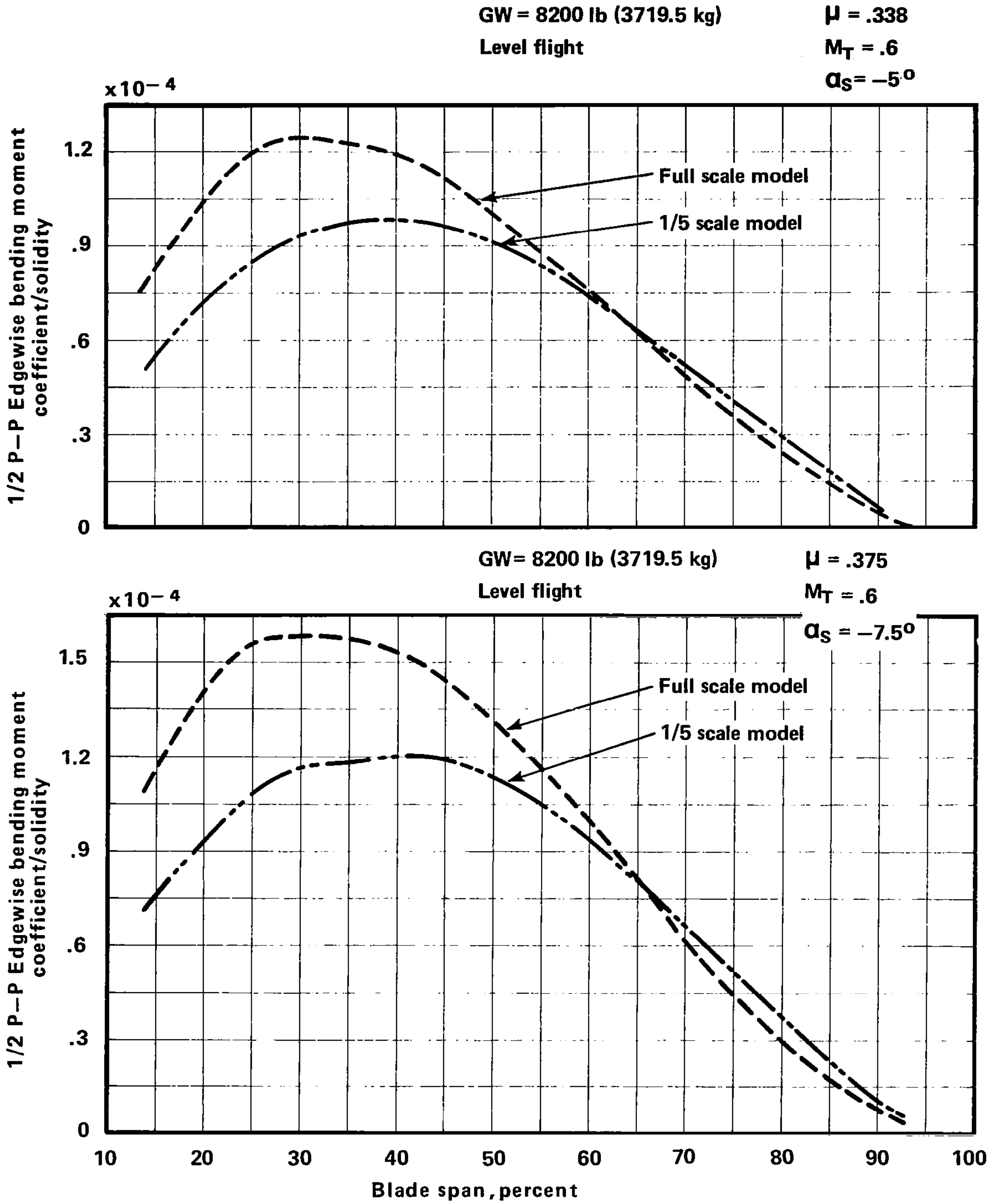

Figures 23, 24 — Calculated 1/2 P—P edgewise bending moment versus blade span. Effect of mass and edgewise stiffness distribution differences between full scale and 1/5 scale model blades.

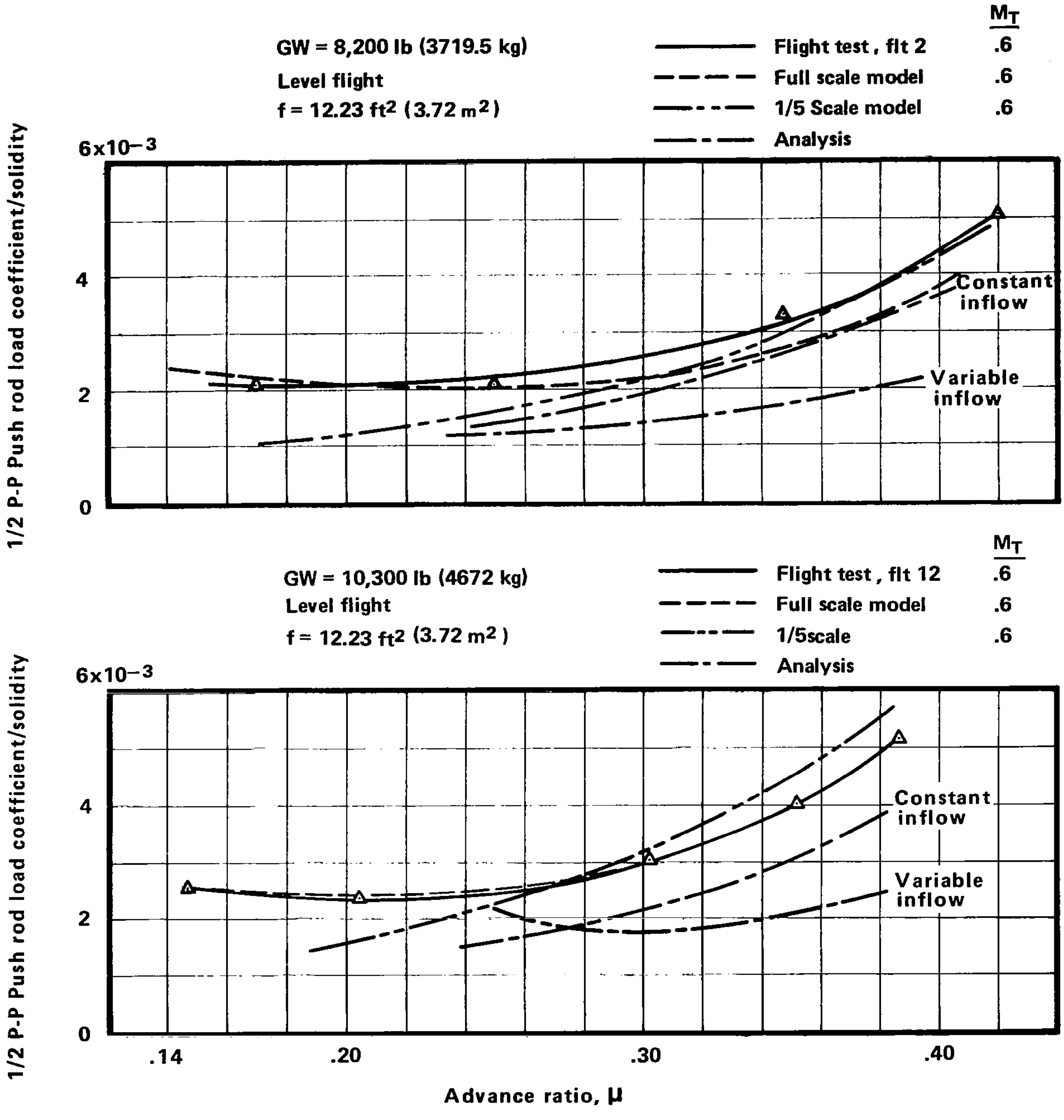

Figures 25, 26 — Main rotor blade vibratory push rod load coefficient/solidity versus advance ratio. Flight test compared with model tests and analysis.

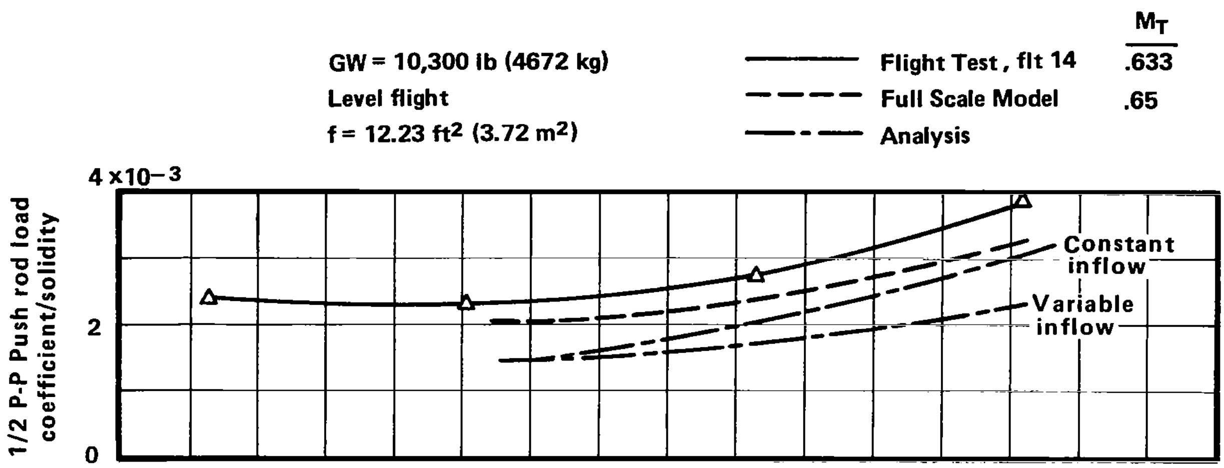

Figure 27—Main rotor blade vibratory push rod load coefficient/solidity versus advance ratio. Flight test compared with model tests and analysis.

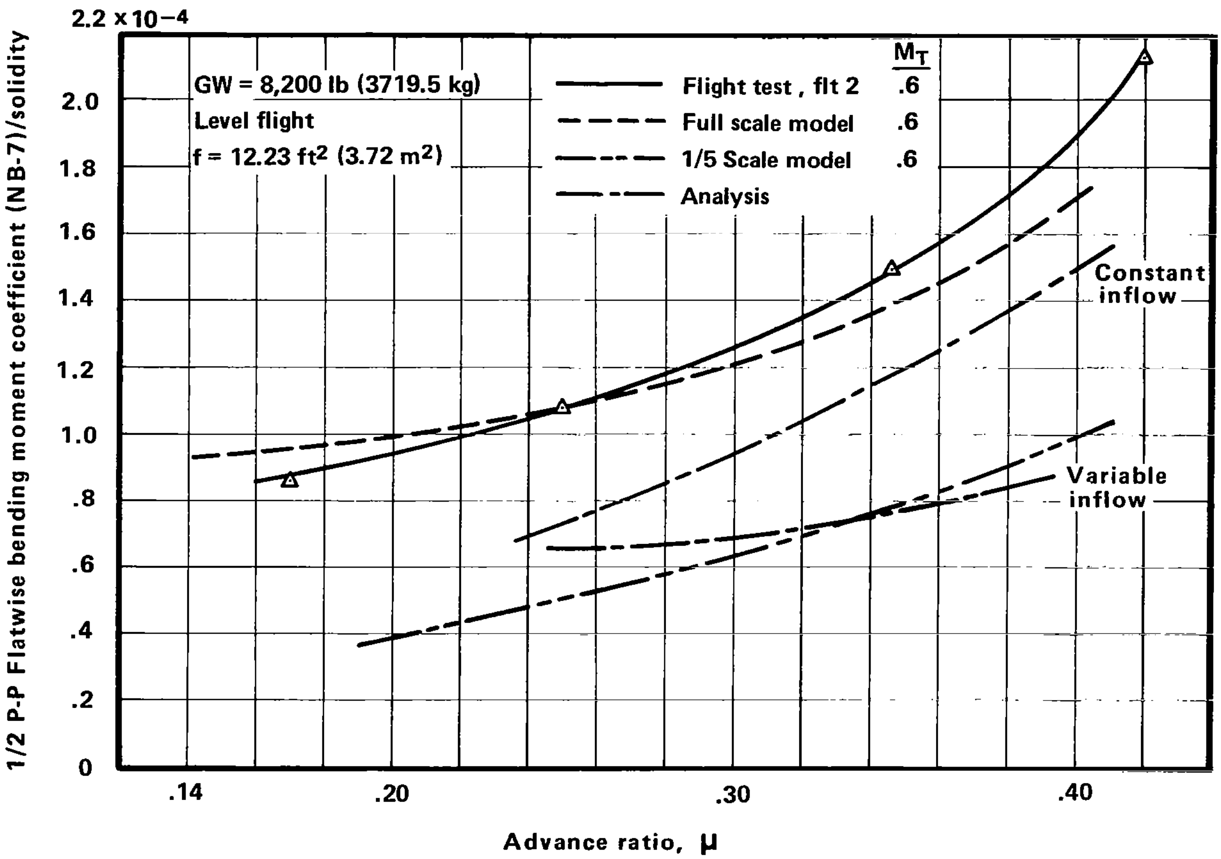

Figure 28 —Main rotor blade vibratory flatwise bending moment coefficient (NB-7)/solidity. versus advance ratio. Flight test compared with model tests and analysis.

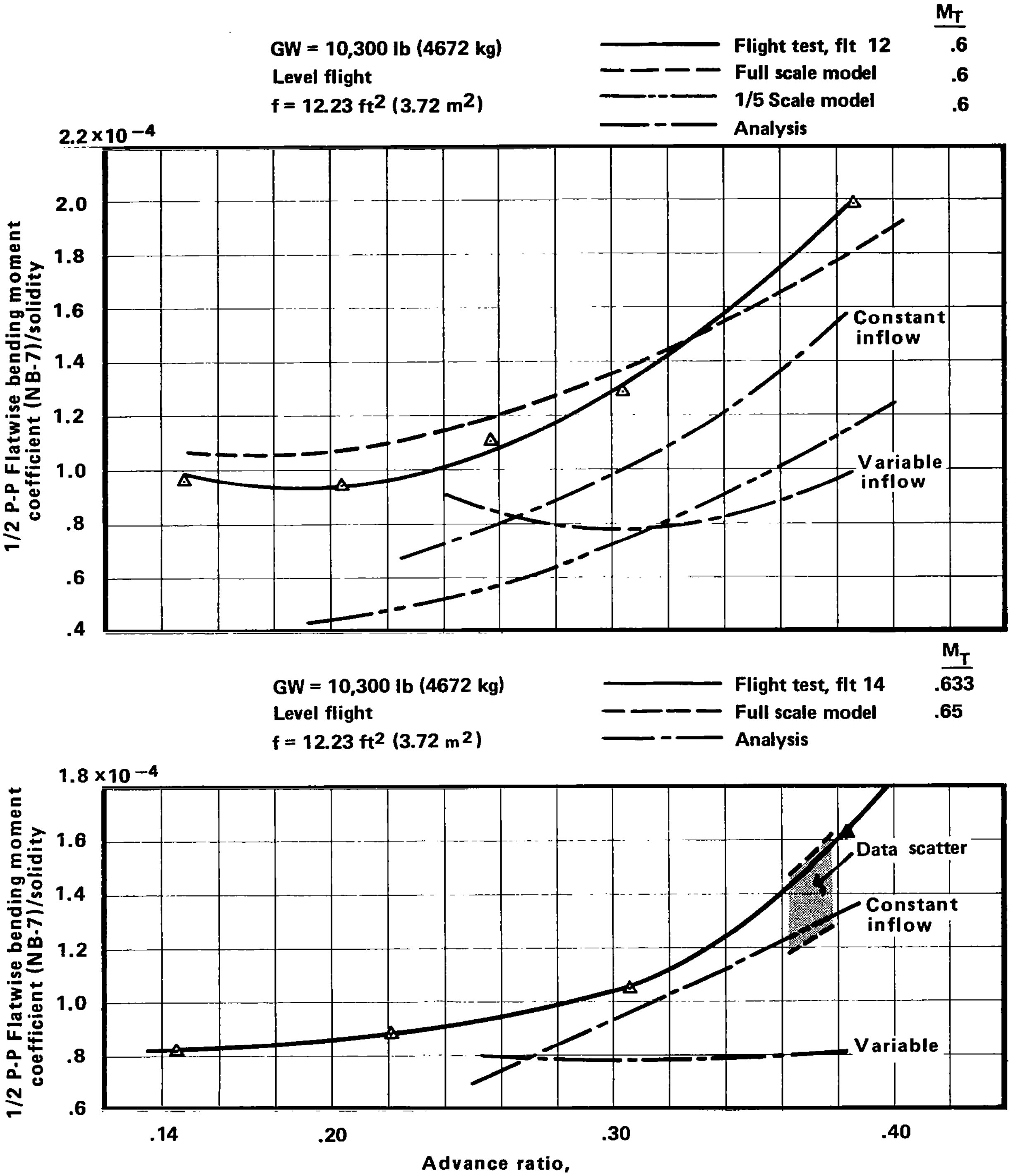

Figures 29, 30- Main rotor blade vibratory flatwise bending moment coefficient (NB-7)/solidity. versus advance ratio. Flight test compared with model tests and analysis.

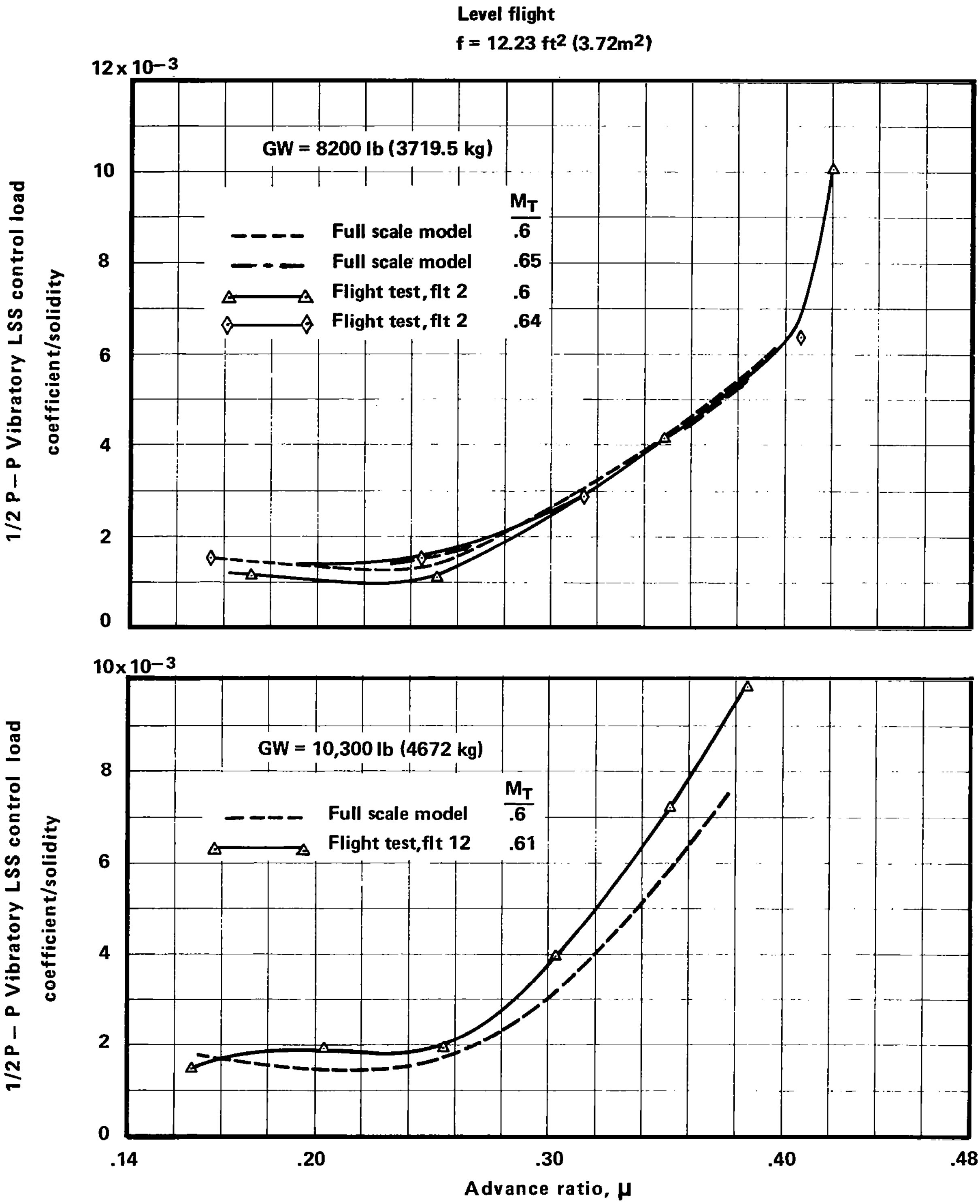

Figures 31, 32 — Flight and wind tunnel lateral stationary star control load coefficient/solidity versus advance ratio.

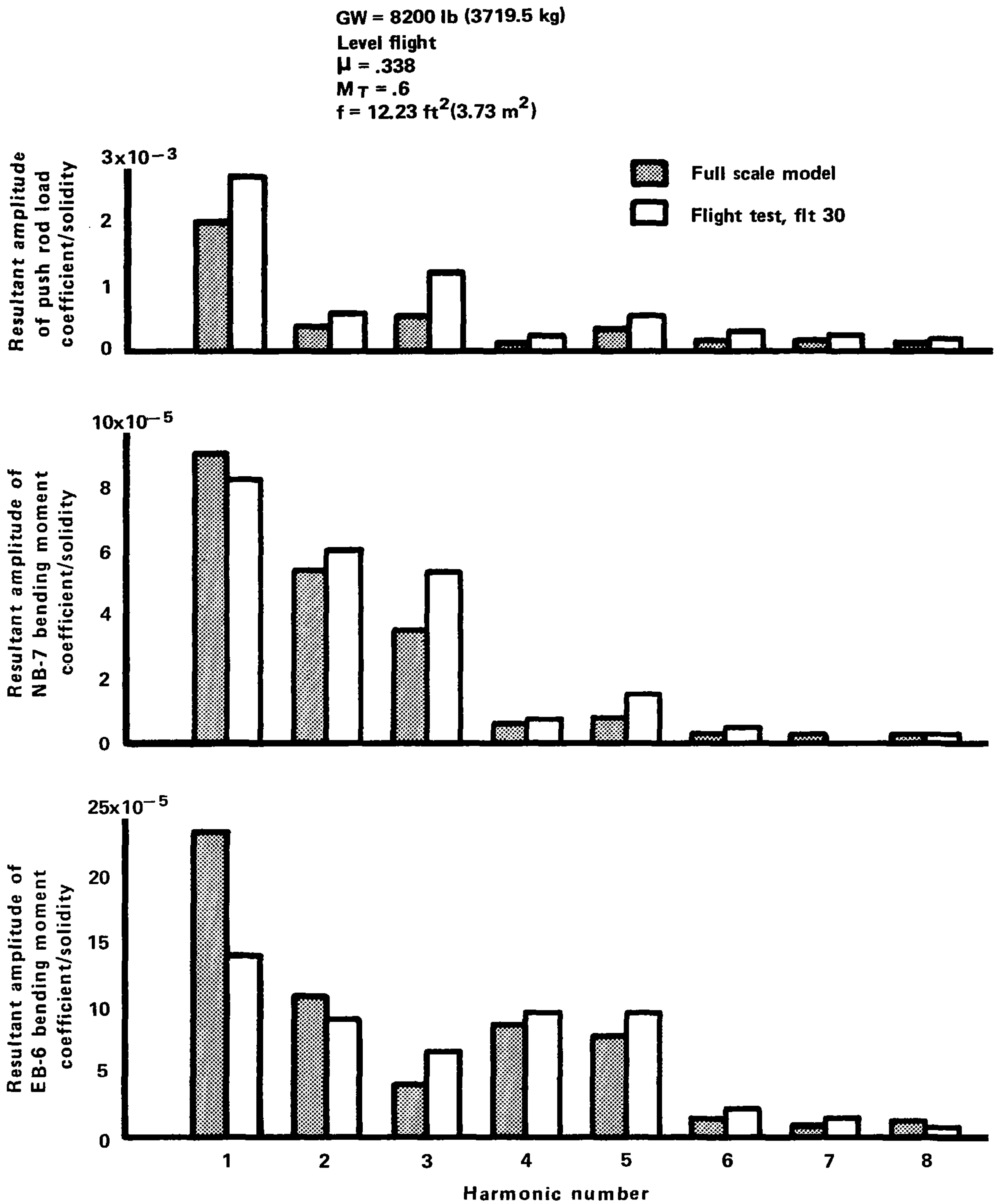

Figures 33, 34, 35 — Resultant amplitude of main rotor blade load versus harmonic number. Flight and full scale model.

GW = 8200 lb (3719.5 kg)
Level flight
μ = .4
M_T = .6
f = 12.23 ft^2 (3.73 m^2)

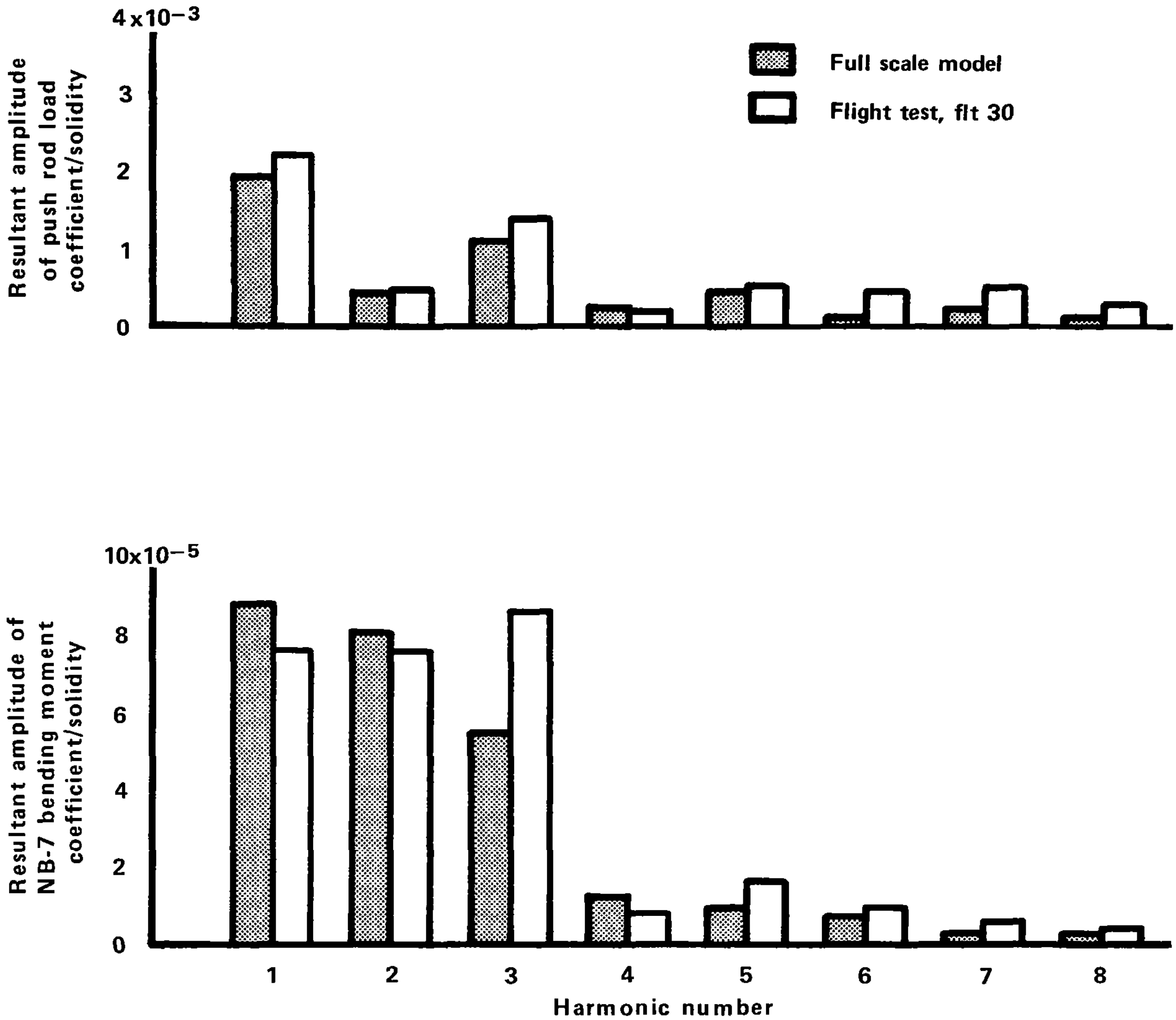

Figures 36, 37 — Resultant amplitude of main rotor blade load versus harmonic number. Flight and full scale model.

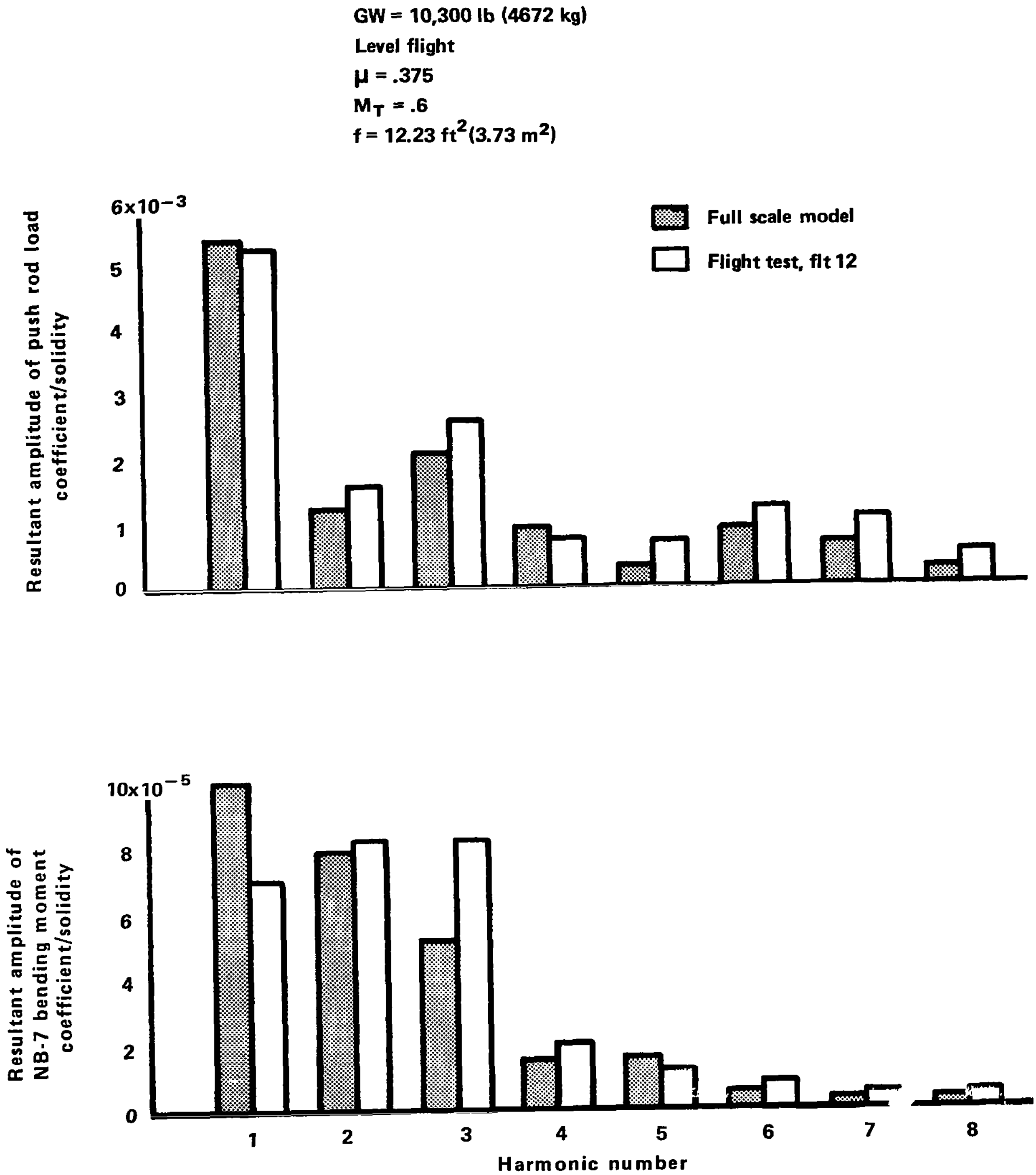

Figures 38, 39 — Resultant amplitude of main rotor blade load versus harmonic number. Flight and full scale model.

GW = 10,300 lb (4672 kg)
Level flight
μ = .375
M_T = .65
f = 12.23 ft^2(3.73 m^2)

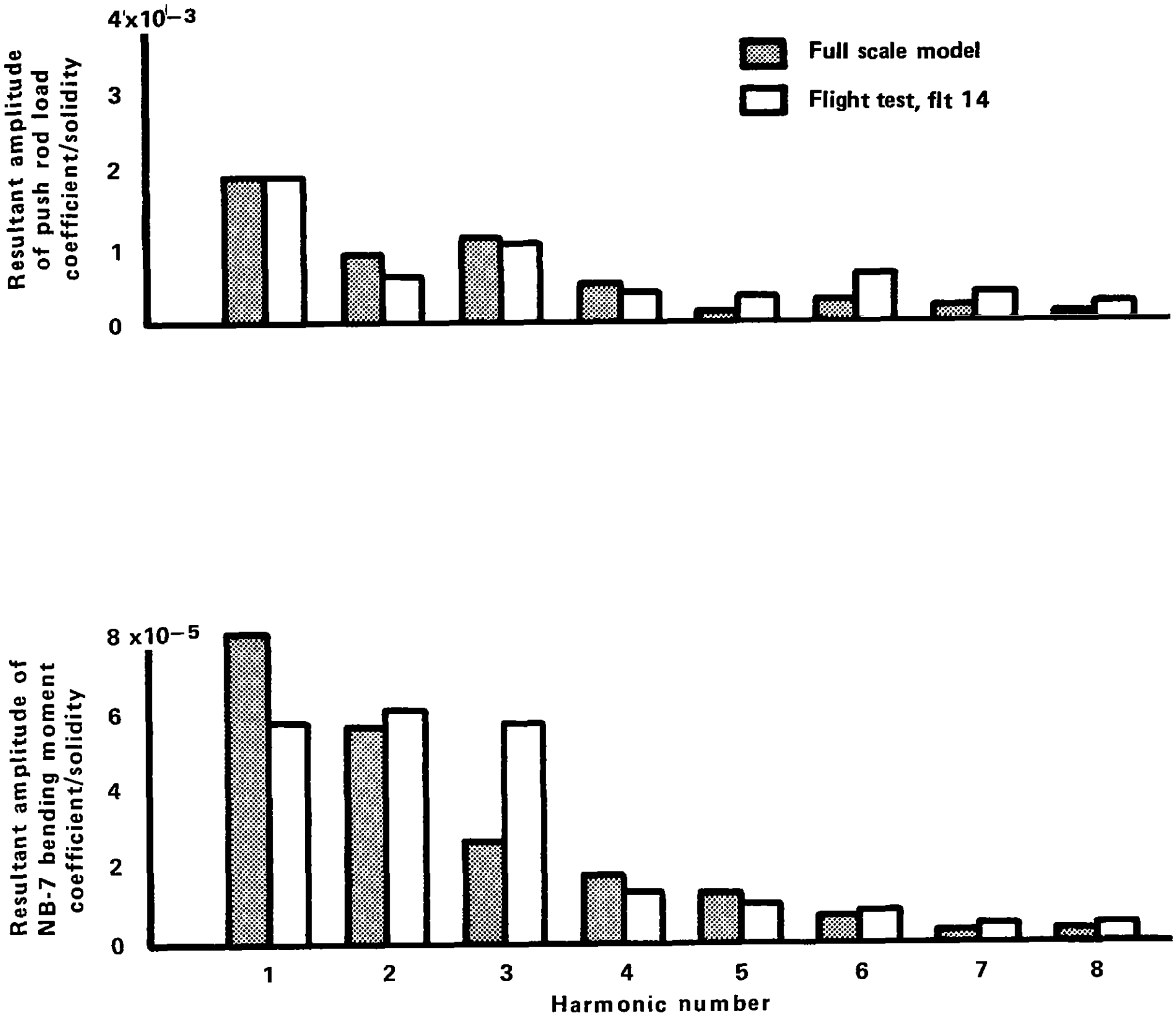

Figures 40, 41 — Resultant amplitude of main rotor blade load versus harmonic number. Flight and full scale model.

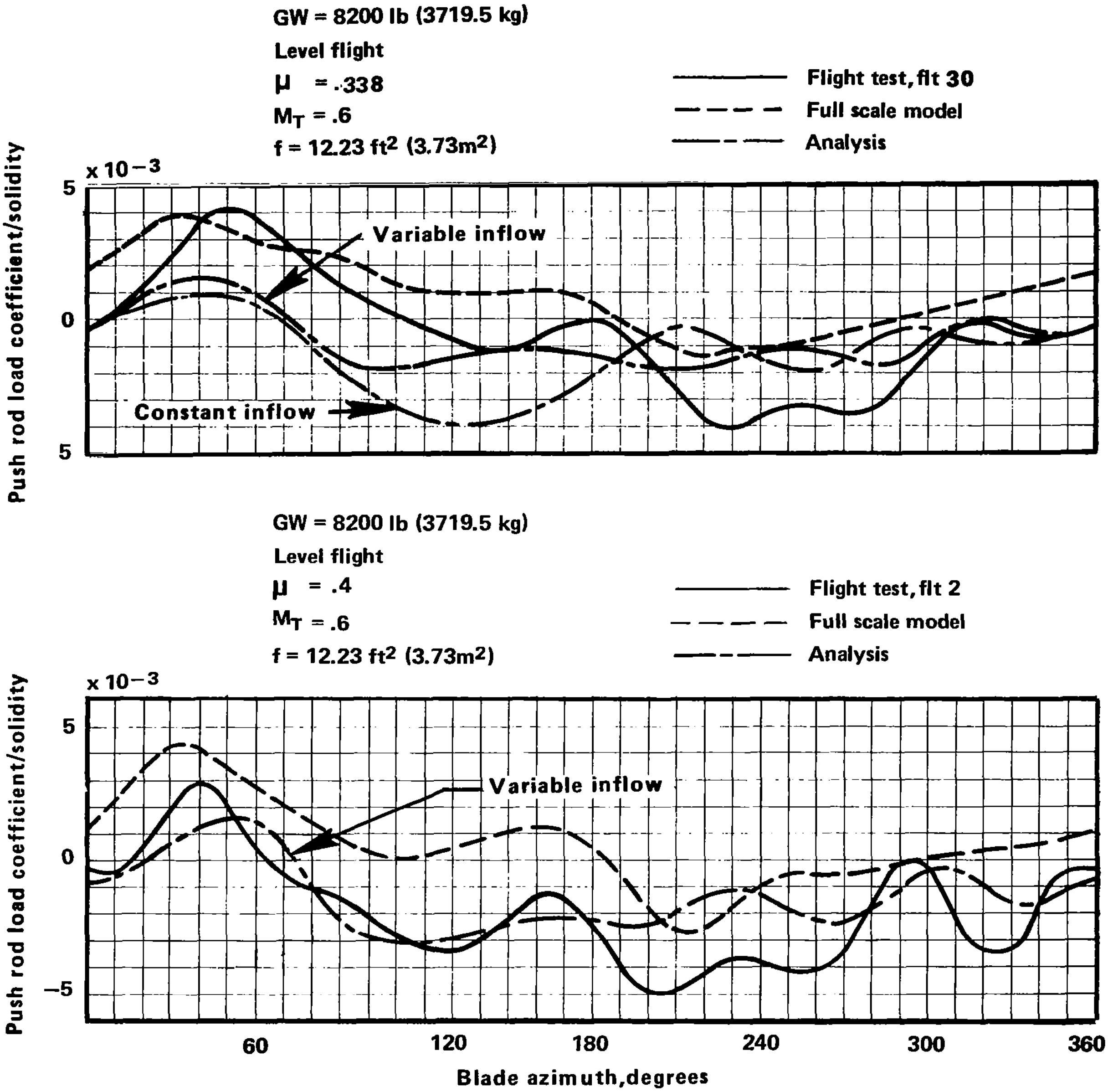

Figures 42, 43 — Main rotor blade push rod load coefficient/solidity versus blade azimuth. Flight test compared with full scale model and analysis.

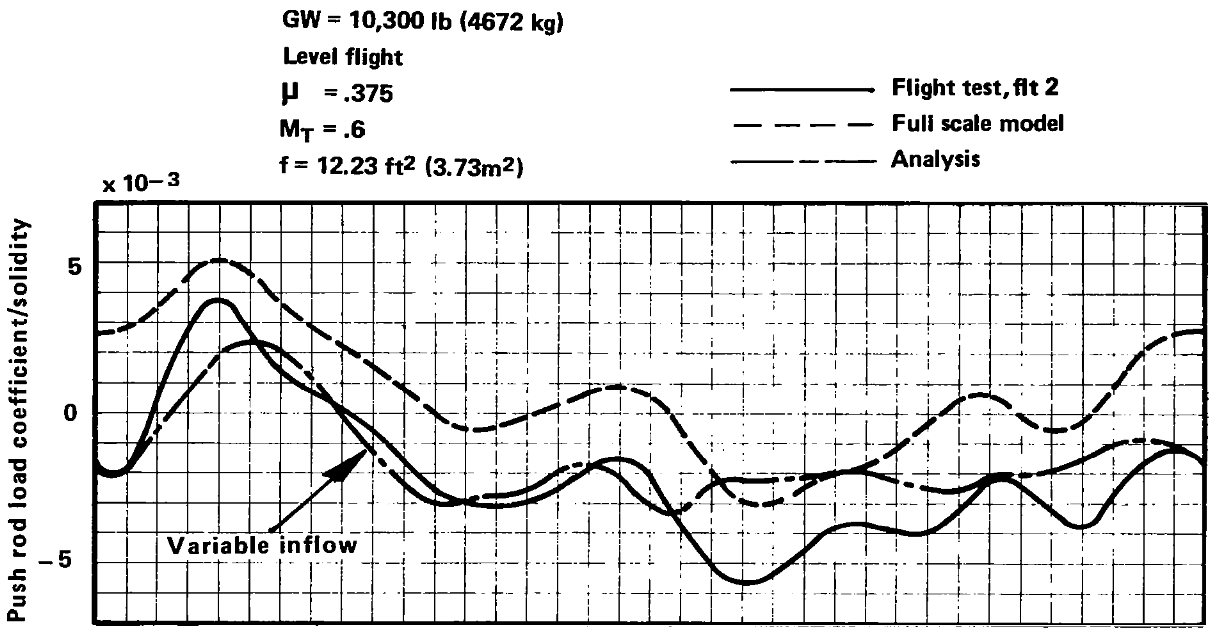

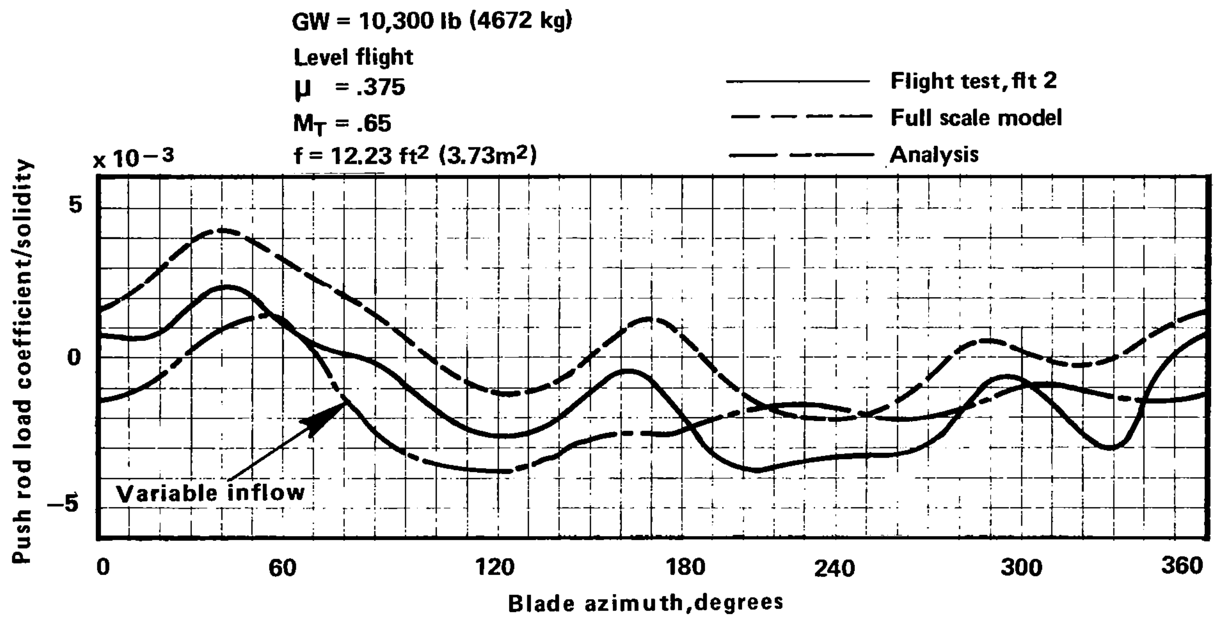

Figures 44, 45 – Main rotor blade push rod load coefficient/solidity versus blade azimuth. Flight test compared with full scale model and analysis.

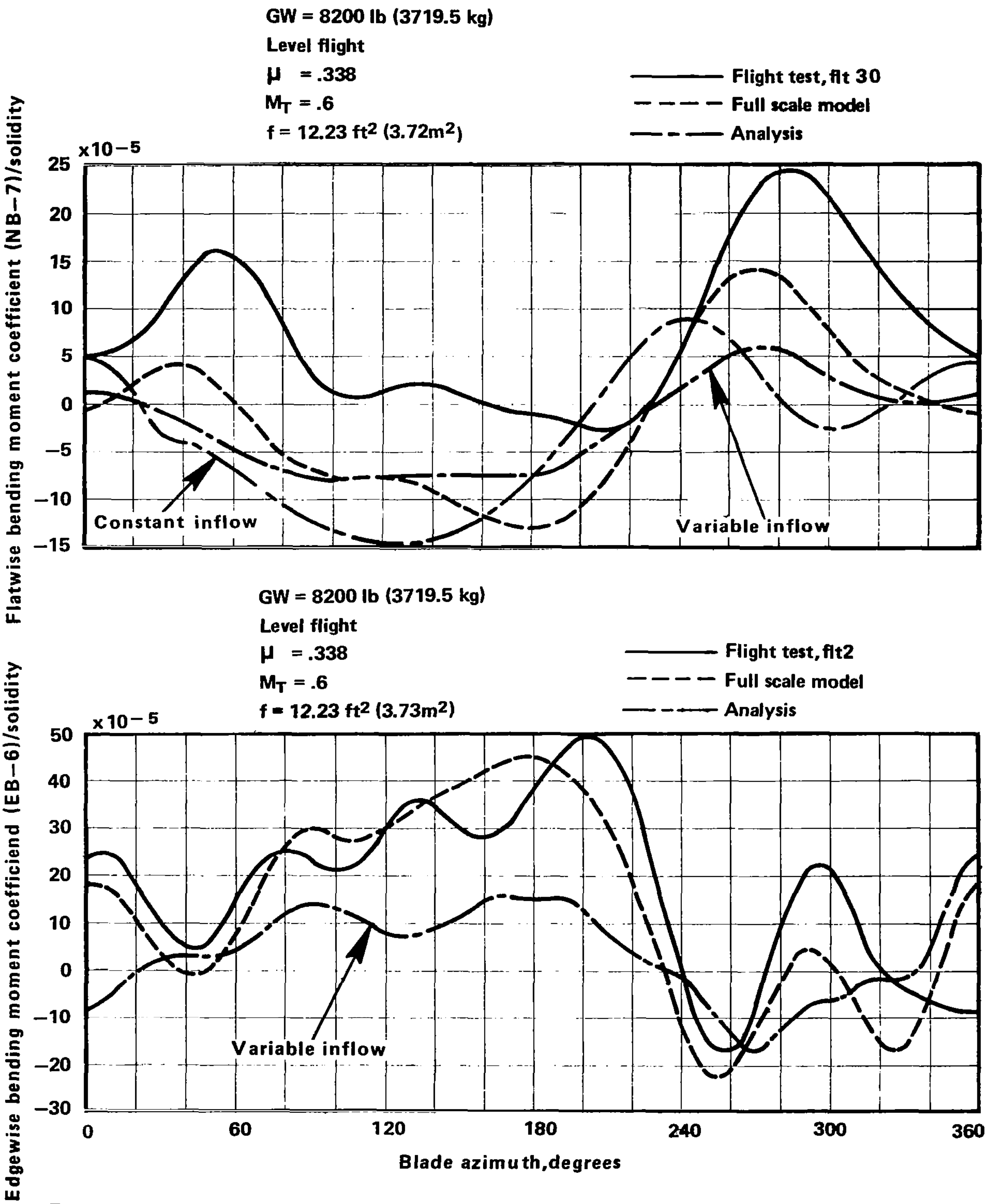

Figures 46, 47 — Main rotor blade bending moment coefficient/solidity versus blade azimuth. Flight test compared with full scale model and analysis.

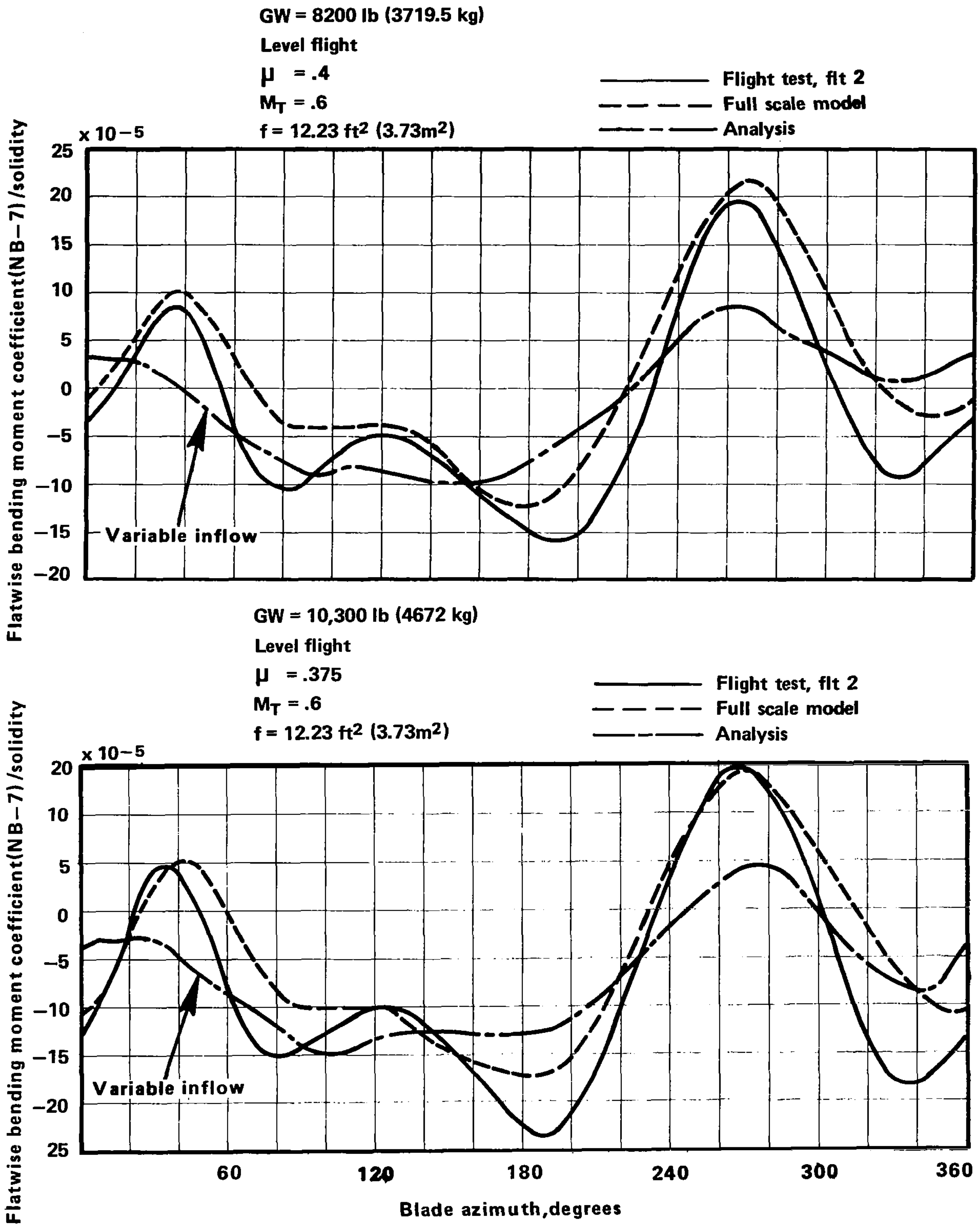

Figures 48, 49 — Main rotor blade flatwise bending moment coefficient/solidity versus blade azimuth. Flight test compared with full scale model and analysis.

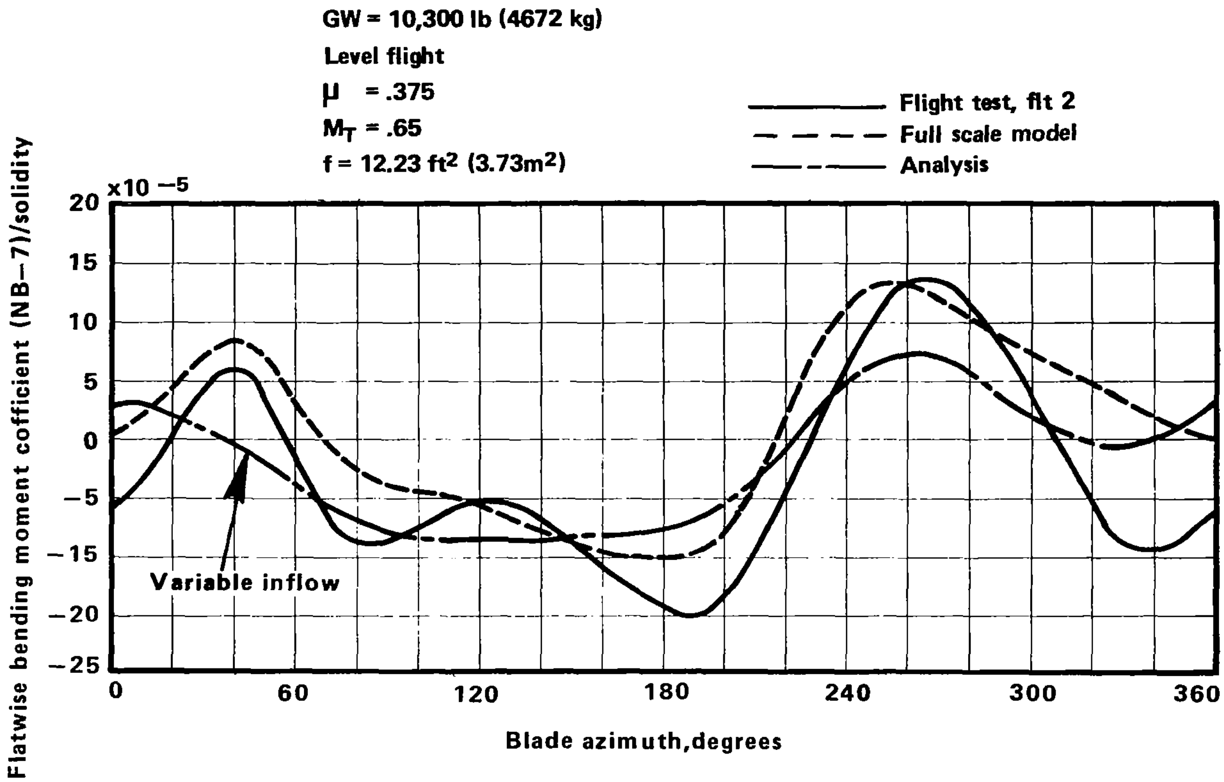

Figure 50 – Main rotor blade flatwise bending moment coefficient/solidity versus blade azimuth. Flight test compared wiht full scale model and analysis.

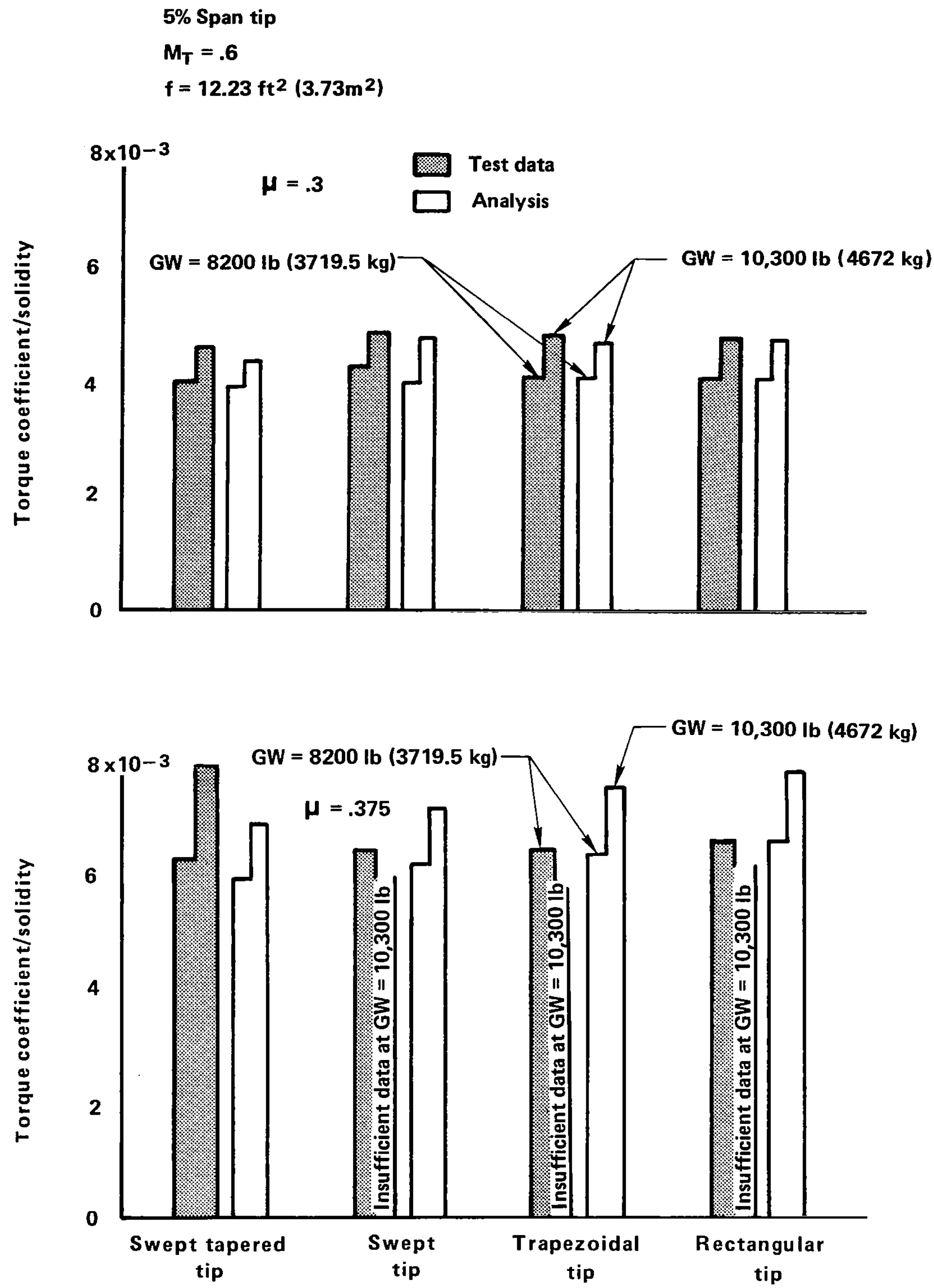

Figures 51, 52 — Effect of tip configuration on trimmed level flight performance. Full scale model test data compared with analysis.

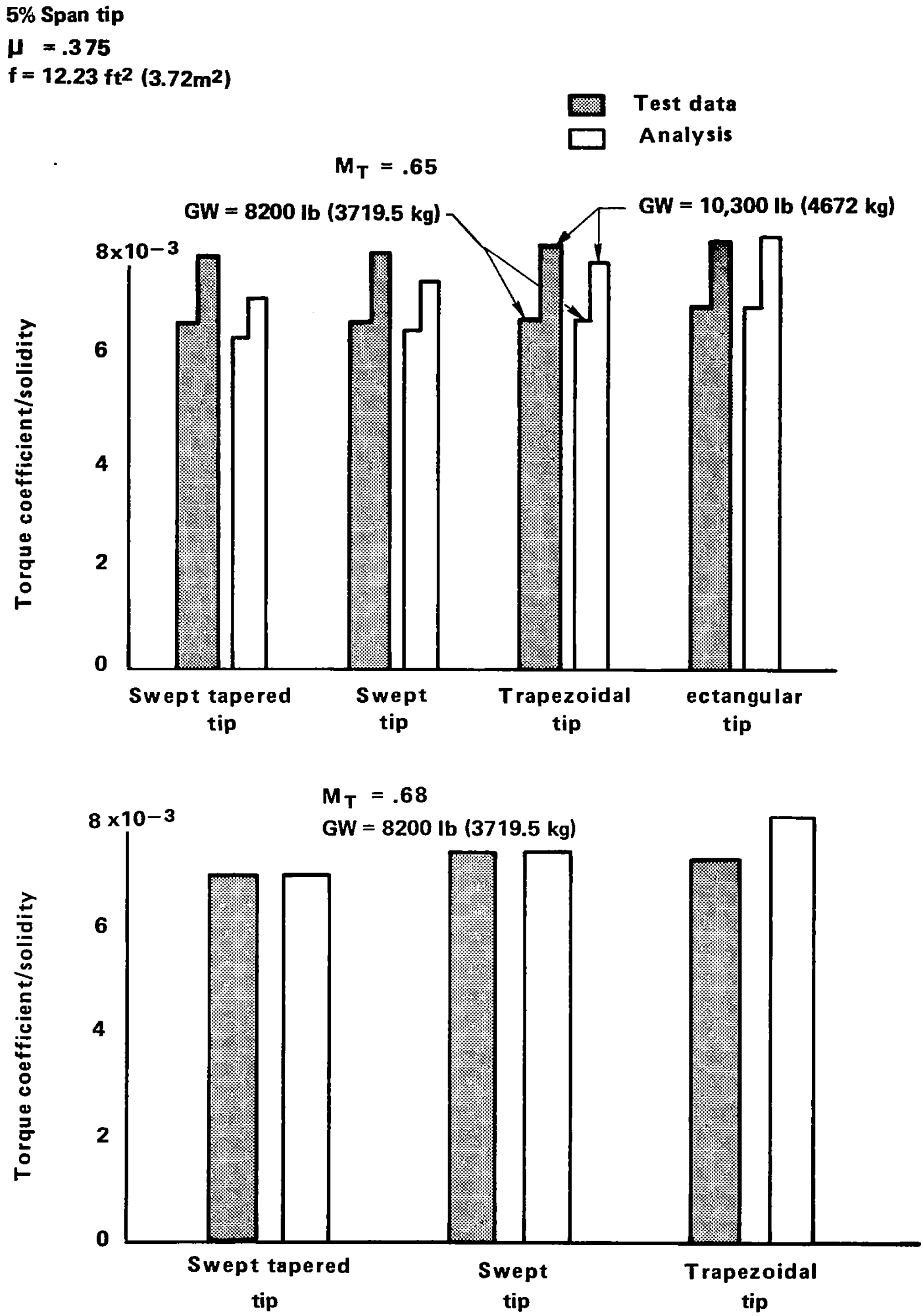

Figures 53, 54 – Effect of tip configuration on trimmed level flight performance. Full scale date compared with analysis.

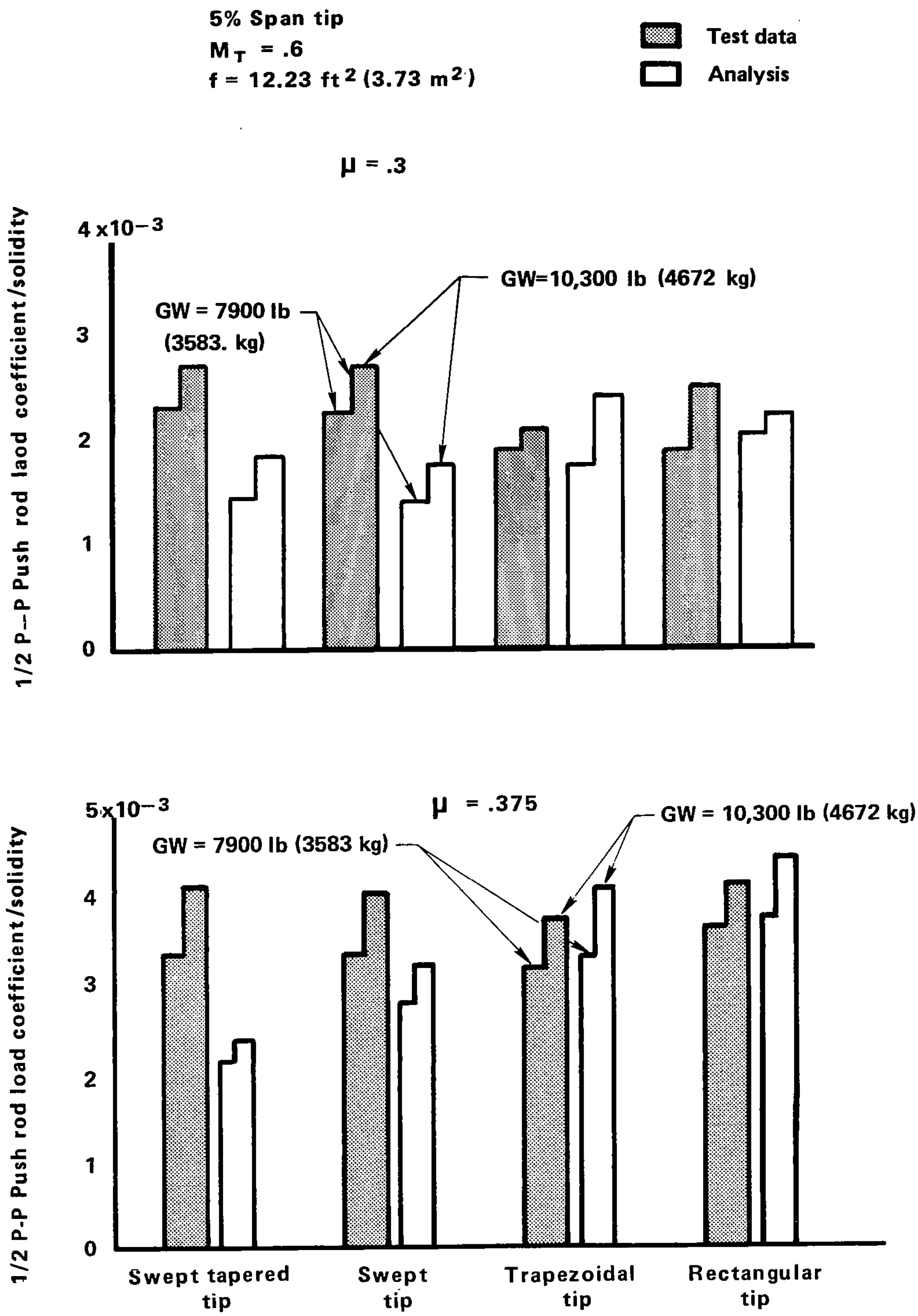

Figures 55, 56 — Effect of tip configuration on blade vibratory push rod load. Full scale model test data and comparison with analysis.

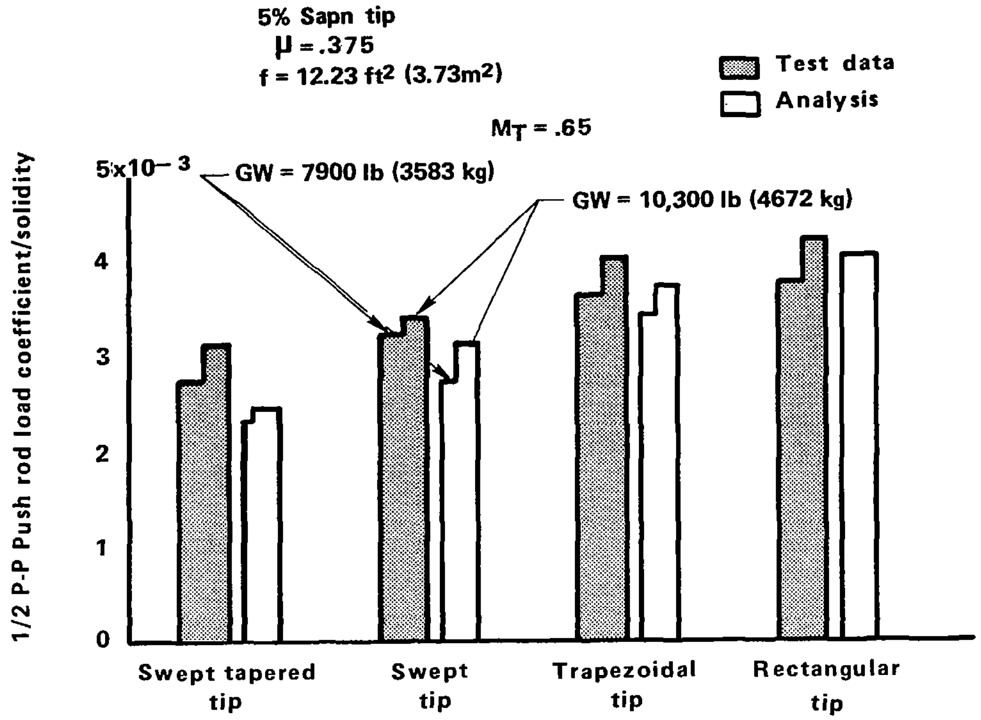

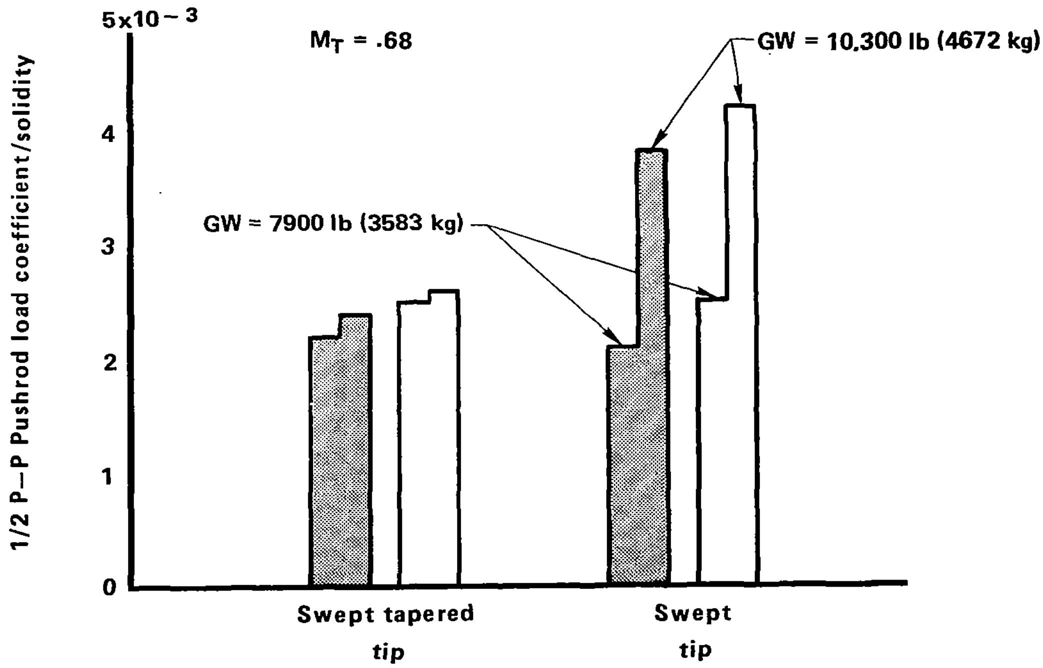

Figures 57, 58 – Effect of tip configuration on blade vibratory push rod load. Full scale model test data and comparison with analysis.

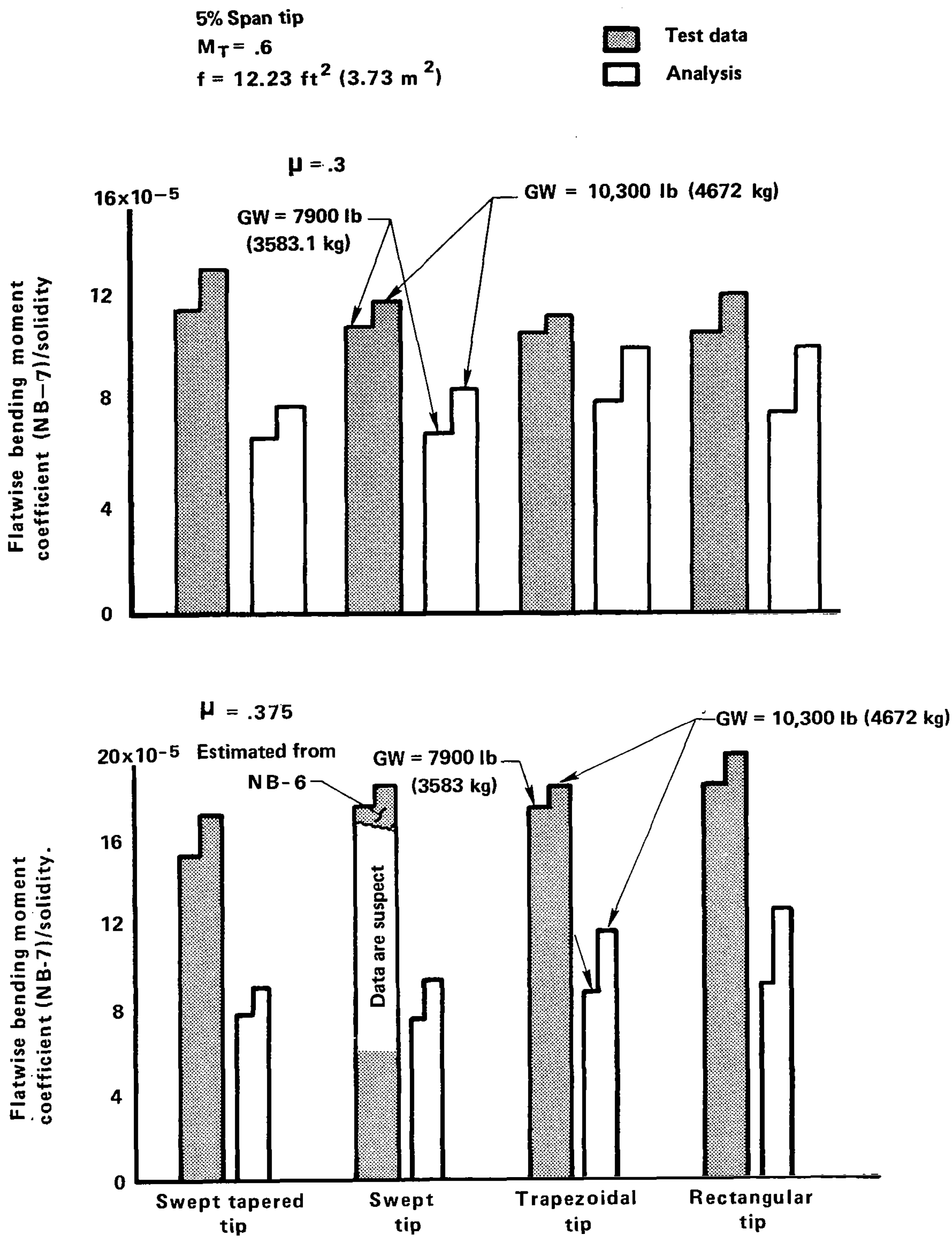

Figures 59, 60 —Effect of tip configuration on blade vibratory flatwise bending moment (NB-7). Full scale test model data and comparsion with analysis.

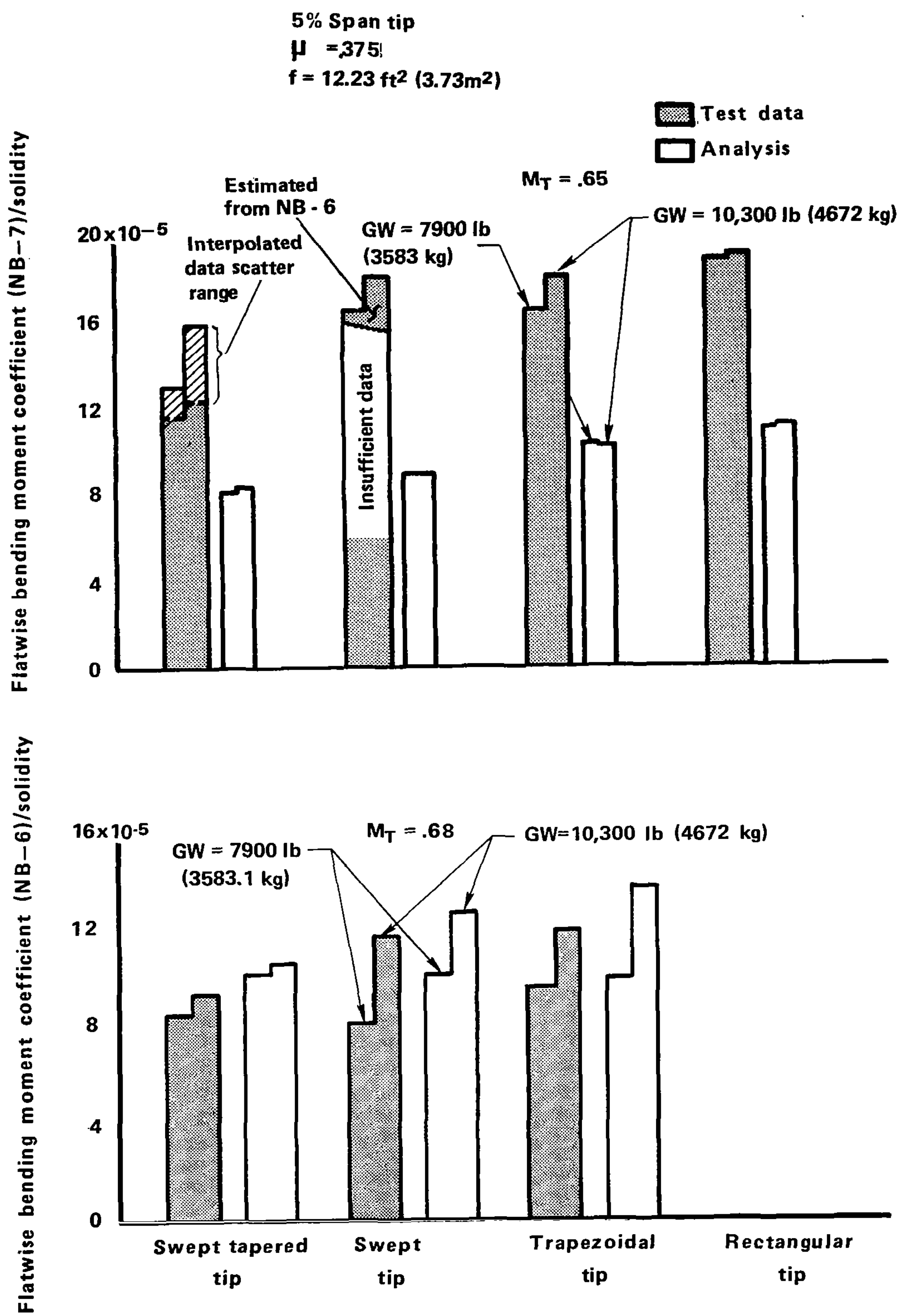

Figures 61, 62 —Effect of tip configuration on blade vibratory flatwise bending moment (NB-7). Full scale test model data and comparsion with analysis.

5% Span tip
M_T = .6
f = 12.23 ft² (3.73m²)

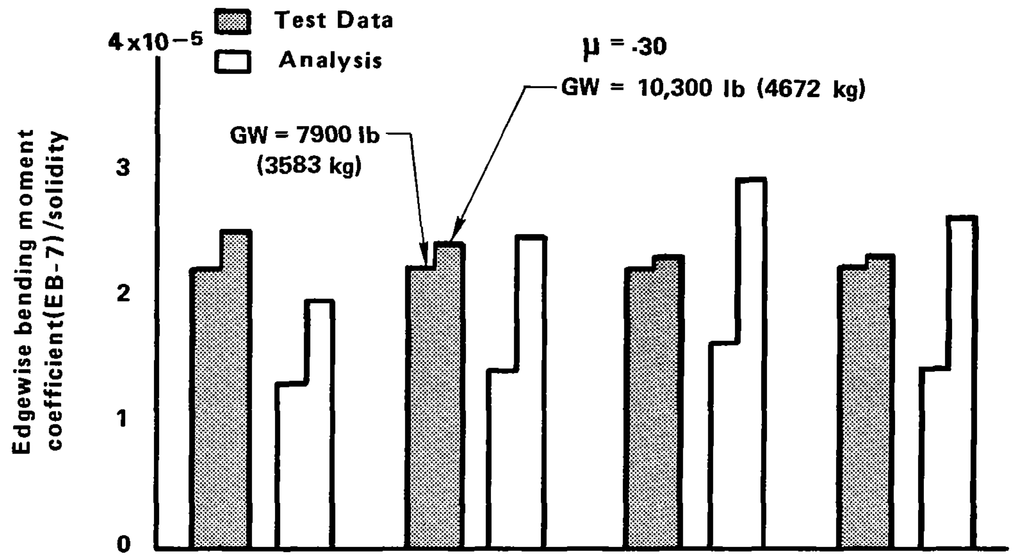

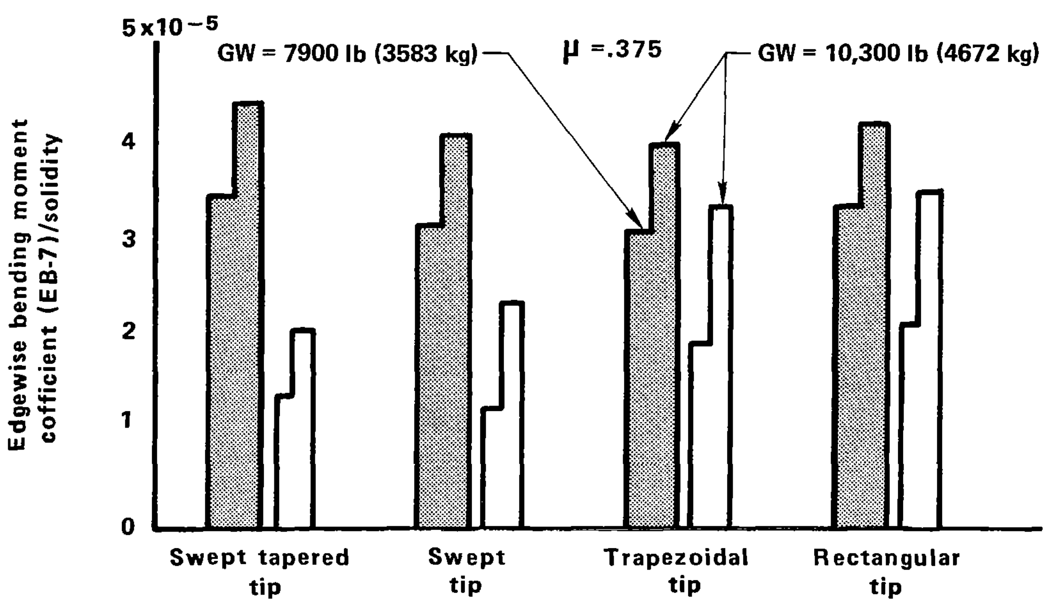

Figures 63, 64– Effect of tip configuration on blade vibratory edgewise bending moment (EB - 7). Full scale model test data and comparison with analysis.

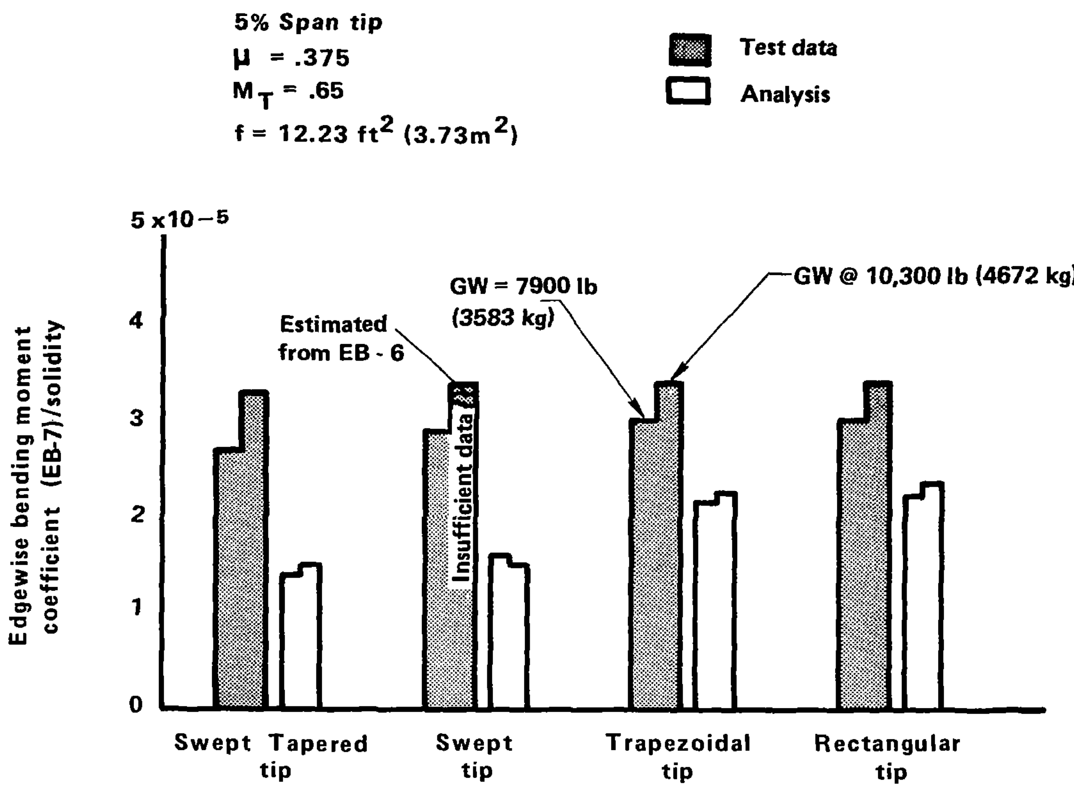

Figure 65 — Effect of tip configuration on blade vibratory edgewise bending moment (EB - 7). Full scale model test data and comparison with analysis.

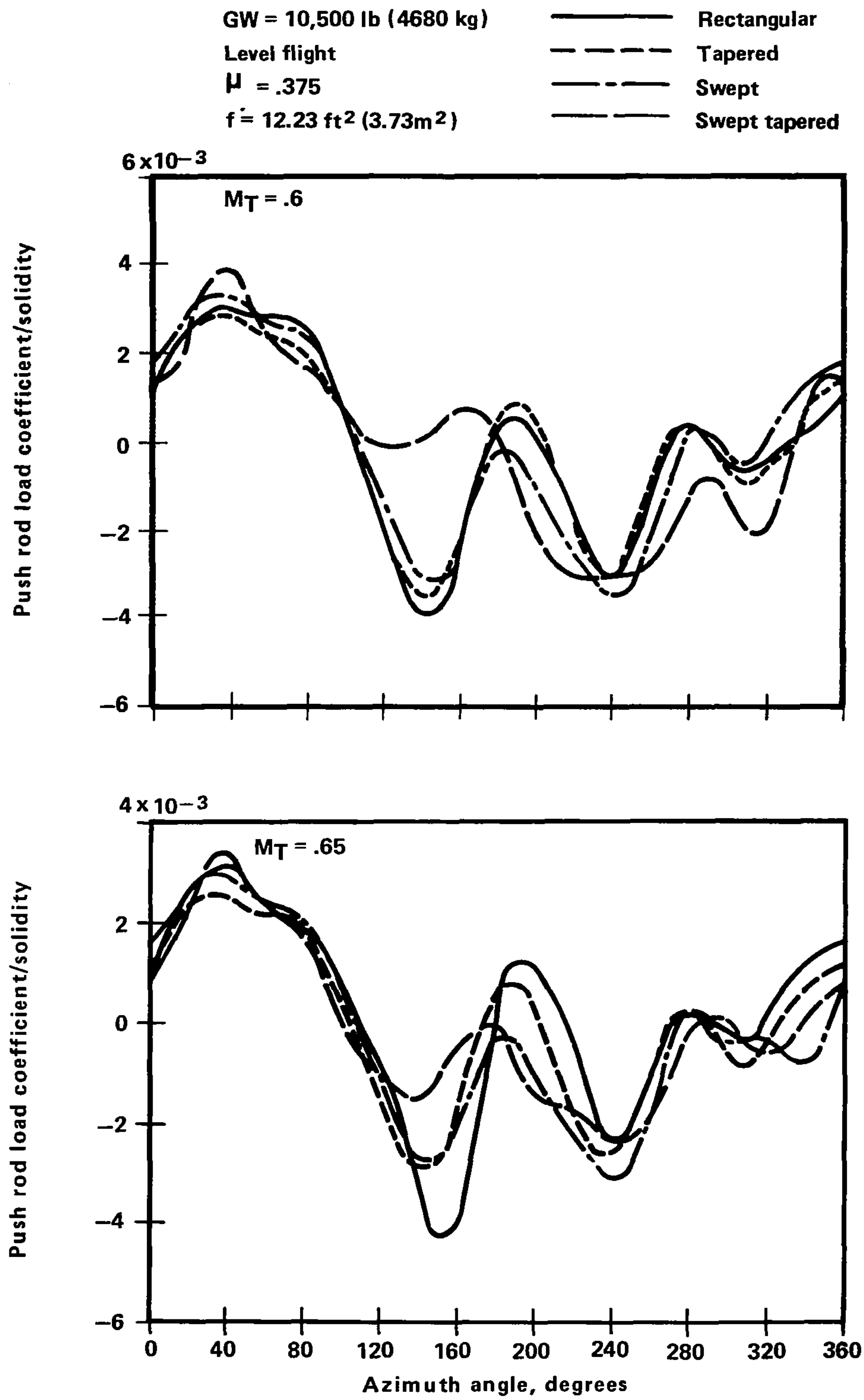

Figures 66, 67 — Effect of tip configuration on blade push rod load time history.

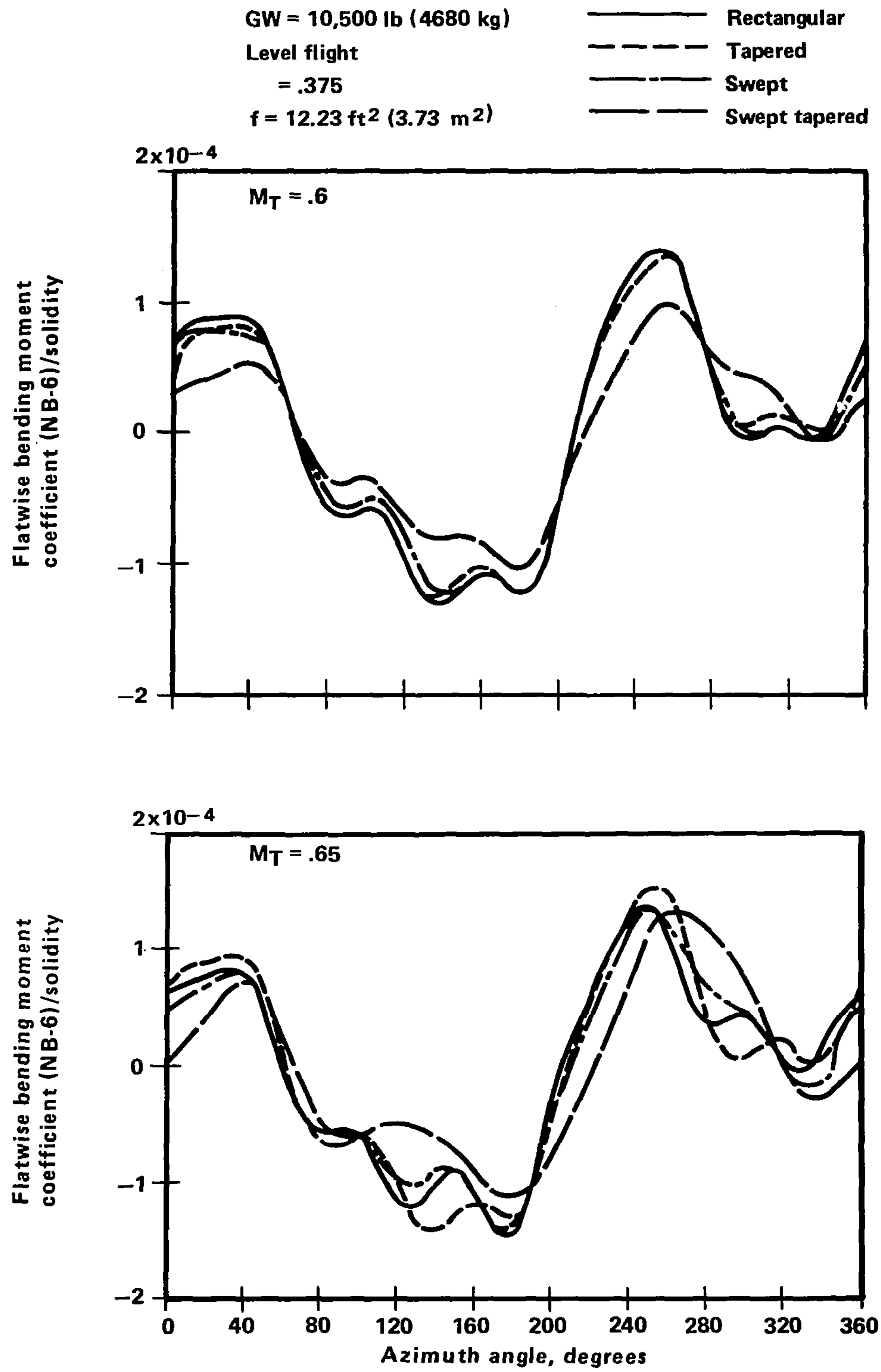

Figures 68, 69 – Effect of tio configuration on blade flatwise bending moment (NB–6) time history

Level flight
f = 12.23 ft² (3.72m²)

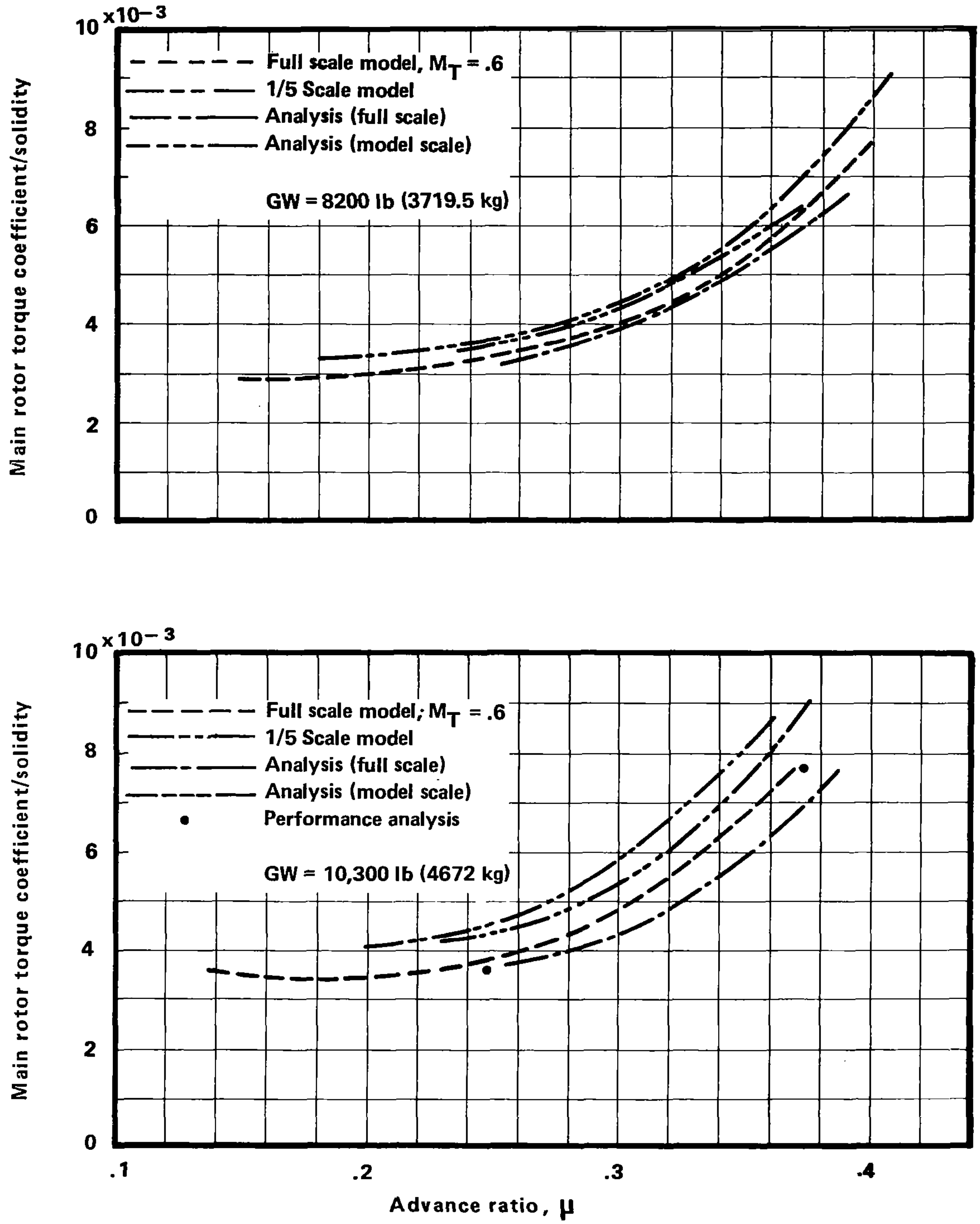

Figures 70, 71 — Main rotor torque coefficient/solidity versus advance ratio. Model tests compared with analysis.

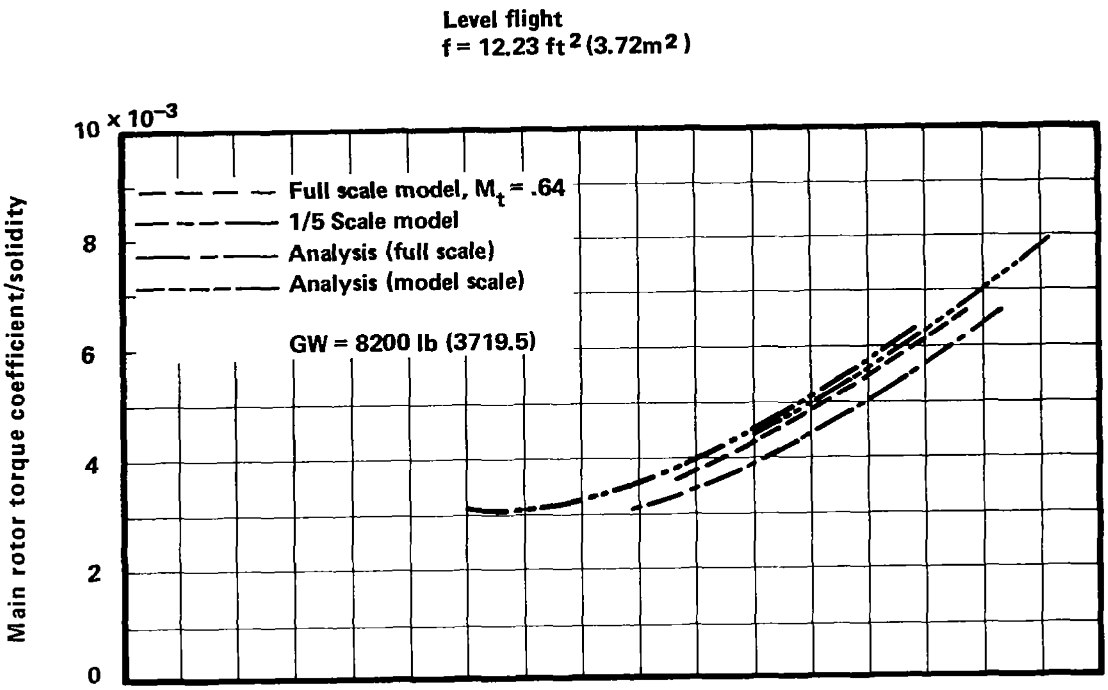

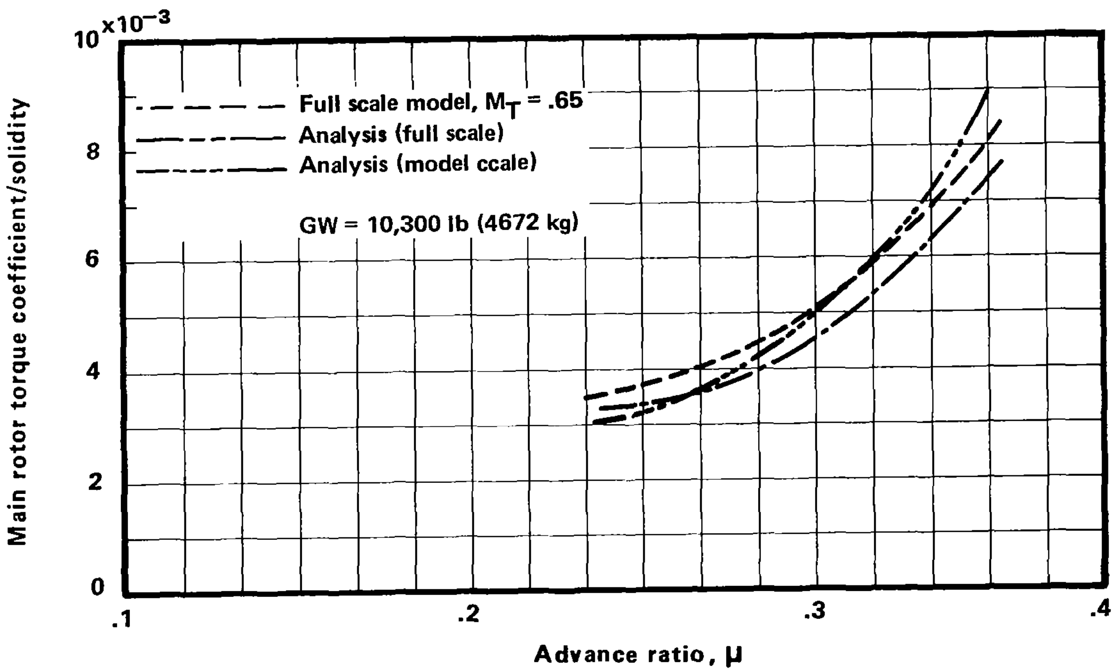

Figures 72, 73 — Main rotor torque coefficient/solidity versus advance ratio. Model tests compared with analysis.

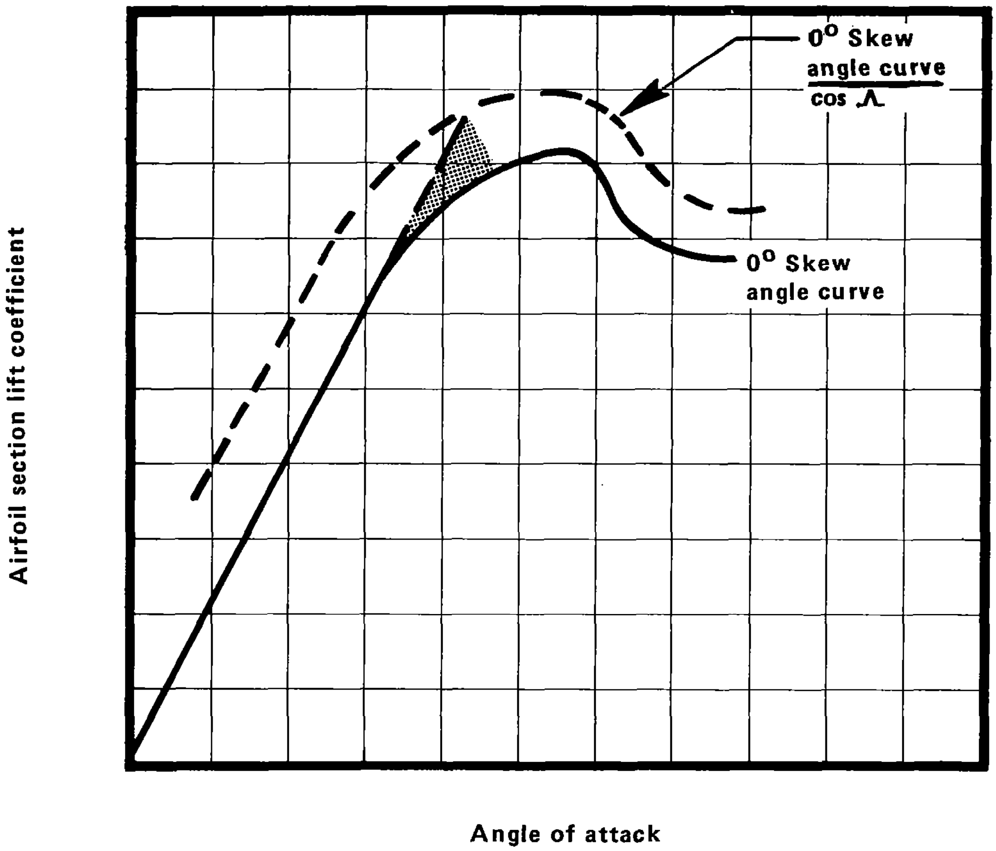

Figure 74 — Y201 Skewed flow lift stall model.

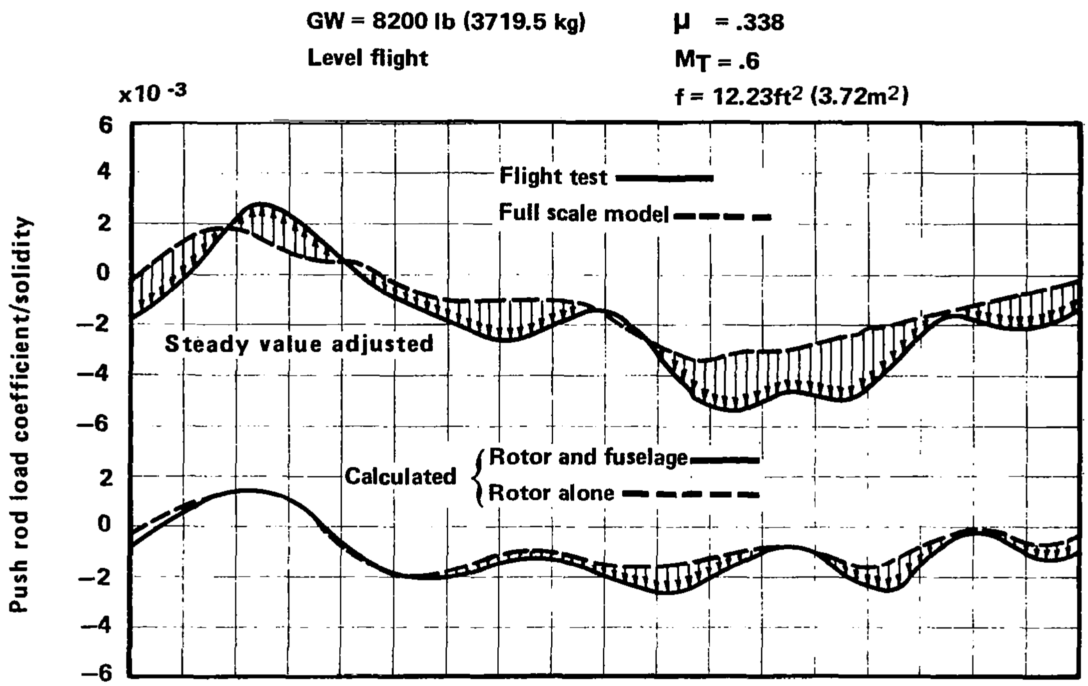

Figure 75 — Effect of fuselage on blade push rod load time history. Test and calculated results.

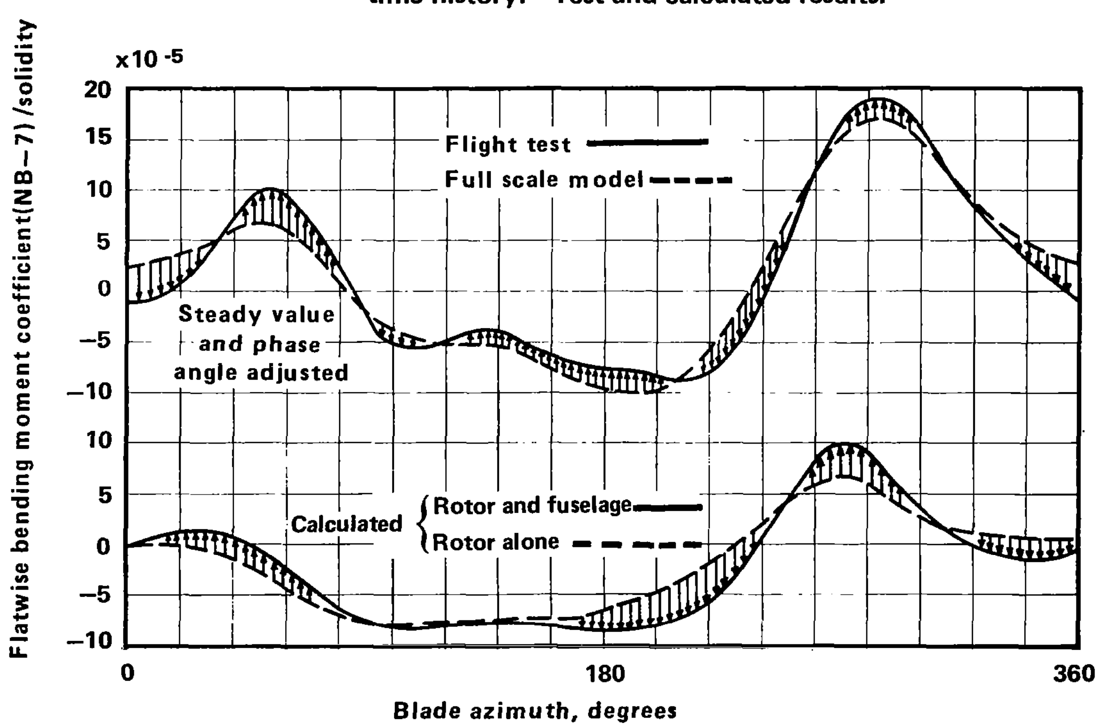

Figure 76 — Effect of fuselage on blade flatwise bending moment time history. Test and calculated results.

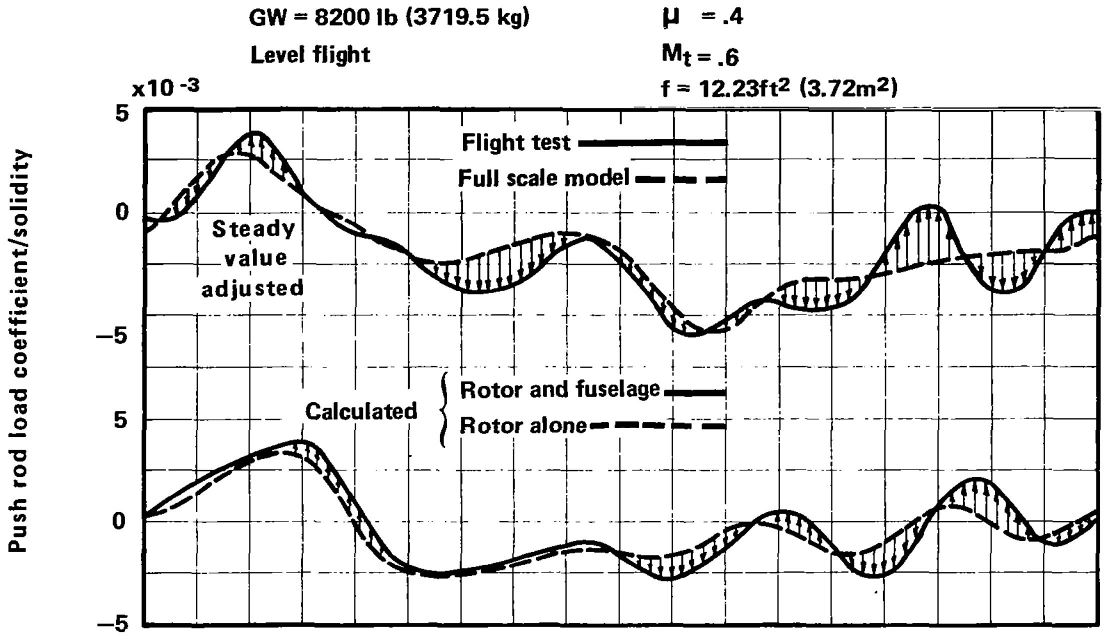

Figure 77 —Effect of fuselage on blade push rod load time history. Test and calculated results.

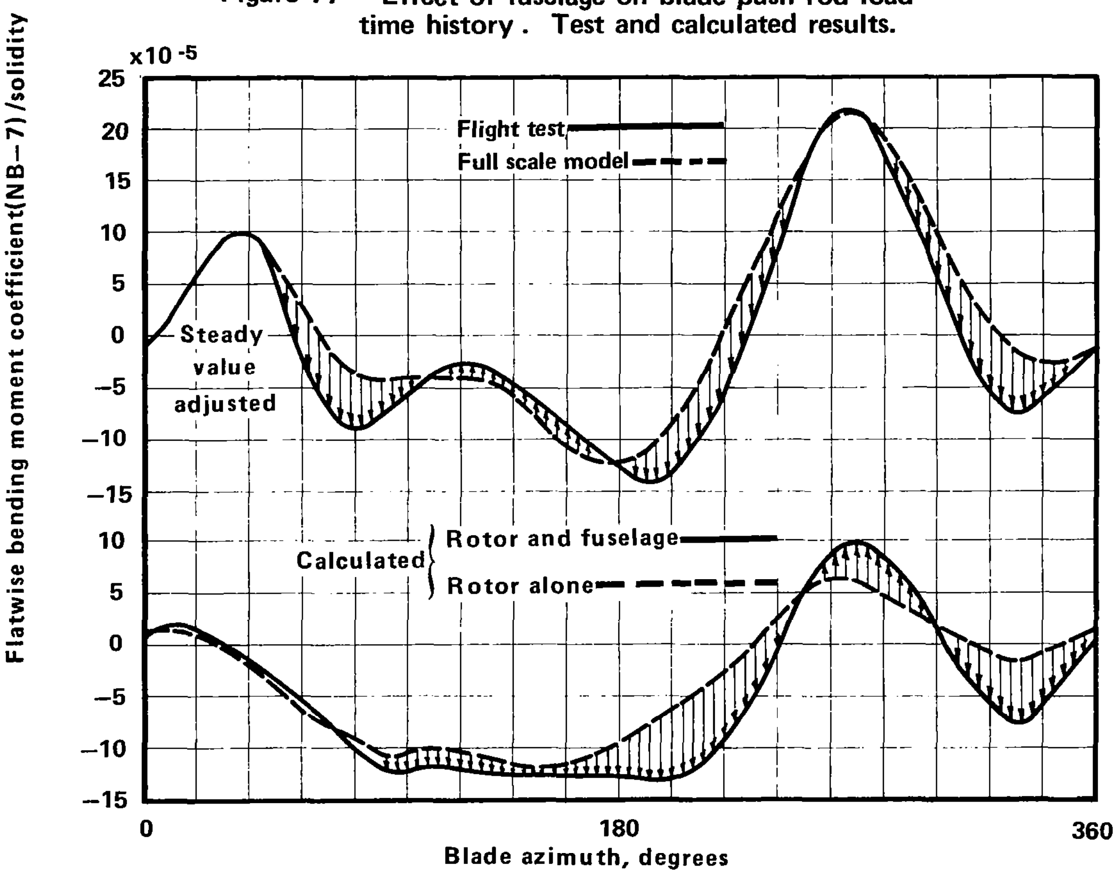

Figure 78 — Effect of fuselage on blade flatwise bending moment time history. Test and calculated results.

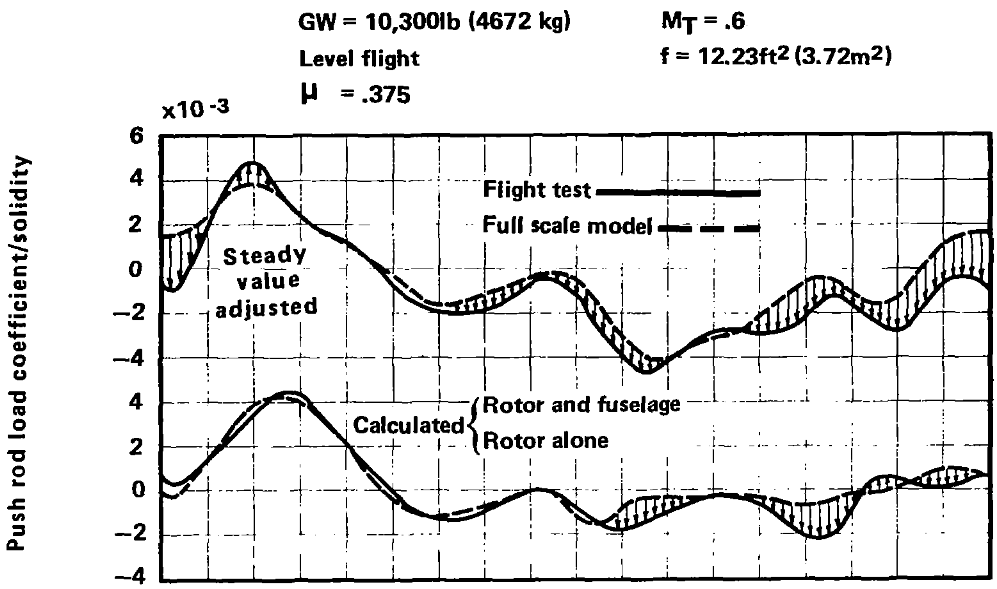

Figure 79 — Effect of fuselage on blade push rod load time history. Test and calculated results.

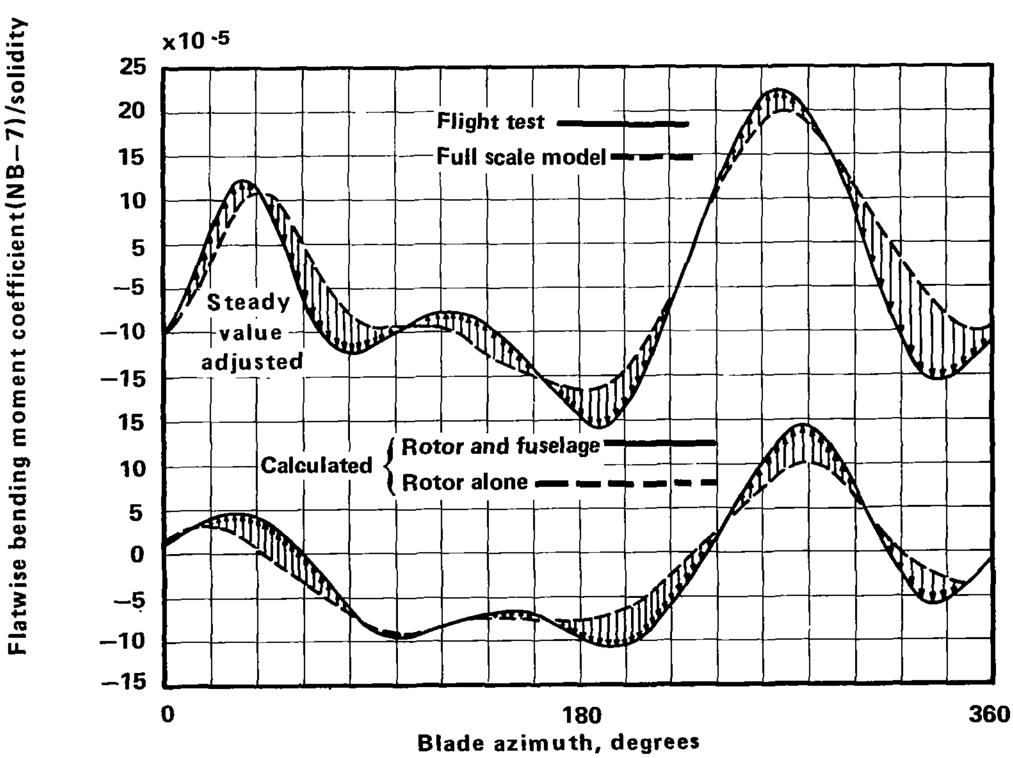

Figure 80 — Effect of fuselage on blade flatwise bending moment. time history. Test and calculated results.

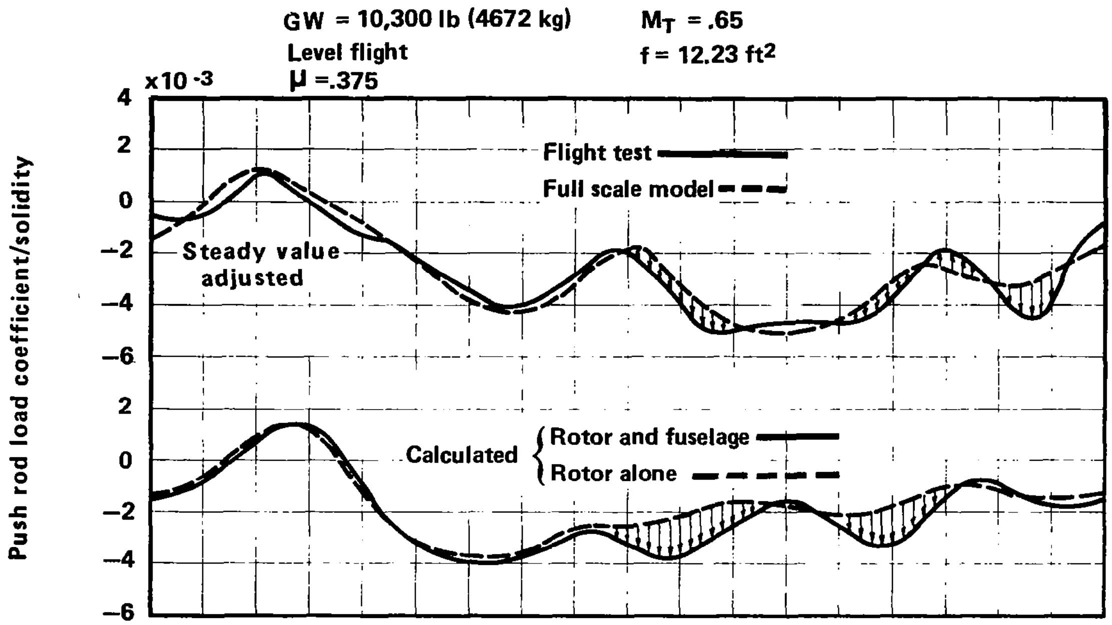

Figure 81 – Effect of fuselage on blade push rod load time history. Test and calculated results.

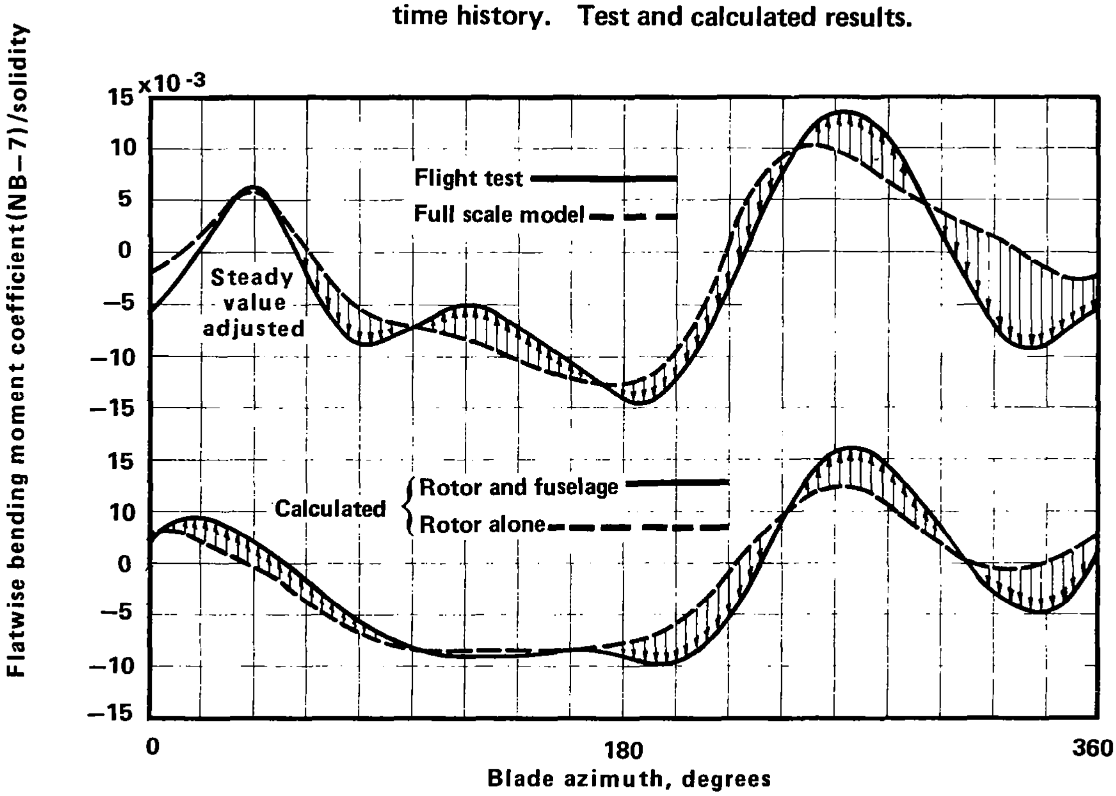

Figure 82 – Effect of fuselage on blade flatwise bending moment time history. Test and calculated results.

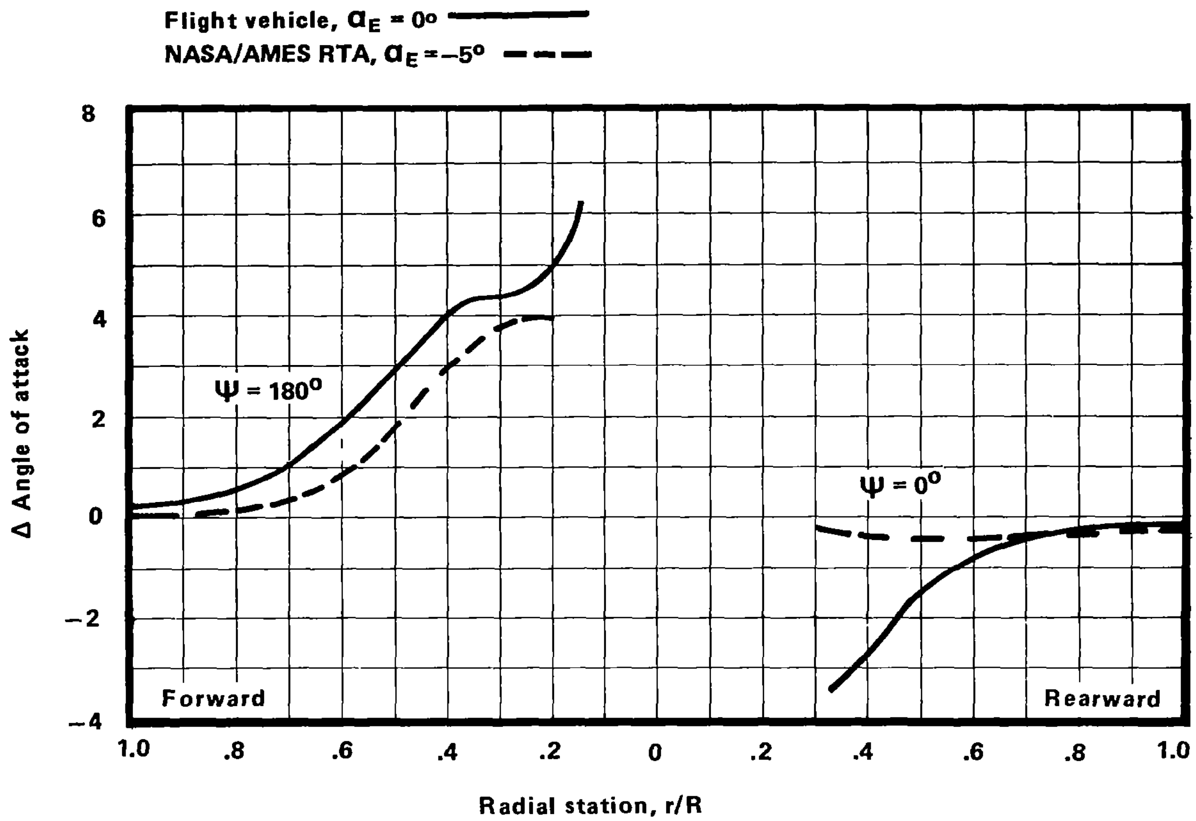

Figure 83 — Effect of fuselage flow on rotor blade local angle of attack in the longitudinal plane of symmetry.

APPENDIX A

ATRS Flight Test Rotor Blade Structural and Mass Properties

In the following table, the blade is represented as a series of 15 radial segments arranged from the coincident flap-lag hinge outboard. The radial length of each segment (Δr) is given nondimensionalized by rotor radius (R). The radius (r) of the midpoint of each segment is also given nondimensionalized by rotor radius. The segment mass is the total mass of the segment. The other properties represent average values for the segment. The elastic axis-quarter chord offset is essentially zero except for the tips segments.

TABLE A.1 BLADE SEGMENT DATA

$\Delta r/R$	r/R	Segment Mass		Segment Torsional Inertia		Modulus Weighted Centroid Distance Forward of Elastic Axis		Center of Gravity Distance Forward of Elastic Axis	
		Slugs	(kg)	Slug-Ft^2	(kg-m^2)	Ft	(cm)	Ft	(cm)
.0540	.0649	.325	(4.743)	.00166	(.0023)	0.0	(0.0)	0.0	(0.0)
.0975	.1406	.541	(7.896)	.02407	(.0326)	.0833	(.254)	-.0792	(-2.414)
.1136	.2462	.259	(3.780)	.02572	(.0346)	-.00183	(-.056)	-.0550	(-1.676)
.0758	.3409	.170	(2.481)	.01652	(.0224)	-.00367	(-.112)	-.0572	(1.743)
.0758	.4167	.170	(2.481)	.01617	(.0219)	-.00334	(-.102)	-.0572	(-1.743)
.0758	.4925	.182	(2.656)	.01754	(.0238)	-.002166	(-.066)	-.176	(-5.364)
.0758	.5683	.218	(3.181)	.01924	(.0261)	-.00167	(-.0509)	-.0242	(-.738)
.0758	.6441	.228	(3.327)	.01965	(.0266)	-.00134	(-.041)	.0484	(1.475)
.0568	.7104	.173	(2.525)	.01589	(.0215)	-.00134	(-.041)	.0594	(1.811)
.0568	.7672	.187	(2.729)	.01706	(.0231)	-.0140	(-.427)	.0594	(1.811)
.0379	.8145	.101	(1.474)	.00946	(.0128)	-.0140	(-.427)	-.0026	(-.079)
.0568	.8619	.151	(2.204)	.01473	(.0200)	-.0140	(-.427)	0.0	(0.0)
.0610	.9208	.265	(3.867)	.01979	(.0268)	-.0140	(-.427)	-.0132	(-4.02)
.0246	.9636	.044	(0.642)	.003787	(.0051)	-.0051	(-1.32)	-.1584	(-4.828)
.0246	.9882	.022	(0.321)	.004869	(.0066)	-.2391	(-7.29)	-.4256)	(-12.942)

TABLE A.1 Continued

Δr/R	r/R	Flatwise Stiffness $EI_f \times 10^{-6}$		Edgewise Stiffness $EI_e \times 10^{-6}$		Torsional Stiffness $GJ \times 10^{-6}$		Chord C		Blade Twist θ1
		$Lb\text{-}in^2$	($kgf\text{-}cm^2$)	$Lb\text{-}in^2$	($kgf\text{-}cm^2$)	$LB\text{-}in^2$	($kgf\text{-}cm^2$)	Ft	(cm)	Deg
.0540	.0649	11.60	(33.95)	11.52	(33.71)	15.00	(43.90)	0.0	(0.0)	0.0
.0975	.1406	21.67	(63.42)	152.5	(446.3)	16.20	(47.41)	.777	(23.68)	2.04
.1136	.2462	9.69	(28.36)	232.7	(681.0)	11.30	(33.07)	1.304	(39.75)	4.45
.0758	.3409	7.36	(21.54)	232.5	(680.4)	9.02	(26.40)	1.304	(39.75)	4.09
.0758	.4167	5.99	(17.53)	232.1	(679.2)	7.55	(22.09)	1.304	(39.75)	3.33
.0758	.4925	5.40	(15.80)	225.5	(659.9)	7.0	(20.49)	1.304	(39.75)	2.58
.0758	.5693	5.40	(15.80)	225.5	(659.9)	7.0	(20.49)	1.304	(39.75)	1.82
.0758	.6441	5.40	(15.80)	225.5	(659.9)	7.0	(20.49)	1.304	(39.75)	1.06
.0568	.7104	5.67	(16.59)	248.0	(725.8)	7.133	(20.87)	1.304	(39.75)	.40
.0568	.7672	5.72	(16.74)	248.0	(725.8)	7.160	(20.95)	1.304	(39.75)	-.17
.0379	.8145	5.52	(16.15)	240.0	(702.3)	7.018	(20.54)	1.298	(39.56)	-.64
.0568	.8619	5.31	(15.54)	198.5	(580.9)	6.876	(20.12)	1.292	(39.37)	-1.12
.0610	.9208	5.27	(15.42)	207.4	(606.9)	6.810	(19.93)	1.292	(39.37)	-1.71
.0246	.9636	2.99	(8.75)	144.8	(423.7)	3.100	(9.07)	1.205	(36.73)	-2.13
.0246	.9882	1.09	(3.19	60.40	(176.8)	.979	(2.86)	.923	(28.13)	-2.38

TABLE A.1 Concluded

$\Delta r/R$	r/R	Distance From e.a. Fwd to C/4 (+ for C/4 Fwd)		Modulus Weighted Radius of Gyration About Elastic Axis $\left[\frac{1}{EA}\int y^2 EdA\right]^{1/2}$		Structural Area EA X 10^{-6}	
		Ft	(cm)	Ft	(cm)	Lb	(kgf)
.054	.0649	0.0	(0.0)	.0658	(2.006)	31.0	(14.1)
.0975	.1406	-.0042	(-.128)	.187	(5.700)	24.0	(10.9)
.1136	.2462	-.0216	(-.658)	.239	(7.285)	18.0	(8.2)
.0758	.3409	-.087	(-.570)	.239	(7.285)	18.0	(8.2)
.0758	.4167	-.0172	(-.524)	.239	(7.285)	18.0	(8.2)
.0758	.4925	-.017	(-.518)	.238	(7.285)	17.5	(7.9)
.0758	.5683	-.017	(-.518)	.238	(7.285)	17.5	(7.9)
.0758	.6441	-.017	(-.518)	.238	(7.285)	17.5	(7.9)
.0568	.7104	-.0448	(-1.366)	.244	(7.437)	19.0	(8.6)
.0568	.7672	-.0448	(-1.366)	.244	(7.437)	19.0	(8.6)
.0379	.8145	-.042	(-1.280	.255	(7.772)	19.0	(8.6)
.0568	.8619	-0.398	(-1.218)	.267	(8.137)	19.0	(8.6)
.0610	.9208	-.0398	(-1.213)	.267	(8.137)	19.0	(8.6)
.0246	.9636	-.1584	(-4.828)	.285	(8.687)	12.0	(5.4)
.0246	.9882	-.4246	(-12.942)	.231	(7.041)	8.0	(3.6)

Table A.2 Miscellaneous Blade and Control System Properties

Item	Units	Quantity	
Blade Mass	Slugs (kg)	3.04	(44.37)
Blade First Moment of Inertia about Lag Hinge	Slug-Ft (kg-m)	29.08	(129.35)
Blade Second Moment of Inertia about Flap Hinge	Slug-Ft^2 (kg-m^2)	408.67	(554.08)
Elastomeric Hinge Flap and Hinge Spring Constant	Ft-Lb/Rad. (m-kgf/Rad.)	1192.0	(164.80)
Effective Control System Stiffness	Ft-Lb/Rad. (m-kgf/Rad.)	23600.0	(3262.82)
Elastomeric Hinge Bearing Torsional Stiffness	Ft-Lb/Rad. (m-kgf/Rad.)	683.0	(94.93)
Collective Pitch for Zero Static Elastomeric Hinge Torsion	Deg.	7.0	
Structural Damping (bending and torsion)	%	3.0	
Radius	Ft (m)	22.0	(6.71)
Flap and Lag Hinge Offset	Ft (cm)	.8333	(25.40)
Aerodynamic Root Cutout	Ft (cm)	3.67	(111.86)

APPENDIX B

Table B.1 ATRS Full Scale Model Blade Swept Tapered and Alternate Tips Structural and Mass Properties

ITEM	QUANTITY							
Tip Configuration	Swept Tapered		Trapezoidal		Swept Untapered		Rectangular	
Segment r/R	.9636	.9882	.9636	.9882	.9636	.9882	.9636	.9882
Segment Δr/R	.0246	.0246	.0246	.0246	.0246	.0246	.0246	.0246
Segment Mass, slugs	.044	.022	.049	.014	.050	.025	.058	.022
(kg)	(.642)	(.321)	(.715)	(.204)	(.730)	(.365)	(.846)	(.321)
Segment Torsional Inertia, Slug-ft^2	.00379	.00487	.0038	.0011	.0054	.0097	.0048	.0043
(kg-m^2)	(.0051)	(.0066)	(.0052)	(.0015)	(.0073)	(.0132)	(.0065)	(.01058)
Centroid Distance Forward of Elastic Axis, ft	-.0433	-.2391	-.0141	-.0141	-.0308	-.165	-.0132	-.0132
(cm)	(1.320)	(-7.288)	(-.430)	(-.430)	(-.939)	(-5.029)	(-.402)	(-.402)
Center of Gravity Distance Forward of Elastic Axis, ft	-.1584	-.4246	-.202	-.1496	-.2926	-.4708	-.209	-.209
(cm)	(-4.828)	(-12.942)	(-6.157)	(-4.560)	(-8.918)	(-14.350)	(-6.370)	(-.6370)
Chord, ft	1.205	.923	1.205	.923	1.292	1.292	1.292	1.292
(cm)	(36.728)	(28.133)	(36.728)	(28.133)	(39.380)	(39.380)	(39.380)	(39.380)
Quarter Chord Distance Forward of Elastic Axis, ft	-.055	-.3608	0.0	0.0	-.0374	-.2464	0.0	0.0
(cm)	(-1.676)	(-10.997)			(-1.140)	(-7.510)		

Table B.1 Concluded

ITEM	QUANTITY			
Tip Configuration	Swept Tapered	Trapezoidal	Swept Untapered	Rectangular
Total Tip Mass, slugs	.066	.063	.075	.080
(kg)	(.963)	(.919)	(1.095)	(1.168)
Total Tip Chordwise Mass Moment, Slug-ft, + fwd (kg-m)	-.0163 (-.0725)	-.0119 (-.0529)	-.0264 (-.1174)	-.0167 (-.0743)
Total Tip Moment of Inertia, Slug-ft^2	.00856	.0049	.0151	.0086
(kg-m^2)	(.0116)	(.0066)	(.0205)	(.0117)
Tip Outboard Chord/Inboard Chord	.6	.6	1.0	1.0
Tip Leading Edge Sweep (deg)	35.0	6.9	20.0	0.0
Tip Quarter Chord Sweep (deg)	30.0	0.0	20.0	0.0
Tip Trailing Edge Sweep (deg)	10.0	-19.9	20.0	0.0

APPENDIX C

1/5 Scale Model Blade and Mass Properties (Converted to Full Scale Values)

In the following table, the blade is represented as a series of 15 radial segments arranged from the coincident flap-lag hinge outboard. The radial length of each segment (Δr) is given nondimensionalized by rotor radius (R). The radius (r) of the midpoint of each segment is also given nondimensionalized by rotor radius. The segment mass is the total mass of the segment.

The other properties represent average values for the segment. The elastic axis-quarter chord offset is essentially zero.

Table C.1 Blade Segment Data

ΔR	r/R	Segment Mass		Center of Gravity Distance Fwd of C/4		Flatwise Stiffness $EI_F \times 10^{-6}$	
		Slugs	(kg)	Ft	(cm)	$Lb\text{-}in^2$	($kgf\text{-}cm^2$)
.054	.0649	.325	(4.743)	0.0	(0.0)	11.6	(33.94)
.0975	.1406	.562	(8.202)	-.046	(-1.40)	21.67	(63.41)
.1136	.2462	.360	(5.254)	-.089	(-2.71)	9.69	(28.35)
.0758	.3409	.235	(3.430)	-.089	(-2.71)	7.36	(21.54)
.0758	.4167	.252	(3.678)	-.089	(-2.71)	5.99	(17.53)
.0758	.4925	.280	(4.086)	.044	(1.34)	5.4	(15.80)
.0758	.5683	.272	(3.970)	.034	(1.04)	5.4	(15.80)
.0758	.6441	.243	(3.546)	.064	(1.95)	5.4	(15.80)
.0568	.7104	.184	(2.685)	.064	(1.95)	5.67	(16.59)
.0568	.7672	.183	(2.671)	.064	(1.95)	5.72	(16.74)
.0379	.8145	.122	(1.780)	.064	(1.95)	5.52	(16.15)
.0568	.8619	.182	(2.656)	.064	(1.95)	5.31	(15.54)
.0619	.9208	.368	(5.371)	.110	(3.35)	5.27	(15.42)
.0246	.9636	.090	(1.313)	-.159	(-4.85)	2.99	(8.75)
.0246	.9882	.028	(0.409)	-.188	(-5.73)	1.09	(3.19)

Table C.1 Concluded

ΔR	r/R	Edgewise Stiffness $EI_e \times 10^{-6}$ Lb-In^2	(kgf-cm^2)	Torsional Stiffness $GJ \times 10^{-6}$ Lb-In^2	(kgf-cm^2)
.054	.0649	11.519	(33.70)	15.00	(43.89)
.0975	.1406	152.52	(446.27)	16.20	(47.40)
.1136	.2462	155.0	(453.53)	11.30	(33.06)
.0758	.3409	152.0	(444.75)	9.02	(26.39)
.0758	.4167	152.0	(444.75)	7.55	(22.09)
.0758	.4925	152.0	(444.75)	7.00	(20.48)
.0758	.5683	152.0	(444.75)	7.00	(20.48)
.0758	.6441	152.0	(444.75)	7.00	(20.40
.0568	.7104	152.0	(444.75)	7.13	(20.86)
.0568	.7672	152.0	(444.75)	7.16	(20.95)
.0379	.8145	152.0	(444.75)	7.01	(20.51)
.0568	.8619	152.0	(444.75)	6.88	(20.13)
.0610	.9208	207.35	(606.71)	6.81	(19.93)
.0246	.9636	144.83	(423.77)	22.0	(64.37)
.0246	.9882	100.0	(292.60)	.98	(2.87)

APPENDIX D

Miscellaneous ATRS Rotor Head and Aircraft Physical Properties

Table D.1 Main Rotor Properties

ITEM	UNITS	QUANTITY
Direction of Rotation		Forward Blade From Starboard to Port
Number of Blades		4
Rotor Solidity		.0748
Typical Equivalent Viscous Lag Hinge Damping	Ft-lb-sec (m-kgf-sec)	2000. (276.6)
Radial Station of Damper Outboard End	Ft (m)	2.133 (.650)
Distance of Damper Outboard End Aft of Feathering Axis	Ft (m)	.417 (.127)
Radial Station of Damper Inboard End	Ft (m)	.766 (.233)
Distance of Damper Inbord End Aft of Feathering Axis	Ft (m)	.557 (.170)
Collective Pitch for Feathering and Damper Axis Coplanar with 6° Coning	Deg	-2.0
Blade pushrod Horn Length	Ft (m)	.542 (.165)
Radial Position of Blade Pushrod at Horn	Ft (m)	1.137 (.347)
Radial Position of Blade Pushrod at Swashplate	Ft (m)	1.219 (.372)
Blade Pushrod Length	Ft (m)	1.167 (.356)
Collective Pitch ($\theta_{.75}$) for Horizontal Pitch Horn	Deg	20.
Blade Lag Angle for Coplanar Blade Pushrod and Rotor Shaft	Deg	13.0
Radial Position of Stationary Pushrods	Ft (m)	.7083 (.216)
Azimuth Position of FLSS Pushrod	Deg	60.6
Azimuth Position of ALSS Pushrod	Deg	241.0
Azimuth Position of LSS Pushrod	Deg	331.0
See Figure 7 for Blade Natural Frequencies		

APPENDIX D CONTINUED

Table D.2 Tail Rotor Properties

ITEM	UNITS	QUANTITY
Number of Blades		4
Direction of Rotation		Top Blade Aft
Radius	Ft (m)	4.0 (1.219)
Aerodynamic Root Cut Out (Blade)	Ft (m)	1.0 (.305)
Blade Chord at 75% Radius	Ft (m)	.542 (.165)
Nominal Blade Twist	Deg	-8^{o}

Table D.3 Main Rotor/Tail Rotor Locations

ITEM	UNITS	QUANTITY
Main Rotor Station	Inches (cm)	200. (508)
Main Rotor Waterline	Inches (cm)	157. (399)
Main Rotor Buttline	Inches (cm)	0.
Tail Rotor Station	Inches (cm)	518. (1316)
Tail Rotor Waterline	Inches (cm)	162.88 (414)
Tail Rotor Buttline	Inches (cm)	19. (48)
Main Rotor Built-in Shaft Angle	Deg	5.0
Tail Rotor Built-in Cant Angle	Deg	0.
Main Rotor/Tail Rotor Gear Ratio		.182

APPENDIX D CONCLUDED

Table D.4 Flight Test Vehicle Inertia and C.G. Location Data

Gross Weight		I_{Roll}		I_{Pitch}		I_{Yaw}	
lb	(kg)	lb-in-sec^2	(kgf-cm-sec^2)	lb-in-sec^2	(kgf-cm-sec^2)	lb-in-sec^2	(kgf-cm-sec^2)
8200	(3719.5)	26800	(30877)	156000	(179731)	141000	(162450)
10300	(4672)	33000	(38020)	168000	(193557)	146000	(168210)
10300	(4672)	33900	(39057)	183000	(210839)	166000	(191253)

Gross Weight		C.G.$_{Station}$		C.G.$_{Waterline}$		C.G.$_{Buttline}$
lb	(kg)	Inches	(cm)	Inches	(cm)	Inches
8200	(3719.5)	210	(533)	93.7	(238)	0
10300	(4672)	210	(533)	90.8	(231)	0
10300	(4672)	197	(500)	89.8	(228)	0

APPENDIX D CONCLUDED

Table D.5 Damper Force Versus Damper Stroke Velocity

Force		Stroke Velocity	
lb	(kgf)	in/sec	(cm/sec)
35	(15.9)	.1	(.254)
100	(45.4)	.2	(.508)
220	(99.8)	.3	(.762)
400	(181.4)	.4	(1.016)
610	(276.7)	.5	(1.270)
950	(430.9)	.6	(1.524)
1280	(580.6)	.7	(1.778)
1500	(6803.9)	.76	(1.930)
1500	(6803.9)	3.0	(7.620)

APPENDIX E

Airfoil Section Aerodynamic Characteristics

Full scale section characteristics for the SC-1095 and SC-1095R8 airfoils are presented in Tables E1 and E2 of this appendix. These data were obtained from two-dimensional steady tests conducted in the 8 ft. octagonal cross section wind tunnel at United Technology Research Center during 1975. Data was obtained using the Sikorsky Tunnel Spanning apparatus. This test technique uses a tunnel spanning airfoil that isolates a 8-inch span metric section at the spanwise mid point. Forces and moments on this section are measured with an internal balance system. In addition, upper and lower surface pressure taps provide an independent measure of section lift and pitching moment. Also, a wake rake is used to determine section drag prior to divergence. The angle-of-attack is referenced to the airfoil section's chordline. The airfoil moments are resolved about the quarter chord position.

Model scale section coefficients for the SC-1095 and SC-1095R8 airfoils are presented in Tables E3 and E4 respectively. Supporting tests for this data was obtained in the NASA Langley 6" x 28" variable density tunnel during 1977. Use of the variable density facility permitted data to be obtained at both high Reynolds numbers representative of full scale rotor and reduced Reynolds numbers applicable to the 1/5th scale model rotor. The Langley results were analyzed to define incremental changes in section lift and drag coefficients that were applied to the baseline full scale data obtained at the United Technologies Research Center. This approach was adapted to reflect Reynolds number changes in the section characteristics without introducing bias due to a change in the test facility and procedures. It should be noted that no Reynolds number corrections were applied to the pitching moment coefficient data. This decision was based on a Reynolds number insensitivity noted in the Langley data.

Table E.1 - Aerodynamic coefficients for full scale airfoil section SC1095

```
CLDAT
 ** SC1095 .5 TAB -3 DEF. LIFT BASED ON 1975 TSR TESTS **
 ALPHA       CL
NPTS  #23.    MACH #0.0          THICK #.095
 -180.     0.        -172.     .78       -160.      .64       -150.     .95
-30.0     -1.0      -10.0     -.88      -8.0      -.76      -6.0      -.6
-5.0      -.50      -3.0      -.30      9.4       1.11      10.3      1.18
11.0      1.21      11.8      1.21      12.6      1.17      16.0      .95
 30.       1.        150.      -.95      156.      -.70      158.      -.66
 160.      -.64      172.      -.78      180.      0.
NPTS  #23.    MACH #0.3          THICK #.095
 -180.     0.        -172.     .78       -160.      .64       -150.     .95
-30.0     -1.0      -10.0     -.88      -8.0      -.76      -6.0      -.6
-5.0      -.50      -3.0      -.30      9.4       1.11      10.3      1.18
11.0      1.21      11.8      1.21      12.6      1.17      16.0      .95
 30.       1.        150.      -.95      156.      -.70      158.      -.66
 160.      -.64      172.      -.78      180.      0.
NPTS  #13.    MACH #0.4          THICK #.095
-30.0     -1.0      -10.0     -.58      -8.0      -.64      -6.5      -.61
-5.0      -.52      -3.6      -.4       8.4       1.07      9.4       1.16
10.5      1.2       11.5      1.17      13.5      1.04      16.0      .96
30.0      1.0
NPTS  #13.    MACH #0.5          THICK #.095
-30.0     -1.0      -10.0     -.72      -8.0      -.72      -6.5      -.66
-5.0      -.55      -3.5      -.4       6.0       .84       7.5       1.0
8.8       1.07      9.8       1.08      11.5      1.06      16.0      1.1
30.0      1.0
NPTS  #12.    MACH #0.6          THICK #.095
-30.0     -1.0      -10.0     -.54      -8.0      -.59      -6.4      -.62
-5.0      -.58      -3.6      -.44      5.0       .79       6.0       .86
7.5       .90       10.0      .95       15.0      1.09      30.0      1.0
NPTS  #12.    MACH #0.7          THICK #.095
-30.0     -1.0      -10.0     -.66      -7.0      -.74      -6.0      -.74
-5.0      -.72      -4.0      -.60      4.0       .75       4.8       .80
6.0       .83       9.0       .89       15.0      1.03      30.0      1.0
NPTS  #11.    MACH #0.75         THICK #.095
-30.0     -1.0      -10.0     -.72      -6.0      -.73      -5.0      -.72
-4.0      -.65      -2.5      -.45      2.3       .54       2.9       .63
3.8       .70       15.0      .93       30.0      1.0
NPTS  # 14   MACH  #     .8000   THICK #      .0950
  -30.0     -.95      -14.0     -.80      -12.0     -.79      -10.0     -.81
   -6.0    -0.690      -2.0    -0.250      0.0     0.070       2.0     0.350
    4.0     0.560       6.0     0.705      8.0     0.805       9.0     0.840
   15.0     0.85       30.0     1.0
NPTS  # 14   MACH  #     .850    THICK #      .095
  -30.0     -.95      -16.0     -.803     -13.0     -.772     -10.0     -.74
   -6.0    -0.680      -2.0    -0.290      0.0    -0.045       2.0     0.230
    4.0     0.460       6.0     0.640      8.0     0.760       9.0     0.802
   15.0     .85        30.0     1.0
NPTS  # 14   MACH  #     .9000   THICK #      .0950
  -30.0     -.95      -16.0     -.754     -13.0     -.712     -10.0     -.67
   -6.0    -0.663      -2.0    -0.310      0.0    -0.150       1.0     0.000
    2.0     0.133       4.0     0.390      6.0     0.640       8.0     0.765
   10.0     .81        30.0     1.0
NPTS  # 13   MACH  #     .950    THICK #     .095
  -30.0     -.95      -16.0     -.741     -13.0     -.696     -10.0     -.651
   -6.0    -0.641      -2.0    -0.270      0.0    -0.090       2.0     0.180
    4.0     0.435       6.0     0.680      8.0     0.795      10.0     0.810
   30.0     1.0
NPTS  # 13   MACH  #     1.0     THICK #     .095
  -30.0    -.9500     -16.0     -.726     -13.0     -.6780    -10.0     -.630
   -6.0    -.6150      -2.0     -.2400     0.0     -.0500      2.0      .200
    4.0     .4490       6.0     .7000      8.0      .8060     10.0      .850
   30.0     1.0
NPTS  # 13   MACH  #     2.0     THICK #     .095
  -30.0    -.9500     -16.0     -.7260    -13.0     -.6780    -10.0     -.630
   -6.0    -.6150      -2.0     -.2400     0.0     -.0500      2.0      .200
    4.0     .4490       6.0     .7000      8.0      .8060     10.0      .850
   30.0     1.0
```

Table E.1 - continued

```
CDDAT
 ** SC1095 .5 TAB -3 DEF. DRAG BASED ON 1975 TSR TESTS **
 ALPHA        CD
NPTS  #34.     MACH #0.0          THICK #.095
 -180.     .02      -179.     .025     -175.     .065     -172.     .11
 -150.     .642     -115.     1.88     -90.      2.08     -65.      1.88
-30.0     .63      -10.0     .21      -8.6      .059     -7.6      .03
-6.9      .016     -6.3      .012     -5.5      .0095    -4.0      .0085
0.0       .0083    4.0       .0095    7.5       .012     9.0       .015
10.0      .0185    10.8      .025     12.0      .056     15.0      .21
30.0      .63       30.1      .63      65.       1.88     65.1      1.88
 90.       2.08     150.      .64      172.      .11      175.      .065
 179.      .025     180.      .02
NPTS  #34.     MACH #0.3          THICK #.095
 -180.     .02      -179.     .025     -175.     .065     -172.     .11
 -150.     .642     -115.     1.88     -90.      2.08     -65.      1.88
-30.0     .63      -10.0     .21      -8.6      .059     -7.6      .03
-6.9      .016     -6.3      .012     -5.5      .0095    -4.0      .0085
0.0       .0083    4.0       .0095    7.5       .012     9.0       .015
10.0      .0185    10.8      .025     12.0      .056     15.0      .21
30.0      .63       30.1      .63      65.       1.88     65.1      1.88
 90.       2.08     150.      .64      172.      .11      175.      .065
 179.      .025     180.      .02
NPTS  #18.     MACH #0.4          THICK #.095
-30.0     .63      -10.0     .215     -7.2      .06      -6.6      .03
-6.2      .024     -5.4      .014     -4.8      .011     -3.8      .0085
0.0       .0083    4.0       .0083    6.0       .0105    8.0       .014
9.0       .017     9.8       .02      10.2      .027     10.6      .04
15.0      .220     30.0      .63
NPTS  #18.     MACH #0.5          THICK #.095
-30.0     .63      -10.0     .15      -8.0      .05      -6.7      .03
-5.7      .02      -5.5      .014     -4.8      .01      -3.8      .0085
0.0       .0083    3.0       .0085    4.5       .0095    5.8       .0125
7.0       .02      8.0       .03      9.00      .055     12.0      .160
15.0      .24      30.0      .63
NPTS  #16.     MACH #0.6          THICK #.095
-30.0     .63      -10.0     .16      -5.6      .036     -4.7      .021
-4.2      .015     -3.5      .012     -2.5      .009     -1.5      .0083
1.5       .0083    3.0       .0095    4.0       .012     4.8       .0175
5.6       .03      7.2       .07      15.0      .277     30.0      .63
NPTS  #14.     MACH #0.7          THICK #.095
-30.0     .63      -10.0     .21      -4.0      .039     -3.6      .028
-3.0      .02      -2.3      .013     -1.4      .009     0.0       .0083
.8        .0085    1.9       .009     2.5       .013     3.0       .02
15.0      .308     30.0      .63
NPTS  #14.     MACH #0.75         THICK #.095
-30.0     .63      -10.0     .185     -3.2      .03      -2.5      .02
-2.0      .015     -1.4      .011     -.5       .0085    .0        .0085
.6        .0095    1.2       .011     1.6       .016     2.0       .0225
15.0      .32      30.0      .63
NPTS  #20.     MACH #0.80         THICK #.095
 -30.0     .63      -12.0     .290     -10.0     .225     -8.0      .160
  -6.0     .100     -4.0      .065     -3.0      .0420    -2.0      .028
  -1.0     .021     -0.5      .019      0.0      .017      0.5      .020
   1.0     .025      2.0      .040      4.0      .090      6.0      .1280
   8.0     .1700    10.0      .225     12.0      .285     30.0      .63
NPTS  #17.     MACH #0.90         THICK #.095
 -30.0     .630     -12.0     .330     -10.0     .262     -8.0      .203
  -6.0     .149     -4.0      .115     -2.0      .066     -1.0      .055
   0.0     .050      1.0      .060      2.0      .080      4.0      .120
   6.0     .167      8.0      .210     10.0      .262     12.0      .3225
  30.0     .63
NPTS  #15.     MACH #1.00         THICK #.095
 -30.0     .630     -12.0     .370     -10.0     .297     -8.0      .248
  -6.      .202     -4.0      .152     -2.0      .117      0.0      .090
   2.      .1175     4.0      .1525     6.0      .203      8.0      .249
  10.      .298     12.0      .3630    30.0      .630
NPTS  #15.     MACH #2.00         THICK #.095
 -30.0     .630     -12.0     .362     -10.0     .297     -8.0      .248
  -6.0     .202     -4.0      .152     -2.0      .117      0.0      .090
   2.0     .1175     4.0      .1525     6.0      .203      8.0      .249
  10.0     .298     12.0      .3425    30.0      .630
```

Table E.1 - concluded

```
CMDAT
** SC1095 .5 TAB -3 DEF. MOMENT BASED ON 1975 TSR TESTS **
 ALPHA         CM
NPTS  #29.   MACH  #      .0000   THICK #     .0950
   -180.00   -.01300   -174.00    .35900   -160.00    .30000   -145.00    .48100
   -125.00    .55700    -90.00    .55500    -60.00    .39500    -30.00    .16500
 -30.0      .1437    -10.0      .0799     -8.0      -.0009     12.0      .0084
  16.0     -.1482     30.0     -.1437     30.1      -.1437     34.9      -.222
     35.00   -.22200     45.00   -.29500     60.00   -.39500     80.00   -.50000
     95.00   -.55500    110.00   -.56000    125.00   -.55700    135.00   -.53800
    145.00   -.48100    150.00   -.43800    160.00   -.30000    174.00   -.35900
    180.00   -.01300
NPTS  #29.   MACH  #      .3000   THICK #     .0950
   -180.00   -.01300   -174.00    .35900   -160.00    .30000   -145.00    .48100
   -125.00    .55700    -90.00    .55500    -60.00    .39500    -30.00    .16500
 -30.0      .1437    -10.0      .0799     -8.0      -.0009     12.0      .0084
  16.0     -.1482     30.0     -.1437     30.1      -.1437     34.9      -.222
     35.00   -.22200     45.00   -.29500     60.00   -.39500     80.00   -.50000
     95.00   -.55500    110.00   -.56000    125.00   -.55700    135.00   -.53800
    145.00   -.48100    150.00   -.43800    160.00   -.30000    174.00   -.35900
    180.00   -.01300
NPTS  #  9   MACH  #      .4000   THICK #     .0950
 -30.0      .1437    -10.0      .1364     -6.0      -.0009      6.0      .0052
  10.0      .0110     11.2     -.0039     12.4      -.0952     16.0     -.1329
  30.0     -.1437
NPTS  #  9   MACH  #      .5000   THICK #     .0950
 -30.0      .1437    -10.0      .1336     -6.0      -.0019      9.0      .0038
  10.0     -.0130     12.0     -.0860     14.0      -.1254     16.0     -.1548
  30.0     -.1437
NPTS  #  9   MACH  #      .6000   THICK #     .0950
 -30.0      .1437    -10.0      .0975     -5.0      -.0069      6.2      .0073
   7.4     -.0099     11.0     -.0879     13.2      -.1263     16.0     -.1549
  30.0     -.1437
NPTS  # 10   MACH  #      .7000   THICK #     .0950
 -30.0      .1437    -10.0      .0847     -6.0       .0834     -4.0     -.0134
   2.0      .0032      4.0     -.0132      6.0      -.0814      8.0     -.0954
  15.0     -.1560     30.0     -.1437
NPTS  # 10   MACH  #      .7500   THICK #     .0950
 -30.0      .1437    -10.0      .1235     -6.0       .1236     -2.8     -.0209
   1.4     -.0071      2.6     -.0319      4.0      -.0942      5.4     -.1135
  15.0     -.1581     30.0     -.1437
NPTS  #15.   MACH  #     .8       THICK # .095
    -30.00    .15000     -8.00    .07500     -6.00    .06000     -4.00    .03500
     -2.00   -.01200       .00   -.02000       .50   -.01500      1.00   -.01200
      1.50   -.01700      2.00   -.02900      4.00   -.07500      6.00   -.10000
      8.00   -.11500     18.00   -.13000     30.00   -.15000
NPTS  #17.   MACH  #     .9       THICK # .095
    -30.00    .14000     -8.00    .12000     -6.00    .09700     -4.00    .04300
     -2.00   -.01200       .00   -.02000       .10   -.00100       .25    .01200
       .50    .01700       .75    .00900      1.00   -.00700      1.50   -.03000
      2.00   -.03500      4.00   -.08300      6.00   -.13700      8.00   -.16000
     30.00   -.19000
NPTS  #17.   MACH  #     1.       THICK # .095
    -30.00    .14000     -8.00    .12000     -6.00    .09700     -4.00    .04300
     -2.00   -.01200       .00   -.02000       .10   -.00100       .25    .01200
       .50    .01700       .75    .00900      1.00   -.00700      1.50   -.0300
      2.00   -.03500      4.00   -.08300      6.00   -.13700      8.00   -.16000
     30.00   -.19000
NPTS  #17.   MACH  #     2.       THICK # .095
    -30.00    .14000     -8.00    .12000     -6.00    .09700     -4.00    .04300
     -2.00   -.01200       .00   -.02000       .10   -.00100       .25    .01200
       .50    .01700       .75    .00900      1.00   -.00700      1.50   -.03000
      2.00   -.03500      4.00   -.08300      6.00   -.13700      8.00   -.16000
     30.00   -.19000
```

Table E.2 - Aerodynamic coefficients for full scale airfoil section SC1095-R8

```
CLDAT2
 ** SC1095 R8 .5 TAB -3  LIFT BASED ON  1975 TSR TEST **
 ALPHA        CL
NPTS  #26.    MACH #0.0         THICK #0.09
 -180.     0.      -172.      .78       -160.      .64       -158.      .66
  -30.0     -1.0      -10.0    -.80      -7.5       -.73      -6.7       -.60
   -5.      -.44       5.       .74      10.        1.30      11.        1.38
   12.      1.44      13.      1.49      14.        1.53      15.2       1.21
   19.      1.08      30.      1.0       30.1       1.        149.9      -.95
 150.      -.95      156.      -.7      158.       -.66      160.       -.64
 172.      -.78      180.      0.
NPTS  #26.    MACH #0.3         THICK #0.09
 -180.     0.      -172.      .78      -160.       .64      -158.       .66
  -30.0     -1.0      -10.0    -.80      -7.5       -.73      -6.7       -.60
   -5.      -.44       5.       .74      10.        1.30      11.        1.38
   12.      1.44      13.      1.49      14.        1.53      15.2       1.21
   19.      1.08      30.      1.0       30.1       1.        149.9      -.95
 150.      -.95      156.      -.7      158.       -.66      160.       -.64
 172.      -.78      180.      0.
NPTS  #13.    MACH #0.4         THICK #0.09
 -30.0   -1.0     -10.0     -.74      -8.6       -.71      -7.0       -.64
   -5.      -.45       7.      1.04       8.        1.15       9.        1.22
   10.      1.27      11.2     1.29      12.        1.13      18.        1.12
   30.      1.0
NPTS  #14.    MACH #0.5         THICK #0.09
 -30.0   -1.0     -10.0     -.6       -8.5       -.66      -7.0       -.65
   -5.      -.47       6.       .93       7.        1.00       8.        1.04
    9.      1.06      10.      1.08      11.        1.09      12.        1.11
   16.      1.11      30.      1.0
NPTS  #18.    MACH #0.6         THICK #0.09
 -30.0   -1.0     -10.0     -.6       -7.0       -.6       -6.0       -.58
   -5.      -.50      -4.      -.36      -3.        -.24      -2.        -.12
   -1.      -.02       0.       .14       3.         .61       4.         .75
    5.       .84       6.       .90       7.         .92      14.        1.04
   15.      1.07      30.      1.0
NPTS  #15.    MACH #0.7         THICK #0.09
 -30.0   -1.0     -10.0     -.6       -7.0       -.6       -5.8       -.59
   -5.      -.55      -4.      -.44      -3.        -.31      -2.        -.17
    2.       .57       3.       .71       4.         .81       5.         .85
   9.4       .92      15.       .98      30.        1.0
NPTS  #15.    MACH #0.75        THICK #0.09
  -30.0     -1.0      -10.0     -.7       -6.5       -.7       -5.7       -.69
   -5.      -.65      -4.      -.54      -3.        -.38      -2.        -.2
   1.4       .55       2.       .63       3.         .70       4.         .74
   7.0       .83      15.       .95      30.        1.0
NPTS  # 14   MACH  #       .8000   THICK  #      .0900
  -30.0     -.95     -14.0     -.80     -12.0       -.79     -10.0      -.81
   -6.0   -0.690      -2.0    -0.250      0.0      0.070      2.0      0.350
    4.0    0.560       6.0     0.705      8.0      0.805      9.0      0.840
   15.0    0.85       30.0     1.0
NPTS  # 14   MACH  #       .850    THICK  #      .090
  -30.0     -.95     -16.0     -.803    -13.0      -.772     -10.0      -.74
   -6.0   -0.680      -2.0    -0.290      0.0     -0.045      2.0      0.230
    4.0    0.460       6.0     0.640      8.0      0.760      9.0      0.802
   15.0     .85       30.0     1.0
NPTS  # 14   MACH  #       .9000   THICK  #      .0900
  -30.0     -.95     -16.0     -.754    -13.0      -.712     -10.0      -.67
   -6.0   -0.663      -2.0    -0.310      0.0     -0.150      1.0      0.000
    2.0    0.138       4.0     0.390      6.0      0.640      8.0      0.765
   10.0     .81       30.0     1.0
NPTS  # 13   MACH  #       .950    THICK  #      .090
  -30.0     -.95     -16.0     -.741    -13.0      -.696     -10.0      -.651
   -6.0   -0.641      -2.0    -0.270      0.0     -0.090      2.0      0.180
    4.0    0.435       6.0     0.680      8.0      0.795     10.0      0.810
   30.0    1.0
NPTS  # 13   MACH  #      1.0      THICK  #      .090
  -30.0    -.9500    -16.0     -.726    -13.0      -.6780    -10.0      -.630
   -6.0    -.6150     -2.0     -.2400     0.0      -.0500      2.0       .200
    4.0     .4490      6.0      .7000     8.0       .8060     10.0       .850
   30.0    1.0
NPTS  # 13   MACH  #      2.0      THICK  #      .090
  -30.0    -.9500    -16.0     -.7260   -13.0      -.6780    -10.0      -.630
   -6.0    -.6150     -2.0     -.2400     0.0      -.0500      2.0       .200
    4.0     .4490      6.0      .7000     8.0       .8060     10.0       .850
   30.0    1.0
```

```
CDDAT2
 ** SC1095 R8 .5 TAB -3  DRAG BASED ON  1975 TSR TEST **
 ALPHA        CD
NPTS  #32.    MACH #0.0          THICK #0.09
 -180.     .02       -179.      .025      -175.      .065      -172.      .11
 -150.     .642      -115.     1.88        -65.     1.88        -30.      .63
-30.0     .63       -10.0       .25       -7.0      .086       -6.0      .05
  -5.6       .039      -4.8       .028       -4.       .018      -3.       .011
   0.        .009       4.        .010        9.       .013      10.       .014
  11.        .018      12.        .022       13.       .030      14.       .064
  16.3      .178      29.9      .63        30.       .63       65.      1.88
 150.       .642     172.       .110      175.       .065     180.       .02
NPTS  #32.    MACH #0.3          THICK #0.09
 -180.     .02       -179.      .025      -175.      .065      -172.      .11
 -150.     .642      -115.     1.88        -65.     1.88        -30.      .63
-30.0     .63       -10.0       .25       -7.0      .086       -6.0      .05
  -5.6       .039      -4.8       .028       -4.       .018      -3.       .011
   0.        .009       4.        .010        9.       .013      10.       .014
  11.        .018      12.        .022       13.       .030      14.       .064
  16.3      .178      29.9      .63        30.       .63       65.      1.88
 150.       .642     172.       .110      175.       .065     180.       .02
NPTS  #19.    MACH #0.4          THICK #0.09
-30.0     .63       -10.0       .26       -7.0      .101       -6.0      .062
  -5.        .034      -4.5       .020       -4.       .013      -3.       .010
  -2.        .008       1.        .008        3.       .009       6.       .011
   8.        .015       9.        .0175      10.       .027      11.       .050
  12.8       .136      15.        .23        30.       .63
NPTS  #19.    MACH #0.5          THICK #0.09
-30.0     .63       -10.0      .27        -7.0      .106       -6.0      .07
  -5.        .038      -4.        .024       -3.       .015      -2.       .010
  -1.        .0085      0.        .008        2.       .008       4.       .0095
   5.        .011       6.        .018        7.       .027       8.       .044
  12.        .178      15.        .28        30.       .63
NPTS  #20.    MACH #0.6          THICK #0.09
-30.0     .63       -10.0      .268       -8.0      .137       -6.0      .081
  -5.        .045      -4.6       .035       -4.       .025      -3.       .017
  -2.        .012      -1.        .0085       0.       .008       1.       .008
   2.        .010       3.        .016        4.       .025       5.       .038
   6.        .060      10.5       .176       15.       .3        30.      .63
NPTS  #14.    MACH #0.7          THICK #0.09
 -30.0     .63       -10.0      .31        -7.0      .155       -6.0      .094
  -5.        .060      -3.        .027       -2.       .013      -1.       .010
   0.        .010       1.        .0115       2.       .025       8.       .160
  15.        .32       30.        .63
NPTS  #15.    MACH #0.75         THICK #0.09
 -30.0     .63        -10.0     .326       -7.0      .168       -6.0      .109
  -5.        .085      -2.4      .020       -2.        .015      -1.       .012
   0.        .0135      1.       .024        4.        .095       6.       .134
   7.2       .155      15.       .33        30.        .63
NPTS  #20.    MACH #0.80         THICK #.090
 -30.0     .63       -12.0      .290      -10.0      .225       -8.0      .170
  -6.0     .122       -4.0      .075       -3.0      .0420      -2.0      .023
  -1.0     .026       -0.5      .0255       0.0      .025        0.5      .035
   1.0     .042        2.0      .070        4.0      .108        6.0      .1480
   8.0     .1850      10.0      .230       12.0      .285       30.0      .63
NPTS  #17.    MACH #0.90         THICK #.090
 -30.0     .630      -12.0      .330      -10.0      .262       -8.0      .210
  -6.0     .163       -4.0      .115       -2.0      .066       -1.0      .063
   0.0     .060        1.0      .078        2.0      .100        4.0      .138
   6.0     .182        8.0      .221       10.0      .262       12.0      .3225
  30.0     .63
NPTS  #15.    MACH #1.00         THICK #.090
 -30.0     .630      -12.0      .370      -10.0      .297       -8.0      .248
  -6.      .202       -4.0      .152       -2.0      .117        0.0      .100
   2.      .1360       4.0      .1700       6.0      .215        8.0      .255
  10.      .298       12.0      .3630      30.0      .630
NPTS  #15.    MACH #2.00         THICK #.090
 -30.0     .630      -12.0      .362      -10.0      .297       -8.0      .248
  -6.0     .202       -4.0      .152       -2.0      .117        0.0      .100
   2.0     .1360       4.0      .1700       6.0      .215        8.0      .255
  10.0     .298       12.0      .3425      30.0      .630
```

Table E.2 - concluded

```
CMDAT2
  ** SC1095 R8 .5 TAB -3  MOMENT BASED ON 1975 TSR TEST **
 ALPHA         CM
NPTS  #33.   MACH  #      .0000   THICK #      .0900
   -180.00   -.01300   -174.00    .35900   -160.00    .30000   -145.00    .48100
   -125.00    .55700    -90.00    .55500    -60.00    .39500    -30.00    .16500
 -30.0       .1437    -10.0      .1065     -7.4       .0989     -6.4      .0052
  -5.0       .0032      4.0      .0019     14.0       .0135     15.2     -.0932
  19.0      -.1303     30.0     -.1437     30.1      -.1437     34.9     -.222
     35.00   -.22200     45.00   -.29500     60.00   -.39500     80.00   -.50000
     95.00   -.55500    110.00   -.56000    125.00   -.55700    135.00   -.53800
    145.00   -.48100    150.00   -.43800    160.00   -.30000    174.00   -.35900
    180.00   -.01300
NPTS  #33.   MACH  #      .3000   THICK #      .0900
   -180.00   -.01300   -174.00    .35900   -160.00    .30000   -145.00    .48100
   -125.00    .55700    -90.00    .55500    -60.00    .39500    -30.00    .16500
 -30.0       .1437    -10.0      .1065     -7.4       .0989     -6.4      .0052
  -5.0       .0032      4.0      .0019     14.0       .0135     15.2     -.0932
  19.0      -.1303     30.0     -.1437     30.1      -.1437     34.9     -.222
     35.00   -.22200     45.00   -.29500     60.00   -.39500     80.00   -.50000
     95.00   -.55500    110.00   -.56000    125.00   -.55700    135.00   -.53800
    145.00   -.48100    150.00   -.43800    160.00   -.30000    174.00   -.35900
    180.00   -.01300
NPTS  # 10   MACH  #      .4000   THICK #      .0900
 -30.0       .1437    -10.0      .1427     -7.0       .1356     -6.0      .0038
  -5.0       .0019      8.0      .0124     11.2       .0115     12.2     -.1299
  18.0      -.1341     30.0     -.1437
NPTS  #  9   MACH  #      .5000   THICK #      .0900
 -30.0       .1437    -10.0      .1108     -9.0       .0952     -7.0      .0483
  -5.0       .0045      8.0      .0031     12.0      -.0800     16.0     -.1293
  30.0      -.1437
NPTS  # 11   MACH  #      .6000   THICK #      .0900
 -30.0       .1437    -25.0      .1267    -20.0       .1047    -15.0      .0878
 -10.0       .0707     -3.0     -.0004      5.0       .0087      8.0     -.0490
  13.0      -.1415     15.0     -.1352     30.0      -.1437
NPTS  # 15   MACH  #      .7000   THICK #      .0900
 -30.0       .1437    -25.0      .1416    -20.0       .1397    -15.0      .1327
 -10.0       .1306     -3.0     -.0119       .0      -.0025      1.0     -.0064
   2.0      -.0073      3.0     -.0241      4.0      -.0569      6.0     -.1105
   8.0      -.1347     15.0     -.1470     30.0      -.1437
NPTS  # 18   MACH  #      .7500   THICK #      .0900
 -30.0       .1437    -25.0      .1361    -20.0       .1335    -15.0      .1260
 -10.0       .1234     -8.0      .1039     -6.0       .0544     -4.0     -.0291
  -3.0      -.0335     -2.0     -.0245       .0      -.0146      1.0     -.0197
   2.0      -.0459      3.0     -.0943      4.0      -.1154      5.0     -.1177
  15.0      -.1526     30.0     -.1437
NPTS  #15.   MACH  #     .8       THICK #.090
    -30.00    .15000     -8.00    .07500     -6.00    .06000     -4.00    .03500
     -2.00   -.01200       .00   -.02000       .50   -.01500      1.00   -.01200
      1.50   -.01700      2.00   -.02900      4.00   -.07500      6.00   -.10000
      8.00   -.11500     18.00   -.13000     30.00   -.15000
NPTS  #17.   MACH  #     .9       THICK #.090
    -30.00    .14000     -8.00    .12000     -6.00    .09700     -4.00    .04300
     -2.00   -.01200       .00   -.02000       .10   -.00100       .25    .01200
       .50    .01700       .75    .00900      1.00   -.00700      1.50   -.03000
      2.00   -.03500      4.00   -.08300      6.00   -.13700      8.00   -.16000
     30.00   -.19000
NPTS  #17.   MACH  #    1.        THICK #.090
    -30.00    .14000     -8.00    .12000     -6.00    .09700     -4.00    .04300
     -2.00   -.01200       .00   -.02000       .10   -.00100       .25    .01200
       .50    .01700       .75    .00900      1.00   -.00700      1.50   -.0300
      2.00   -.03500      4.00   -.08300      6.00   -.13700      8.00   -.16000
     30.00   -.19000
NPTS  #17.   MACH  #    2.        THICK #.090
    -30.00    .14000     -8.00    .12000     -6.00    .09700     -4.00    .04300
     -2.00   -.01200       .00   -.02000       .10   -.00100       .25    .01200
       .50    .01700       .75    .00900      1.00   -.00700      1.50   -.03000
      2.00   -.03500      4.00   -.08300      6.00   -.13700      8.00   -.16000
     30.00   -.19000
```

Table E.3 - Aerodynamic coefficients for model scale airfoil section SC1095

CLDAT 109501
** SC1095-75T CL DATA ** MODEL SCALE ** 1975 TESTS
ALPHA CL

NPTS	#27.	MACH	#0.0	THICK	#0.095		
-180.	0.	-172.	.78	-160.	.64	-158.	.66
-150.	.95	-30.	-1.	-20.	-.975	-15.	-.96
-14.	-1.07	-9.	-.19	-7.	-.3	-6.	-.39
-5.5	-.45	-5.	-.45	-4.	-.4	11.	1.21
12.	1.25	12.5	1.23	13.	1.16	16.	.98
30.	1.	150.	-.95	156.	-.70	158.	-.66
160.	-.64	172.	-.78	180.	0.		
NPTS	#27.	MACH	#0.3	THICK	#0.095		
-180.	0.	-172.	.78	-160.	.64	-158.	.66
-150.	.95	-30.	-1.	-20.	-.975	-15.	-.96
-14.	-1.07	-9.	-.19	-7.	-.3	-6.	-.39
-5.5	-.45	-5.	-.45	-4.	-.4	11.	1.21
12.	1.25	12.5	1.23	13.	1.16	16.	.98
30.	1.	150.	-.95	156.	-.70	158.	-.66
160.	-.64	172.	-.78	180.	0.		
NPTS	17.	MACH	0.4	THICK	0.095		
-30.	-.95	-25.	-.96	-15.	-.97	-10.	-.24
-8.	-.3	-7.	-.35	-6.	-.44	-5.	-.45
-4.	-.42	9.	1.1	10.	1.17	11.	1.19
12.	1.13	13.	1.06	14.	1.03	16.	.96
30.	1.						
NPTS	24.	MACH	0.5	THICK	0.095		
-30.	-.95	-25.	-.92	-15.	-.94	-11.	-.39
-10.	-.4	-9.	-.39	-8.	-.33	-7.	-.29
-6.	-.32	-5.	-.32	-4.	-.44	6.	.78
7.	.89	8.	.96	9.	1.	10.	1.01
11.	.99	12.	.96	13.	1.03	14.	1.07
15.	1.08	16.	1.06	18.	1.07	30.	1.
NPTS	16.	MACH	0.6	THICK	0.095		
-30.	-.95	-25.	-.94	-15.	-.92	-13.	-.69
-12.	-.66	-11.	-.62	-10.	-.61	-9.	-.57
-8.	-.55	-7.	-.53	-6.	-.52	-5.	-.5
-4.	-.47	5.	.75	6.39	.938	30.	.938
NPTS	12.	MACH	0.7	THICK	0.095		
-30.	-.95	-25.	-.935	-15.	-.905	-10.	-.78
-9.	-.75	-8.	-.74	-6.	-.68	-5.	-.66
-4.	-.58	4.41	.79	15.	.79	30.	.79
NPTS	9.	. MACH	0.75	THICK	0.095		
-30.	-.95	-15.	-.93	-8.	-.75	-4.	-.6
-2.	-.34	2.	.47	3.38	.75	4.	.75
30.	.75						
NPTS	14.	MACH	0.80	THICK	0.095		
-30.0	-.95	-14.0	-.80	-12.0	-.79	-10.0	-.81
-6.0	-0.690	-2.0	-0.250	0.0	0.070	2.0	0.350
4.0	0.560	6.0	0.705	8.0	0.805	9.0	0.840
15.0	0.85	30.0	.86				
NPTS	14.	MACH	0.85	THICK	0.095		
-30.0	-.95	-16.0	-.803	-13.0	-.772	-10.0	-.74
-6.0	-0.680	-2.0	-0.290	0.0	-0.045	2.0	0.230
4.0	0.460	6.0	0.640	8.0	0.760	9.0	0.802
15.0	.85	30.0	.86				
NPTS	14.	MACH	0.90	THICK	0.095		
-30.0	-.95	-16.0	-.754	-13.0	-.712	-10.0	-.67
-6.0	-0.663	-2.0	-0.310	0.0	-0.150	1.0	0.000
2.0	0.138	4.0	0.390	6.0	0.640	8.0	0.765
10.0	.81	30.0	.86				
NPTS	13.	MACH	0.95	THICK	0.095		
-30.0	-.95	-16.0	-.741	-13.0	-.696	-10.0	-.651
-6.0	-0.641	-2.0	-0.270	0.0	-0.090	2.0	0.180
4.0	0.435	6.0	0.680	8.0	0.795	10.0	0.810
30.0	.86						
NPTS	13.	MACH	1.00	THICK	0.095		
-30.0	-.9500	-16.0	-.726	-13.0	-.6780	-10.0	-.630
-6.0	-.6150	-2.0	-.2400	0.0	-.0500	2.0	.200
4.0	.4490	6.0	.7000	8.0	.8060	10.0	.850
30.0	.86						
NPTS	13.	MACH	2.00	THICK	0.095		
-30.0	-.9500	-16.0	-.7260	-13.0	-.6780	-10.0	-.630
-6.0	-.6150	-2.0	-.2400	0.0	-.0500	2.0	.200
4.0	.4490	6.0	.7000	8.0	.8060	10.0	.850
30.0	.86						

Table E.3 - continued

```
CDDAT  109502
 ** SC1095-75T CDDATA ** MODEL SCALE ** 1975 TESTS
 ALPHA                        CD
NPTS   34.   MACH    0.0         THICK  0.095
 -180.     .0222     -179.     .0272    -175.      .0672    -172.      .1122
 -150.     .6442     -115.    1.8822     -90.     2.0822     -65.     1.8822
  -30.     .6322      -13.     .0240     -12.      .0196     -10.      .0137
   -8.     .0102       -4.     .0097       0.      .0097       2.      .0102
    4.     .0107        6.     .0112       8.      .0132       9.      .0152
   10.     .0192       11.     .0222      12.      .0282      13.      .0922
   14.     .1472       15.     .1872      30.      .6322      65.     1.8822
   90.    2.0822      150.     .6422     172.      .1122     175.      .0672
  179.     .0272      180.     .0222
NPTS   34.   MACH    0.3         THICK  0.095
 -180.     .0222     -179.     .0272    -175.      .0672    -172.      .1122
 -150.     .6442     -115.    1.8822     -90.     2.0822     -65.     1.8822
  -30.     .6322      -13.     .0240     -12.      .0196     -10.      .0137
   -8.     .0104       -4.     .0097       0.      .0097       2.      .0102
    4.     .0107        6.     .0112       8.      .0132       9.      .0152
   10.     .0192       11.     .0222      12.      .0282      13.      .0922
   14.     .1472       15.     .1872      30.      .6322      65.     1.8822
   90.    2.0822      150.     .6422     172.      .1122     175.      .0672
  179.     .0272      180.     .0222
NPTS   19.   MACH    0.4         THICK  0.095
  -30.     .6322      -14.     .1492     -13.      .1782     -12.      .0247
  -11.     .0182      -10.     .0154      -8.      .0117      -6.      .0107
   -4.     .0102        0.     .0102       4.      .0107       6.      .0127
    8.     .0162        9.     .0182      10.      .0232      11.      .0592
   13.     .1322       15.     .1992      30.      .6322
NPTS   20.   MACH    0.5         THICK  0.095
  -30.     .6322      -13.     .1572     -12.      .1222     -10.      .0702
   -9.     .0422       -8.     .0228      -7.      .0127      -4.      .0102
   -2.     .0097        2.     .0097       4.      .0102       5.      .0107
    6.     .0132        7.     .0182       8.      .0282       9.      .0482
   10.     .0822       12.     .1552      13.      .1882      30.      .6322
NPTS   23.   MACH    0.6         THICK  0.095
  -30.     .6322      -20.     .3622     -17.      .3122     -14.      .2482
  -12.     .1932      -10.     .1292      -9.      .0972      -8.      .0722
   -7.     .0522       -6.     .0282      -4.      .0147      -3.      .0117
   -2.     .0107        2.     .0097       3.      .0107       4.      .0132
    5.     .0172        6.     .0312       9.      .0992      12.      .1822
   17.     .3122       20.     .3622      30.      .6322
NPTS   19.   MACH    0.7         THICK  0.095
  -30.     .6322      -12.     .2452     -10.      .1792      -8.      .1152
   -6.     .0622       -4.     .0322      -3.      .0192      -2.      .0142
   -1.     .0107        0.     .0102       1.      .0107       2.      .0127
    3.     .0182        4.     .0382       8.      .1282       9.      .1472
   10.     .1642       12.     .2402      30.      .6322
NPTS   17.   MACH    0.75        THICK  0.095
  -30.     .6322      -12.     .2698     -10.      .2042      -8.      .1402
   -6.     .0822       -4.     .0472      -3.      .0252      -2.      .0157
   -1.     .0112        0.     .0102       1.      .0122       2.      .0232
    4.     .0682        6.     .1072       8.      .1472      12.      .2632
   30.     .6322
NPTS   20.   MACH    0.80        THICK  0.095
  -30.0    .6322    -12.0      .2922    -10.0      .2272     -8.0      .1622
   -6.0    .1022     -4.0      .0672     -3.0      .0442     -2.0      .0302
   -1.0    .0232     -0.5      .0212      0.0      .0192      0.5      .0222
    1.0    .0272      2.0      .0422      4.0      .0922      6.0      .1302
    8.0    .1722     10.0      .2272     12.0      .2872     30.0      .6322
NPTS   17.   MACH    0.90        THICK  0.095
  -30.0    .6322    -12.0      .3322    -10.0      .2642     -8.0      .2052
   -6.0    .1512     -4.0      .1172     -2.0      .0682     -1.0      .0572
    0.0    .0522      1.0      .0622      2.0      .0822      4.0      .1222
    6.0    .1692      8.0      .2122     10.0      .2642     12.0      .3247
   30.0    .6322
NPTS   15.   MACH    1.00        THICK  0.095
  -30.0    .6322    -12.0      .3722    -10.0      .2992     -8.0      .2502
   -6.     .2042     -4.0      .1544     -2.0      .1192      0.0      .0922
    2.     .1197      4.0      .1547      6.0      .2052      8.0      .2512
   10.     .3002     12.0      .3652     30.0      .6322
NPTS   15.   MACH    2.00        THICK  0.095
  -30.0    .6322    -12.0      .3642    -10.0      .2992     -8.0      .2502
   -6.0    .2042     -4.0      .1544     -2.0      .1192      0.0      .0922
    2.0    .1197      4.0      .1547      6.0      .2052      8.0      .2512
   10.0    .3002     12.0      .3447     30.0      .6322
```

Table E.3 - concluded

```
CMDAT  109503
** SC1095 1975 TSR CM DATA ** MODEL SCALE **
ALPHA                      CM
NPTS   29.    MACH   0.00          THICK  0.095
   -180.00    -.01300   -174.00     .35900   -160.00    .30000   -145.00     .48100
   -125.00     .55700    -90.00     .55500    -60.00    .39500    -30.00     .16500
  -20.0     .0950      -13.0      -.023      -4.0      -.012      11.5       .005
   13.0     -.007       16.0      -.08       20.0      -.135      30.0      -.165
     35.00    -.22200     45.00    -.29500     60.00   -.39500     80.00    -.50000
     95.00    -.55500    110.00    -.56000    125.00   -.55700    135.00    -.53800
    145.00    -.48100    150.00    -.43800    160.00   -.30000    174.00    -.35900
    180.00    -.01300
NPTS   29.    MACH   0.20          THICK   .095
   -180.00    -.01300   -174.00     .35900   -160.00    .30000   -145.00     .48100
   -125.00     .55700    -90.00     .55500    -60.00    .39500    -30.00     .16500
  -20.0     .0950      -13.0      -.023      -4.0      -.012      11.5       .005
   13.0     -.007       16.0      -.08       20.0      -.135      30.0      -.165
     35.00    -.22200     45.00    -.29500     60.00   -.39500     80.00    -.50000
     95.00    -.55500    110.00    -.56000    125.00   -.55700    135.00    -.53800
    145.00    -.48100    150.00    -.43800    160.00   -.30000    174.00    -.35900
    180.00    -.01300
NPTS   29.    MACH   0.30          THICK  0.095
   -180.00    -.01300   -174.00     .35900   -160.00    .30000   -145.00     .48100
   -125.00     .55700    -90.00     .55500    -60.00    .39500    -30.00     .16500
  -20.0     .095       -13.0      -.023      -6.0      -.02        6.0       0.0
  12.2      .01         13.0      -.03       20.0      -.135      30.0      -.165
     35.00    -.22200     45.00    -.29500     60.00   -.39500     80.00    -.50000
     95.00    -.55500    110.00    -.56000    125.00   -.55700    135.00    -.53800
    145.00    -.48100    150.00    -.43800    160.00   -.30000    174.00    -.35900
    180.00    -.01300
NPTS   14.    MACH   0.40          THICK  0.095
    -30.00     .18500    -27.00     .17600    -24.00    .16700    -20.00     .14000
    -17.00     .10800    -14.00     .06500    -13.00    .02000    -12.00    -.02800
  -10.0     -.02       -4.0       -.02       10.0       .019      13.0      -.055
  20.0      -.140       30.0      -.185
NPTS   14.    MACH   0.50          THICK  0.095
    -30.00     .21300    -28.00     .18800    -24.00    .14800    -20.00     .10000
    -17.00     .06500    -14.00     .03500    -12.00    .00000    -10.00    -.03000
   -4.0     -.02        9.0        .022      11.0      -.05       14.0      -.075
  20.0      -.14        30.0      -.213
NPTS   16.    MACH   0.60          THICK  0.095
    -30.00     .23400    -27.00     .19600    -23.00    .15500    -20.00     .12200
    -17.00     .08500    -14.00     .05000    -12.00    .03700    -10.00     .02000
   -6.0     -.042       6.0        .018       9.0      -.012      11.0      -.045
  12.0      -.065       20.0      -.148      30.0      -.234
NPTS  #12.    MACH  #       .7         THICK #  .095
    -30.00     .20000    -20.00     .13000    -12.00    .08500     -8.00     .03600
   -4.0     -.037       2.0        0.0        4.0       0.0        6.0      -.045
  8.0       -.06        10.0      -.065      20.0      -.15       30.0      -.20
NPTS  #12.    MACH  #       .75        THICK #  .095
  -30.0     .160       -10.0       .070      -8.0       .05       -4.0      -.005
  -2.0      -.03        0.0       -.015       2.0      -.015       4.0      -.055
  6.0       -.070       8.0       -.080      20.0      -.15       30.0      -.165
NPTS  #17.    MACH  #       .8         THICK #  .095
    -30.00     .14000     -8.00     .12000     -6.00    .09700     -4.00     .04300
     -2.00    -.01200       .00    -.02000       .10   -.00100       .25     .01200
       .50     .01700       .75     .00900      1.00   -.00700      1.50    -.03000
      2.00    -.03500      4.00    -.08300      6.00   -.13700      8.00    -.16000
     30.00    -.19000
NPTS  #17.    MACH  #       .9         THICK # .095
    -30.00     .14000     -8.00     .12000     -6.00    .09700     -4.00     .04300
     -2.00    -.01200       .00    -.02000       .10   -.00100       .25     .01200
       .50     .01700       .75     .00900      1.00   -.00700      1.50    -.03000
      2.00    -.03500      4.00    -.08300      6.00   -.13700      8.00    -.16000
     30.00    -.19000
NPTS  #17.    MACH  #      1.          THICK #  .095
    -30.00     .14000     -8.00     .12000     -6.00    .09700     -4.00     .04300
     -2.00    -.01200       .00    -.02000       .10   -.00100       .25     .01200
       .50     .01700       .75     .00900      1.00   -.00700      1.50    -.0300
      2.00    -.03500      4.00    -.08300      6.00   -.13700      8.00    -.16000
     30.00    -.19000
NPTS  #17.    MACH  #      2.          THICK # .095
    -30.00     .14000     -8.00     .12000     -6.00    .09700     -4.00     .04300
     -2.00    -.01200       .00    -.02000       .10   -.00100       .25     .01200
       .50     .01700       .75     .00900      1.00   -.00700      1.50    -.03000
      2.00    -.03500      4.00    -.08300      6.00   -.13700      8.00    -.16000
     30.00    -.19000
```

Table E.4 - Aerodynamic coefficients for model scale airfoil section SC1096-R8

```
CLDAT2 109581
 ** SC1095-R8 CL DATA ** MODEL SCALE **
  APLHA                   CL
NPTS   30.   MACH   0.0        THICK  0.098
 -180.      0.       -172.     .78      -160.     .64      -158.     .66
 -150.      .95      -30.      -1.      -20.      -.975    -15.      -.26
 -11.6      -.32     -11.4     -.75     -10.      -.72     -9.       -.68
 -8.        -.63     -7.       -.57     -6.       -.49     -5.       -.4
 9.         1.14     10.       1.25     11.1      1.37     14.       1.37
 16.2       1.1      20.       1.04     30.       1.       150.      -.95
 150.       -.95     156.      -.7      158.      -.66     160.      -.64
 172.       -.78     180.      0.
NPTS   30.   MACH   0.3        THICK  0.098
 -180.      0.       -172.     .78      -160.     .64      -158.     .66
 -150.      .95      -30.      -1.      -20.      -.975    -15.      -.26
 -11.6      -.32     -11.4     -.75     -10.      -.72     -9.       -.68
 -8.        -.63     -7.       -.57     -6.       -.49     -5.       -.4
 9.         1.14     10.       1.25     11.1      1.37     14.       1.37
 16.2       1.1      20.       1.04     30.       1.       150.      -.95
 150.       -.95     156.      -.7      158.      -.66     160.      -.64
 172.       -.78     180.      0.
NPTS   14.   MACH   0.4        THICK  0.098
 -30.       -.95     -25.      -.96     -14.      -.28     -9.4      -.29
 -8.8       -.53     -8.       -.52     -7.       -.51     -6.       -.47
 -5.        -.39     -4.       -.27     9.        1.15     12.8      1.15
 18.        1.07     30.       1.
NPTS   14.   MACH   0.4        THICK  0.098
 -30.       -.95     -25.      -.92     -14.      -.58     -10.      -.56
 -9.        -.55     -8.       -.53     -7.       -.51     -6.       -.49
 -5.        -.4      -1.       .02      6.41      .92      10.       .92
 20.        .92      30.       .92
NPTS   12.   MACH   0.6        THICK  0.098
 -30.       -.95     -25.      -.94     -13.      -.54     -5.       -.40
 -3.        -.23     -1.       .01      1.        .28      3.        .57
 4.         .72      5.36      .87      15.       .87      30.       .87
NPTS   13.   MACH   0.7        THICK  0.098
 -30.       -.95     -25.      -.935    -15.      -.905    -9.       -.51
 -6.        -.45     -5.       -.4      -4.       -.36     -3.       -.25
 -1.        .04      1.        .37      3.5       .75      15.       .75
 30.        .75
NPTS   13.   MACH   0.75       THICK  0.098
 -30.       -.95     -15.      -.93     -12.      -.9      -9.       -.68
 -5.        -.52     -4.       -.47     -3.       -.36     1.        .44
 2.         .58      3.        .65      4.26      .71      15.       .71
 30.        .71
NPTS   11.   MACH   0.80       THICK  0.098
 -30.0      -.95     -14.0     -.80     -12.0     -.79     -10.0     -.81
 -6.0       -0.690   -2.0      -0.250   0.0       0.070    2.0       0.350
 3.75       0.670    15.0      0.670    30.0      0.670
NPTS   14.   MACH   0.85       THICK  0.098
 -30.0      -.95     -16.0     -.803    -13.0     -.772    -10.0     -.74
 -6.0       -0.680   -2.0      -0.290   0.0       -0.045   2.0       0.230
 4.0        0.460    6.0       0.640    8.0       0.760    9.0       0.802
 15.0       .82      30.0      .82
NPTS   14.   MACH   0.90       THICK  0.098
 -30.0      -.95     -16.0     -.754    -13.0     -.712    -10.0     -.67
 -6.0       -0.663   -2.0      -0.310   0.0       -0.150   1.0       0.000
 2.0        0.138    4.0       0.390    6.0       0.640    8.0       0.765
 10.0       .81      30.0      .82
NPTS     13.   MACH             .950    THICK  0.098
 -30.0      -.95     -16.0     -.741    -13.0     -.696    -10.0     -.651
 -6.0       -0.641   -2.0      -0.270   0.0       -0.090   2.0       0.180
 4.0        0.435    6.0       0.680    8.0       0.795    10.0      0.810
 30.0       .82
NPTS     13.   MACH             1.0     THICK  0.098
 -30.0      -.9500   -16.0     -.726    -13.0     -.6780   -10.0     -.630
 -6.0       -.6150   -2.0      -.2400   0.0       -.0500   2.0       .200
 4.0        .4490    6.0       .7000    8.0       .8060    10.0      .850
 30.0       .82
NPTS     13.   MACH             2.0     THICK  0.098
 -30.0      -.9500   -16.0     -.7260   -13.0     -.6780   -10.0     -.630
 -6.0       -.6150   -2.0      -.2400   0.0       -.0500   2.0       .200
 4.0        .4490    6.0       .7000    8.0       .8060    10.0      .850
 30.0       .82
```

Table E.4 - continued

CDDAT2 109582

** SC1095-R8 CD DATA ** MODEL SCALE **

ALPHA	CD						
NPTS 32.	MACH 0.0		THICK 0.098				
-180.	.0263	-179.	.0313	-175.	.0713	-172.	.1163
-150.	.6483	-115.	1.8863	-65.	1.8863	-30.	.6363
-8.0	.0943	-7.	.0673	-6.	.0483	-5.	.0283
-4.	.0193	-3.	.0153	-2.	.0143	2.	.0153
4.	.0163	6.	.0168	8.	.0183	10.	.0203
12.	.0223	13.	.0243	14.	.0288	15.	.0463
16.	.0913	17.	.1763	30.	.6363	65.	1.8863
150.	.6483	172.	.1163	175.	.0713	180.	.0263
NPTS 32.	MACH 0.30		THICK 0.098				
-180.	.0246	-1836	.0296	-175.	.0696	-172.	.1146
-150.	.6466	-115.	1.8846	-65.	1.8846	-30.	.6346
-8.0	.0926	-7.	.0656	-6.	.0466	-5.	.0266
-4.	.0176	-3.	.0136	-2.	.0126	2.	.0136
4.	.0146	6.	.0151	8.	.0166	10.	.0186
12.	.0206	13.	.0226	14.	.0271	15.	.0446
16.	.0896	17.	.1746	30.	.6346	65.	1.8846
150.	.6466	172.	.1146	175.	.0696	180.	.0246
NPTS 20.	MACH 0.40		THICK 0.098				
-30.	.6342	-10.	.1492	-8.0	.0952	-7.	.0692
-6.	.0482	-5.	.0312	-4.	.0172	-3.	.0137
-2.	.0122	2.	.0122	4.	.0132	6.	.0147
8.	.0167	9.	.0182	10.	.0227	11.	.0322
12.	.0542	13.	.1192	13.5	.1742	30.	.6342
NPTS 27.	MACH 0.50		THICK 0.098				
-30.	.6336	-13.	.2086	-10.5	.1786	-10.	.1536
-9.	.1246	-8.	.1006	-7.	.0746	-6.	.0546
-5.	.0386	-4.	.0241	-3.	.0176	-2.	.0136
-1.	.0121	0.	.0116	2.	.0116	4.	.0126
5.	.0136	6.	.0166	7.	.0246	8.	.0386
9.	.0546	10.	.0746	11.	.1006	12.	.1316
13.	.1716	13.5	.1936	30.	.6336		
NPTS 29.	MACH 0.60		THICK 0.098				
-30.	.6331	-20.	.3631	-14.	.2491	-11.3	.1931
-11.	.1831	-10.	.1561	-9.	.1291	-8.	.1051
-7.	.0811	-6.	.0601	-5.	.0431	-4.	.0311
-3.	.0211	-2.	.0131	-1.	.0121	0.	.0111
1.	.0106	2.	.0111	3.	.0131	4.	.0181
5.	.0281	6.	.0451	7.	.0651	8.	.0861
9.	.1111	10.	.1351	11.	.1631	12.	.1921
30.	.6331						
NPTS 23.	MACH 0.70		THICK 0.098				
-30.	.6326	-12.	.2456	-10.6	.1776	-10.	.1646
-9.	.1426	-8.	.1196	-7.	.0986	-6.	.0786
-5.	.0586	-4.	.0426	-3.	.0266	-2.	.0136
-1.	.0121	0.	.0116	1.	.0121	2.	.0166
3.	.0346	4.	.0556	6.	.0946	9.	.1606
9.5	.1726	12.	.2406	30.	.6326		
NPTS 19.	MACH 0.75		THICK 0.098				
-30.	.6324	-12.	.2700	-10.	.2044	-8.	.1504
-3.	.0324	-2.5	.0204	-2.	.0164	-1.	.0159
0.	.0154	1.	.0264	2.	.0514	3.	.0724
4.	.0914	5.	.1084	6.	.1254	7.	.1424
10.	.2064	12.	.2634	30.	.6324		
NPTS 20.	MACH 0.80		THICK 0.098				
-30.0	.6321	-12.0	.2921	-10.0	.2271	-8.0	.1721
-6.0	.1241	-4.0	.0771	-3.0	.0441	-2.0	.0301
-1.0	.0281	-0.5	.0276	0.0	.0271	0.5	.0371
1.0	.0441	2.0	.0721	4.0	.1101	6.0	.1501
8.0	.1841	10.0	.2271	12.0	.2871	30.0	.6321
NPTS 17.	MACH 0.90		THICK 0.098				
-30.0	.6316	-12.0	.3316	-10.0	.2636	-8.0	.2116
-6.0	.1646	-4.0	.1166	-2.0	.0676	-1.0	.0646
0.0	.0616	1.0	.0796	2.0	.1016	4.0	.1396
6.0	.1836	8.0	.2226	10.0	.2636	12.0	.3241
30.0	.6316						
NPTS 15.	MACH 1.00		THICK 0.098				
-30.0	.631	-12.0	.371	-10.0	.298	-8.0	.249
-6.	.203	-4.0	.153	-2.0	.118	0.0	.101
2.	.1370	4.0	.1710	6.0	.216	8.0	.256
10.	.299	12.0	.3640	30.0	.631		
NPTS 15.	MACH 2.00		THICK 0.098				
-30.0	.630	-12.0	.362	-10.0	.297	-8.0	.248
-6.0	.202	-4.0	.152	-2.0	.117	0.0	.100
2.0	.1360	4.0	.1700	6.0	.215	8.0	.255
10.0	.298	12.0	.3425	30.0	.630		

```
CMDAT2 109583
** SC1095-R8 1975 TSR CM DATA ** MODEL SCALE **
ALPHA                  CM
NPTS  #29.   MACH  #      .0       THICK # .098
   -180.00   -.01300   -174.00    .35900   -160.00    .30000   -145.00    .48100
   -125.00    .55700    -90.00    .55500    -60.00    .39500    -30.00    .16500
  -20.0    .095      -13.0     -.023      -4.0      -.03       9.0       0.0
   16.0    .012       17.0     -.07       20.0      -.11       30.0      -.165
     35.00   -.22200     45.00   -.29500     60.00   -.39500     80.00   -.50000
     95.00   -.55500    110.00   -.56000    125.00   -.55700    135.00   -.53800
    145.00   -.48100    150.00   -.43800    160.00   -.30000    174.00   -.35900
    180.00   -.01300
NPTS  #29.   MACH  #      .2       THICK # .098
   -180.00   -.01300   -174.00    .35900   -160.00    .30000   -145.00    .48100
   -125.00    .55700    -90.00    .55500    -60.00    .39500    -30.00    .16500
  -20.0    .095      -13.0     -.023      -4.0      -.03       9.0       0.0
   16.0    .012       17.0     -.07       20.0      -.11       30.0      -.165
     35.00   -.22200     45.00   -.29500     60.00   -.39500     80.00   -.50000
     95.00   -.55500    110.00   -.56000    125.00   -.55700    135.00   -.53800
    145.00   -.48100    150.00   -.43800    160.00   -.30000    174.00   -.35900
    180.00   -.01300
NPTS  #29.   MACH  #      .3       THICK # .098
   -180.00   -.01300   -174.00    .35900   -160.00    .30000   -145.00    .48100
   -125.00    .55700    -90.00    .55500    -60.00    .39500    -30.00    .16500
  -20.0    .095      -13.0     -.023      -5.0      -.03       2.0       -.01
  15.2     .015       16.0     -.070      20.0      -.115      30.0      -.165
     35.00   -.22200     45.00   -.29500     60.00   -.39500     80.00   -.50000
     95.00   -.55500    110.00   -.56000    125.00   -.55700    135.00   -.53800
    145.00   -.48100    150.00   -.43800    160.00   -.30000    174.00   -.35900
    180.00   -.01300
NPTS  #15.   MACH  #      .4       THICK # .098
    -30.00    .18500    -27.00    .17600    -24.00    .16700    -20.00    .14000
    -17.00    .10800    -14.00    .06500    -13.00    .02000    -12.00   -.02800
  -10.0    -.02       -7.0     -.045      5.7       0.0        12.0      .02
  13.0     -.05       20.0     -.130      30.0      -.185
NPTS  #14.   MACH  #      .5       THICK # .098
    -30.00    .21300    -28.00    .18800    -24.00    .14800    -20.00    .10000
    -17.00    .06500    -14.00    .03500    -12.00    .00000    -10.00   -.03000
  -7.0     -.04       4.5      0.0        8.7       .015       13.2      -.065
  20.0     -.130      30.0     -.213
NPTS  #15.   MACH  #      .6000    THICK # .098
    -30.00    .23400    -27.00    .19600    -23.00    .15500    -20.00    .12200
    -17.00    .08500    -14.00    .05000    -12.00    .03700    -10.00    .02000
  -5.0     -.035      -3.      -.035      5.2       .003       7.2       -.002
  13.0     -.10       20.0     -.15       30.0      -.234
NPTS  #12.   MACH  #      .7       THICK # .098
    -30.00    .20000    -20.00    .13000    -12.00    .08500     -8.00    .03600
  -5.0     -.03       -3.0     -.045      1.2       -.011      3.2       -.01
  4.2      -.05       10.0     -.08       20.0      -.15       30.0      -.200
NPTS  #12.   MACH  #      .75      THICK # .098
    -30.00    .16000    -10.00    .07000     -8.00    .05000     -6.00    .03000
  -5.0     -.005      -3.      -.055      -1.0      -.035      1.0       -.027
  3.0      -.06       8.0      -.09       20.0      -.15       30.0      -.20
NPTS  #14.   MACH  #      .8       THICK # .098
    -30.00    .15000     -8.00    .07500     -6.00    .06000     -4.00    .03500
     -2.00   -.03000       .00   -.03500       .50   -.03250      1.00   -.03000
      1.50   -.035        2.0    -.042        4.0    -.07500      6.00   -.10000
      8.00   -.11500     30.0    -.200
NPTS  #14.   MACH  #      .9       THICK # .098
    -30.00    .15000     -8.00    .07500     -6.00    .06000     -4.00    .03500
     -2.00   -.03000       .00   -.03500       .50   -.03250      1.00   -.03000
      1.50   -.035        2.0    -.042        4.0    -.07500      6.00   -.10000
      8.00   -.11500     30.0    -.200
NPTS  #14.   MACH  #      1.       THICK # .098
    -30.00    .15000     -8.00    .07500     -6.00    .06000     -4.00    .03500
     -2.00   -.03000       .00   -.03500       .50   -.03250      1.00   -.03000
      1.50   -.035        2.0    -.042        4.0    -.07500      6.00   -.10000
      8.00   -.11500     30.0    -.200
NPTS  #14.   MACH  #      2.       THICK # .098
    -30.00    .15000     -8.00    .07500     -6.00    .06000     -4.00    .03500
     -2.00   -.03000       .00   -.03500       .50   -.03250      1.00   -.03000
      1.50   -.035        2.0    -.042        4.0    -.07500      6.00   -.10000
      8.00   -.11500     30.0    -.200
```

APPENDIX F

Fuselage and Empennage Aerodynamic Force and Moment Data

SUMMARY

Fuselage and empennage aerodynamic forces for the flight test vehicle are presented in this appendix as determined from 1/5th scale unpowered model testing. Also presented is the method for calculating airframe lift and drag using the 1/5 scale model data.

SYMBOLS

$C_{D_{HT}}$	horizontal tail drag coefficient, $D_{HT}/q_{HT}\ S_{HT}$
$C_{D_{VT}}$	vertical tail drag coefficient, $D_{VT}/q_{VT}\ S_{VT}$
$C_{L_{HT}}$	horizontal tail lift coefficient, $L_{HT}/q_{HT}\ S_{HT}$
$C_{L_{VT}}$	vertical tail lift coefficient, $L_{VT}/q_{HT}\ S_{HT}$
D_{AF}	total airframe drag
D_{FUS}	fuselage drag force
D_{HT}	horizontal tail drag force
D_{VT}	vertical tail drag force
F_Y	fuselage side force
i_{HT}	horizontal tail incidence
L_{FUS}	fuselage lift force
L_{HT}	horizontal tail lift force
L_{VT}	vertical tail lift force
L_r	fuselage rolling moment
M_F	fuselage pitching moment
N_y	fuselage yawing moment
q	free stream dynamic pressure, $\frac{1}{2}\rho V^2$

q_{HT} effective dynamic pressure at the horizontal tail location

q_{VT} effective dynamic pressure at the vertical tail location

S_{HT} horizontal tail reference area

S_{VT} vertical tail reference a

V free stream velocity

α_{FUS} fuselage angle of attack

α_{HT} horizontal tail angle of attack

ΔD_{FUS} fuselage drag increment due to yaw

ΔL_{FUS} fuselage lift increment due to yaw

ΔM_{FUS} fuselage pitching moment increment due to yaw

$\Delta\alpha_{FUS}$ fuselage rotor induced angle of attack

$\Delta\alpha_{HT}$ horizontal tail rotor induced angle of attack

ε local flow angle at horizontal tail location, positive down

θ_B fuselage pitch attitude, positive nose up

ρ ambient air density

σ local sideflow angle at the vertical tail location, positive from the left

ϕ roll angle, positive right-wing down

ψ yaw angle, positive nose right

The following summarizes the data presented in the figures of this appendix.

Figures 1F, 2F, and 3F:

1/5 scale model fuselage lift, drag, and pitching moment divided by dynamic pressure, plotted as a function of angle of attack.

Figures 4F, 5F, 6F, 7F, 8F, and 9F:

1/5 scale model fuselage delta pitch moment, delta lift, delta drag, side force, roll moment, and yaw moment, divided by dynamic pressure and plotted as a function of yaw angle.

Figures 10F and 11F:

Plots of horizontal tail lift and drag coefficients versus angle of attack.

Figures 12F and 13F:

Plots of vertical tail lift (side force) and drag coefficients versus angle of attack (yaw).

Figure 14F and 15F:

Horizontal tail downflow angle and dynamic pressure ratio variation with angle of attack.

Figure 15F and 17F:

Vertical tail sideflow angle and dynamic pressure ratio variation with yaw angle.

Figure 18F and 19F:

Fuselage and horizontal tail downwash delta angle of attack change versus forward speed.

Table F.1:

ATRS fuselage and tail surface geometric data.

Table F.2:

ATRS tail surface geometric description data.

Table F.3:

ATRS Aircraft gross weight and center of gravity limits data.

Table F.3:

Tail rotor data.

The data in Figures 1F through 9F and 14F through 17F have been derived from 1/5 scale wind tunnel test results as labeled. The data on Figures 10F through 13F are based on established NACA two-dimensional coefficients for the respective airfoils, with finite span effect corrections theoretically derived by the DATCOM method. Figures 18F and 19F are derived from Sikorsky Aircraft's GENHEL simulation program.

Correction factors must be added to the sums of experimental and theoretical drag data shown in Figures 2F, 6F, 11F, and 13F to obtain the total equivalent airframe drag area of 12.23 ft^2 (level flight trim value). This value was from flight test data obtained from the instrumented flight test vehicle shown in Figure 2. These corrections consider items not included on the model, such as tail rotor and hub, interference, airflow momentum drag from cooling systems, and miscellaneous minor pertuberances. These corrections sum to 4.36 ft^2 and should be added to the sum of data from Figures 2F, 6F, 11F and 13F to obtain the test aircraft total configuration drag. Figure 8 presents the variation of total airframe drag with local fuselage angle of attack. It is shown to be independent of rotor lift and speed because these parameters have only a minor effect on drag for realistic values of effective angle of attack in trimmed level flight.

Calculation of Airframe Lift and Drag

Airframe lift is a function of rotor lift and must be calculated iteratively for each flight condition. The airframe lift increment was calculated as the sum of the fuselage and horizontal tail contributions accordingly, the airframe lift, L_{AF}, is expressed as

$$L_{AF} = L_{FUS} + L_{HT} \tag{1F}$$

where L_{FUS} and L_{HT} are the fuselage and horizontal tail contributions, respectively.

L_{FUS} is calculated as

$$L_{FUS} = (L/q)_{FUS}\ q \tag{2F}$$

where $q = \frac{1}{2}\rho V^2$ (free stream dynamic pressure, lb/ft^2 or $Kg\ (m^2)$ and $(L/q)_{FUS}$ is obtained from Figure 1F at the appropriate effective fuselage angle of attack, α_{FUS}. α_{FUS} is expressed as

$$\alpha_{FUS} = \theta_B + \Delta\alpha_{FUS} \tag{3F}$$

where θ_B is body pitch attitude (deg) for level flight and $\Delta\alpha_{FUS}$ is the correction angle due to main rotor downwash. Body pitch angles are obtained from either flight test data or GENHEL simulation and $\Delta\alpha_{FUS}$ is obtained from Figure 18F.

The horizontal tail lift contribution is expressed as

$$L_{HT} = C_{L_{HT}}\ (Q_{HT}/q)\ q\ S_{HT} \tag{4F}$$

Horizontal tail lift coefficient, $C_{L_{HT}}$, and dynamic pressure ratio (q_{HT}/q) are obtained from Figures 10F and 14F, respectively. The horizontal tail area,

S_{HT}, is 18.5 ft^2 (1.719 M^2). It should be noted that the angle of attack for determining the horizontal tail C_L, $\cdot\alpha_{HT}$, differs from the fuselage angle of attack due to different interference factors. In this case,

$$\alpha_{HT} = i_{HT} + \Delta\alpha_{HT} - \varepsilon + \theta_B \qquad (5F)$$

where i_{HT} is tail incidence, $\Delta\alpha_{HT}$ is the correction for main rotor wake interference obtained from Figure 19F and ε is the self-induced downwash angle at the horizontal tail presented in Figure 19F.

The approach is further illustrated by the following worked example which also includes an evaluation of the drag.

Data:

Flight No. 12	
Gross Weight	= 10,300 lb
Advance ratio (μ)	= 0.3
Rotational tip Mach No. (M_T)	= 0.6
Level flight speed (V)	= 120.8 knots-TAS
Body pitch attitude (θ_B)	= 0.4^o
Body yaw attitude (ψ)	= 2.0^o
Ambient air density (ρ)	= 0.002278 $\frac{lb\ sec^2}{ft^4}$
Horizontal tail area (S_{HT})	= 18.5 ft^2
Vertical tail area (S_{VT})	= 19.7 ft^2

Calculations:

From equation 3F and Figure 18F

$$\alpha_{FUS} = 0.4 - 2.20$$
$$= -1.8^o$$

Corresponding to this angle of attack, the fuselage lift obtained from Figure 1F and equation 2F is (the effects of yaw and roll are negligible)

$$\Delta L_{FUS} = -0.07 \times \tfrac{1}{2} \times 0.002278 \times (1.689 \times 120.8)^2$$
$$= -3.32 \text{ lb}$$

Using equation 5F and Figures 19 and 14F the angle of attack for the horizontal tail is:

$$\alpha_{HT} = 2. - 3.50 - 2.20 + 0.4$$
$$= -3.3^0$$

From Figure 10F and equation 4F:

$$\Delta L_{HT} = 0.50 \times 0.74 \times \tfrac{1}{2} \times 0.002278 \times (1.689 \times 120.8)^2 \times 18.5$$
$$= -324.56 \text{ lb}$$

The total configuration lift is given by equation 1F:

$$\Delta L_{AF} = -3.32 - 324.56$$
$$= -327.88 \text{ lb}$$

The drag is obtained using the data presented in Figures 2F, 6F, 11F and 13F together with the correction factor of 4.36 ft^2 as was discussed earlier.

From Figure 2F

$$\frac{D_{FUS}}{q} = 6.6 \text{ ft}^2$$

From Figure 6F

$$\frac{\Delta D_{FUS}}{q} = 0.5 \text{ ft}^2$$

From Figure 11F

$$D_{D_{HT}} = 0.0028$$

and from Figure 13F

$$C_{D_{VT}} = 0.013$$

Converting the drag coefficients to equivalent flat plate drag areas, summing and adding the correction of 4.36 gives

$$D_{AF}/q = 6.6 + 0.5 + .028 \times 18.5 + .013 \times 19.7 + 4.36$$

$$= 12.23 \text{ ft}^2$$

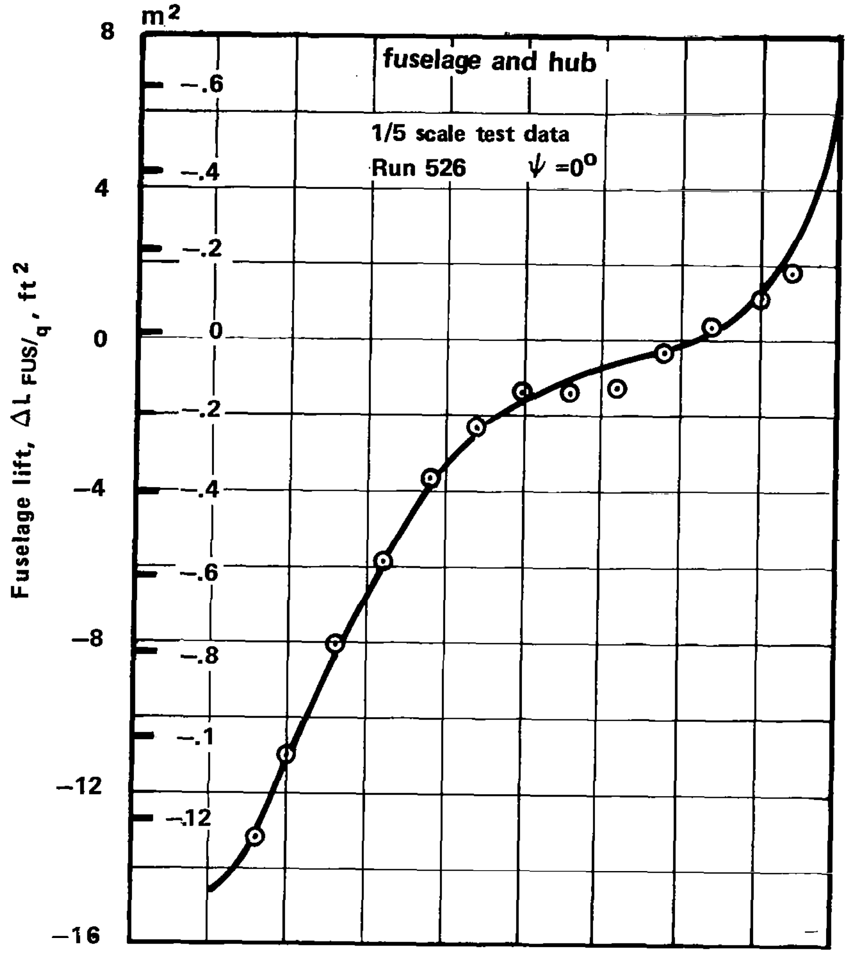

Figure 1F – ATRS fuselage lift 1/5 angle of attack

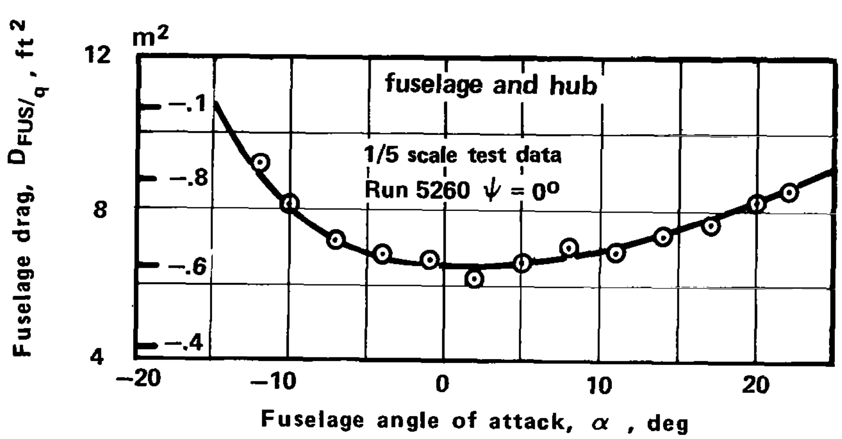

Figure 2F – ATRS fuselage drag vs angle of attack

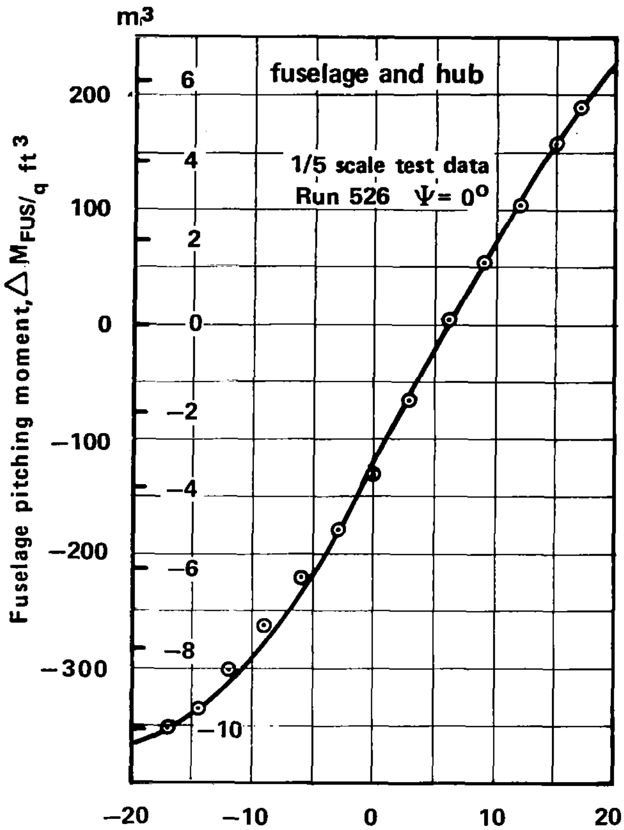

Figure 3F — ATRS fuselage pitching moment vs angle of attack

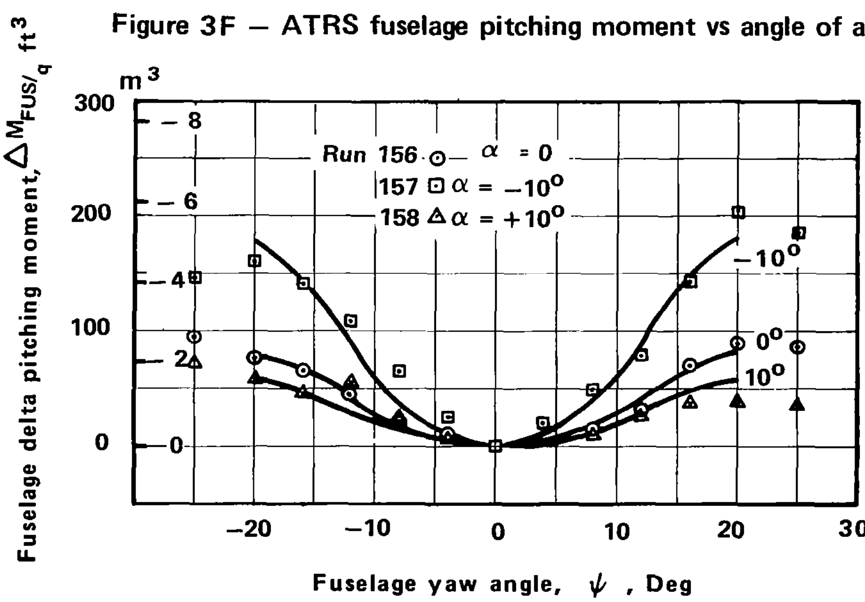

Figure 4F — ARTS variation of fuselage pitching monent vs yaw angle

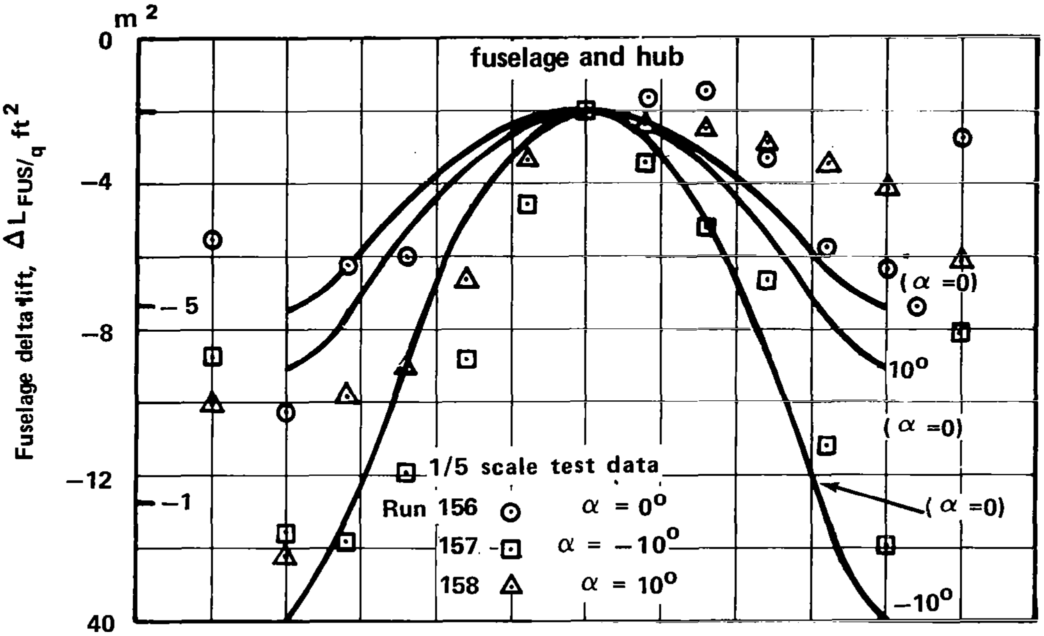

Figure 5F – ATRS variation of fuselage lift with yaw angle

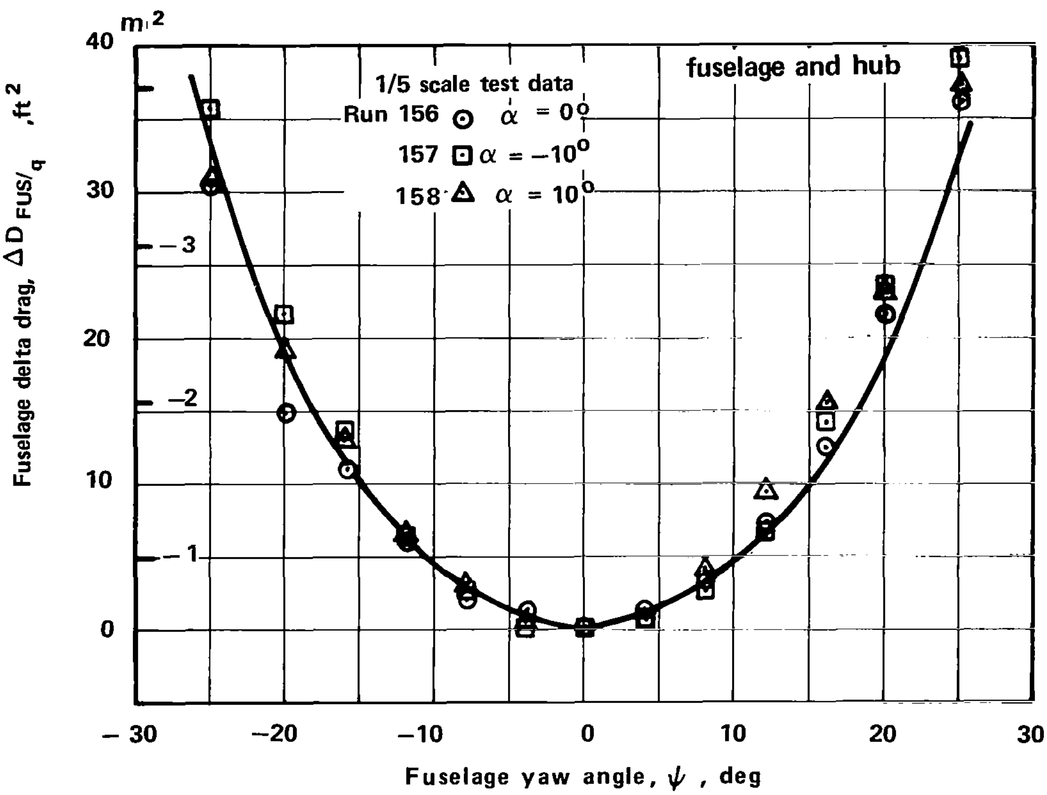

Figure 6F – ATRS variation of fuselage drag with yaw angle

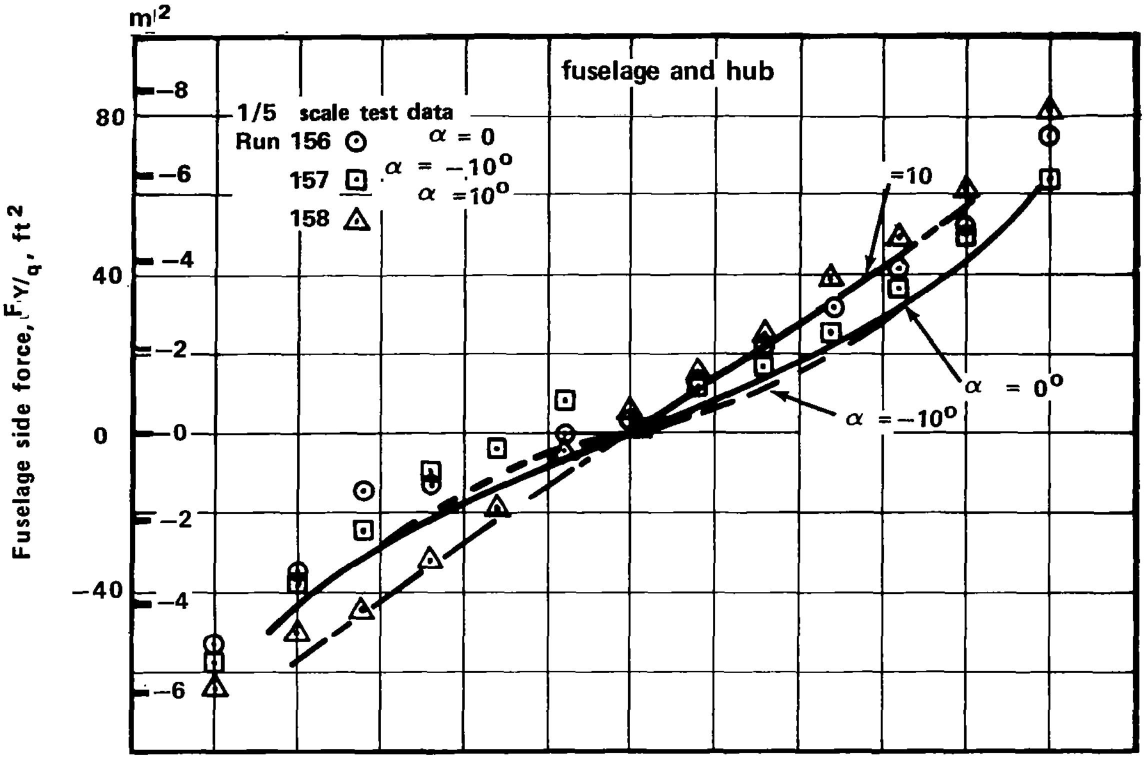

Figure 7F — ARTS variation of fuselage side force with yaw angle

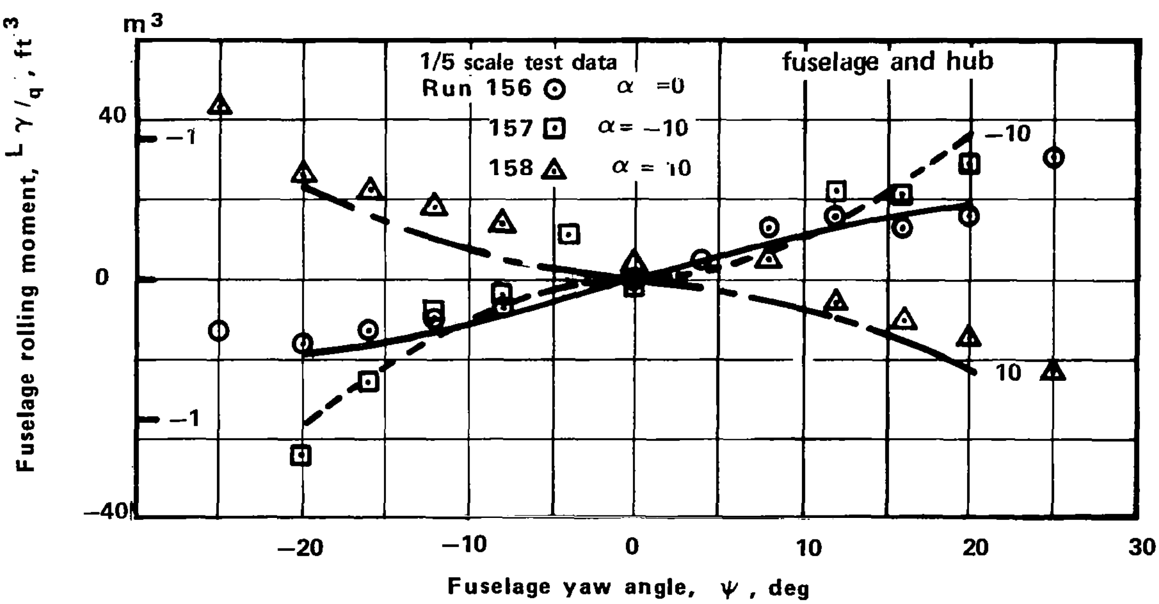

Figure 8F — ARTS variation of fuselage rolling moment with yaw angle

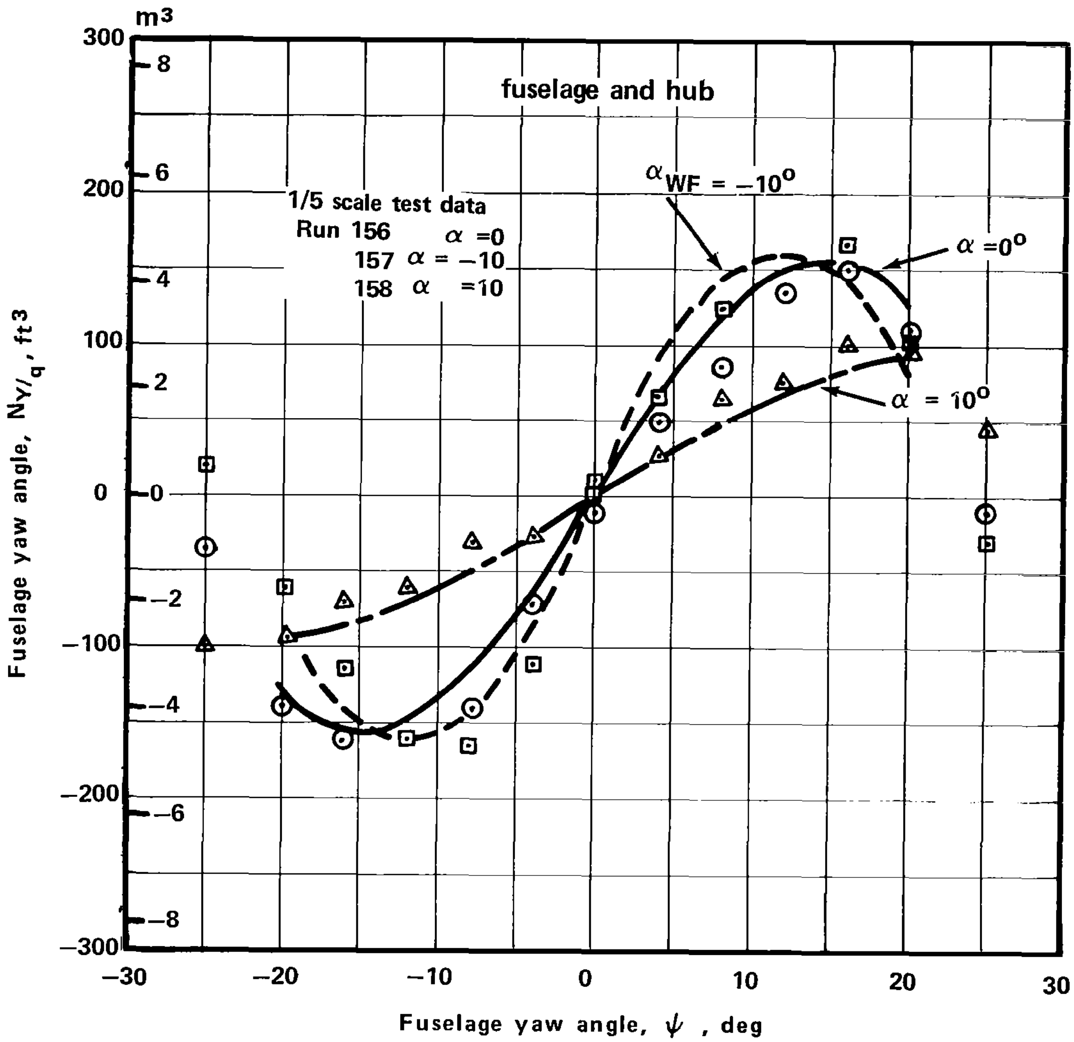

Figure 9F – ATRS variation of fuselage yawing moment with yaw angle

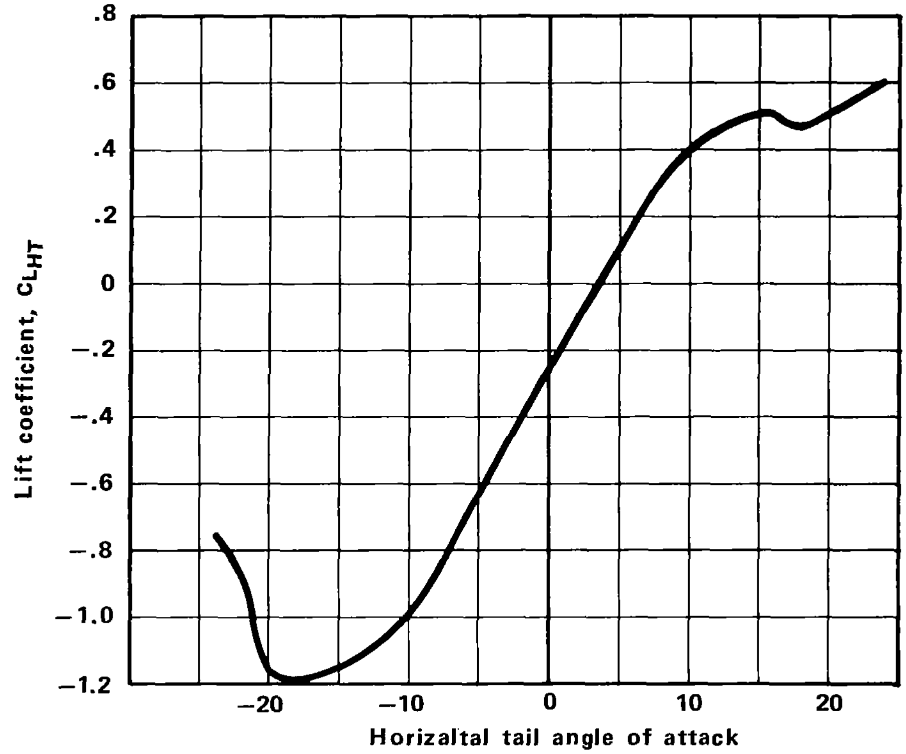

Figure 10 F — ATRS horizontal tail lift coefficient vs angle of attack (theoretical)

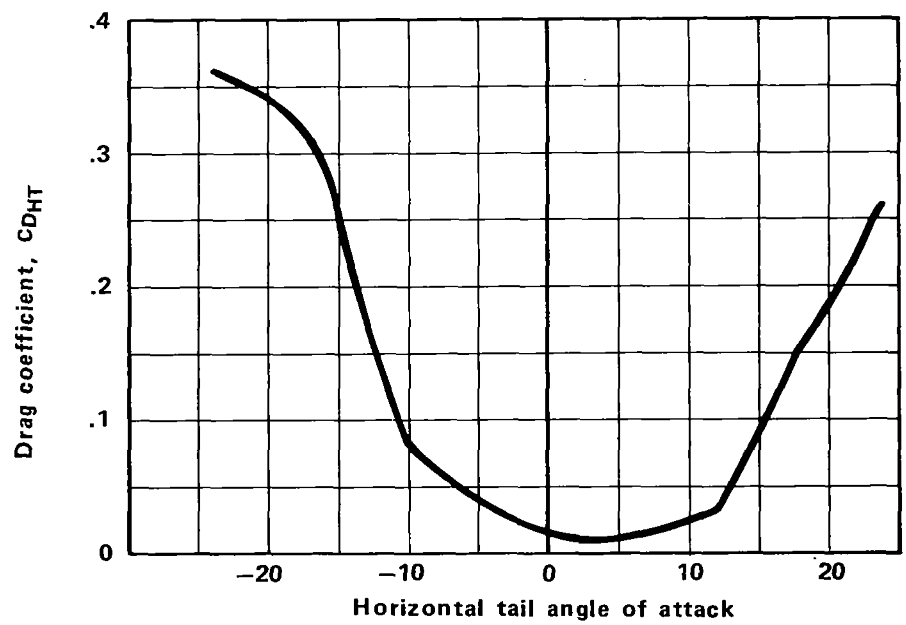

Figure 11 F — ATRS horizontal tail drag coefficient vs angle of attack (theoretical)

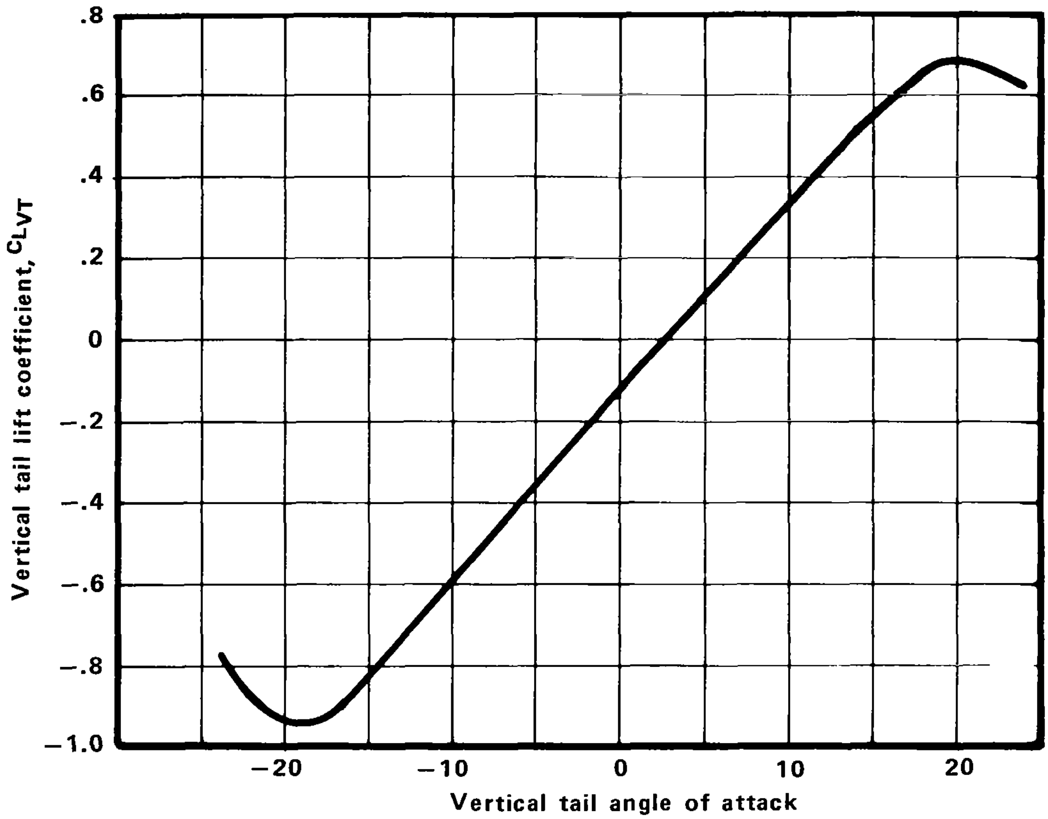

Figure 12 F – ATRS vertical tail lift coefficient vs. angle of attack (theoretical)

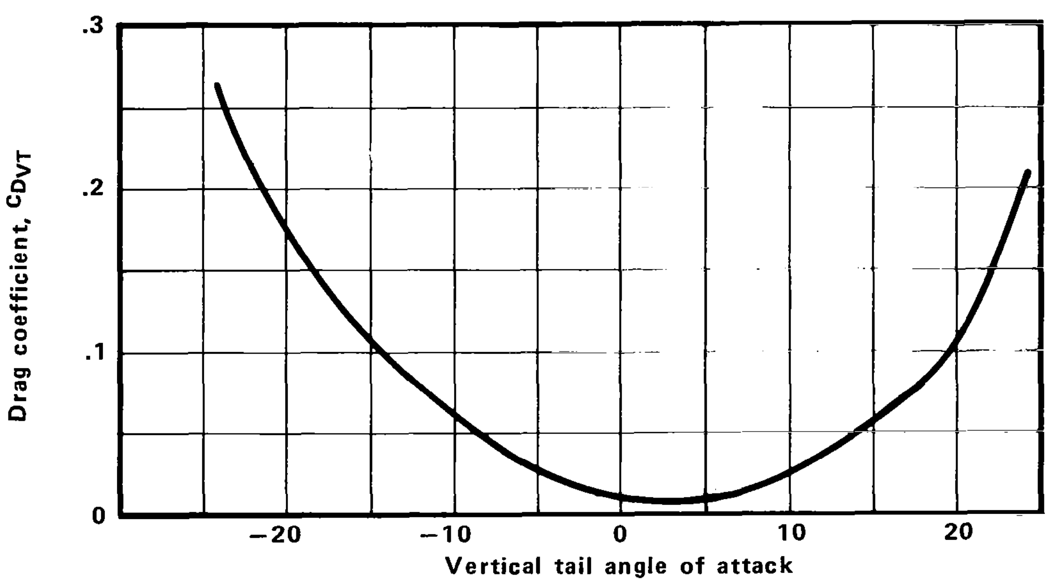

Figure 13 F – ATRS vertical tail drag coefficient vs. angle of attack (theoretical)

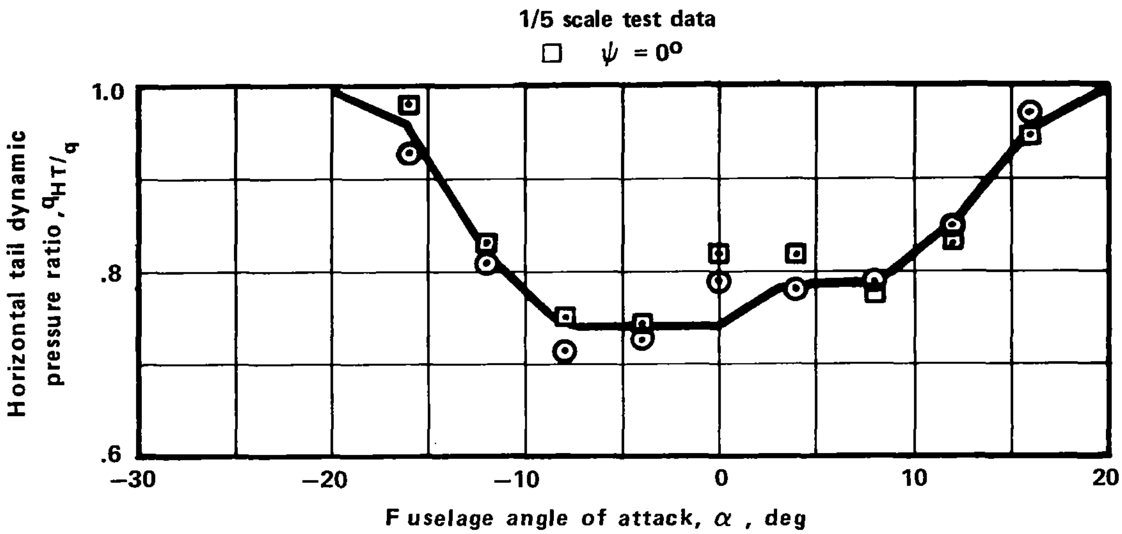

Figure 14 F — ATRS horizontal tail dynamic pressure ratio variation with angle of attack.

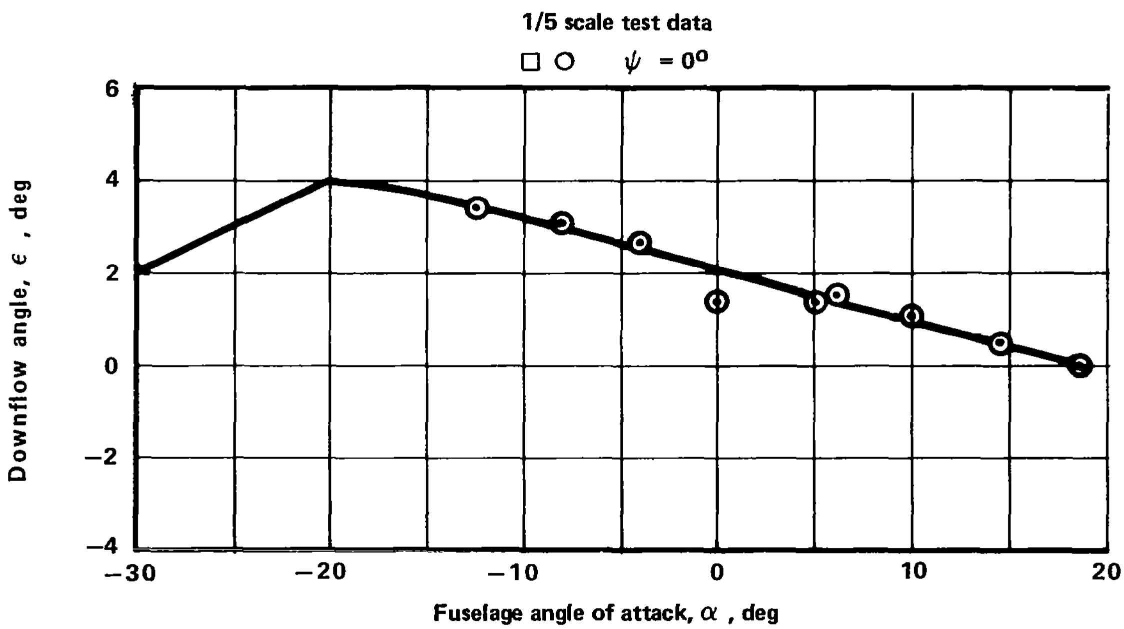

Figure 15 F — ATRS horizontal tail downflow angle variation with angle of attack.

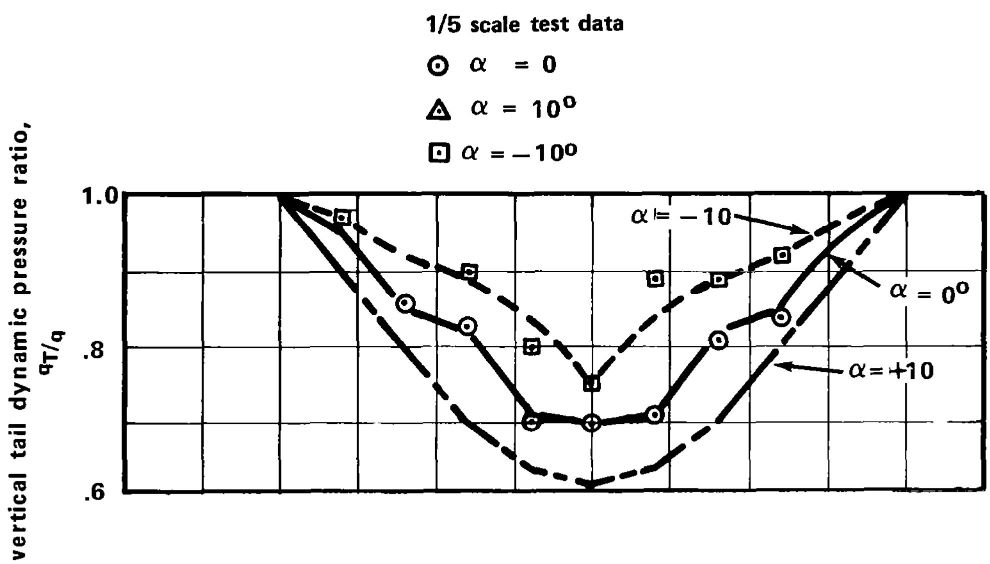

Figure 16F – ATRS vertical dynamic pressure ratio variation with yaw angle

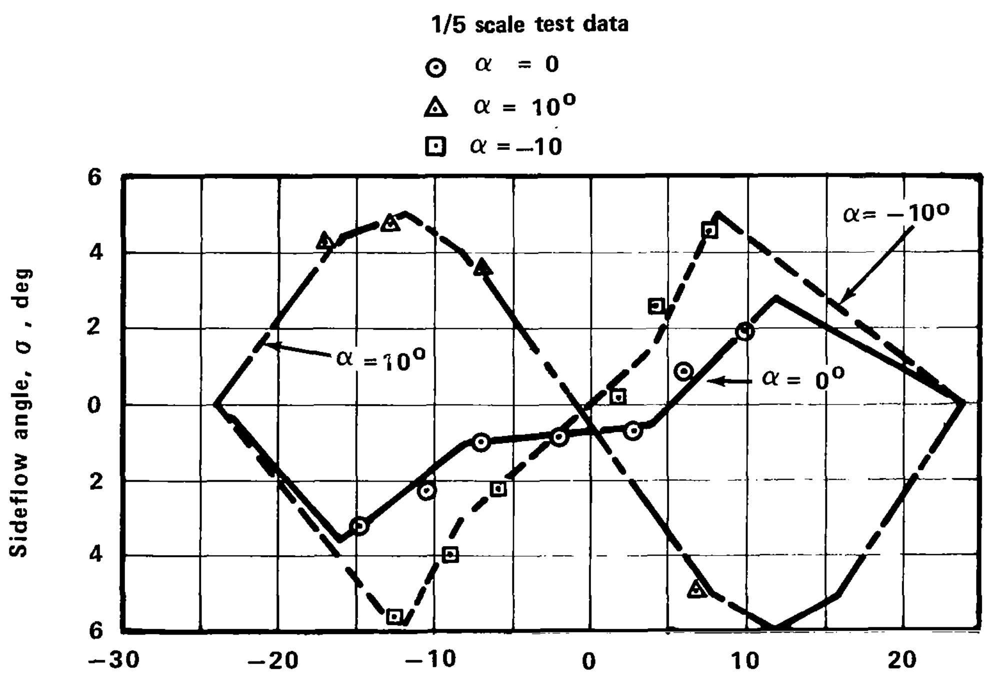

Figure 17F – Vertical tail sideflow angle variation with yaw angle.

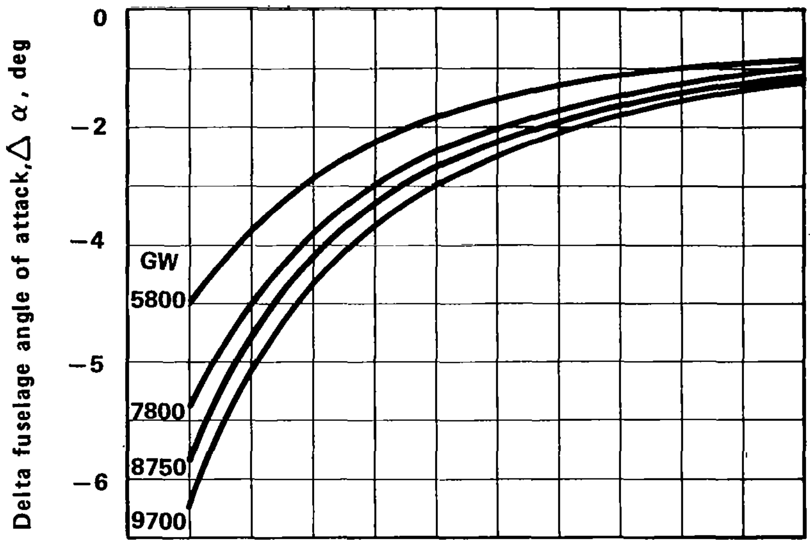

Figure 18F —Effect of rotor on body angle of attack

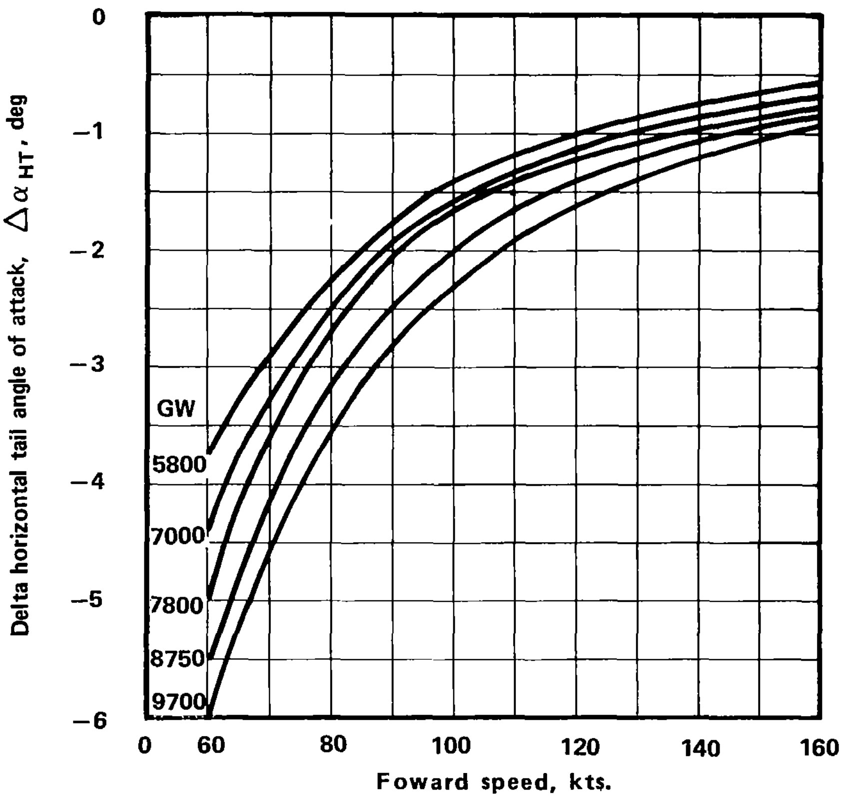

Figure 19F —Effect of rotor on tail angle of attack

TABLE F.1 ATRS FUSELAGE AND TAIL SURFACE GEOMETRIC DATA

Item	Fuselage Station	Water Line	Butt Line
Main Rotor Center (5^{0} forward shaft tile)	200	157	0
Tail Rotor Center (0^{0} yaw and cant angle)	518	163	19
Horizontal Stabilizer Aerodynamic Center of Pressure	474	101	0
Vertical Stabilizer Aerodynamic Center of Pressure	490	141	0
Reference Point for Figures 1F-17F Data	200	90	0

TABLE F.2 ATRS TAIL SURFACE GEOMETRIC DESCRIPTION DATA

Item	Units	Horizontal Stabilizer	Vertical Stabilizer
Area	ft^2 (m^2)	18.5 (1.72)	19.7 (1.35)
Span	in. (cm)	116.0 (294.6)	70.0 (177.8)
Root Chord	in. (cm)	32.0 (81.3)	52.0 (15.8)
Tip Chord	in. (cm)	13.8 (3.51)	29.0 (73.7)
Aspect Ratio	-	5.0	1.7
Taper Ratio	-	.43	.56
Sweep (1/4 Chord)	deg.	3.5	36.5
Airfoil Section	-	4412(INVERTED)	63_4 - 421
Incidence (Geometric)	deg.	+2.0	0

TABLE F.3 ATRS AIRCRAFT CG LIMIT DATA

Gross Weight (lb)	(kg)	Fuselage Station	Water Line
5,700	(2586)	210.	103.7
6,500 6,500	(2948)	193. 210.	103.8 98.6
7,500 7,500	(3402)	193. 210.	100.8 98.6
8,500	(3856)	193.	97.7
8,750	(3969)	210.	95.4
10,000 10,000	(4536)	197. 206.	97.7 93.9

NOTE: Lateral CG offset between 6.5 in. right and 4.5 inches left up to 7,500 lb gross weight (3402 kg), decreasing to 5.0 in. (12.7 cm) right and 3.5 in. (8.89 cm) left at 10,000 lb gross weight (4536 kg).

APPENDIX G

Description of Coupled Normal Modes (Y201)/Variable Inflow (F389) Elastic Rotor Analysis

The analysis employed in this study is identified as Y201, which was funded by the Eustis and Ames directorates of USAAMRDL, as well as the United Technologies Research Center and Hamilton Standard Division of United Technologies Corporation. The basic blade equations of motion were developed under army contract No. DA-44-177-AMC-322(T), as reported in Reference 7. A current version of the program was developed under Contract DAAJ02-71-C-0024, Reference 8.

The Y201 aeroelastic rotor program contains state-of-the-art representations for all primary factors influencing rotor airloads prediction. The approach includes both dynamic and aerodynamic considerations required to determine rotor blade motions and resultant airload distributions. These analytic models are integrated into a single analysis and can be selectively employed to vary the sophistication of the airloads prediction technique. The basic mathematical model in the Y201 airloads analysis represents each blade as a segmented dynamic and aerodynamic body. Mass, stiffness and damping properties are defined for each segment which, when combined with the appropriate end constraints at the rotor head, permit calculation of the blade response to imparted airloads. Since the airloads themselves are also functions of the blade dynamic response, an iterative technique is used to converge the airload and dynamic behavior. The rotor inflow logic can be exercised on several levels of complexity. As such, only the simplest constant inflow representation is addressed directly within the Y201 analysis. The more complicated wake inflow representations are accessed through a separate analysis, F389SR, which is linked with Y201.

Rotor blade flatwise, edgewise, and torsional bending modes and frequencies are calculated internal to the program. The blade model was run with three flatwise elastic modes, two edgewise modes, and one torsion mode. These are in addition to the articulated flapping and lag modes.

The rotor model uses the normal modes of vibration of the blade to form a set of approximately uncoupled differential equations which are integrated with respect to time to calculate the response of the blade. Up to second order products of small terms in the flatwise and edgewise equations, and third order products in the torsion equation have been retained.

The analysis yields rotor performance, vibratory blade moments, stresses, push rod loads and non-linear aeroelastic stability. These results are used to evaluate or design the rotor system. Variables can include blade c.g. offset distributions, aerodynamic center offset distributions resulting from airfoil characteristics or blade planform variations, blade stiffness distributions, and control system stiffness.

A simple viscous lag damper is used on the blade. The aerodynamic model uses a blade-element yawed flow analysis. The yawed flow capability was developed for the Army ATL in 1977 and is a steady flow analysis. Table look-up of experimental data is used to obtain coefficients of appropriate airfoil lift, drag, and pitching moment. A multiple airfoil capability is also available up to two different airfoil sections along the blade span. Tip sweep back may be included with steady flow models. Presently, the aerodynamic sweep is assumed to be the geometric sweep of the blade tip quarter chord, uncorrected for three-dimensional flow effects.

Rotor trim is primarily accomplished through internal iteration on the governing rotor control inputs. An exception is rotor shaft angle setting which requires an external iteration. Rotor collective pitch and the rotor lateral and longitudinal cyclic pitch settings are internally controlled to obtain a specified lift and predetermined roll and pitch moment values.

As mentioned previously, the Y201 analysis accesses either an internally calculated uniform downwash or a radial and azimuthally variable downwash generated with the linked F389SR analysis. In either case, the downwash plays an important role in the airload determination since the effective blade section lift angles are the sum of the local airfoil section geometric angle and the flow angle induced by the local downwash.

This program is known as the UTRC Rotorcraft Prescribed Wake Induced Velocity Analysis. Descriptions of the analysis, applications, and comparisons with test data are presented in Reference 9, 10 and 11.

The F389R prescribed rotor wake inflow program computes rotor inflow distributions for interface with the Y201 airloads analysis. Since the inflow velocities are based on the evaluation of velocities induced by a representation of the wake structure, the method can describe radial and azimuthal inflow variations in great detail. The use of representative wake induced downwash distributions has a strong effect on predicted airloads. This is particularly true in regard to the higher harmonic airload excitations. The non-uniform downwash distributions were calculated with an assumed classical, skewed helical wake.

Stated briefly, the mathematical model in the rotor inflow program consists of the representation of each blade by a segmented lifting line, and the helical wake of the rotor by discrete, segmented vortex filaments. The vorticity of the trailing wake results from the spanwise variation of bound circulation. The blades are divided into a finite number of radial segments, and the induced velocity at the center of each selected blade segment is computed by summing the contributions of each bound and trailing wake segment. The contribution of each vortex segment is obtained through use of the Biot-Savart equation.

In the generation of the analytical results for this study, two complete cycles of the coupled Y201/F389SR analysis were performed. This involved one execution of Y201 with constant inflow to initiate the F389SR program and two subsequent F389SR/Y201 passes.

APPENDIX H

Description of Wing and Body Aerodynamic Technique (WABAT)

The Sikorsky developed Wing And Body Aerodynamic Techniques (WABAT) program is a versatile three-dimensional potential flow method. Its primary function is the calculation of body surface pressures, surface flow velocities, and off-body velocity distributions for both non-lifting and lifting bodies. The basic potential flow solution is based on the distributed source method developed by Hess and Smith in Reference 12 while the lifting elements are represented with a modified Multhopp lifting surface procedure developed from Reference 13. The program is capable of calculating both the body pressure distribution, required for evaluating rotor flow effects on body surface excitation, and off-body potential flow velocities, needed for assessing rotor load interference.

The WABAT analysis is comprised of separate body paneling and panel source solution programs. The body paneling definition program was developed to simplify the generation of a suitable model for arbitrary body shapes. Program inputs generally describe cross sections of the body by combinations of curved and straight line segments. Figure H1 illustrates a typical airframe panel model generated with the geometry model.

For prediction of rotor load variations induced by the airframe, the ability to predict off-body velocities in the rotor plane is important. WABAT has this capability which is demonstrated as follows for a selected rotor/fuselage configuration. The predicted nondimensionalized interference velocities at the rotor plane are depicted in Figure H2. As illustrated, the interference is highest in the nose region where the rotor inflow is decreased by the nose structures and the forward pylon geometry. These effects are shown in detail in Figure H3 which shows the effect on section angle of attack when the blade passes the nose region. The net effect of the entire fuselage flow field on the rotor loads was obtained by combining the fuselage and rotor induced flows and comparing the resulting blade load pattern with that obtained without the airframe effects. The resulting angle of attack comparison for the .30 blade radial station is shown in Figure H4. Although the interference effects are most pronounced at 180°, significant load distortions appear around the entire azimuth. These results were obtained by coupling the WABAT analysis with the UTRC Rotorcraft Wake Analysis (F389 SR), and then using the total inflow in a normal modes aeroelastic rotor analysis.

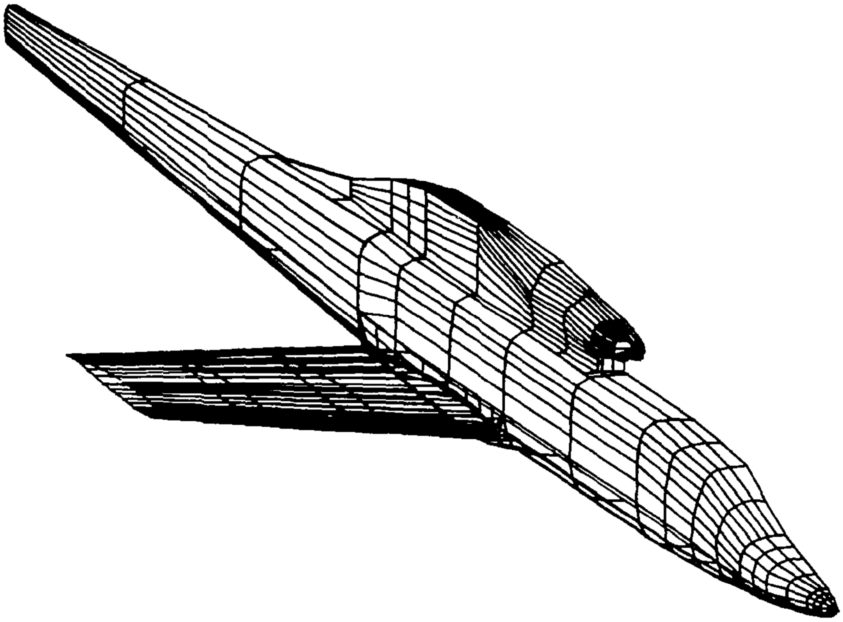

Figure H1 — Typical airframe panel model.

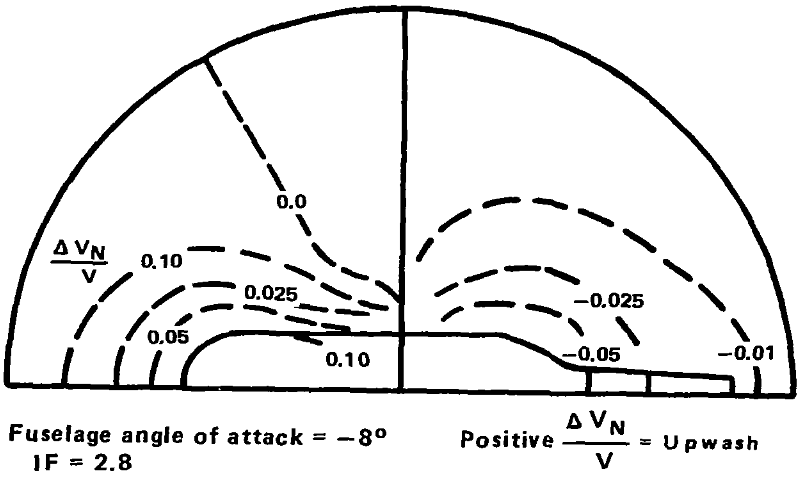

Figure H2 — Predicted body induced velocities at rotor plane.

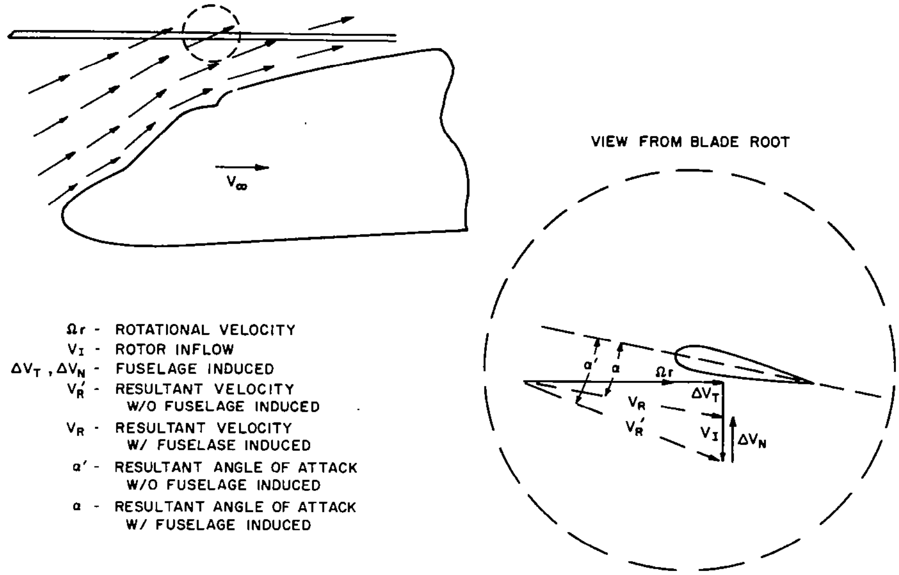

Figure H3 – Nose region upwash alters local angle of attack.

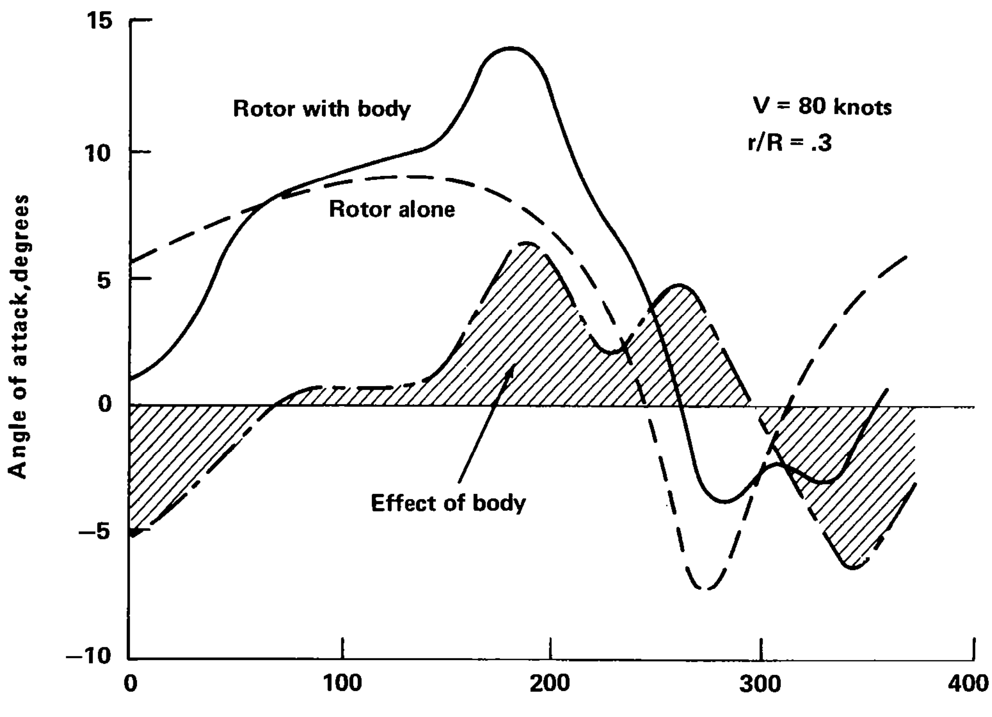

Figure H4 – Blade angle of attack change due to body interference.

APPENDIX I

Description of Full Scale Model Wind Tunnel Test Facility

The large scale wind tunnel at the NASA/Ames Research Center, Mountain View, California is located on the Moffett Field Naval Air Station. The tunnel is a closed throat, closed return type with a test section 40 feet (12.2m) high and 80 feet (24.4m) wide. The wind tunnel has a nominal maximum speed capability of 200 knots and is powered by six 6000 horsepower (4406 Kw) electric motors. Rotor forces and moments are measured by a six-component mechanical balance.

The rotor hub was mounted at the center of the wind tunnel test section as shown in Reference 1. Figure 4 shows the entire test model installed in the NASA/Ames wind tunnel.

APPENDIX J

Description of 1/5th Scale Model Test Facility

The United Technology Research Center Large Subsonic Wind Tunnel is a single return, closed throat facility with interchangeable 18 foot (5.5m) and 8 foot (2.4m) test sections. The 1/5th scale model test was conducted in the 18 foot (5.5m) octagonally shaped test section. Maximum tunnel velocity in the 18 foot (5.5m) test section is approximately 175 knots. Stagnation temperature of the airstream can be held constant by means of air exchanger values. Stagnation pressure is equal to atmospheric pressure. Electric power was supplied to the model by one of two motor generator sets capable of developing a maximum of 325 HP (239 Kw) each at a variable frequency of 0-400 Hz. A 25 channel static data acquisition system (STADAS) was used to record and process tunnel test conditions and model static data. The STADAS system is directly linked to a PDP-6 computer.

The rotor hub was mounted at the center of the wind tunnel test section at zero fuselage pitch. Because the model pitches about a point 10.6 feet (3.2m) below the rotor hub, the hub drops below the centerline of the test section by the amount:

$$z = 10.6\ (1 - \cos \alpha_f) \text{ in feet}$$

or

$$z = 3.2\ (1 - \cos \alpha_f) \text{ in meters}$$

The 1/5 scale model is shown installed in the UTRC wind tunnel in Figure 6.

APPENDIX K

NASA/Ames Rotor Test Apparatus Outside Contour Geometric Description

The NASA/Ames Rotor Test Apparatus (RTA) was used to test the Advanced Rotor System in the NASA/Ames 40' x 80' tunnel (Figure 3). In order to analytically assess the impact of the velocities induced at the rotor due to the RTA module a geometric description of the module was developed, which is compatible with Sikorsky Aircraft's three-dimensional aerodynamic analysis. The aerodynamic analysis used was developed by Sikorsky and is designated, the Wing and Body Aerodynamic Technique (WABAT). This analysis is a potential flow analysis and calculates local velocities and pressures at points on the surface as well as off the surface. See Appendix H.

A half-body geometric description for symmetrical bodies is used in the analysis. The body is modeled by representing the surface of a number of approximately flat panels. Table K1 presents the coordinates of the panel nodal points. Each panel is described independently and, consequently, nodal points are duplicated if shared by more than one panel. All panels are described by four nodal points even if the panel is triangular rather than a quadrilateral.

In Table K1, the four node points are described by its Cartesian coordinate points. In the coordinate system used the X,Y,Z points correspond to:

X - Buttline

Y - Waterline

Z - Body Station

Units - Inches

As indicated by the table, the RTA module half body is described by 300 panels.

It should be noted that the actual module has small fairing approximately mid-length of the body located near the bottom of the module (Figure 3). The fairings cover the attachment fittings for the balance support struts. These fairings have not been modeled since their size and distance from the rotor is sufficient to assume that their aerodynamic influence on the rotor is significant.

Table K.1 - Rotor test apparatus outside contour coordinates

PANEL	X1	Y1	Z1	X2	Y2	Z2	X3	Y3	Z3	X4	Y4	Z4
1	.000	200.000	82.000	.000	207.460	83.330	1.551	207.297	83.330	.000	200.000	82.000
2	.000	200.000	82.000	1.551	207.297	83.330	3.034	206.815	83.330	.000	200.000	82.000
3	.000	200.000	82.000	3.034	206.815	83.330	4.385	206.035	83.330	.000	200.000	82.000
4	.000	200.000	82.000	4.385	206.035	83.330	5.544	204.992	83.330	.000	200.000	82.000
5	.000	200.000	82.000	5.544	204.992	83.330	6.461	203.730	83.330	.000	200.000	82.000
6	.000	200.000	82.000	6.461	203.730	83.330	7.095	202.305	83.330	.000	200.000	82.000
7	.000	200.000	82.000	7.095	202.305	83.330	7.419	200.780	83.330	.000	200.000	82.000
8	.000	200.000	82.000	7.419	200.780	83.330	7.419	199.220	83.330	.000	200.000	82.000
9	.000	200.000	82.000	7.419	199.220	83.330	7.095	197.695	83.330	.000	200.000	82.000
10	.000	200.000	82.000	7.095	197.695	83.330	6.461	196.270	83.330	.000	200.000	82.000
11	.000	200.000	82.000	6.461	196.270	83.330	5.544	195.008	83.330	.000	200.000	82.000
12	.000	200.000	82.000	5.544	195.008	83.330	4.385	193.965	83.330	.000	200.000	82.000
13	.000	200.000	82.000	4.385	193.965	83.330	3.034	193.185	83.330	.000	200.000	82.000
14	.000	200.000	82.000	3.034	193.185	83.330	1.551	192.703	83.330	.000	200.000	82.000
15	.000	200.000	82.000	1.551	192.703	83.330	.000	192.540	83.330	.000	200.000	82.000
16	.000	207.460	83.330	.000	214.400	87.330	2.994	214.085	87.330	1.551	207.297	83.330
17	1.551	207.297	83.330	2.994	214.085	87.330	5.857	213.155	87.330	3.034	206.815	83.330
18	3.034	206.815	83.330	5.857	213.155	87.330	8.464	211.650	87.330	4.385	206.035	83.330
19	4.385	206.035	83.330	8.464	211.650	87.330	10.701	209.635	87.330	5.544	204.992	83.330
20	5.544	204.992	83.330	10.701	209.635	87.330	12.471	207.200	87.330	6.461	203.730	83.330
21	6.461	203.730	83.330	12.471	207.200	87.330	13.695	204.450	87.330	7.095	202.305	83.330
22	7.095	202.305	83.330	13.695	204.450	87.330	14.321	201.505	87.330	7.419	200.780	83.330
23	7.419	200.780	83.330	14.321	201.505	87.330	14.321	198.495	87.330	7.419	199.220	83.330
24	7.419	199.220	83.330	14.321	198.495	87.330	13.695	195.550	87.330	7.095	197.695	83.330
25	7.095	197.695	83.330	13.695	195.550	87.330	12.471	192.800	87.330	6.461	196.270	83.330
26	6.461	196.270	83.330	12.471	192.800	87.330	10.701	190.365	87.330	5.544	195.008	83.330
27	5.544	195.008	83.330	10.701	190.365	87.330	8.464	188.350	87.330	4.385	193.965	83.330
28	4.385	193.965	83.330	8.464	188.350	87.330	5.857	186.845	87.330	3.034	193.185	83.330
29	3.034	193.185	83.330	5.857	186.845	87.330	2.994	185.915	87.330	1.551	192.703	83.330
30	1.551	192.703	83.330	2.994	185.915	87.330	.000	185.600	87.330	.000	192.540	83.330
31	.000	214.400	87.330	.000	219.200	92.660	3.992	218.780	92.660	2.994	214.085	87.330
32	2.994	214.085	87.330	3.992	218.780	92.660	7.809	217.540	92.660	5.857	213.155	87.330
33	5.857	213.155	87.330	7.809	217.540	92.660	11.286	215.533	92.660	8.464	211.650	87.330
34	8.464	211.650	87.330	11.286	215.533	92.660	14.268	212.847	92.660	10.701	209.635	87.330
35	10.701	209.635	87.330	14.268	212.847	92.660	16.628	209.600	92.660	12.471	207.200	87.330
36	12.471	207.200	87.330	16.628	209.600	92.660	18.260	205.933	92.660	13.695	204.450	87.330
37	13.695	204.450	87.330	18.260	205.933	92.660	19.095	202.007	92.660	14.321	201.505	87.330
38	14.321	201.505	87.330	19.095	202.007	92.660	19.095	197.993	92.660	14.321	198.495	87.330
39	14.321	198.495	87.330	19.095	197.993	92.660	18.260	194.067	92.660	13.695	195.550	87.330
40	13.695	195.550	87.330	18.260	194.067	92.660	16.628	190.400	92.660	12.471	192.800	87.330
41	12.471	192.800	87.330	16.628	190.400	92.660	14.268	187.153	92.660	10.701	190.365	87.330
42	10.701	190.365	87.330	14.268	187.153	92.660	11.286	184.467	92.660	8.464	188.350	87.330
43	8.464	188.350	87.330	11.286	184.467	92.660	7.809	182.460	92.660	5.857	186.845	87.330

Table K.1 - continued

44	5.857	186.845	87.330	7.809	182.460	92.660	3.992	181.220	92.660	2.994	185.915	87.330
45	2.994	185.915	87.330	3.992	181.220	92.660	.000	180.800	92.660	.000	185.600	87.330
46	.000	219.200	92.660	.000	222.660	99.330	4.711	222.165	99.330	3.992	218.780	92.660
47	3.992	218.780	92.660	4.711	222.165	99.330	9.217	220.701	99.330	7.809	217.540	92.660
48	7.809	217.540	92.660	9.217	220.701	99.330	13.319	218.332	99.330	11.286	215.533	92.660
49	11.286	215.533	92.660	13.319	218.332	99.330	16.840	215.163	99.330	14.268	212.847	92.660
50	14.268	212.847	92.660	16.840	215.163	99.330	19.624	211.330	99.330	16.628	209.600	92.660
51	16.628	209.600	92.660	19.624	211.330	99.330	21.551	207.002	99.330	18.260	205.933	92.660
52	18.260	205.933	92.660	21.551	207.002	99.330	22.536	202.369	99.330	19.095	202.007	92.660
53	19.095	202.007	92.660	22.536	202.369	99.330	22.536	197.631	99.330	19.095	197.993	92.660
54	19.095	197.993	92.660	22.536	197.631	99.330	21.551	192.998	99.330	18.260	194.067	92.660
55	18.260	194.067	92.660	21.551	192.998	99.330	19.624	188.670	99.330	16.628	190.400	92.660
56	16.628	190.400	92.660	19.624	188.670	99.330	16.840	184.837	99.330	14.268	187.153	92.660
57	14.268	187.153	92.660	16.840	184.837	99.330	13.319	181.668	99.330	11.286	184.467	92.660
58	11.286	184.467	92.660	13.319	181.668	99.330	9.217	179.299	99.330	7.809	182.460	92.660
59	7.809	182.460	92.660	9.217	179.299	99.330	4.711	177.835	99.330	3.992	181.220	92.660
60	3.992	181.220	92.660	4.711	177.835	99.330	.000	177.340	99.330	.000	180.800	92.660
61	.000	222.660	99.330	.000	225.460	110.498	5.293	224.904	110.498	4.711	222.165	99.330
62	4.711	222.165	99.330	5.293	224.904	110.498	10.355	223.259	110.498	9.217	220.701	99.330
63	9.217	220.701	99.330	10.355	223.259	110.498	14.965	220.598	110.498	13.319	218.332	99.330
64	13.319	218.332	99.330	14.965	220.598	110.498	18.921	217.036	110.498	16.840	215.163	99.330
65	16.840	215.163	99.330	18.921	217.036	110.498	22.049	212.730	110.498	19.624	211.330	99.330
66	19.624	211.330	99.330	22.049	212.730	110.498	24.214	207.868	110.498	21.551	207.002	99.330
67	21.551	207.002	99.330	24.214	207.868	110.498	25.320	202.661	110.498	22.536	202.369	99.330
68	22.536	202.369	99.330	25.320	202.661	110.498	25.320	197.339	110.498	22.536	197.631	99.330
69	22.536	197.631	99.330	25.320	197.339	110.498	24.214	192.132	110.498	21.551	192.998	99.330
70	21.551	192.998	99.330	24.214	192.132	110.498	22.049	187.270	110.498	19.624	188.670	99.330
71	19.624	188.670	99.330	22.049	187.270	110.498	18.921	182.964	110.498	16.840	184.837	99.330
72	16.840	184.837	99.330	18.921	182.964	110.498	14.965	179.402	110.498	13.319	181.668	99.330
73	13.319	181.668	99.330	14.965	179.402	110.498	10.355	176.741	110.498	9.217	179.299	99.330
74	9.217	179.299	99.330	10.355	176.741	110.498	5.293	175.096	110.498	4.711	177.835	99.330
75	4.711	177.835	99.330	5.293	175.096	110.498	.000	174.540	110.498	.000	177.340	99.330
76	.000	225.460	110.498	.000	228.260	121.665	5.876	227.642	121.665	5.293	224.904	110.498
77	5.293	224.904	110.498	5.876	227.642	121.665	11.494	225.817	121.665	10.355	223.259	110.498
78	10.355	223.259	110.498	11.494	225.817	121.665	16.611	222.863	121.665	14.965	220.598	110.498
79	14.965	220.598	110.498	16.611	222.863	121.665	21.001	218.910	121.665	18.921	217.036	110.498
80	18.921	217.036	110.498	21.001	218.910	121.665	24.474	214.130	121.665	22.049	212.730	110.498
81	22.049	212.730	110.498	24.474	214.130	121.665	26.877	208.733	121.665	24.214	207.868	110.498
82	24.214	207.868	110.498	26.877	208.733	121.665	28.105	202.954	121.665	25.320	202.661	110.498
83	25.320	202.661	110.498	28.105	202.954	121.665	28.105	197.046	121.665	25.320	197.339	110.498
84	25.320	197.339	110.498	28.105	197.046	121.665	26.877	191.267	121.665	24.214	192.132	110.498
85	24.214	192.132	110.498	26.877	191.267	121.665	24.474	185.870	121.665	22.049	187.270	110.498
86	22.049	187.270	110.498	24.474	185.870	121.665	21.001	181.090	121.665	18.921	182.964	110.498
87	18.921	182.964	110.498	21.001	181.090	121.665	16.611	177.137	121.665	14.965	179.402	110.498
88	14.965	179.402	110.498	16.611	177.137	121.665	11.494	174.183	121.665	10.355	176.741	110.498
89	10.355	176.741	110.498	11.494	174.183	121.665	5.876	172.358	121.665	5.293	175.096	110.498
90	5.293	175.096	110.498	5.876	172.358	121.665	.000	171.740	121.665	.000	174.540	110.498
91	.000	228.260	121.665	.000	231.060	132.833	6.458	230.381	132.833	5.876	227.642	121.665
92	5.876	227.642	121.665	6.458	230.381	132.833	12.633	228.375	132.833	11.494	225.817	121.665
93	11.494	225.817	121.665	12.633	228.375	132.833	18.257	225.128	132.833	16.611	222.863	121.665
94	16.611	222.863	121.665	18.257	225.128	132.833	23.082	220.783	132.833	21.001	218.910	121.665
95	21.001	218.910	121.665	23.082	220.783	132.833	26.899	215.530	132.833	24.474	214.130	121.665
96	24.474	214.130	121.665	26.899	215.530	132.833	29.540	209.598	132.833	26.877	208.733	121.665
97	26.877	208.733	121.665	29.540	209.598	132.833	30.890	203.247	132.833	28.105	202.954	121.665
98	28.105	202.954	121.665	30.890	203.247	132.833	30.890	196.753	132.833	28.105	197.046	121.665
99	28.105	197.046	121.665	30.890	196.753	132.833	29.540	190.402	132.833	26.877	191.267	121.665
100	26.877	191.267	121.665	29.540	190.402	132.833	26.899	184.470	132.833	24.474	185.870	121.665
101	24.474	185.870	121.665	26.899	184.470	132.833	23.082	179.217	132.833	21.001	181.090	121.665
102	21.001	181.090	121.665	23.082	179.217	132.833	18.257	174.872	132.833	16.611	177.137	121.665
103	16.611	177.137	121.665	18.257	174.872	132.833	12.633	171.625	132.833	11.494	174.183	121.665

Table K.1 - continued

104	11.494	174.183	121.665	12.633	171.625	132.833	6.458	169.619	132.833	5.876	172.358	121.665
105	5.876	172.358	121.665	6.458	169.619	132.833	.000	168.940	132.833	.000	171.740	121.665
106	.000	231.060	132.833	.000	233.860	144.000	7.040	233.120	144.000	6.458	230.381	132.833
107	6.458	230.381	132.833	7.040	233.120	144.000	13.772	230.933	144.000	12.633	228.375	132.833
108	12.633	228.375	132.833	13.772	230.933	144.000	19.902	227.393	144.000	18.257	225.128	132.833
109	18.257	225.128	132.833	19.902	227.393	144.000	25.163	222.657	144.000	23.082	220.783	132.833
110	23.082	220.783	132.833	25.163	222.657	144.000	29.324	216.930	144.000	26.899	215.530	132.833
111	26.899	215.530	132.833	29.324	216.930	144.000	32.203	210.463	144.000	29.540	209.598	132.833
112	29.540	209.598	132.833	32.203	210.463	144.000	33.674	203.539	144.000	30.890	203.247	132.833
113	30.890	203.247	132.833	33.674	203.539	144.000	33.674	196.461	144.000	30.890	196.753	132.833
114	30.890	196.753	132.833	33.674	196.461	144.000	32.203	189.537	144.000	29.540	190.402	132.833
115	29.540	190.402	132.833	32.203	189.537	144.000	29.324	183.070	144.000	26.899	184.470	132.833
116	26.899	184.470	132.833	29.324	183.070	144.000	25.163	177.343	144.000	23.082	179.217	132.833
117	23.082	179.217	132.833	25.163	177.343	144.000	19.902	172.607	144.000	18.257	174.872	132.833
118	18.257	174.872	132.833	19.902	172.607	144.000	13.772	169.067	144.000	12.633	171.625	132.833
119	12.633	171.625	132.833	13.772	169.067	144.000	7.040	166.880	144.000	6.458	169.619	132.833
120	6.458	169.619	132.833	7.040	166.880	144.000	.000	166.140	144.000	.000	168.940	132.833
121	.000	233.860	144.000	.000	235.120	158.960	7.302	234.353	158.960	7.040	233.120	144.000
122	7.040	233.120	144.000	7.302	234.353	158.960	14.285	232.084	158.960	13.772	230.933	144.000
123	13.772	230.933	144.000	14.285	232.084	158.960	20.643	228.413	158.960	19.902	227.393	144.000
124	19.902	227.393	144.000	20.643	228.413	158.960	26.099	223.500	158.960	25.163	222.657	144.000
125	25.163	222.657	144.000	26.099	223.500	158.960	30.415	217.560	158.960	29.324	216.930	144.000
126	29.324	216.930	144.000	30.415	217.560	158.960	33.401	210.853	158.960	32.203	210.463	144.000
127	32.203	210.463	144.000	33.401	210.853	158.960	34.928	203.671	158.960	33.674	203.539	144.000
128	33.674	203.539	144.000	34.928	203.671	158.960	34.928	196.329	158.960	33.674	196.461	144.000
129	33.674	196.461	144.000	34.928	196.329	158.960	33.401	189.147	158.960	32.203	189.537	144.000
130	32.203	189.537	144.000	33.401	189.147	158.960	30.415	182.440	158.960	29.324	183.070	144.000
131	29.324	183.070	144.000	30.415	182.440	158.960	26.099	176.500	158.960	25.163	177.343	144.000
132	25.163	177.343	144.000	26.099	176.500	158.960	20.643	171.587	158.960	19.902	172.607	144.000
133	19.902	172.607	144.000	20.643	171.587	158.960	14.285	167.916	158.960	13.772	169.067	144.000
134	13.772	169.067	144.000	14.285	167.916	158.960	7.302	165.647	158.960	7.040	166.880	144.000
135	7.040	166.880	144.000	7.302	165.647	158.960	.000	164.880	158.960	.000	166.140	144.000
136	.000	235.120	158.960	.000	235.080	181.385	7.294	234.313	181.385	7.302	234.353	158.960
137	7.302	234.353	158.960	7.294	234.313	181.385	14.268	232.047	181.385	14.285	232.084	158.960
138	14.285	232.084	158.960	14.268	232.047	181.385	20.619	228.380	181.385	20.643	228.413	158.960
139	20.643	228.413	158.960	20.619	228.380	181.385	26.069	223.473	181.385	26.099	223.500	158.960
140	26.099	223.500	158.960	26.069	223.473	181.385	30.380	217.540	181.385	30.415	217.560	158.960
141	30.415	217.560	158.960	30.380	217.540	181.385	33.363	210.840	181.385	33.401	210.853	158.960
142	33.401	210.853	158.960	33.363	210.840	181.385	34.888	203.667	181.385	34.928	203.671	158.960
143	34.928	203.671	158.960	34.888	203.667	181.385	34.888	196.333	181.385	34.928	196.329	158.960
144	34.928	196.329	158.960	34.888	196.333	181.385	33.363	189.160	181.385	33.401	189.147	158.960
145	33.401	189.147	158.960	33.363	189.160	181.385	30.380	182.460	181.385	30.415	182.440	158.960
146	30.415	182.440	158.960	30.380	182.460	181.385	26.069	176.527	181.385	26.099	176.500	158.960
147	26.099	176.500	158.960	26.069	176.527	181.385	20.619	171.620	181.385	20.643	171.587	158.960
148	20.643	171.587	158.960	20.619	171.620	181.385	14.268	167.953	181.385	14.285	167.916	158.960
149	14.285	167.916	158.960	14.268	167.953	181.385	7.294	165.687	181.385	7.302	165.647	158.960
150	7.302	165.647	158.960	7.294	165.687	181.385	.000	164.920	181.385	.000	164.880	158.960
151	.000	235.080	181.385	.000	235.040	203.810	7.285	234.274	203.810	7.294	234.313	181.385
152	7.294	234.313	181.385	7.285	234.274	203.810	14.252	232.011	203.810	14.268	232.047	181.385
153	14.268	232.047	181.385	14.252	232.011	203.810	20.596	228.348	203.810	20.619	228.380	181.385
154	20.619	228.380	181.385	20.596	228.348	203.810	26.040	223.446	203.810	26.069	223.473	181.385
155	26.069	223.473	181.385	26.040	223.446	203.810	30.345	217.520	203.810	30.380	217.540	181.385
156	30.380	217.540	181.385	30.345	217.520	203.810	33.325	210.828	203.810	33.363	210.840	181.385
157	33.363	210.840	181.385	33.325	210.828	203.810	34.848	203.663	203.810	34.888	203.667	181.385
158	34.888	203.667	181.385	34.848	203.663	203.810	34.848	196.337	203.810	34.888	196.333	181.385
159	34.888	196.333	181.385	34.848	196.337	203.810	33.325	189.172	203.810	33.363	189.160	181.385
160	33.363	189.160	181.385	33.325	189.172	203.810	30.345	182.480	203.810	30.380	182.460	181.385
161	30.380	182.460	181.385	30.345	182.480	203.810	26.040	176.554	203.810	26.069	176.527	181.385
162	26.069	176.527	181.385	26.040	176.554	203.810	20.596	171.652	203.810	20.619	171.620	181.385
163	20.619	171.620	181.385	20.596	171.652	203.810	14.252	167.989	203.810	14.268	167.953	181.385

Table K.1 - continued

164	14.268	167.953	181.385	14.252	167.989	203.810	7.285	165.726	203.810	7.294	165.687	181.385
165	7.294	165.687	181.385	7.285	165.726	203.810	.000	164.960	203.810	.000	164.920	181.385
166	.000	235.040	203.810	.000	235.000	226.235	7.277	234.235	226.235	7.285	234.274	203.810
167	7.285	234.274	203.810	7.277	234.235	226.235	14.236	231.974	226.235	14.252	232.011	203.810
168	14.252	232.011	203.810	14.236	231.974	226.235	20.572	228.316	226.235	20.596	228.348	203.810
169	20.596	228.348	203.810	20.572	228.316	226.235	26.010	223.420	226.235	26.040	223.446	203.810
170	26.040	223.446	203.810	26.010	223.420	226.235	30.311	217.500	226.235	30.345	217.520	203.810
171	30.345	217.520	203.810	30.311	217.500	226.235	33.287	210.816	226.235	33.325	210.828	203.810
172	33.325	210.828	203.810	33.287	210.816	226.235	34.808	203.659	226.235	34.848	203.663	203.810
173	34.848	203.663	203.810	34.808	203.659	226.235	34.808	196.341	226.235	34.848	196.337	203.810
174	34.848	196.337	203.810	34.808	196.341	226.235	33.287	189.184	226.235	33.325	189.172	203.810
175	33.325	189.172	203.810	33.287	189.184	226.235	30.311	182.500	226.235	30.345	182.480	203.810
176	30.345	182.480	203.810	30.311	182.500	226.235	26.010	176.580	226.235	26.040	176.554	203.810
177	26.040	176.554	203.810	26.010	176.580	226.235	20.572	171.684	226.235	20.596	171.652	203.810
178	20.596	171.652	203.810	20.572	171.684	226.235	14.236	168.026	226.235	14.252	167.989	203.810
179	14.252	167.989	203.810	14.236	168.026	226.235	7.277	165.765	226.235	7.285	165.726	203.810
180	7.285	165.726	203.810	7.277	165.765	226.235	.000	165.000	226.235	.000	164.960	203.810
181	.000	235.000	226.235	.000	234.960	248.660	7.269	234.196	248.660	7.277	234.235	226.235
182	7.277	234.235	226.235	7.269	234.196	248.660	14.219	231.937	248.660	14.236	231.974	226.235
183	14.236	231.974	226.235	14.219	231.937	248.660	20.549	228.283	248.660	20.572	228.316	226.235
184	20.572	228.316	226.235	20.549	228.283	248.660	25.980	223.393	248.660	26.010	223.420	226.235
185	26.010	223.420	226.235	25.980	223.393	248.660	30.276	217.480	248.660	30.311	217.500	226.235
186	30.311	217.500	226.235	30.276	217.480	248.660	33.249	210.803	248.660	33.287	210.816	226.235
187	33.287	210.816	226.235	33.249	210.803	248.660	34.768	203.654	248.660	34.808	203.659	226.235
188	34.808	203.659	226.235	34.768	203.654	248.660	34.768	196.346	248.660	34.808	196.341	226.235
189	34.808	196.341	226.235	34.768	196.346	248.660	33.249	189.197	248.660	33.287	189.184	226.235
190	33.287	189.184	226.235	33.249	189.197	248.660	30.276	182.520	248.660	30.311	182.500	226.235
191	30.311	182.500	226.235	30.276	182.520	248.660	25.980	176.607	248.660	26.010	176.580	226.235
192	26.010	176.580	226.235	25.980	176.607	248.660	20.549	171.717	248.660	20.572	171.684	226.235
193	20.572	171.684	226.235	20.549	171.717	248.660	14.219	168.062	248.660	14.236	168.026	226.235
194	14.236	168.026	226.235	14.219	168.062	248.660	7.269	165.804	248.660	7.277	165.765	226.235
195	7.277	165.765	226.235	7.269	165.804	248.660	.000	165.040	248.660	.000	165.000	226.235
196	.000	234.960	248.660	.000	232.016	282.926	6.656	231.316	282.926	7.269	234.196	248.660
197	7.269	234.196	248.660	6.656	231.316	282.926	13.022	229.248	282.926	14.219	231.937	248.660
198	14.219	231.937	248.660	13.022	229.248	282.926	18.819	225.902	282.926	20.549	228.283	248.660
199	20.549	228.283	248.660	18.819	225.902	282.926	23.793	221.423	282.926	25.980	223.393	248.660
200	25.980	223.393	248.660	23.793	221.423	282.926	27.727	216.008	282.926	30.276	217.480	248.660
201	30.276	217.480	248.660	27.727	216.008	282.926	30.449	209.893	282.926	33.249	210.803	248.660
202	33.249	210.803	248.660	30.449	209.893	282.926	31.841	203.347	282.926	34.768	203.654	248.660
203	34.768	203.654	248.660	31.841	203.347	282.926	31.841	196.653	282.926	34.768	196.346	248.660
204	34.768	196.346	248.660	31.841	196.653	282.926	30.449	190.107	282.926	33.249	189.197	248.660
205	33.249	189.197	248.660	30.449	190.107	282.926	27.727	183.992	282.926	30.276	182.520	248.660
206	30.276	182.520	248.660	27.727	183.992	282.926	23.793	178.577	282.926	25.980	176.607	248.660
207	25.980	176.607	248.660	23.793	178.577	282.926	18.819	174.098	282.926	20.549	171.717	248.660
208	20.549	171.717	248.660	18.819	174.098	282.926	13.022	170.752	282.926	14.219	168.062	248.660
209	14.219	168.062	248.660	13.022	170.752	282.926	6.656	168.684	282.926	7.269	165.804	248.660
210	7.269	165.804	248.660	6.656	168.684	282.926	.000	167.984	282.926	.000	165.040	248.660
211	.000	232.016	282.926	.000	229.072	317.192	6.044	228.437	317.192	6.656	231.316	282.926
212	6.656	231.316	282.926	6.044	228.437	317.192	11.825	226.559	317.192	13.022	229.248	282.926
213	13.022	229.248	282.926	11.825	226.559	317.192	17.088	223.520	317.192	18.819	225.902	282.926
214	18.819	225.902	282.926	17.088	223.520	317.192	21.605	219.453	317.192	23.793	221.423	282.926
215	23.793	221.423	282.926	21.605	219.453	317.192	25.177	214.536	317.192	27.727	216.008	282.926
216	27.727	216.008	282.926	25.177	214.536	317.192	27.649	208.984	317.192	30.449	209.893	282.926
217	30.449	209.893	282.926	27.649	208.984	317.192	28.913	203.039	317.192	31.841	203.347	282.926
218	31.841	203.347	282.926	28.913	203.039	317.192	28.913	196.961	317.192	31.841	196.653	282.926
219	31.841	196.653	282.926	28.913	196.961	317.192	27.649	191.016	317.192	30.449	190.107	282.926
220	30.449	190.107	282.926	27.649	191.016	317.192	25.177	185.464	317.192	27.727	183.992	282.926
221	27.727	183.992	282.926	25.177	185.464	317.192	21.605	180.547	317.192	23.793	178.577	282.926
222	23.793	178.577	282.926	21.605	180.547	317.192	17.088	176.480	317.192	18.819	174.098	282.926
223	18.819	174.098	282.926	17.088	176.480	317.192	11.825	173.441	317.192	13.022	170.752	282.926

Table K.1 - continued

224	13.022	170.752	282.926	11.825	173.441	317.192	6.044	171.563	317.192	6.656	168.684	282.926
~~225~~	~~6.656~~	~~168.684~~	~~282.926~~	~~6.044~~	~~171.563~~	~~317.192~~	~~.000~~	~~170.928~~	~~317.192~~	~~.000~~	~~167.984~~	~~282.926~~
226	.000	229.072	317.192	.000	226.128	351.458	5.432	225.557	351.458	6.044	228.437	317.192
227	6.044	228.437	317.192	5.432	225.557	351.458	10.627	223.869	351.458	11.825	226.559	317.192
228	11.825	226.559	317.192	10.627	223.869	351.458	15.358	221.138	351.458	17.088	223.520	317.192
229	17.088	223.520	317.192	15.358	221.138	351.458	19.417	217.483	351.458	21.605	219.453	317.192
230	21.605	219.453	317.192	19.417	217.483	351.458	22.628	213.064	351.458	25.177	214.536	317.192
231	25.177	214.536	317.192	22.628	213.064	351.458	24.849	208.074	351.458	27.649	208.984	317.192
232	27.649	208.984	317.192	24.849	208.074	351.458	25.985	202.731	351.458	28.913	203.039	317.192
233	28.913	203.039	317.192	25.985	202.731	351.458	25.985	197.269	351.458	28.913	196.961	317.192
234	28.913	196.961	317.192	25.985	197.269	351.458	24.849	191.926	351.458	27.649	191.016	317.192
235	27.649	191.016	317.192	24.849	191.926	351.458	22.628	186.936	351.458	25.177	185.464	317.192
236	25.177	185.464	317.192	22.628	186.936	351.458	19.417	182.517	351.458	21.605	180.547	317.192
237	21.605	180.547	317.192	19.417	182.517	351.458	15.358	178.862	351.458	17.088	176.480	317.192
238	17.088	176.480	317.192	15.358	178.862	351.458	10.627	176.131	351.458	11.825	173.441	317.192
239	11.825	173.441	317.192	10.627	176.131	351.458	5.432	174.443	351.458	6.044	171.563	317.192
240	6.044	171.563	317.192	5.432	174.443	351.458	.000	173.872	351.458	.000	170.928	317.192
241	.000	226.128	351.458	.000	223.184	385.724	4.820	222.677	385.724	5.432	225.557	351.458
242	5.432	225.557	351.458	4.820	222.677	385.724	9.430	221.180	385.724	10.627	223.869	351.458
243	10.627	223.869	351.458	9.430	221.180	385.724	13.627	218.756	385.724	15.358	221.138	351.458
244	15.358	221.138	351.458	13.627	218.756	385.724	17.229	215.513	385.724	19.417	217.483	351.458
245	19.417	217.483	351.458	17.229	215.513	385.724	20.078	211.592	385.724	22.628	213.064	351.458
246	22.628	213.064	351.458	20.078	211.592	385.724	22.049	207.164	385.724	24.849	208.074	351.458
247	24.849	208.074	351.458	22.049	207.164	385.724	23.057	202.423	385.724	25.985	202.731	351.458
248	25.985	202.731	351.458	23.057	202.423	385.724	23.057	197.577	385.724	25.985	197.269	351.458
249	25.985	197.269	351.458	23.057	197.577	385.724	22.049	192.836	385.724	24.849	191.926	351.458
250	24.849	191.926	351.458	22.049	192.836	385.724	20.078	188.408	385.724	22.628	186.936	351.458
251	22.628	186.936	351.458	20.078	188.408	385.724	17.229	184.487	385.724	19.417	182.517	351.458
252	19.417	182.517	351.458	17.229	184.487	385.724	13.627	181.244	385.724	15.358	178.862	351.458
253	15.358	178.862	351.458	13.627	181.244	385.724	9.430	178.820	385.724	10.627	176.131	351.458
254	10.627	176.131	351.458	9.430	178.820	385.724	4.820	177.323	385.724	5.432	174.443	351.458
255	5.432	174.443	351.458	4.820	177.323	385.724	.000	176.816	385.724	.000	173.872	351.458
256	.000	223.184	385.724	.000	220.240	419.990	4.208	219.798	419.990	4.820	222.677	385.724
257	4.820	222.677	385.724	4.208	219.798	419.990	8.232	218.490	419.990	9.430	221.180	385.724
258	9.430	221.180	385.724	8.232	218.490	419.990	11.897	216.375	419.990	13.627	218.756	385.724
259	13.627	218.756	385.724	11.897	216.375	419.990	15.041	213.543	419.990	17.229	215.513	385.724
260	17.229	215.513	385.724	15.041	213.543	419.990	17.528	210.120	419.990	20.078	211.592	385.724
261	20.078	211.592	385.724	17.528	210.120	419.990	19.249	206.254	419.990	22.049	207.164	385.724
262	22.049	207.164	385.724	19.249	206.254	419.990	20.129	202.116	419.990	23.057	202.423	385.724
263	23.057	202.423	385.724	20.129	202.116	419.990	20.129	197.884	419.990	23.057	197.577	385.724
264	23.057	197.577	385.724	20.129	197.884	419.990	19.249	193.746	419.990	22.049	192.836	385.724
265	22.049	192.836	385.724	19.249	193.746	419.990	17.528	189.880	419.990	20.078	188.408	385.724
266	20.078	188.408	385.724	17.528	189.880	419.990	15.041	186.457	419.990	17.229	184.487	385.724
267	17.229	184.487	385.724	15.041	186.457	419.990	11.897	183.625	419.990	13.627	181.244	385.724
268	13.627	181.244	385.724	11.897	183.625	419.990	8.232	181.510	419.990	9.430	178.820	385.724
269	9.430	178.820	385.724	8.232	181.510	419.990	4.208	180.202	419.990	4.820	177.323	385.724
270	4.820	177.323	385.724	4.208	180.202	419.990	.000	179.760	419.990	.000	176.816	385.724
271	.000	220.240	419.990	.000	215.200	445.600	3.160	214.868	445.600	4.208	219.798	419.990
272	4.208	219.798	419.990	3.160	214.868	445.600	6.182	213.886	445.600	8.232	218.490	419.990
273	8.232	218.490	419.990	6.182	213.886	445.600	8.934	212.297	445.600	11.897	216.375	419.990
274	11.897	216.375	419.990	8.934	212.297	445.600	11.296	210.171	445.600	15.041	213.543	419.990
275	15.041	213.543	419.990	11.296	210.171	445.600	13.164	207.600	445.600	17.528	210.120	419.990
276	17.528	210.120	419.990	13.164	207.600	445.600	14.456	204.697	445.600	19.249	206.254	419.990
277	19.249	206.254	419.990	14.456	204.697	445.600	15.117	201.589	445.600	20.129	202.116	419.990
278	20.129	202.116	419.990	15.117	201.589	445.600	15.117	198.411	445.600	20.129	197.884	419.990
279	20.129	197.884	419.990	15.117	198.411	445.600	14.456	195.303	445.600	19.249	193.746	419.990
280	19.249	193.746	419.990	14.456	195.303	445.600	13.164	192.400	445.600	17.528	189.880	419.990
281	17.528	189.880	419.990	13.164	192.400	445.600	11.296	189.829	445.600	15.041	186.457	419.990
~~262~~	~~15.041~~	~~186.457~~	~~419.990~~	~~11.296~~	~~189.829~~	~~445.600~~	~~8.934~~	~~187.703~~	~~445.600~~	~~11.897~~	~~183.625~~	~~419.990~~
283	11.897	183.625	419.990	8.934	187.703	445.600	6.182	186.114	445.600	8.232	181.510	419.990

Table K.1 - concluded

284	8.232	181.510	419.990	6.182	186.114	445.600	3.160	185.132	445.600	4.208	180.202	419.990
~~285~~	~~4.208~~	~~180.202~~	~~419.990~~	~~3.160~~	~~185.132~~	~~445.600~~	~~.000~~	~~184.800~~	~~445.600~~	~~.000~~	~~179.760~~	~~419.990~~
286	.000	215.200	445.600	.000	210.400	470.000	2.162	210.173	470.000	3.160	214.868	445.600
287	3.160	214.868	445.600	2.162	210.173	470.000	4.230	209.501	470.000	6.182	213.886	445.600
288	6.182	213.886	445.600	4.230	209.501	470.000	6.113	208.414	470.000	8.934	212.297	445.600
289	8.934	212.297	445.600	6.113	208.414	470.000	7.729	206.959	470.000	11.296	210.171	445.600
290	11.296	210.171	445.600	7.729	206.959	470.000	9.007	205.200	470.000	13.164	207.600	445.600
291	13.164	207.600	445.600	9.007	205.200	470.000	9.891	203.214	470.000	14.456	204.697	445.600
292	14.456	204.697	445.600	9.891	203.214	470.000	10.343	201.087	470.000	15.117	201.589	445.600
293	15.117	201.589	445.600	10.343	201.087	470.000	10.343	198.913	470.000	15.117	198.411	445.600
294	15.117	198.411	445.600	10.343	198.913	470.000	9.891	196.786	470.000	14.456	195.303	445.600
295	14.456	195.303	445.600	9.891	196.786	470.000	9.007	194.800	470.000	13.164	192.400	445.600
296	13.164	192.400	445.600	9.007	194.800	470.000	7.729	193.041	470.000	11.296	189.829	445.600
297	11.296	189.829	445.600	7.729	193.041	470.000	6.113	191.586	470.000	8.934	187.703	445.600
298	8.934	187.703	445.600	6.113	191.586	470.000	4.230	190.499	470.000	6.182	186.114	445.600
299	6.182	186.114	445.600	4.230	190.499	470.000	2.162	189.827	470.000	3.160	185.132	445.600
300	3.160	185.132	445.600	2.162	189.827	470.000	.000	189.600	470.000	.000	184.800	445.600

APPENDIX L

Normal Component of Flight Vehicle Induced Velocities At Rotor Plane

The following tables present the predicted induced velocity component normal to the plane of the rotor, for each of four flight conditions studied in the main report. The fuselage induced velocity component is normalized by the free stream velocity and is evaluated around the rotor azimuth at 15 blade radial stations, selected to be the center of each of the 15 blade segments used in the normal modes elastic blade analyses. A positive fourier series of argument ψ is used to express the interference velocity. For each blade segment, the first number is the steady amplitude coefficient. The next set of 12 coefficients is the harmonic amplitudes of the cos $(n\psi)$ terms of the series in assending order. The last set of 12 coefficients is the harmonic amplitudes of the $(n\psi)$ terms of the series. The data in Table L.1 are valid for the two flight conditions studied at low gross weight (see Table VII, page 44) because, as the calculations were performed, blade coning and flapping relative to the rotor shaft are nearly the same for the two flight conditions. Table L.2 and L.3 cover one flight condition each.

GW = 8200 lb (3719.5 kg) μ = .338, .4 M_T = .6

Table L.1 - Harmonics of normal component of flight vehicle induced velocities at rotor plane

Blade segment mean station, r/R	Fourier series amplitude coefficient
.0649	0.111404E+00 -0.585325E-01 0.336887E-01 -0.666425E-02 -0.743823E-03 -0.117297E-02 -0.104244E-02 -0.140798E-03 0.504172E-04 0.420667E-04 0.598794E-04 -0.143657E-05 -0.323906E-06 0.133878E-08 0.194026E-09 0.217309E-08 -0.155220E-09 -0.186265E-08 0.100893E-08 0.535510E-08 0.201787E-08 0.205667E-08 -0.737297E-09 0.283277E-08 0.0
.1406	0.405048E-01 -0.778932E-01 0.208659E-01 -0.222066E-01 -0.291731E-02 -0.652741E-02 -0.169449E-02 -0.818522E-03 0.163686E-03 0.389516E-03 0.413871E-03 0.346866E-03 0.170218E-03 0.100893E-08 -0.252233E-09 0.159101E-08 0.776102E-10 -0.112535E-08 -0.100893E-08 0.232831E-09 0.120296E-08 -0.388051E-09 -0.128037E-08 -0.213428E-09 0.0
.2462	0.102059E-01 -0.665029E-01 0.171147E-01 -0.166797E-01 0.405476E-02 -0.431385E-02 0.539345E-03 -0.139897E-02 -0.204475E-03 -0.650983E-03 -0.268856E-03 -0.400213E-03 -0.122736E-03 0.805206E-09 -0.485064E-09 0.776102E-09 -0.368051E-10 -0.737297E-09 -0.174623E-08 -0.147459E-08 0.814907E-09 -0.659687E-09 -0.970128E-09 -0.649986E-09 0.0
.3409	0.434492E-02 -0.653257E-01 0.165634E-01 -0.196934E-01 0.711667E-02 -0.456221E-02 0.261155E-02 -0.599483E-03 0.974475E-03 0.102076E-03 0.411093E-03 0.155226E-03 0.133494E-03 0.620882E-09 -0.717894E-09 0.620882E-09 -0.155220E-09 -0.582077E-09 -0.205667E-08 -0.182384E-08 0.853712E-09 -0.737297E-09 -0.892517E-09 -0.902219E-09 0.0
.4167	0.431409E-02 -0.572084E-01 0.150969E-01 -0.197599E-01 0.652030E-02 -0.564971E-02 0.208885E-02 -0.126752E-02 0.608981E-03 -0.155524E-03 0.195954E-03 0.737757E-04 0.603596E-04 0.591778E-09 -0.271636E-09 0.814907E-09 0.0 -0.465661E-09 -0.186265E-08 -0.162981E-08 0.853712E-09 -0.698492E-09 -0.795505E-09 -0.863414E-09 0.0
.4925	0.388297E-02 -0.455100E-01 0.129096E-01 -0.165511E-01 0.556996E-02 -0.518485E-02 0.170504E-02 -0.142529E-02 0.408844E-03 -0.348615E-03 0.610083E-04 -0.874761E-04 0.146431E-06 0.[illegible]04466E-09 -0.368649E-09 0.698492E-09 -0.232831E-09 -0.426856E-09 -0.151340E-08 -0.112535E-08 0.776102E-09 -0.582077E-09 -0.601479E-09 -0.659687E-09 0.0
.5683	0.308077E-02 -0.339366E-01 0.102589E-01 -0.123272E-01 0.451096E-02 -0.390496E-02 0.147429E-02 -0.110667E-02 0.412277E-03 -0.204626E-03 0.100939E-03 -0.795407E-04 0.185583E-04 0.271636E-09 -0.339545E-09 0.504466E-09 -0.776102E-10 -0.232831E-09 -0.110595E-08 -0.892517E-09 0.504466E-09 -0.407454E-09 -0.446259E-09 -0.480213E-09 0.0

Table L.1 - concluded

Blade segment mean station r/R	Fourier series amplitude coefficient
.6441	0.204721E-02 -0.247650E-01 0.749370E-02 -0.878618E-02 0.330864E-02 -0.276022E-02 0.113547E-02 -0.785144E-03 0.361191E-03 -0.199200E-03 0.120840E-03 -0.503766E-04 0.335730E-04 0.295889E-09 -0.194026E-09 0.349246E-09 -0.776102E-10 -0.155220E-09 -0.873115E-09 -0.717894E-09 0.329843E-09 -0.291038E-09 -0.349246E-09 -0.354097E-09 0.0
.7104	0.120916E-02 -0.187629E-01 0.537922E-02 -0.646210E-02 0.233356E-02 -0.200388E-02 0.810070E-03 -0.569625E-03 0.272240E-03 -0.144726E-03 0.102521E-03 -0.344358E-04 0.320814E-04 0.184324E-09 -0.184324E-09 0.232831E-09 0.0 -0.145519E-09 -0.601479E-09 -0.533570E-09 0.281337E-09 -0.252233E-09 -0.261934E-09 -0.276486E-09 0.0
.7672	0.616771E-03 -0.147926E-01 0.388820E-02 -0.494326E-02 0.162531E-02 -0.151520E-02 0.550634E-03 -0.431874E-03 0.186414E-03 -0.110883E-03 0.737673E-04 -0.265477E-04 0.241987E-04 0.123691E-09 -0.106714E-09 0.174623E-09 -0.582077E-10 -0.970128E-10 -0.485064E-09 -0.436557E-09 0.223129E-09 -0.184324E-09 -0.223129E-09 -0.235256E-09 0.0
.8145	0.241308E-03 -0.121895E-01 0.291598E-02 -0.395919E-02 0.116352E-02 -0.119924E-02 0.376719E-03 -0.342179E-03 0.124975E-03 -0.885300E-04 0.507719E-04 -0.212089E-04 0.172602E-04 0.143094E-09 -0.150370E-09 0.145519E-09 0.194026E-10 -0.970128E-10 -0.378350E-09 -0.349246E-09 0.155220E-09 -0.174623E-09 -0.164922E-09 -0.208577E-09 0.0
.8619	-0.355698E-04 -0.100733E-01 0.215992E-02 -0.317036E-02 0.808946E-03 -0.947840E-03 0.241810E-03 -0.272098E-03 0.744200E-04 -0.729653E-04 0.291008E-04 -0.196703E-04 0.988813E-05 0.104289E-09 -0.970128E-10 0.116415E-09 -0.582077E-10 -0.679089E-10 -0.310441E-09 -0.320142E-09 0.126117E-09 -0.140669E-09 -0.145519E-09 -0.177048E-09 0.0
.9208	-0.264348E-03 -0.796557E-02 0.147029E-02 -0.239753E-02 0.497594E-03 -0.700707E-03 0.128345E-03 -0.200322E-03 0.340733E-04 -0.541449E-04 0.131814E-04 -0.147108E-04 0.482541E-05 0.751849E-10 -0.970128E-10 0.727596E-10 -0.485064E-11 -0.582077E-10 -0.242532E-09 -0.271636E-09 0.921621E-10 -0.121266E-09 -0.121266E-09 -0.150370E-09 0.0
.9636	-0.366808E-03 -0.673890E-02 0.110973E-02 -0.195775E-02 0.342257E-03 -0.561630E-03 0.740994E-04 -0.160394E-03 0.147426E-04 -0.443644E-04 0.481948E-05 -0.129913E-04 0.189619E-05 0.654836E-10 -0.751849E-10 0.436557E-10 -0.194026E-10 -0.679089E-10 -0.198876E-09 -0.237681E-09 0.679089E-10 -0.106714E-09 -0.921621E-10 -0.134605E-09 0.0
.9882	-0.407332E-03 -0.612458E-02 0.943323E-03 -0.174108E-02 0.273701E-03 -0.493280E-03 0.517731E-04 -0.140151E-03 0.771995E-05 -0.385408E-04 0.248293E-05 -0.109567E-04 0.126136E-05 0.618456E-10 -0.388051E-10 0.388051E-10 -0.970128E-11 -0.339545E-10 -0.189175E-09 -0.208577E-09 0.485064E-10 -0.970128E-10 -0.921621E-10 -0.124904E-09 0.0

GW = 10,300. lb (4672 kg) μ = .375 M_T = .6

Table L.2 - Harmonics of Normal Component of Flight Vehicle Induced Velocities at Rotor Plane

Blade segment mean station, r/R	Fourier series amplitude coefficient
.0649	0.110838E+00 -0.545712E-01 0.321541E-01 -0.542486E-02 -0.779167E-03 -0.126106E-02 -0.102640E-02 -0.210642E-03 0.439831E-04 0.376890E-04 0.575065E-04 0.169413E-04 -0.802265E-05 0.164922E-08 0.100893E-08 0.244472E-08 0.0 -0.162981E-08 0.139698E-08 0.543272E-08 0.194026E-08 0.225070E-08 -0.931323E-09 0.292979E-08 0.0
.1406	0.395553E-01 -0.746248E-01 0.171830E-01 -0.203224E-01 -0.437931E-02 -0.633814E-02 -0.214048E-02 -0.859177E-03 0.956110E-04 0.425770E-03 0.449401E-03 0.407590E-03 0.194430E-03 0.108654E-08 -0.504466E-09 0.126117E-08 0.388051E-10 -0.116415E-08 -0.814907E-09 0.388051E-09 0.116415E-08 -0.329843E-09 -0.116415E-08 -0.300740E-09 0.0
.2462	0.100387E-01 -0.647734E-01 0.142729E-01 -0.149956E-01 0.268973E-02 -0.366623E-02 0.266094E-04 -0.123509E-02 -0.409900E-03 -0.638006E-03 -0.384268E-03 -0.432917E-03 -0.165699E-03 0.708193E-09 -0.485064E-09 0.582077E-09 -0.388051E-10 -0.776102E-09 -0.151340E-08 -0.135818E-08 0.853712E-09 -0.659687E-09 -0.100893E-08 -0.688791E-09 0.0
.3409	0.376329E-02 -0.626765E-01 0.126156E-01 -0.173027E-01 0.504869E-02 -0.340488E-02 0.189862E-02 -0.164297E-03 0.800198E-03 0.258432E-03 0.389198E-03 0.224351E-03 0.136121E-03 0.611180E-09 -0.601479E-09 0.698492E-09 -0.155220E-09 -0.582077E-09 -0.186265E-08 -0.186265E-08 0.853712E-09 -0.776102E-09 -0.892517E-09 -0.941024E-09 0.0
.4167	0.287099E-02 -0.542207E-01 0.109466E-01 -0.172202E-01 0.419835E-02 -0.444102E-02 0.119386E-02 -0.865671E-03 0.348365E-03 -0.603220E-04 0.137318E-03 0.823366E-04 0.544132E-04 0.611180E-09 -0.407454E-09 0.659687E-09 -0.116415E-09 -0.582077E-09 -0.151340E-08 -0.159101E-08 0.659687E-09 -0.814907E-09 -0.795505E-09 -0.863414E-09 0.0
.4925	0.260773E-02 -0.428523E-01 0.940461E-02 -0.143141E-01 0.354054E-02 -0.408666E-02 0.878076E-03 -0.104239E-02 0.143435E-03 -0.247872E-03 -0.744383E-05 -0.672270E-04 -0.120596E-04 0.465661E-09 -0.426856E-09 0.504466E-09 -0.776102E-10 -0.388051E-09 -0.128057E-08 -0.116415E-08 0.543271E-09 -0.601479E-09 -0.601479E-09 -0.727596E-09 0.0
.5683	0.219093E-02 -0.319338E-01 0.769579E-02 -0.105879E-01 0.299708E-02 -0.302039E-02 0.837299E-03 -0.771271E-03 0.194629E-03 -0.179461E-03 0.356346E-04 -0.466394E-04 0.359203E-05 0.305590E-09 -0.320142E-09 0.426856E-09 0.0 -0.271636E-09 -0.970128E-09 -0.892517E-09 0.426856E-09 -0.426856E-09 -0.426856E-09 -0.494765E-09 0.0

Table L.2 - concluded

Blade segment Mean Station, r/R	Fourier Series Amplitude Coefficient
.6441	0.150725E-02 -0.234293E-01 0.574496E-02 -0.756723E-02 0.225760E-02 -0.212000E-02 0.683039E-03 -0.525783E-03 0.200022E-03 -0.105872E-03 0.688251E-04 -0.120975E-04 0.206343E-04 0.203727E-09 -0.203727E-09 0.300740E-09 0.0 -0.232831E-09 -0 737297E-09 -0.679089E-09 0.310441E-09 -0.300740E-09 -0.339545E-09 -0.358947E-09 0.0
.7104	0.899154E-03 -0.179106E-01 0.417022E-02 -0.562905E-02 0.159655E-02 -0.155953E-02 0.488251E-03 -0.384378E-03 0.154324E-03 -0.737677E-04 0.624240E-04 -0.226690E-05 0.215207E-04 0.160071E-09 -0.135818E-09 0.203727E-09 -0.485064E-10 -0.174623E-09 -0.543271E-09 -0.523869E-09 0.232831E-09 -0.252233E-09 -0.271636E-09 -0.281337E-09 0.0
.7672	0.453963E-03 -0.142591E-01 0.303366E-02 -0.437129E-02 0.109866E-02 -0.120941E-02 0.319279E-03 -0.304562E-03 0.100063E-03 -0.617362E-04 0.431365E-04 -0.386581E-05 0.157444E-04 0.157646E-09 -0.135818E-09 0.145519E-09 -0.291038E-10 -0.145519E-09 -0.417155E-09 -0.417155E-09 0.184324E-09 -0.184324E-09 -0.213428E-09 -0.227980E-09 0.0
.8145	0.166476E-03 -0.118548E-01 0.228297E-02 -0.355388E-02 0.769992E-03 -0.983630E-03 0.204083E-03 -0.253584E-03 0.607419E-04 -0.540431E-04 0.285657E-04 -0.446893E-05 0.114032E-04 0.111565E-09 -0.679089E-10 0.116415E-09 -0.970128E-11 -0.970128E-10 -0.339545E-09 -0.378350E-09 0.145519E-09 -0.155220E-09 -0.164922E-09 -0.201301E-09 0.0
.8619	-0.468138E-04 -0.988419E-02 0.169659E-02 -0.289004E-02 0.518504E-03 -0.800046E-03 0.115143E-03 -0.213203E-03 0.272459E-04 -0.509609E-04 0.124009E-04 -0.950042E-05 0.531306E-05 0.776102E-10 -0.135818E-09 0.970128E-10 0.0 -0.106714E-09 -0.291038E-09 -0.300740E-09 0.106714E-09 -0.140669E-09 -0.150370E-09 -0.179474E-09 0.0
.9208	-0.222282E-03 -0.789706E-02 0.116226E-02 -0.222527E-02 0.301690E-03 -0.611822E-03 0.431677E-04 -0.167938E-03 0.131608E-05 -0.444057E-04 -0.489090E-07 -0.120260E-04 0.577294E-06 0.873115E-10 -0.582077E-10 0.582077E-10 -0.970128E-11 -0.776102E-10 -0.223129E-09 -0.261934E-09 0.873115E-10 -0.130967E-09 -0.116415E-09 -0.152795E-09 0.0
.9636	-0.301145E-03 -0.672770E-02 0.881694E-03 -0.183942E-02 0.195515E-03 -0.501281E-03 0.111066E-04 -0.139578E-03 -0.906042E-05 -0.385617E-04 -0.449326E-05 -0.115638E-04 -0.100477E-05 0.606330E-10 -0.557823E-10 0.485064E-10 -0.145519E-10 -0.727596E-10 -0.179474E-09 -0.237681E-09 0.582077E-10 -0.111565E-09 -0.945874E-10 -0.134605E-09 0.0
.9882	-0.331983E-03 -0.613700E-02 0.752514E-03 -0.164632E-02 0.149806E-03 -0.445357E-03 -0.117065E-05 -0.124501E-03 -0.123991E-04 -0.348364E-04 -0.564717E-05 -0.106302E-04 -0.136392E-05 0.557823E-10 -0.460811E-10 0.485064E-10 0.485064E-11 -0.533570E-10 -0.174623E-09 -0.208577E-09 0.582077E-10 -0.101863E-09 -0.897368E-10 -0.132180E-09 0.0

GW = 10,300 lb (4672 kg) μ = .375 M_T = .65

Table L.3 - Harmonics of normal component of flight vehicle induced veolcities at rotor plane

Blade segment mean station, r/R	Fourier series amplitude coefficient
.0649	0.111948E+00 -0.556634E-01 0.330015E-01 -0.583748E-02 -0.803494E-03 -0.125285E-02 -0.104943E-02 -0.194940E-03 0.402073E-04 0.626041E-04 0.460689E-04 0.860953E-05 -0.114948E-05 0.145519E-08 0.892517E-09 0.228950E-08 -0.232831E-09 -0.194026E-08 0.108654E-08 0.574316E-08 0.201787E-08 0.213428E-08 -0.853712E-09 0.279397E-08 0.0
.1406	0.402085E-01 -0.760878E-01 0.185470E-01 -0.213300E-01 -0.402540E-02 -0.657280E-02 -0.205202E-02 -0.869258E-03 0.134415E-03 0.439412E-03 0.462837E-03 0.422920E-03 0.196205E-03 0.514168E-09 -0.388051E-09 0.141639E-08 0.155220E-09 -0.116415E-08 -0.892517E-09 0.776102E-10 0.116415E-08 -0.426856E-09 -0.116415E-08 -0.300740E-09 0.0
.2462	0.101652E-01 -0.657057E-01 0.154339E-01 -0.157659E-01 0.320919E-02 -0.398011E-02 0.184558E-03 -0.134401E-02 -0.377897E-03 -0.676540E-03 -0.373064E-03 -0.444522E-03 -0.162952E-03 0.679089E-09 -0.504466E-09 0.659687E-09 -0.116415E-09 -0.776102E-09 -0.159101E-08 -0.139698E-08 0.931323E-09 -0.659687E-09 -0.911920E-09 -0.756700E-09 0.0
.3409	0.413125E-02 -0.641954E-01 0.141371E-01 -0.184196E-01 0.588119E-02 -0.386855E-02 0.220834E-02 -0.299567E-03 0.896715E-03 0.226942E-03 0.419801E-03 0.217948E-03 0.144233E-03 0.611180E-09 -0.679089E-09 0.659687E-09 0.388051E-10 -0.659687E-09 -0.194026E-08 -0.194026E-08 0.892517E-09 -0.776102E-09 -0.873115E-09 -0.960426E-09 0.0
.4167	0.336496E-02 -0.558329E-01 0.124979E-01 -0.184511E-01 0.505600E-02 -0.499156E-02 0.150828E-02 -0.104528E-02 0.427136E-03 -0.108509E-03 0.147449E-03 0.686802E-04 0.506296E-04 0.649986E-09 -0.620882E-09 0.853712E-09 -0.194026E-09 -0.465661E-09 -0.166862E-08 -0.155220E-08 0.776102E-09 -0.698492E-09 -0.776102E-09 -0.911920E-09 0.0
.4925	0.307093E-02 -0.442609E-01 0.107439E-01 -0.153781E-01 0.430368E-02 -0.458039E-02 0.117372E-02 -0.121088E-02 0.231133E-03 -0.292647E-03 0.123422E-04 -0.770461E-04 -0.922118E-05 0.475363E-09 -0.388051E-09 0.620882E-09 -0.232831E-09 -0.426856E-09 -0.139698E-08 -0.124176E-08 0.659687E-09 -0.582077E-09 -0.620882E-09 -0.717894E-09 0.0
.5683	0.253171E-02 -0.329579E-01 0.870446E-02 -0.113864E-01 0.358492E-02 -0.340294E-02 0.107610E-02 -0.909720E-03 0.272590E-03 -0.220932E-03 0.576958E-04 -0.589375E-04 0.839029E-05 0.300740E-09 -0.368649E-09 0.504466E-09 -0.776102E-10 -0.368649E-09 -0.102834E-08 -0.911920E-09 0.446259E-09 -0.407454E-09 -0.494765E-09 -0.514168E-09 0.0

Table L.3 - concluded

Blade Segment mean station, r/R	Fourier series amplitude coefficient
.6441	0.171987E-02 -0.241077E-01 0.644321E-02 -0.812034E-02 0.267266E-02 -0.239163E-02 0.857605E-03 -0.628726E-03 0.261345E-03 -0.139430E-03 0.892277E-04 -0.236832E-04 0.260654E-04 0.247383E-09 -0.223129E-09 0.320142E-09 -0.970128E-10 -0.174623E-09 -0.776102E-09 -0.698492E-09 0.349246E-09 -0.271636E-09 -0.329843E-09 -0.358947E-09 0.0
.7104	0.102000E-02 -0.183564E-01 0.465017E-02 -0.601241E-02 0.188598E-02 -0.175011E-02 0.612267E-03 -0.458045E-03 0.199739E-03 -0.988258E-04 0.787457E-04 -0.116549E-04 0.261963E-04 0.164922E-09 -0.164922E-09 0.203727E-09 -0.582077E-10 -0.194026E-09 -0.562674E-09 -0.562674E-09 0.232831E-09 -0.232831E-09 -0.271636E-09 -0.276486E-09 0.0
.7672	0.514714E-03 -0.145539E-01 0.336825E-02 -0.464154E-02 0.130266E-02 -0.134391E-02 0.407228E-03 -0.356503E-03 0.132737E-03 -0.798172E-04 0.548858E-04 -0.112837E-04 0.190292E-04 0.160071E-09 -0.101863E-09 0.164922E-09 -0.485064E-10 -0.116415E-09 -0.436557E-09 -0.436557E-09 0.232831E-09 -0.203727E-09 -0.208577E-09 -0.232831E-09 0.0
.8145	0.191465E-03 -0.120545E-01 0.252680E-02 -0.375205E-02 0.919198E-03 -0.108261E-02 0.267441E-03 -0.291998E-03 0.838443E-04 -0.676019E-04 0.367973E-04 -0.100599E-04 0.137248E-04 0.123691E-09 -0.106714E-09 0.106714E-09 -0.194026E-10 -0.776102E-10 -0.349246E-09 -0.378350E-09 0.145519E-09 -0.174623E-09 -0.174623E-09 -0 208577E-09 0.0
.8619	-[illegible] 481299E-04 -0.100140E-01 0.187044E-02 -0.303378E-02 0.625534E-03 -0.871601E-03 0.159937E-03 -0.240487E-03 0.434967E-04 -0.602337E-04 0.183777E-04 -0.130161E-04 0.708627E-05 0.897368E-10 -0.727596E-10 0.776102E-10 0.970128E-11 -0.873115E-10 -0.300740E-09 -0.300740E-09 0.970128E-10 -0.145519E-09 -0.145519E-09 -0.179474E-09 0.0
.9208	-0.244516E-03 -0.796491E-02 0.127420E-02 -0.231950E-02 0.371317E-03 -0.658482E-03 0.714600E-04 -0.185325E-03 0.112157E-04 -0.501778E-04 0.345244E-05 -0.141646E-04 0.158909E-05 0.751849E-10 -0.291038E-10 0.630583E-10 -0.194026E-10 -0.679089E-10 -0.223129E-09 -0.271636E-09 0.727596E-10 -0.121266E-09 -0.121266E-09 -0.155220E-09 0.0
.9636	-0.332449E-03 -0.676463E-02 0.962095E-03 -0.190809E-02 0.246104E-03 -0.535185E-03 0.311196E-04 -0.151963E-03 -0.230261E-05 -0.425911E-04 -0.220301E-05 -0.130302E-04 -0.363764E-06 0.739722E-10 -0.460811E-10 0.339545E-10 -0.970128E-11 -0.630583E-10 -0.189175E-09 -0.208577E-09 0.727596E-10 -0.106714E-09 -0.994381E-10 -0.139456E-09 0.0
.9882	-0.366764E-03 -0.616019E-02 0.818646E-03 -0.170329E-02 0.191798E-03 -0.473461E-03 0.151617E-04 -0.134639E-03 -0.701044E-05 -0.380928E-04 -0.387389E-05 -0.118014E-04 -0.878087E-06 0.727596E-10 -0.485064E-10 0.436557E-10 -0.145519E-10 -0.339545E-10 -0.184324E-09 -0.218279E-09 0.533570E-10 -0.970128E-10 -0.921621E-10 -0.128542E-09 0.0

APPENDIX M

ATRS Blade Airfoil Coordinates

The following tables present the ATRS blade airfoil surface coordinates normalized by the airfoil chord. The X coordinate is parallel to the airfoil chord and is zero at the airfoils' most forward extremity. The Y coordinate is perpendiuclar to the X coordinate, positive in the direction of the upper surface. The coordinates are referenced to the chord except for the SC-1095 airfoil, which is referenced to a line parallel to, but located .17% chord above the airfoil chord.

Table M.1 SC-1095 Airfoil coordinates

Upper surface		Lower surface	
X/C	Y/C	X/C	Y/C
0.0	0.0	0.0	0.0
0.0008200	0.0039660	0.0015000	-0.0045890
0.0039700	0.0091750	0.0052400	-0.0090190
0.0096600	0.0152640	0.0111900	-0.0136550
0.0183300	0.0219940	0.0194300	-0.0183320
0.0299900	0.0287360	0.0300900	-0.0228170
0.0445700	0.0349250	0.0432100	-0.0268230
0.0619900	0.0401600	0.0587600	-0.0301220
0.0821700	0.0442810	0.0766900	-0.0326180
0.1049900	0.0473760	0.0969400	-0.0343760
0.1302500	0.0500600	0.1194500	-0.0356080
0.1577500	0.0521800	0.1441000	-0.0366080
0.1872900	0.0539200	0.1707700	-0.0376320
0.2186600	0.0550200	0.1992900	-0.0387180
0.2349500	0.0553800	0.2294600	-0.0393250
0.2516300	0.0555220	0.2450900	-0.0393920
0.2686500	0.0555560	0.2610600	-0.0394470
0.2859800	0.0554370	0.2773300	-0.0394000
0.3036100	0.0551880	0.2938700	-0.0392680
0.3215000	0.0548320	0.3106500	-0.0390670
0.3396100	0.0543890	0.3276500	-0.0388090
0.3579300	0.0538760	0.3448300	-0.0385060
0.3764200	0.0533060	0.3621700	-0.0381680
0.3950500	0.0526880	0.3796500	-0.0378020
0.4138000	0.0520280	0.3972300	-0.0374130
0.4326200	0.0513280	0.4149200	-0.0370030
0.4515000	0.0505870	0.4327000	-0.0365730
0.4704200	0.0498000	0.4505900	-0.0361190
0.4893400	0.0489610	0.4686100	-0.0356380
0.5082500	0.0480630	0.4868000	-0.0351230
0.5271400	0.0470950	0.5051900	-0.0345660
0.5459900	0.0460470	0.5237900	-0.0339580
0.5648100	0.0449100	0.5426200	-0.0332880
0.5835900	0.0436730	0.5616700	-0.0325470
0.6023200	0.0423260	0.5809300	-0.0317250
0.6209800	0.0408720	0.6003700	-0.0308130
0.6395600	0.0393000	0.6199700	-0.0298040
0.6580200	0.0376160	0.6396800	-0.0286940
0.6763400	0.0358230	0.6594700	-0.0274820
0.6944700	0.0339350	0.6792800	-0.0261730
0.7123900	0.0319640	0.6990600	-0.0247730
0.7300500	0.0299320	0.7187600	-0.0232990
0.7474200	0.0278610	0.7383100	-0.0217690
0.7644600	0.0257780	0.7576700	-0.0202070
0.7811300	0.0237120	0.7767600	-0.0186460
0.7974000	0.0216950	0.7955200	-0.0171180
0.8132300	0.0197570	0.8138600	-0.0156630
0.8286000	0.0178200	0.8317200	-0.0143170
0.8578000	0.0144010	0.8490200	-0.0131170
0.8847800	0.0107400	0.8656600	-0.0120980
0.9093200	0.0076470	0.8815800	-0.0107710
0.9312300	0.0048860	0.9109300	-0.0083240
0.9503600	0.0024750	0.9365300	-0.0061900
0.9665400	0.0004360	0.9579900	-0.0044010
0.9734900	-0.0002830	0.9750400	-0.0031170
0.9896000	-0.0010618	0.9875800	-0.0023390
1.0000000	-0.0017000	1.0000000	-0.0017000

Table M.2 SC-1095R8 Airfoil coordinates

Upper surface X/C	Upper surface Y/C	Lower surface X/C	Lower surface Y/C
0.0	0.0	0.0	0.0
0.0008200	0.0050470	0.0015000	-0.0075230
0.0039700	0.0128660	0.0052400	-0.0121080
0.0096600	0.0217500	0.0111900	-0.0153640
0.0183300	0.0307540	0.0194300	-0.0177590
0.0299900	0.0392540	0.0300900	-0.0194550
0.0445700	0.0473600	0.0432100	-0.0207000
0.0619900	0.0528920	0.0587600	-0.0219420
0.0821700	0.0573750	0.0766900	-0.0227870
0.1049900	0.0609810	0.0969400	-0.0234150
0.1302500	0.0637490	0.1194500	-0.0239310
0.1577500	0.0657359	0.1441000	-0.0244140
0.1872900	0.0670059	0.1707700	-0.0249100
0.2186600	0.0676209	0.1992900	-0.0254340
0.2349500	0.0677040	0.2294600	-0.0259670
0.2516300	0.0676469	0.2450900	-0.0262250
0.2686500	0.0674599	0.2610600	-0.0264680
0.2859800	0.0671479	0.2773300	-0.0266880
0.3036100	0.0667199	0.2938700	-0.0268800
0.3215000	0.0661829	0.3106500	-0.0270340
0.3396100	0.0655450	0.3276500	-0.0271460
0.3579300	0.0648119	0.3448300	-0.0272100
0.3764200	0.0639910	0.3621700	-0.0272230
0.3950500	0.0630890	0.3796500	-0.0271820
0.4138000	0.0621130	0.3972300	-0.0270890
0.4326200	0.0610690	0.4149200	-0.0269440
0.4515000	0.0599640	0.4327000	-0.0267530
0.4704200	0.0588020	0.4505900	-0.0265230
0.4893400	0.0575910	0.4686100	-0.0262600
0.5082500	0.0563290	0.4868000	-0.0259770
0.5271400	0.0549620	0.5051900	-0.0256880
0.5459900	0.0535140	0.5237900	-0.0253340
0.5648100	0.0519880	0.5426200	-0.0248840
0.5835900	0.0503880	0.5616700	-0.0243450
0.6023200	0.0487180	0.5809300	-0.0237210
0.6209800	0.0469820	0.6003700	-0.0230200
0.6395600	0.0451860	0.6199700	-0.0222470
0.6580200	0.0433350	0.6396800	-0.0214110
0.6763400	0.0414360	0.6594700	-0.0205200
0.6944700	0.0394980	0.6792800	-0.0195800
0.7123900	0.0375270	0.6990600	-0.0186010
0.7300500	0.0355320	0.7187600	-0.0175880
0.7474200	0.0335200	0.7383100	-0.0165520
0.7644600	0.0315020	0.7576700	-0.0154500
0.7811300	0.0294860	0.7767600	-0.0144300
0.7974000	0.0274800	0.7955200	-0.0133590
0.8132300	0.0254940	0.8138600	-0.0122900
0.8286000	0.0235340	0.8317200	-0.0112290
0.8578000	0.0197310	0.8490200	-0.0101830
0.8847800	0.0161300	0.8656600	-0.0091580
0.9093200	0.0127890	0.8815800	-0.0081690
0.9312300	0.0097580	0.9109300	-0.0062670
0.9503600	0.0070800	0.9365300	-0.0045560
0.9665400	0.0047890	0.9579900	-0.0030710
0.9734900	0.0038000	0.9750400	-0.0018530
0.9896000	0.0014970	0.9875800	-0.0009340
1.0000000	0.0000010	1.0000000	-0.0000020

Table M.3 SC-1013R8 Airfoil coordinates

Upper surface		Lower surface	
X/C	Y/C	X/C	Y/C
0.0	0.0	0.0	0.0
0.0008200	0.0069777	0.0015000	-0.0104008
0.0039700	0.0177877	0.0052400	-0.0167398
0.0096600	0.0300702	0.0111900	-0.0212413
0.0183300	0.0425185	0.0194300	-0.0245525
0.0299900	0.0542701	0.0300900	-0.0268973
0.0445700	0.0654769	0.0432100	-0.0286185
0.0619900	0.0731251	0.0587600	-0.0303356
0.0821700	0.0793230	0.0766900	-0.0315039
0.1049900	0.0843084	0.0969400	-0.0323721
0.1302500	0.0881354	0.1194500	-0.0330855
0.1577500	0.0908824	0.1441000	-0.0337533
0.1872900	0.0926382	0.1707700	-0.0344390
0.2186600	0.0934885	0.1992900	-0.0351634
0.2349500	0.0936033	0.2294600	-0.0359003
0.2516300	0.0935244	0.2450900	-0.0362570
0.2686500	0.0932659	0.2610600	-0.0365930
0.2859800	0.0928345	0.2773300	-0.0368971
0.3036100	0.0922428	0.2938700	-0.0371626
0.3215000	0.0915004	0.3106500	-0.0373755
0.3396100	0.0906184	0.3276500	-0.0375304
0.3579300	0.0896050	0.3448300	-0.0376188
0.3764200	0.0884699	0.3621700	-0.0376368
0.3950500	0.0872229	0.3796500	-0.0375801
0.4138000	0.0858735	0.3972300	-0.0374515
0.4326200	0.0844301	0.4149200	-0.0372511
0.4515000	0.0829024	0.4327000	-0.0369870
0.4704200	0.0812959	0.4505900	-0.0366690
0.4893400	0.0796216	0.4686100	-0.0363054
0.5082500	0.0778769	0.4868000	-0.0359142
0.5271400	0.0759870	0.5051900	-0.0355146
0.5459900	0.0739850	0.5237900	-0.0350252
0.5648100	0.0718753	0.5426200	-0.0344031
0.5835900	0.0696632	0.5616700	-0.0336579
0.6023200	0.0673544	0.5809300	-0.0327952
0.6209800	0.0649543	0.6003700	-0.0318260
0.6395600	0.0624713	0.6199700	-0.0307573
0.6580200	0.0599122	0.6396800	-0.0296015
0.6763400	0.0572868	0.6594700	-0.0283697
0.6944700	0.0546074	0.6792800	-0.0270701
0.7123900	0.0518824	0.6990600	-0.0257166
0.7300500	0.0491243	0.7187600	-0.0243161
0.7474200	0.0463426	0.7383100	-0.0228838
0.7644600	0.0435526	0.7576700	-0.0213602
0.7811300	0.0407655	0.7767600	-0.0199500
0.7974000	0.0379921	0.7955200	-0.0184693
0.8132300	0.0352464	0.8138600	-0.0169914
0.8286000	0.0325366	0.8317200	-0.0155245
0.8578000	0.0272788	0.8490200	-0.0140784
0.8847800	0.0223003	0.8656600	-0.0126613
0.9093200	0.0176813	0.8815800	-0.0112939
0.9312300	0.0134908	0.9109300	-0.0086644
0.9503600	0.0097884	0.9365300	-0.0062988
0.9665400	0.0066210	0.9579900	-0.0042458
0.9734900	0.0052536	0.9750400	-0.0025618
0.9896000	0.0020697	0.9875800	-0.0012913
1.0000000	0.0000014	1.0000000	-0.0000028

1. Report No. NASA CR-3714	2. Government Accession No.	3. Recipient's Catalog No.
4. Title and Subtitle ANALYSIS AND CORRELATION OF TEST DATA FROM AN ADVANCED TECHNOLOGY ROTOR SYSTEM		5. Report Date August 1983
		6. Performing Organization Code
7. Author(s) D. Jepson, R. Moffitt, K. Hilzinger, J. Bissell		8. Performing Organization Report No. SER-510034
9. Performing Organization Name and Address United Technologies Corporation Sikorsky Aircraft Division Stratford, Conn. 06602		10. Work Unit No. T4947YA
		11. Contract or Grant No. NAS2-10211
12. Sponsoring Agency Name and Address National Aeronautics and Space Administration Washington, D.C. 20546		13. Type of Report and Period Covered Contractor Report
		14. Sponsoring Agency Code 505-42-11

15. Supplementary Notes
Point of Contact: W. Johnson, Ames Research Center, MS 247-1, Moffett Field, CA 94035 (415) 965-5043 or FTS 448-5043

16. Abstract
Comparisons have been made of the performance and blade vibratory loads characteristics for an advanced rotor system as predicted by analysis and as measured in a 1/5 scale model wind tunnel test, a full scale model wind tunnel test and flight test. The principal objective of the study was to determine the accuracy with which the various tools available at the various stages in the design/development process (analysis, model test etc.) could predict final characteristics as measured on the aircraft. A secondary objective was to evaluate the accuracy of the analyses in predicting the effects of systematic tip planform variations investigated in the full scale wind tunnel test.

17. Key Words (Suggested by Author(s))	18. Distribution Statement
helicopter analysis helicopter wind tunnel test helicopter flight test	Unclassified - Unlimited Subject Category 02

19. Security Classif. (of this report)	20. Security Classif. (of this page)	21. No. of Pages	22. Price*
Unclassified	Unclassified	170	A08

*For sale by the National Technical Information Service, Springfield, Virginia 22161

NASA-Langley, 1983